Reliability and optimization, application to safety of aircraft structures

Liu Chu

▶ **To cite this version:**

Liu Chu. Reliability and optimization, application to safety of aircraft structures. Mechanics [physics.med-ph]. INSA de Rouen, 2016. English. ⟨NNT : 2016ISAM0008⟩. ⟨tel-01430044⟩

HAL Id: tel-01430044

https://theses.hal.science/tel-01430044v1

Submitted on 9 Jan 2017

HAL is a multi-disciplinary open access archive for the deposit and dissemination of scientific research documents, whether they are published or not. The documents may come from teaching and research institutions in France or abroad, or from public or private research centers.

L'archive ouverte pluridisciplinaire **HAL**, est destinée au dépôt et à la diffusion de documents scientifiques de niveau recherche, publiés ou non, émanant des établissements d'enseignement et de recherche français ou étrangers, des laboratoires publics ou privés.

HAL Authorization

Normandie Université

THESE

Pour obtenir le diplôme de doctorat
Mécanique

Préparée au sein de INSA Rouen

Reliability and optimization, application to safety of the aircraft structures

Présentée et soutenue par
Liu CHU

Thèse soutenue publiquement le 24 Mars 2016 devant le jury composé de		
M. P.BREITKOPF	Directeur de recherche CNRS	Rapporteur
M. X.L. GONG	Professeur à l'U.T de Troyes	Rapporteur
M. A. CHEROUAT	Professeur à l'U.T de Troyes	Examinateur
M. M. EID	PhD Ingénieur-Chercheur, au CEA, Paris	Encadrant
M. A. EL HAMI	Professeur à l'INSA de Rouen	Directeur de thèse
M. E. SOUZA	Professeur à l'INSA de Rouen	Directeur de thèse

Thèse dirigée par José Eduardo SOUZA DE CURSI, Addelkhalak EL HAMI , laboratoire LOFIMS

INSA INSTITUT NATIONAL DES SCIENCES APPLIQUÉES ROUEN

SPMI ECOLE DOCTORALE

LOFIMS

Acknowledgement

In three years of Ph.D study, many people give me help and support in the research work. Firstly, I would like to express my sincere gratitude to my supervisor Prof. Eduardo Souza de Cursi, his guidance always keeps me in the right way of study, constructive ideas from him in the process of discussion inspire me a lot and are also very helpful in the work. His deep mathematical foundation and extraordinary experiences in research teach me how to be an excellent researcher.

Secondly, Prof. El Hami, as co-director of my thesis, also provides lots of significant help. His passion in professional research encourages me to have progress in the difficult questions. In addition, I also want to appreciate M.M.Eid for his time and patience in the discussion.

Thirdly, thanks to my colleagues in the laboratory of LOFIMS (Laboratoire d'Optimisation et FIabilité en Mécanique des Structures) for their kindness and accompany in every day. The time spent with them is a cherish memory for myself no matter where I will stay or who I will work with in the future.

At last, I appreciate the organization of China Scholarship Council, the scholarship from my country covers the expense of three years. My family always stand by my side, it makes me have the courage to face and come over the difficulty. Even though they never require my appreciation or feedback, I want to present my best sincerely acknowledgement to my family.

Abstract

Tremendous struggles of researchers in the field of aerodynamic design and aircraft production were made to improve wing airfoil by optimization techniques. The development of computational fluid dynamic (CFD) in computer simulation cuts the expense of aerodynamic experiment while provides convincing results to simulate complicated situation of aircraft. In our work, we chose a special and important part of aircraft, namely, the structure of wing.

Reliability based optimization is one of the most appropriate methods for structural design under uncertainties. It struggles to seek for the best compromise between cost and safety while considering system uncertainties by incorporating reliability measures within the optimization. Despite the advantages of reliability based optimization, its application to practical engineering problem is still quite challenging.

In our work, uncertainty analysis in numerical simulation is introduced and expressed by probability theory. Monte Carlo simulation as an effective method to propagate the uncertainties in the finite element model of structure is applied to simulate the complicate situations that may occur. To improve efficiency of Monte Carlo simulation in sampling process, Latin Hypercube sampling is performed. However, the huge database of sampling is difficult to provide explicit evaluation of reliability. Polynomial chaos expansion is presented and discussed. Kriging model as a surrogate model play an important role in the reliability analysis.

Traditional methods of optimization have disadvantages in unacceptable time-complexity or natural drawbacks of premature convergence because of finding the nearest local optima of low quality. Simulated Annealing is a local search-based heuristic, Genetic Algorithm draws inspiration from the principles and mechanisms of natural selection, that makes us capable of escaping from being trapped into a local optimum. In reliability based design optimization, these two methods were performed as the procedure of optimization. The loop of reliability analysis is running in surrogate model.

Key words: optimization, reliability, uncertainty analysis, heuristic method, Kriging model

Résumé

Les chercheurs dans le domaine de la conception aérodynamique et de la fabrication des avions ont fait beaucoup d'effort pour améliorer les performances des ailes par des techniques d'optimisation. Le développement de la mécanique des fluides numérique a permi de réduire les dépenses en soufflerie tout en fournissant des résultats convaincants pour simuler des situations compliquées des aéronefs. Dans cette thèse, il a été choisi une partie spéciale et importante de l'avion, à savoir, la structure de l'aile.

L'optimisation basée sur la fiabilité est une méthode plus appropriées pour les structures sous incertitudes. Il se bat pour obtenir le meilleur compromis entre le coût et la sécurité tout en tenant compte des incertitudes du système en intégrant des mesures de fiabilité au sein de l'optimisation. Malgré les avantages de l'optimisation de la fiabilité en fonction, son application à un problème d'ingénierie pratique est encore assez difficile.

Dans notre travail, l'analyse de l'incertitude dans la simulation numérique est introduite et exprimée par la théorie des probabilités. La simulation de Monte Carlo comme une méthode efficace pour propager les incertitudes dans le modèle d'éléments finis de la structure est ici appliquée pour simuler les situations compliquées qui peuvent se produire. Pour améliorer l'efficacité de la simulation Monte Carlo dans le processus d'échantillonnage, la méthode de l'Hypercube Latin est effectuée. Cependant, l'énorme base de données de l'échantillonnage rend difficile le fait de fournir une évaluation explicite de la fiabilité. L'expansion polynôme du chaos est présentée et discutée. Le modèle de Kriging comme un modèle de substitution jouet un rôle important dans l'analyse de la fiabilité.

Les méthodes traditionnelles d'optimisation ont des inconvénients à cause du temps de calcul trop long ou de tomber dans un minimum local causant une convergence prématurée. Le recuit simulé est une méthode heuristique basée sur une recherche locale, les Algorithmes Génétiques puisent leur inspiration dans les principes et les mécanismes de la sélection naturelle, qui nous rendent capables d'échapper aux pièges des optimums locaux. Dans l'optimisation de la conception de base de la fiabilité, ces deux méthodes ont été mise en place comme procédure d'optimisation. La boucle de l'analyse de fiabilité est testée sur le modèle de substitution.

Mots – clés : optimisation, fiabilité, analyse de l'incertitude, méthode heuristique, modèle de Kriging

Table of Contents

Acknowledgement ..... **I**

Abstract ..... **II**

Résumé ..... **III**

Chapter 1 Introduction **1**

1.1 Introduction of background 1

1.2 Outline of the dissetation 2

Chapter 2 Uncertainty analysis **5**

2.1 Uncertainty classification 5

2.2 Sources of uncertainty 8

2.3 Uncertainty representation and modeling 9

2.3.1 Probability theory 9

2.3.2 Evidence theory 11

2.3.3 Possibility theory 12

2.3.4 Interval analysis 13

2.3.5 Convex modeling 13

2.4 Model validation 13

2.4.1 Pearson correlation coefficient 15

2.4.2 Spearman correlation coefficient 15

2.4.3 Kendall correlation coefficient 17

2.5 Sensitivity analysis 19

2.6 Uncertainty propagation 21

2.6.1 Monte Carlo simulation 21

2.6.2 Taylor series approximation 23

2.6.3 Reliability analysis 24

2.6.4 Decomposition based uncertainty analysis 24

2.7 Conclusion 25

Chapter 3 Monte Carlo Simulation **27**

3.1 Mathematical formulation of Monte Carlo Integration 27

3.1.1 Plain (crude) Monte Carlo Algorithm 28

3.1.2 Geometric Monte Carlo Algorithm 29

3.2 Advanced Monte Carlo Methods 30

3.2.1 Importance Sampling Algorithm 31

3.2.2 Weight Functions Approach 33
3.2.3 Latin Hypercube Sampling approach 33
3.3 Random Interpolation Quadratures 34
3.4. Iterative Monte Carlo Methods for Linear Equations 36
3.4.1 Iterative Monte Carlo Algorithms 37
3.4.2 Convergence and mapping 40
3.5 Morkov Chain Monte Carlo methods for Eigen-value Problem 40
3.5.1 Formulation of Eigen-value problem 41
3.5.2 Method for Choosing the Number of Iterations k 44
3.5.3 Method for choosing the number of chains 45
3.6 Examples 46
3.6.1 Importance sampling 46
3.6.2 Latin Hypercube sampling in Finite element model of structure 50
3.7 Conclusion 56
Chapter 4 Stochastic Expansion for Probability analysis 57
4.1 Fundamental of PCE 57
4.2 Stochastic approximation 58
4.3 Hermite Polynomials and Gram-Charlier Series 60
4.4 Karhunen-Loeve (KL) Transform 63
4.5 KL Expansion to solve Eigen value problem 65
4.6 Spectral Stochastic Finite Element Method 67
4.6.1 Role of KL expansion in SSFEM 67
4.6.2 Role of PCE in SSFEM 69
4.7 Examples 71
4.7.1 Orthogonal polynomial 71
4.7.2 Gram-Charlier series 74
4.7.3 Surrogate model for reliability analysis 75
4.8 Conclusion 87
Chapter 5 Reliability based design optimization 89
5.1 General remarks of RBDO 90
5.1.1 Single Objective Optimization Description 91
5.1.2 Multiple-Objective Optimization description 93
5.2 First –order reliability method 95
5.2.1 First – order second moment method 96

5.2.2 Hasofer and lind safety-index 98
5.2.3 Hasofer Lind- Rackwitz Fiessler (HL-RF) Method 103
5.2.4 FORM with adaptive approximations 105
5.3 Second-order Reliability Method (SORM) 106
5.3.1 First- and Second-order Approximation of Limit-state Function 107
5.3.2 Breitung's Formulation 111
5.3.3 Tvedt's Formulation 112
5.3.4 SORM with adaptive approximations 113
5.4 Mathematical Formulation of RBDO 113
5.4.1 RIA based RBDO 115
5.4.2 PMA based RBDO 115
5.5 Robust design optimization 116
5.6 Reliability based optimization in surrogate model 117
5.7 Conclusion 129
Chapter 6 Examples 130
6.1 Cumulative Damage Analysis of Wing Structure by Stochastic Simulation 130
6.1.1 Stochastic simulation in Finite Element Model 130
6.1.2 Fatigue Analysis 134
6.1.3 Probability density 136
6.1.4 Conclusion 140
6.2 Airfoil shape optimization by heurist algorithms in surrogated model 141
6.2 .1 Airfoil CFD model 141
6.2.2 Surrogate model 143
6.2.3 Optimization 150
6.2.4 Conclusion 156
Chapter 7 Conclusion 157
Chapter 8 Résumé de la thèse en français 159
8.1 Motivation et objectif 159
8.2 Organisation du mémoire 160
8.2.1 Chapitre 2: Analyse de l'incertitude 161
8.2.2 Chapitre 3: simulation de Monte Carlo 162
8.2.3 Chapitre 4: Expansion stochastique pour l'analyse de probabilité 168
8.2.4 Chapitre 5: Fiabilité et optimisation 176
8.2.5 Chapitre 6: Exemples 183

8.3 Conclusion..... 199
List of figures..... 201
List of tables 203
Reference 204

Chapter 1 Introduction

1.1 Introduction of background

As result of impressive advances in computational capability of hardware and software in recent decades, computational methods are gradually replacing empirical methods[1]. In the process of design and analyze aircraft components, more time and energy are spent in applying computational tools instead of conducting physical experiments[2].

For wing design, the requirement of new tools capable of accurate predicting aerodynamic behavior is performed. Numerical simulation of computational fluid dynamics can be applied for early detection of unwanted effects regarding stability and control behavior[3]. In the same time, uncertainty is an inevitable issue in the field of research. Since aircrafts have complicated operation environment and sophisticated mechanical structural itself.

The uncertainties in the aircraft can cause system performance to change or fluctuate, or even contribute to severe deviation and result in unprecedented function fault and mission failure. The consideration of uncertainty in the stage of design process is necessary[4]. According to specific characteristics of uncertainty, it should be represented in the research and design process by reasonable approaches.

The traditional analysis of deterministic Finite Element Model ignores the fluctuation of parameters as uncertain variables in the real operation environment. Application of Monte Carlo Method to probabilistic structural analysis problems is comparatively recent[5]. It is a powerful mathematical tool for determining the approximate probability of a specific event that is the outcome of a series of stochastic processes.

Monte Carlo methods are useful and reliable only when a huge amount of sampling was performed[6]. It means heavy calculation burden of repeating sampling and time-consuming process to deal with result databases for grasping the key information. In the one hand, the struggles for reducing calculation expense in Monte Carlo Simulation are considerable. Among them, Latin Hypercube Sampling is one of advanced methods due to its advantage of having memory and effectiveness in the repeating sampling simulation[7]. In the other hand, sensitivity analysis is a way to

predict the importance level of one variable to the final outcome. By creating a given set of scenarios, the analyst can determine how changes in one variable will impact the target variable.

After perform Monte Carlo simulation in finite element models of aircraft structure, the huge database for the following reseach is also a big challenge to resarchers. Stochastic expansion for probability analysis is a promising method to provide believeable evalution in the next reliability analysis in our work. It also plays an important role in reducing the heavy calculation burden of reliability based design optimization.

1.2 Outline of the dissetation

In chapter 2, methods of uncertainty analysis are presented. Firstly, the uncertainty classification and sources of uncertainty in the simulated-design are discussed.Then we demonstrated uncertainty representation and modeling as concluded in the literatures. After that, model validation and sensitivity analysis are also taken into consideration. In the last part of this chapter, mentods of uncertatiny propagation are showed and discussed.

Chapter 3 begins with the introduction of mathematical formulation of Monte Carlo Integration. Next, we present advanced Monte Carlo methods, as importance sampling and Latin Hypercube sampling. Then, random interpolation quadratures, iterative Monte Carlo methods for linear equations and Morkow Chain Monte Carlo methods for Eigen-value problem are also demonstated in this chapter. Lastly, we have a numerical example of importance sampling method. Monte Carlo simulation in fininte element model of wing structure in chapter 3 is performed as original work.

In Chapter 4, stochastic expansion for probability analysis is discussed. The fundamental theory of polynomial chaos expansion is presented in the first part of this chapter. Next, Hermite pomynomial and Gram – Charlier series are expressed. Then Karhunen – Loeve transform as a very useful method in simulation is also presented. In this chapter, we also explain the spectral stochastic finite element method, role of Karhunen – Loeve expansion and role of polynomial chaos expansion in spectral stochastic finite element method are demonstrated. Based on these theories, we also have serveral examples of stochastic expansion for probability analysis.

Chapter 5 presents reliability based design optimization. At first, general remarks of RBDO is illustrated. Then, first order and second order reliability method are explained. Next, we demonstrate mathematical formulation of RBDO. Robust design optimization is also introduced in this chapter. In the last part, examples of numerical simulation are presented.

In Chapter 6, two complet examples are demonstrated. The first example is cumulatice damage analysis of wing structure by stochastic simulation. As one of the most essential components in the aircraft structure, wing often operates in very complicated environment. It causes difficulties in identifying the exact values for the parameters in the models to simulate the real situation. In this example, a deterministic finite element model is created, the corresponding parameters in the model are sampled by Monte Carlo Method in numerous times. The process of stochastic simulation provides a useful database for the following cumulative damage analysis. Gaussian, Rayleigh, and Weibull distribution are proposed and used to express the probability density function for maximum stress in the wing structure. The last expression of probability distribution for maximum stress in the wing structure is polynomial function. In this method, sensitivity analysis was performed to find the most important several input variables. The relationship between the input variables and output variables in the database of stochastic simulation is obtained by linear regression method in the form of polynomial function. All of these four expressions were applied and discussed in cumulative damage analysis for wing structure.

The second example is airfoil shape optimization by heurist algorithms in surrogated model. Many struggles of researchers and designers in the field of aerodynamic design and aircraft production were made to improve wing airfoil by optimization techniques. Despite the development of computational fluid dynamic (CFD) in computer simulation, airfoil shape optimization is still quite challenging. In this example, we propose an effective method to have airfoil shape optimization by heuristic algorithms in surrogate model. To create an appropriate surrogate model, Monte Carlo simulation was performed by repeating computational fluid dynamic calculation, and reliable information was captured from this black box and concluded as Kriging interpolators. In order to prevent the premature convergence in the process optimization, attempts in heuristic algorithms for optimization were made.

The results of genetic algorithm and simulated annealing algorithm were tested in CFD to confirm the reliability of the method proposed in this paper.

Chapter 7 presents a summary of this dissertation, conclusions concerning the results and recommentations for future work.

Chapter 2 Uncertainty analysis

In the process of structural design, uncertainties include prediction errors induced by design model assumption and simplification; performance uncertainty arising from material properties, manufacturing tolerance; and uncertainty of load conditions applied on the structure during operation [2]. These uncertainties can cause system performance to change or fluctuate, or even contribute to severe deviation and result in unanticipated or even unprecedented function fault and mission failure.

Uncertainty analysis is the premise of uncertainty-based design optimization. It includes adopting suitable taxonomy to comprehensively identify and classify uncertainty sources; utilizing appropriate mathematical tools to represent and model these uncertainties; and applying sensitivity analysis approaches to screen out uncertainties with minor effects on design so as to simplify the problems.

2.1 Uncertainty classification

In different research fields, there are different definitions and taxonomies for the term of uncertainty. In computational modeling and simulation process, uncertainty is regarded as a potential deficiency in phases or activities of the modeling process caused by lack of knowledge[2] .

In some literatures, uncertainty is defined as the incompleteness in knowledge, and causes model-based predictions to differ from reality in a manner described by some distribution function[8] . In another useful functional definition it is defined as the information/knowledge gap between what is known and what needs to be known for optimal decisions with minimal risks[9].

From the perspective of systems engineering and taking the whole lifecycle into account during the design phase, the definition of uncertainty is as follows:

- Uncertainty: the incompleteness in knowledge and the inherent variability of the system and its environment.
- A robust system is defined to be relatively insensitive to variations in both the system components and the environment. The degree of tolerance to these variations is measured with robustness [4].
- Reliability is defined as the likelihood that an item will perform its intended

function without failure for a specified period of time under stated operating conditions[10].

To address uncertainty classification, the most popular uncertainty taxonomy is in risk assessment, which classifies uncertainty into two general categories: aleatory and epistemic.

- Aleatory uncertainty describes the inherent variation associated with the physical system or the environment under consideration. Sources of aleatory uncertainty can commonly be singled out from other contributors to nondeterministic simulation. Because their representation as distributed quantities can take on values in an established or known range, but the exact value will vary by chance from unit to unit or from time to time[11]. Aleatory uncertainty is also referred to in the literature as stochastic uncertainty, variability, inherent uncertainty, and cannot be eliminated by collection of more information or data.

- Epistemic uncertainty is due to lack of knowledge, and exists as a potential inaccuracy in any phase or activity of the modeling process. The first feature that our definition stresses is “potential”, in other words, the deficiency may or may not exist. It is possible that there is no deficiency even though lack of knowledge when model the phenomena correctly. The second key feature is that its fundamental cause is incomplete information due to vagueness, non-specificity, or dissonance. Epistemic uncertainty is known as subjective or cognitive, also referred to as reducible uncertainty and ignorance [6].

This taxonomy is widely accepted and has been applied in numerous fields. The conclusion of the difference between aleatoty uncertainty and epistemic uncertainty is clearly showed in Fig 2-1.

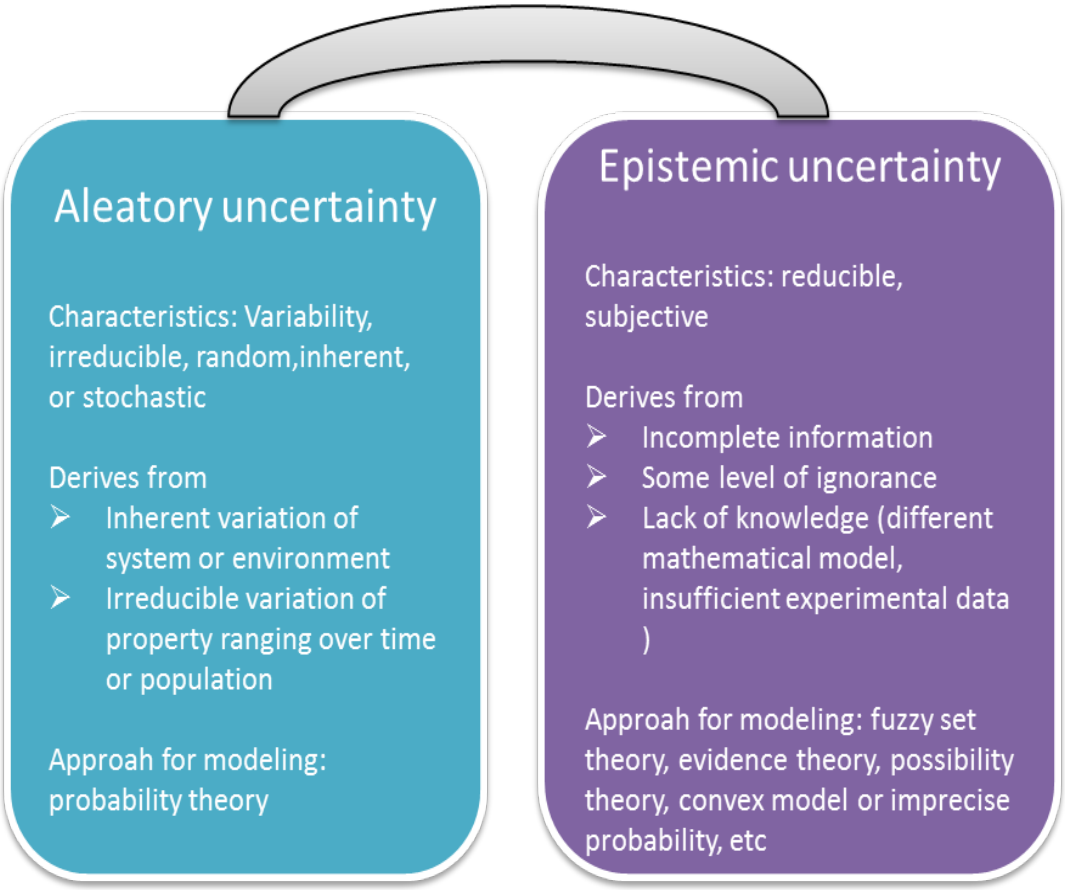

Fig 2 - 1 Comparison between aleatory uncertainty and epistemic uncertainty

Besides aleatory and epistemic uncertainty, errors exist as a recognizable deficiency in phases of modeling and simulation. An error can be either acknowledged or unacknowledged.

Acknowledged errors[12] are deficiencies recognized or introduced by the analysts. Examples of acknowledged errors are finite precision arithmetic in a digital computer, approximations made to simplify the modeling of a physical process, and conversion of partial differential equations into discrete equations, or lack of spatial convergence. Acknowledged errors can be estimated, bounded, or ordered.

Examples of unacknowledged errors are blunders or mistakes. They can be programming errors, input or output errors, and compilation and linkage errors. There are no straightforward methods for estimating, bounding, or ordering the contribution of unacknowledged errors.

2.2 Sources of uncertainty

In the process of simulation-based design, uncertainties origins from four sources: input, operational environment, model uncertainties, and measurement; as showed in Fig 2-2 ,

- Input uncertainties are caused by imprecise or even ambiguous requirements and problems description.
- Uncertainties in operational environment are due to unknown or uncontrollable external disturbances.
- Model uncertainties include model structure uncertainty and model parameter uncertainty. Model structure uncertainty, also mentioned as non-parametric uncertainty, is mainly due to assumptions underlying the model which may not capture the physics characteristics correctly. While model parameter uncertainty is mainly due to limited information in estimating the model parameters for a given fixed model form.
- For uncertainties exist in measurement, they arise when the response of interest is not directly computable from the math model.

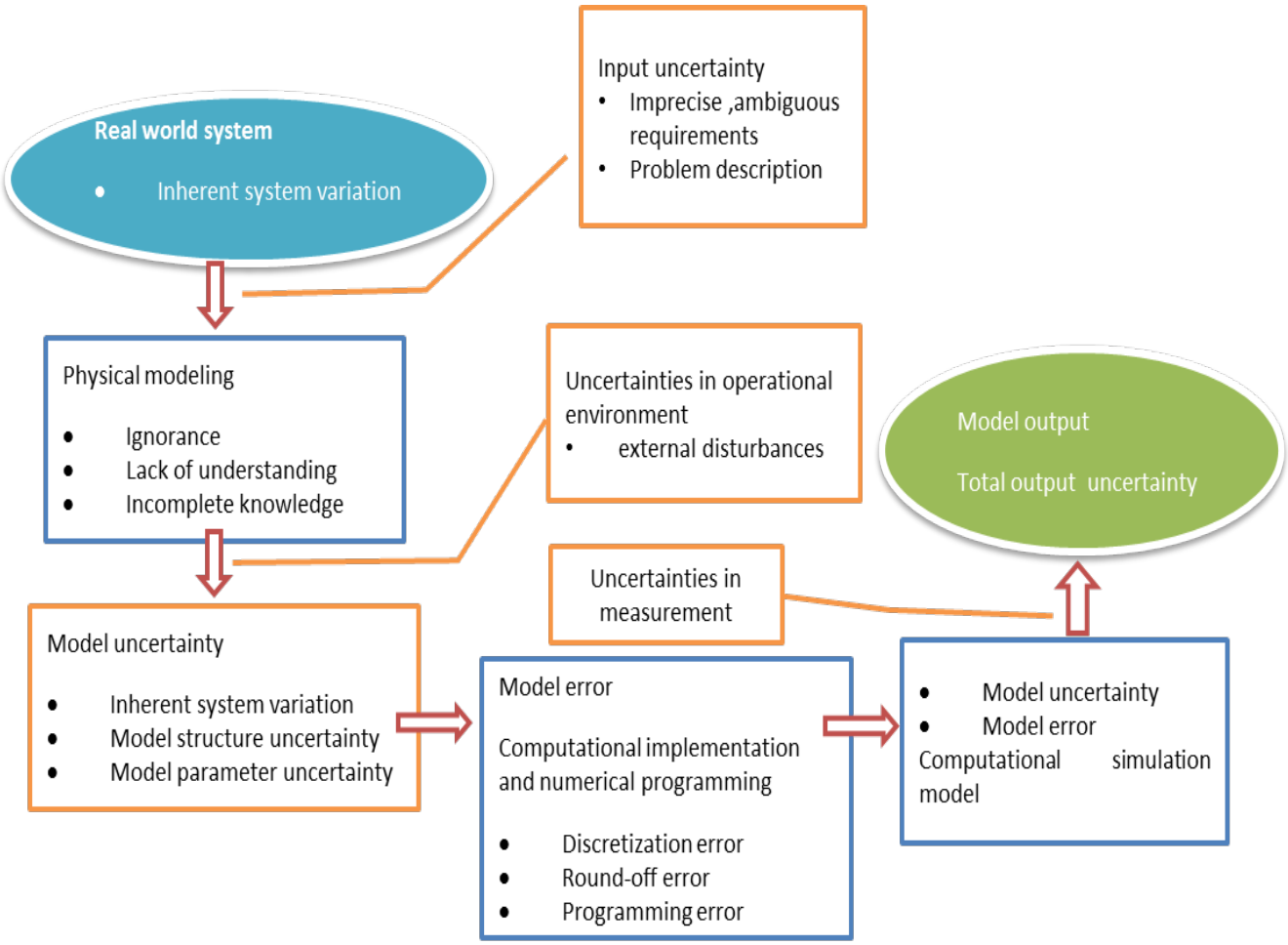

Fig 2 - 2 Uncertainty sources in the simulation-based design

2.3 Uncertainty representation and modeling

According to its specific characteristics, uncertainty should be represented in the research and design process by reasonable approaches. In different context, model input and model parameter uncertainties have different features. The most popular methods in research includes: probability theory, evidence theory, possibility theory, interval analysis, and convex modeling[13].

2.3.1 Probability theory

Probability theory is a more prevalent or better known theory to engineers. Its relative advantages are due to sound theoretical foundation, deep root in the research of non-deterministic design.

In probability theory, uncertainty is represented as random variable or stochastic process. Let X denote the quantity of interest whose probability density function (PDF)

is given by fX(x/p), and cumulative distribution function (CDF), where p refers to the distribution parameters of the random variable X (continuous random variable), and x is a realization of X. For discrete random variable, a sample space is firstly defined which relates to the set of all possible outcomes, each element of the sample space is assigned a probability value between 0 and 1, and the sum of all the elements in the sample space to the “probability” value is called probability mass function (PMF).

In the context of a probabilistic approach, two difficulties are encountered. The first is the choice of the distribution type (normal, lognormal, etc.). The choice of distribution type is known from previous experiences, priori knowledge, or expert opinion, those are quite subjective. The second difficulty is lack of adequate data to estimate the distribution parameters with a high degree of confidence[14].

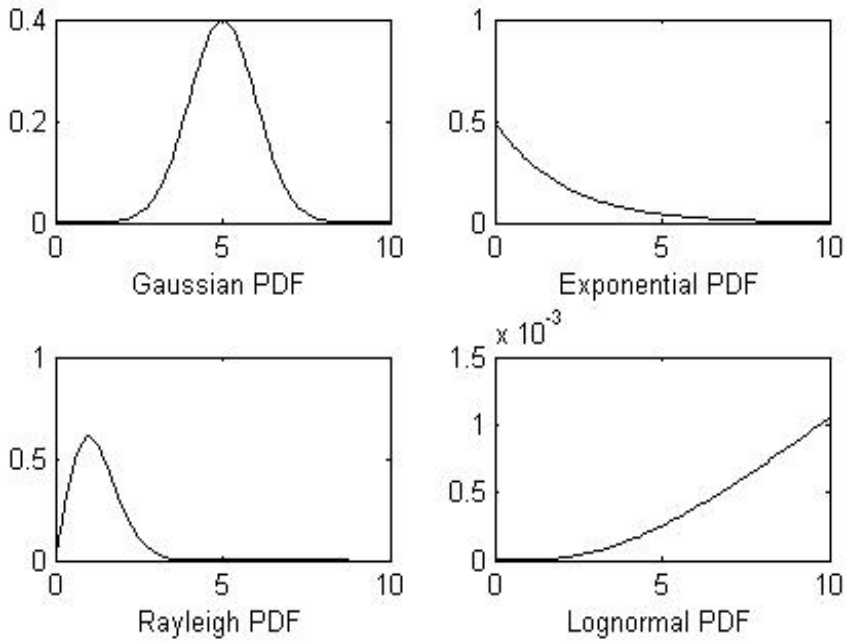

Fig 2 - 3 Examples of probability density function

Classical statistics-based frequentist methodology addresses the uncertainty in the distribution parameters by estimating statistical confidence intervals, which cannot be used further in uncertainty propagation, reliability analysis, etc. In contrast, Bayesian probability interprets the concept of probability as a measure of a state of belief or knowledge of the quantity of interest, not as a frequency or a physical property of a system. It specifies some prior probability subjectively[15] , and then updates in the light of new evidence or observations by means of statistical inference approach. In

this way it can combine pre-existing knowledge with subsequent available information and update the prior knowledge with uncertainties. With the capability of dealing with both aleotory and epistemic uncertainties, the Bayesian theory has been widely applied, especially in reliability engineering.

2.3.2 Evidence theory

Evidence theory (Dempster-Shafer theory, D-S theory) measures uncertainty with belief and plausibility determined from known information. For a proposition, lower and upper bounds of probability with consistent evidence are defined instead of assigning a precise probability[16]. The information or evidence to measure belief and plausibility comes from a wide range of sources (e.g., experimental data, theoretical evidence, experts' opinion concerning belief in value of a parameter or occurrence of an event, etc.). Meanwhile, the evidence can be combined with combination rules[17] .

Evidence theory begins with defining a frame of discernment X, which includes a set of mutually exclusive "elementary" propositions. The elements of the power set 2X can be taken to represent propositions concerning the actual state of the system. Evidence theory assigns a belief mass to each element of the power set by a basic belief assignment function m: $2X \rightarrow [0,1]$ which has the following two properties: the mass of the empty set is zero, and the mass of all the member elements of the power set adds up to a total of 1.

The mass m(A) express the proportion of all relevant and available evidence that supports the claim that the actual state belongs to A. The value of m(A) pertains only to A and makes no additional claims about any subsets of A, each of which has its own mass. From the mass assignments, a probability interval can be defined which contains the precise probability, and the lower and upper bound measures are belief (Bel) and plausibility (Pl) as $Bel(A) \leq P(A) \leq Pl(A)$.

The belief Bel(A) is defined as the sum of mass of all the subsets of A, which represents the amount of all the evidence supporting that the actual state belongs to A, and the plausibility Pl(A) is the sum of mass of all the sets that intersect with A, which represents the amount of all the evidence that does not rule out that the actual state belongs to A:

$$\mathbf{Bel}(\mathbf{A}) = \sum_{\boldsymbol{B}/\boldsymbol{B}\in\boldsymbol{A}} \boldsymbol{m}(\boldsymbol{B}) \quad (2 - 1)$$

$$\mathbf{Pl}(\mathbf{A}) = \sum_{\boldsymbol{B}/\boldsymbol{B}\cap\boldsymbol{A}\neq\emptyset} \boldsymbol{m}(\boldsymbol{B}) \quad (2 - 2)$$

The two measures are related to each other as

$$\mathbf{Pl}(\mathbf{A}) = \mathbf{1} - \mathbf{Bel}(\bar{\boldsymbol{A}}) \qquad \mathbf{Bel}(\mathbf{A}) + \mathbf{Bel}(\bar{\boldsymbol{A}}) \leq \mathbf{1} \quad \mathbf{Pl}(\mathbf{A}) + \mathbf{Pl}(\bar{\boldsymbol{A}}) \geq \mathbf{1} \quad (2 - 3)$$

Where $\bar{A}$ is the complement of A.

The evidence space is characterized with cumulative belief function (CBF) and cumulative plausibility function (CPF).

Evidence theory can deal with the problems both of aleatory and epistemic uncertainties flexibly with its evidence combination rules to update probability measures[18]. It is actually close related to probability theory. When the amount of available information increases, an uncertainty representation with evidence theory can approach that with probability theory [19],[20]. However, it also has limitations when handle highly inconsistent data sources, which may render the evidence combination rule unreliable. Anyway, it has been widely utilized and attracted great research interest in the fields of uncertainty-based information, risk assessment, decision making, and design optimization [21],[22].

2.3.3 Possibility theory

Possibility theory is introduced as an extension of the theory of fuzzy set and fuzzy logic, which can be used to model uncertainties when there is imprecise information or sparse data. The term fuzzy set is in contrast with the conventional set (fixed boundaries).

In possibility theory, uncertain parameters are not treated as random variables but as possibilistic variables, the membership function is extended to possibility distribution. It expresses the degree of an event can occur by analyst as subjective knowledge.

Like evidence theory, possibility theory can deal with both the aletory and epistemic uncertainties[23] . Compared to probability theory, possibility theory can be more conservative in terms of a confidence level. Because the knowledge of the analyst can be easily introduced to the design process and make problems more tractable[24] . The application of fuzzy set and possibility theory is feasible in

engineering design optimization and decision making. Fractile approach, modality optimization approach and spread minimization approach also be developed to solve possibilistic programming problems[25] . Possibility theory can also be applied along with probability theory, the integrated or unified algorithms are necessary to research and exploded[26], [27], [28], [29], [30] .

2.3.4 Interval analysis

Interval analysis is an approach to putting bounds on rounding errors and measurement errors in mathematical computation, and yield reliable results by developing numerical methods. In interval analysis the value of a variable is replaced by a pair of numbers representing the maximum and minimum values that the variable is expected to take. Interval arithmetic rules are applied to perform mathematical operations with the interval numbers, therefore the propagation of the interval bounds through the computational model is implemented, and the bounds on the output variables are achieved[31],[32],[33],[34].

2.3.5 Convex modeling

Convex modeling is a more general approach to represent uncertainties with convex sets[35]. The convex models include energy-bound model, interval model, ellipsoid model, envelope- bound model, slope- bound model, Fourier-bound model, etc.

It is unlikely that the uncertain components are independent with each other and the bounds on the components of the object are reached simultaneously. Therefore, it is more reasonable to apply the convex model with representation of correlations between uncertain components in realistic application. In addition, techniques in interval analysis can be used here, when the convex models are intervals[36],[37].

Besides the foregoing five theories, there are other alternative approaches to represent uncertainties, especially for epistemic uncertainty[38], such as cloud theory mediating between fuzzy set theory and probability distribution, fuzzy random theory and random fuzzy theory with characteristics of both fuzzy set theory and probability theory[39] ,[40].

2.4 Model validation

In uncertainty based design, uncertainty representation models also have model form uncertainties, especially probabilistic models whose distributions are assumed and

fitted based on past experience, expert opinions, experimental data, etc. Hence, it is also necessary to measure the uncertainty of the model to validate the feasibility of the uncertainty representation[41].

Model form uncertainty can be characterized through model accuracy assessment by comparison between simulation results and experimental measurements. This process is also called model validation. It can be determined when the mathematical model of a physical event is sufficiently reliable to represent the actual physical event in the real practice.

To discuss whether a specific distribution is suitable to a data-set, the goodness of fit criteria can be applied. It includes the Pearson test[42], the Kolmogorov-Smirnov test[43], the Anderson-Darling test[44], etc. When the data available to test the hypothesis about probabilistic models are too scarce to allow definite conclusions to choose or discard totally one model among others, Bayesian method can be applied. It has the capability of combining several competing probability distribution types together to describe a random variable. More generally, a complete Bayesian solution is proposed to average over all possible models which can provide better predictive performance than any single model accounting for model uncertainties.

When sampling from random vectors, it is important to control correlation or even dependence patterns between marginal. The bounds on the correlation errors can be useful for the selection of stopping criteria in algorithms employed for correlation control. In order to quantify an error in the correlation of a given sample, one must select a correlation estimator and define a scalar measure of the correlation matrix. Another goal of controlled statistical sampling is usually to perform the sampling with the smallest possible sample size, and yet achieve statistically significant estimates of the response.

The estimated correlation matrix is a symmetric matrix of the order N_{var} and can be written as the sum

$$A = I + L + L^T \tag{2 - 4}$$

Where I is the identity matrix and L is the strictly lower triangular matrix with entries with the range $\langle -1,1 \rangle$. There are N_c correlation that describe pairwise correlations:

$$N_c = \binom{N_{\text{var}}}{2} = \frac{N_{\text{var}}(N_{\text{var}}-1)}{2} \tag{2 - 5}$$

2.4.1 Pearson correlation coefficient

The most well-known correlation measure is the linear Pearson correlation coefficient (PCC)[45]. The PCC takes values from between -1 and +1, inclusive, and provides a measure of the strength of the linear relationship between two variables. The actual PCC between two variables, say X_i and X_j, is estimated using the sample correlation coefficient A_{ij} as

$$A_{ij} = \frac{\sum_{s=1}^{N_{sim}} (\mathrm{x}_{i,s} - \overline{\mathrm{X}}_i)(\mathrm{x}_{\mathrm{j},s} - \overline{\mathrm{X}}_j)}{\sqrt{\sum_{s=1}^{N_{sim}} (\mathrm{x}_{i,s} - \overline{\mathrm{X}}_i)^2 \sum_{s=1}^{N_{sim}} (\mathrm{x}_{\mathrm{j},s} - \overline{\mathrm{X}}_j)^2}} \tag{2 - 6}$$

$$\overline{\mathrm{X}}_i = \frac{1}{N_{sim}} \sum_{s=1}^{N_{sim}} \mathrm{x}_{i,s} \quad , \quad \overline{\mathrm{X}}_j = \frac{1}{N_{sim}} \sum_{s=1}^{N_{sim}} \mathrm{x}_{\mathrm{j},s} \tag{2 - 7}$$

When the actual data $\mathrm{x}_{\mathrm{i},s}$, $s = 1, 2, \cdots, N_{sim}$ of each vector $i = 1, 2, \cdots, N_{\text{var}}$ are standardized into $z_{\mathrm{i},s}$ into vectors that yield zero average and unit sample variance estimates, the formula simplifies to

$$A_{ij} = \frac{\sum r_{\mathrm{i},s} r_{\mathrm{j},s}}{\sqrt{\sum r_{i,s}^2 \sum r_{\mathrm{j},s}^2}} \tag{2 - 8}$$

$$A_{ij} = \frac{1}{N_{sim}} \sum_{s=1}^{N_{sim}} z_{\mathrm{i},s} z_{\mathrm{j},s} \tag{2 - 9}$$

Which is the dot product of two vectors divided by the sample size.

2.4.2 Spearman correlation coefficient

The formula for Spearman correlation coefficient[46] estimation is identical to the one for Pearson linear correlation with the exception that the values of random variables X_i and X_j are replaced with the ranks $\pi_{i,s}$ and $\pi_{\mathrm{j},s}$, $s = 1, 2, \cdots, N_{sim}$. The ranks are

permutation of numbers. It is convenient to transform the ranks into $r_{i,s} = \pi_{s,i} - \bar{\pi}_i$ and $r_{j,s} = \pi_{s,j} - \bar{\pi}_j$.

$$\bar{\pi}_i = \bar{\pi}_j = \bar{\pi} = \frac{1}{N_{sim}} \sum_{s=1}^{N_{sim}} s = \frac{N_{sim}+1}{2} \tag{2 - 10}$$

The rank correlation is then defined as,

$$A_{ij} = \frac{\sum r_{i,s} r_{j,s}}{\sqrt{\sum r_{i,s}^2 \sum r_{j,s}^2}} \tag{2 - 11}$$

By noting that the sum of the first N_{sim} squared integers is $\frac{N_{sim}(N_{sim}+1)(2N_{sim}+1)}{6}$, we find that $\sum r_{i,s}^2 = \sum r_{j,s}^2 = \frac{N_{sim}^3 - N_{sim}}{12}$, and the rank correlation reads:

$$A_{ij} = \frac{12\sum r_{i,s} r_{j,s}}{N_{sim}(N_{sim}^2 - 1)} = \frac{12\sum \pi_{i,s} \pi_{j,s}}{N_{sim}^3 - N_{sim}} - 3\frac{N_{sim}+1}{N_{sim}-1} \tag{2 - 12}$$

In the case of ties, the averaged ranks are used. Note that when LHS is applied to continuous parametric distributions no ties can occur in the generated data. Therefore, we do not consider ties from here on. Another formula exists for Spearman correlation suitable for data with no ties. The correlation coefficient between any two vectors each consisting of permutations of integer ranks from 1 to N_{sim} is

$$A_{ij} = 1 - \frac{6D}{N_{sim}(N_{sim}^2 - 1)} \tag{2 - 13}$$

Where D is the sum of values d_s, the differences between the s^{th} integer elements in the vectors:

$$D = \sum_{s=1}^{N_{sim}} d_s^2 \tag{2 - 14}$$

Every mutual permutation of ranks can be achieved by permuting the ranks π_s of the second variable against the identity permutation corresponding to the ranks of the first variable. Therefore, we may write

$$D = \sum_{s=1}^{N_{sim}} (\mathrm{s} - \pi_s)^2 = 2\left[\sum_{s=1}^{N_{sim}} \mathrm{s}^2 - \sum_{s=1}^{N_{sim}} (\mathrm{s}\,\pi_s)\right] \qquad (2 - 15)$$

This is equal to

$$\frac{N_{sim}(N_{sim}+1)(2N_{sim}+1)}{3} - 2\sum_{s=1}^{N_{sim}} (\mathrm{s}\,\pi_s) \qquad (2 - 16)$$

Spearman correlation can, in general, take any value between -1 and 1, inclusive, depending on the value of the sum $\sum d_s^2$. The lowest correlation is achieved for the reverse ordering of rank numbers and corresponds to the case when the sum D equal $\frac{N_{sim}(N_{sim}^2 - 1)}{3}$. Conversely, the maximum correlation is achieved for identical ranks and the sum equals zero.

2.4.3 Kendall correlation coefficient

Kendall's correlation[47] (nonparametric or distribution-free) coefficient estimates the difference between the probability of concordance and discordance between two variables, x_i and x_j. For data without ties, the estimate is calculated based on the rankings π_i and π_j of N_{sim} samples of two vectors x_i and x_j. Let us index the ranks by $1 \le k, l \le N_{sim}$. The formula for sample correlation is a direct estimation of the difference between the probabilities:

$$A_{ij} = \frac{n_c - n_d}{\binom{N_{sim}}{2}} = \frac{\sum_{k<l}^{N_{sim}} \mathrm{sgn}\left[(\pi_{i,k} - \pi_{i,\mathrm{l}})(\pi_{\mathrm{j},k} - \pi_{\mathrm{j},\mathrm{l}})\right]}{\binom{N_{sim}}{2}} \qquad (2 - 17)$$

Where $\mathrm{sgn}(\mathrm{z}) = -1$ for negative z, +1 for positive z, and zero for z =0.

The numerator counts the difference between concordant pairs n_c and discordant pairs n_d. The denominator is the maximum number of pairs with the same order, the

total number of item pairs with respect to which the ranking can be compared. The number of concordant pairs n_c is the number of item pairs on the order of which both rankings agree. A pair $\left(\pi_{i,k}, \pi_{j,k}\right)$ and $\left(\pi_{i,\mathrm{l}}, \pi_{j,\mathrm{l}}\right)$ of points in the sample is concordant if either $\pi_{i,\mathrm{k}} < \pi_{i,\mathrm{l}}$ and $\pi_{\mathrm{j,k}} < \pi_{\mathrm{j,l}}$ or $\pi_{\mathrm{i,k}} > \pi_{\mathrm{i,l}}$ and $\pi_{\mathrm{j,k}} > \pi_{\mathrm{j,l}}$. Analogically, n_d is the number on which both ranking disagreed.

The number of concordant pairs can be calculated by adding scores: a score of one for every pair of objects that are ranked in the same order and a zero score for every pair that are ranked in different orders:

$$n_c = \sum_{k=1}^{N_{sim}-1} \sum_{l=k+1}^{N_{sim}} \left(\mathrm{l}_{(\pi_{i,k}-\pi_{i,\mathrm{l}})(\pi_{\mathrm{j,k}}-\pi_{\mathrm{j,l}})>0}\right) \qquad (2 - 18)$$

Where the indicator function l_A equals one if A is true, and zero otherwise. Analogically, n_d would count only for opposite orders and the formula would be identical but with opposite orientation of the inequality sign.

In the cases of tied rank, the denominator is usually adjusted. We do not consider ties. Therefore, A_{ij} can be rewritten by exploiting the fact that the number of pairs is the sum of concordant and discordant pairs and therefore the number of discordant pairs is $n_d = \binom{N_{sim}}{2} - n_c$. Then,

$$A_{ij} = \frac{4n_c}{N_{sim}(N_{sim}-1)} - 1 = 1 - \frac{4n_d}{N_{sim}(N_{sim}-1)} \qquad (2 - 19)$$

A straightforward implementation of the algorithm based on the above equations has $\vartheta(\mathrm{N}_{sim}^2)$ complexity. In practice, it is convenient to rearrange the two rank vectors so that the first one is in increasing order.

Kendall's correlation coefficient is intuitively simple to interpret. When compared to the Spearman coefficient, its algebraic structure is much simpler. Note that Spearman's coefficient involves concordance relationship among three sets of observation, which makes the interpretation somewhat more complex than that for

Kendall's coefficient. Regarding the relation between Spearman's correlation (ρ) and Kendall's correlation (τ)

$$\tau - (1-\tau^2) \le 3\tau - 2\rho \le \tau + (1-\tau^2) \qquad (2 - 20)$$

For many joint distribution, correlation coefficients of Spearman and Kendall have different values, as they measure different aspects of the dependence structure. It has long been known about the relationship between the two measurements that, for many distributions exhibiting weak dependence, the sample value of Spearman's is about 50% larger than the sample value of Kendall's.

2.5 Sensitivity analysis

Sensitivity analysis is the study of how the variation in the model output can be apportioned, qualitatively or quantitatively, to different sources of variations in the model input[48]. By means of this technique, uncertainty factors can be systematically studied to measure their effects on the system output, so as to filter out the uncertainty factors with negligible contributions and reduce complexity. With this specific aim, sensitivity analysis in this context is also termed uncertainty importance analysis.

There are numerous approaches to address sensitivity analysis under uncertainty, especially with probability theory. Probabilistic sensitivity analysis methods mainly include differential analysis, response surface methodology, variance decomposition, Fourier amplitude sensitivity test, sampling-based method[49], etc. Among these approaches, sampling-based method is widely applied for its flexibility and ease of implementation.

Once the sample is generated, evaluation of f created the following mapping from analysis inputs to analysis results

$$\left[x_i, \mathrm{y}_i\right],\ i = 1, 2, \cdots, nS$$

Where $y_i = f(x_i)$

Then

$$E(\mathrm{y}) = \sum_{i=1}^{nS} y_i w_i \tag{2 - 21}$$

$$V(\mathrm{y}) = \sum_{i=1}^{nS} \left[E(\mathrm{y}) - y_i \right]^2 w_i \tag{2 - 22}$$

The mapping in $\left[x_i , \mathrm{y}_i \right]$, $i = 1, 2, \cdots, nS$ can be explored with various techniques to determine the effects of the individual elements of x on y.

Differential analysis is based on the partial derivative of f with respect to the elements of x. In its simplest form, differential analysis involves approximating the model by the Taylor series

$$\mathrm{y}(\mathrm{x}) = \mathrm{f}(\mathrm{x}_0) + \sum_{j=1}^{nX} \left[\partial f(\mathrm{x}_0) / \partial x_j \right] \left[x_j - x_{j0} \right] \tag{2 - 23}$$

Where $\mathrm{x}_0 = \left[\mathrm{x}_{10} , \mathrm{x}_{20} , \cdots, \mathrm{x}_{nX,0} \right]$ is a vector of base-case values for the x_j.

One the approximation in the model of Taylor series is determined, variance propagation formulas can be used to determine the uncertainty in y that results from the distribution. In particular,

$$E(\mathrm{y}) = \mathrm{y}(\mathrm{x}_0) + \sum_{j=1}^{nX} \left[\partial f(\mathrm{x}_0) / \partial x_j \right] E\left[x_j - x_{j0} \right] \tag{2 - 24}$$

$$V(\mathrm{y}) = \sum_{j=1}^{nX} \left[\partial f(\mathrm{x}_0) / \partial x_j \right]^2 V(x_j) + 2 \sum_{j=1}^{nX} \sum_{k=j+1}^{nX} \left[\partial f(\mathrm{x}_0) / \partial x_j \right] \times \left[\partial f(\mathrm{x}_0) / \partial x_k \right] Cov(x_j , x_k) \tag{2 - 25}$$

Thus, the Taylor series leads to approximations of the expected value and variance for y that result from the distributions. Sensitivity analysis is based on the use of partial derivatives associated with a Taylor series to determine the effects of the individual elements. If the elements are independent, then the fractional contribution of x_j to the variance of y can be approximated by

$$V(y / x_j) = \left[\partial f(\mathrm{x}_0) / \partial x_j \right]^2 V(x_j) / V(y) \tag{2 - 26}$$

2.6 Uncertainty propagation

Uncertainty analysis is concerned with quantifying uncertainty characteristics of output in the system resulted from model input uncertainties and model uncertainties propagated through computational simulation. Generally uncertainty analysis approaches can be categorized into two types: intrusive and non-intrusive[50].

The intrusive type is mainly related to the physics-based approaches. It involves reformulation of governing equations and modification to the simulation codes so as to incorporate uncertainty directly into the system[51]. Typical example of this type is Polynomial Chaos expansion based approaches, which represent a stochastic process with expansion of orthogonal polynomials. The coefficient of the expansion can be defined by substituting the stochastic process with its polynomial chaos expansion in the original governing equations, which results in a coupled system of deterministic equations to be solved by editing the existing analysis codes.

In contrast to intrusive approaches, non-intrusive approaches treat computer simulation model as black-box and need no modification to existing deterministic simulation codes. So it can be developed for general use and take the advantage of being applicable to legacy codes. With this merit, the preceding Polynomial Chaos expansion based methods are also studied to be solved with non-intrusive approaches. Widely used non-intrusive approaches, include Monte Carlo simulation method, Taylor series approximation method, and some methods specific for reliability analysis[52]. Considering the computational difficulty in application of the conventional uncertainty analysis methods, decomposition based methods are introduced, which can treat uncertainty cross propagation among complex coupling disciplines more efficiently by decomposing the system uncertainty analysis problem into subsystem or disciplinary level.

2.6.1 Monte Carlo simulation

Monte Carlo simulation (MCS) methods (sampling-based methods) are a class of computational algorithms that perform repeated sampling and simulation. If sufficient samples are provided, MCS methods can provide statistical analysis results with arbitrary level of accuracy[53].

MCS is often used as a benchmark for evaluating the performance of new uncertainty analysis techniques. Lots of efforts have been devoted to develop approximation approaches to numerically evaluate this integral[54].

Gauss quadrature approaches and other numerical quadrature and cubature methods are proposed to approximate the multi-dimensional integral with weighted sum of the integrand values at a set of discrete integration points within the integration region. Laplace Approximation approach is proposed to approximate the integrand with second order Taylor series expansion at its minimum so as to derive the integral. Unfortunately, these approximate numerical integration approaches are generally only efficient and accurate for a special type of problem, quadrature based method for polynomial response, and may be not applicable especially for problems with high dimensional uncertainties and complex integrand which has no explicit formula and can only be calculated with time-consuming simulation analysis[55].

The difficulties with the traditional numerical integration approaches as motivation to the development of simulation based MCS integration methods, statistics of the system response by simply performing repeated sampling and simulation can be computed.

The disadvantage of MCS methods is computational prohibitive when simulation model is complex. For problems need iterations of several coupled disciplinary simulations to reach a consistent system response result, the situation becomes even worse[56]. To be more efficient than the random sampling method, several improved MCS methods with different sampling techniques have been developed and proved.

Among these sampling methods, importance sampling (weighted sampling)[57], is pervasively studied. It is expected to reduce error to zero if importance sampling probability density function is correctly selected. However, in realistic engineering problems, generally theoretical optimum importance sampling functions are not practical.

A compromise method is Latin hypercube sampling (LHS) approach[58]. This approach divides the range of each variable into disjoint intervals of equal probability, and one value is randomly selected from each interval. It improves MCS stability and also maintains the tractability of random sampling.

The first-order sensitivity method, as a variance reduction technique, is also utilized to accelerate MCS estimation convergence[59]. It is observed that this sensitivity enhanced method can improve accuracy by one order of magnitude compared to error. The variance reduction techniques are especially important when MCS is applied to estimate small failure probability.

2.6.2 Taylor series approximation

Taylor series approximation methods have been widely used for the relative ease of understanding and implementation[60]. This method can be employed to approximate statistical moments of system output based on partial derivatives of the output f with respect to the elements of the random input vector x. The original simulation model function y=f(x) can be approximated with the first order Taylor series as,

$$+\mathbf{y}(\mathbf{x}) \approx \mathbf{f}(\mathbf{x0}) + \sum_{\boldsymbol{k=0}}^{\boldsymbol{n}} \binom{\boldsymbol{n}}{\boldsymbol{k}} \boldsymbol{x^k a^{n-k}} \qquad (2 - 27)$$

Where x0 is the base point vector at which the derivatives are calculated. The output uncertainty resulting from the random input uncertainties can be determined with uncertainty propagation through this approximation formula.

Taylor series approximation methods have several disadvantages[61]:

(1) Its estimation accuracy is low when the coefficients of variation of the input random vector increase.
(2) The increase of Taylor series expansion order leads to rapidly increase of estimation complexity due to high-order terms and correlations between the elements.
(3) The determination of partial derivatives could be very difficult for complex system simulation models.

As Taylor series approximation methods only deal with the propagation of first two moments rather than the exact distribution of randomness, it belongs to first-order, second-moment methods which are related to the class of problems only concerning the means and variances and their propagation. This is a logical naming convention for the uncertainty propagation techniques with a given choice of the order of approximation and the statistical moment to be used [62]. Besides Taylor series

approximation methods, there are also several other first order, second-moment approaches such as point-estimate-for-probability-moment methods.

2.6.3 Reliability analysis

Reliability of the system is generally difficult to calculate analytical as both the joint probability distribution function p(x) and the failure domain D are seldom accurately defined in an explicit analytical form, and the multidimensional integration can be computationally prohibitive especially for the complex system with time consuming analysis models[63]. Hence, it is motivated to develop various approximation methods, including the preceding numerical integration methods, as well as other integration approximation methods specific for reliability analysis. Laplace multidimensional integral method based asymptotic approximation, main domain of failure coverage base integration, fast Fourier transform (FFT) based method, tail modeling approach, dimension-reduction (DR) methodology, First Order Reliability Method (FORM) and Second Order Reliability Method (SORM), etc[64]. Among these approximation methods, FORM and SORM are most prevailing and wide applied in engineering problems.

To further improve reliability analysis efficiency, response surface methodology (RSM) can be utilized to replace the computationally expensive accurate function so as to reduce calculation burden[65]. Interval analysis, possibility theory, evidence theory and convex uncertainty in reliability analysis are also studied. Besides the methods to determine exact reliability, there are also some approaches dealing with reliability bounds.

2.6.4 Decomposition based uncertainty analysis

For a complex system with close coupled disciplines, tremendous repeating multidisciplinary analysis (MDA), Monte Carlo methods, FORM/SORM make uncertainty analysis computationally prohibitive. As a solution to this problem, decomposition strategies are proposed to decompose the uncertainty analysis problem nested with MDA into several discipline or subsystem uncertainty analysis problems, so as to control each sub-problem within acceptable level and meanwhile take advantages of distributed parallel computing[66].

For MPP based uncertainty analysis, the search procedure of MPP is essentially a double loop algorithm, which includes a MPP search optimization in the outside loop

and a MDA iteration procedure in the inner loop. To improve the search efficiency of MPP, decomposition based approaches have been suggested[67]. In addition, employing concurrent subspace optimization (CSSO) procedure to solve the MPP search optimization problem, so called MPP-CSSO, also greatly improve efficiency with parallelization of disciplinary analysis and optimization [61].

Last but not the least, another solution to address the double loop problem is to decompose MDA from the MPP search and organize them sequentially as a recursive loop. In this sequential approach to reliability analysis for multidisciplinary systems (SARAM), concurrent subsystem analysis can be applied in the separate MDA to further alleviate computational burden [61].

For numerical simulation based reliability analysis, Gibbs sampling[68] is utilized to decompose MDA into disciplinary sub-problems and reduce the consistency of multidisciplinary system at each run. Without consistency constraint on MDA, only the number of disciplines times the disciplinary analysis computation are needed for each run of sample simulation, which can greatly reduce calculation cost compared to the traditional sampling method that needs iterations of disciplinary analysis to obtain a consistent system response at each sample.

2.7 Conclusion

In this chapter, we first discussed the uncertainty classification and sources of uncertainty in numerical simulation. Probability theory, evidence theory, possibility theory, interval analysis and also convex modeling are reminded as theory of uncertainty representation and modeling for uncertainty analysis. To take consideration of in uncertainty representation models it is also necessary to validate the feasibility of the uncertainty representation by Person correlation, Spearman correlation or Kendall correlation.

Sensitivity analysis, also termed uncertainty importance analysis, analyse the influence effect of different sources of variations in the model input to variation in the model output. It can filter out the uncertainty factors with negligible contributions and reduce complexity as discussed in fifth section of this chapter. Quantifying uncertainty characteristics of output in the system resulted from model input uncertainties and model uncertainties propagated through computational simulation

are the key problems in uncertainty analysis, we discussed it in the last section of this thiese.

Chapter 3 Monte Carlo Simulation

Monte Carlo sampling got its name as the code word for work that von Neumann and Ulam were doing during World War II on the Manhatten Project at Los Alamos for the atom bomb where it was used to integrate otherwise intractable mathematical functions[69] (Rubinstein, 1981). However, one of the earliest examples of the use of the Monte Carlo method was in the famous Buffon's needle problem where needles were physically thrown randomly onto a gridded field to estimate the value of *p*. In the beginning of the 20th century the Monte Carlo method was also used to examine the Boltzmann Equation and in 1908 the famous statistician Student (W.S. Gossett) applied the Monte Carlo method for estimating the correlation coefficient in his t-distribution[70].

A basic advantage of sampling methods is their direct utilization of experiments to obtain mathematical solutions or probabilistic information concerning problems whose system equations cannot be solved easily by known procedures[71]. Application of Monte Carlo Method to probabilistic structural analysis problems is comparatively recent, becoming practical only with the advent of digital computers. It is a powerful mathematical tool for determining the approximate probability of a specific event that is the outcome of a series of stochastic processes.

3.1 Mathematical formulation of Monte Carlo Integration

The quality of any algorithm that approximate the true value of the solution depends very much of the convergence rate. One needs to estimate how fast the approximate solution converges to the true solution. Let ξ be a random variable for which the mathematical expectation of $E(\xi) = I$ exists. Formally defined as,

$$E(\xi) = \begin{cases} \int_{-\infty}^{\infty} \xi\, p(\xi) d\xi & where \int_{-\infty}^{\infty} p(x)dx = 1 \ \ when\ \xi\ is\ a\ continuous\ r.v. \\ \sum_{\xi} \xi\, p(\xi) & where \sum_{x} p(x) = 1 \quad when\ \xi\ is\ a\ discrete\ r.v. \end{cases} \tag{3 - 1}$$

The nonnegative function $p(x)$ (continuous or discrete) is called the probability density function. To approximate the variable I , a computation of the arithmetic mean must usually be carried out,

$$\overline{\xi}_N = \frac{1}{N}\sum_{i=1}^{N}\xi_i \qquad (3 - 2)$$

For a sequence of uniformly distributed independent random variables, for which the mathematical expectation exists, the theorem of J. Bernoulli[72] (who proved for the first time the Law of Large Number Theorem) . This means that the arithmetic mean of these variables converges to the mathematical expectation:

$$\xi_N \xrightarrow{p} I \quad as \;\; N \to \infty$$

The sequence of the random variables $\eta_1, \eta_2, \cdots, \eta_N, \cdots$ converges to the constant c if for every $h > 0$, it follow that,

$$\lim_{N\to\infty} P\left\{\left|\eta_N - c\right| \geq h\right\} = 0$$

Thus, when N is sufficiently large $\overline{\xi}_N \approx I$

Suppose that the random variable ξ has a finite variance, the error of the algorithm can be estimated as,

$$D(\xi) = E[\xi - E(\xi)]^2 = E(\xi^2) - [E(\xi)]^2 \qquad (3 - 3)$$

3.1.1 Plain (crude) Monte Carlo Algorithm

Crude Monte Carlo is the simplest possible approach for solving multidimensional integrals. This approach simply applied the definition of the mathematical expectation.

Let Ω be an arbitrary domain and $x \in \Omega \subset R^d$ be a d-dimensional vector.

We consider the problem of the approximate computation of the integral

$$I = \int_\Omega f(x)\,p(x)dx \qquad (3 - 4)$$

Where the non-negative function $p(x)$ is density function $\int_\Omega p(x)dx = 1.$

Let ξ be a random point with probability density function $p(x)$. Introducing the random variable

$$\theta = f(\xi) \qquad (3 - 5)$$

With mathematical expectation equal to the value of integral I

$$E(\theta) = \int_{\Omega} f(x)\, p(x) dx \tag{3 - 6}$$

Let the random points $\xi_1, \xi_2, \ldots, \xi_N$ be independent realizations of the random point ξ with probability density function $p(x)$, then an approximate value of I is

$$\overline{\theta}_N = \frac{1}{N} \sum_{i=1}^{N} \theta_i \tag{3 - 7}$$

If $\overline{\xi}_N = \frac{1}{N} \sum_{i=1}^{N} \xi_i$ were absolutely convergent, then $\overline{\theta}_N$ would be convergent to I.

3.1.2 Geometric Monte Carlo Algorithm

Let the nonnegative function f be bounded,

$0 \le f(x) \le c \quad for \quad x \in \Omega$

Where c is a generic constant. Consider the cylindrical domain

$\tilde{\Omega} = \Omega \times [0, c]$

And the random point $\tilde{\xi} = (\xi_1, \xi_2, \xi_3) \subset \tilde{\Omega}$ with the following probability density function

$$\tilde{p}(x) = \frac{1}{c} p(x_1, x_2) \tag{3 - 8}$$

Let $\tilde{\xi}_1, \ldots, \tilde{\xi}_N$ be independent realization of the random point $\tilde{\xi}$. Introduce the random variable

$$\tilde{\theta} = \begin{cases} c, & if \ \xi_3 < f(\xi_1, \xi_2) \\ 0, & if \ \xi_3 \ge f(\xi_1, \xi_2) \end{cases} \tag{3 - 9}$$

The random variable introduced is a measure of the points below the graph of the function f.

$$E(\tilde{\theta}) = c\,\Pr\{\xi_3 < f(\xi)\} = \int_\Omega dx_1 dx_2 \int_0^{f(x_1,x_2)} \tilde{p}(x_1, x_2, x_3) dx_3 = I \tag{3 - 10}$$

The algorithm consists of generating a sequence of random points uniformly distributed in the third direction and accepting points if they are under the graph of the function and rejecting other points. This is the reason to call this Geometric algorithm an acceptance-rejection technique.

Compare the accuracy of the Geometric and the Plain Monte Carlo algorithm

Let $f \in L_2(\Omega, p)$ guarantees that the variance

$D(\tilde{\theta}) = \int_\Omega f^2(x) p(x) dx \quad - I^2$ in a Plain Monte Carlo algorithm is finite.

For the Geometric Monte Carlo algorithm the following equation holds

$$E(\tilde{\theta}^2) = c^2\,\Pr\{x_3 < f(\xi)\} = cI \tag{3 - 11}$$

Hence the variance is $D(\tilde{\theta}) = cI - I^2$. Because

$$\int_\Omega f^2(x) p(x) dx \le c \int_\Omega f(x) p(x) dx = cI \tag{3 - 12}$$

Therefore, $D(\theta) \le D(\tilde{\theta})$. The last inequality shows that the Plain Monte Carlo algorithm is more accurate than the Geometric one (except for the case when the function f is a constant). Nevertheless, the Geometric algorithm is often preferred, from the algorithmic point of view, because its computational complexity may be less than that of the plain algorithm.

3.2 Advanced Monte Carlo Methods

The probable error in Monte Carlo algorithms will appear when no information about the smoothness of the function is used

$$r_N = c\sqrt{\frac{D\xi}{N}} \tag{3 - 13}$$

It is important for such computational schemes and random variables that a value of ξ is chosen so that the variance is as small as possible. Monte Carlo algorithms with

reduced variance compared to Plain Monte Carlo algorithms are usually called advanced Monte Carlo algorithms. Consider the integral

$$I = \int_{\Omega} f(x)\, p(x) dx \tag{3 - 14}$$

Where $f \in L_2(\Omega, p)$, $x \in \Omega \subset R^d$

Let the function $h(x) \in L_2(\Omega, p)$ be close to $f(x)$ with respect to its L_2 norm; $\|f - h\|_{L_2} \leq \varepsilon$. The value of the integral is supposed as

$$I = \int_{\Omega} h(x)\, p(x) dx = I' \tag{3 - 15}$$

The random variable $\theta' = f(\xi) - h(\xi) + I'$ generates the following estimate for the integral

$$\theta'_N = I' + \frac{1}{N} \sum_{i=1}^{N} [f(\xi_i) - h(\xi_i)] \tag{3 - 16}$$

A possible estimate of the variance of θ' is

$$D(\theta') = \int_{\Omega} [f(x) - h(x)]^2 p(x) dx \quad - (I - I')^2 \leq \varepsilon^2 \tag{3 - 17}$$

This means that the variance and the probable error will be quite small, if the function $h(x)$ is such that the integral I' can be calculated analytically. The function $h(x)$ is often chosen to be piece-wise linear function in order to compute the value of I' easily.

3.2.1 Importance Sampling Algorithm

Importance sampling is a variance reduction technique that can be used in the Monte Carlo method. The basic idea behind importance sampling is that certain values of the input random variables in a simulation have more impact on the parameter being estimated than others. If these "important" values are emphasized by sampling more frequently, then the estimator variance can be reduced. Hence, the basic methodology in importance sampling is to choose a distribution which "encourages" the important values.

Consider the problem of computing the integral

$I_0 = \int_\Omega f(x)dx$, $x \in \Omega \subset R^d$

Ω_0 be the set of points x for which $f(x) = 0$ and $\Omega_+ = \Omega - \Omega_0$

Define the probability density function $p(x)$ to be tolerant to $f(x)$, if $p(x) > 0$ for $x \in \Omega_+$ and $p(x) \geq 0$ for $x \in \Omega_0$.

For an arbitrary tolerant probability density function $p(x)$ for $f(x)$ in Ω. The random variable θ_0 can be defined in the following way:

$$\theta_0(x) = \begin{cases} \dfrac{f(x)}{p(x)}, & x \in \Omega_+ \\ 0, & x \in \Omega_0 \end{cases} \tag{3 - 18}$$

It is interesting to consider the problem of finding a tolerant density, $p(x)$, which minimizes the variance of θ_0. The existence of such a density means that the optimal Monte Carlo algorithm with minimal probability error exists.

In importance sampling, a distribution g which is called importance distribution or instrumental distribution is introduced to apply a change of measure

$$E(\theta) = \mu = \int \frac{p(\mathrm{x})}{g(\mathrm{x})} f(\mathrm{x})\, \mathrm{g}(\mathrm{x})\, \mathrm{dx} \tag{3 - 19}$$

In sampling space, $\mathrm{w}(\mathrm{x}_i)$ are importance weights

$$\mathrm{w}(\mathrm{x}_i) = \frac{p(\mathrm{x}_i)}{g(\mathrm{x}_i)} \quad \text{i=1,…, n} \tag{3 - 20}$$

$$\begin{aligned} E(\theta) &= \int f(\mathrm{x})\, \mathrm{p}(\mathrm{x})\, \mathrm{dx} \\ &= \int \cdots \int \left(\frac{1}{n} \sum_{i=1}^{n} \mathrm{w}(\mathrm{x}_i) f(\mathrm{x}_i)\right) \prod_{i=1}^{n} g(\mathrm{x}_i) dx_i \end{aligned} \tag{3 - 21}$$

Importance sampling methods are frequently used to estimate posterior densities or expectations in state and/or parameter estimation problems in probabilistic models that are too hard to treat analytically, for example in Bayesian networks. It is used to

estimate properties of a particular distribution, while only having samples generated from a different distribution rather than the distribution of interest. Depending on the application, the term may refer to the process of sampling from this alternative distribution, the process of inference, or both.

3.2.2 Weight Functions Approach

If the integrand contains a weight function, in Monte Carlo quadratures with weight functions are considered for the computation of

$$S(g;m) = \int g(\theta)m(\theta)d\theta \tag{3 - 22}$$

The un-normalized posterior density m is expressed as the product of two functions w and f, where w is called the weight function $m(\theta) = w(\theta) f(\theta)$. The weight function is nonnegative and $\int w(\theta)d\theta = 1$, and it is chosen to have similar properties to m.

Most numerical integration algorithms then replace the function $m(\theta)$ by a discrete approximation in the form of:

$$\hat{m}(\theta) = \begin{cases} w_i f(\theta) & , \ \theta = \theta_i \ , i = 1,2,...n, \\ 0 & elsewhere \end{cases} \tag{3 - 23}$$

Then, the intrgral can be estimated by

$$\hat{S}(g;m) = \sum_{i=1}^{N} w_i f(\theta_i) g(\theta_i) \tag{3 - 24}$$

Integration algorithms use the weight function w as the kernel of the approximation of the integrand

$$\begin{aligned} S(g;m) &= \int g(\theta)m(\theta)d\theta \\ &= \int g(\theta)w(\theta) f(\theta)d\theta = E[w(g(\theta) f(\theta))] \end{aligned} \tag{3 - 25}$$

3.2.3 Latin Hypercube Sampling approach

The probability error usually has the form of $R_N = cN^{-0.5}$. The speed of convergence can be increased if an algorithm with a probability error $R_N = cN^{-0.5-\psi(d)}$ can be constructed, where c is a constant, $\psi(d) > 0$ and d is the dimension of the space.

Usually, the exploiting of smoothness is combined with subdividing the domain of integration into a number of non-overlapping sub-domains. This is the reason to call the techniques leading to super-convergent Monte Carlo algorithms stratified sampling, or Latin Hypercube sampling.

LHS also known as the “stratified sampling technique” represents a multivariate sampling method that guarantees non-overlapping design. In LHS, the distribution for each random variable can be subdivided into n equal probability intervals or bins. Each bin has one analysis point. There are n analysis points, randomly mixed, so each of the n bins has 1/n of the distribution probability. The basic steps

- Divide the distribution for each variable into n non-overlapping intervals on the basis of equal probability
- Select one value at random from each interval with respect to its probability density.
- Repeat step (1) and (2) until you have selected values for all random variables, such as $x_1, x_2, ..., x_k$
- Associate the n values obtained for each xi with the n values obtained for the other $x_{j \neq i}$ at random

The regularity of probability intervals on the probability distribution function ensures that each of the input variables has all portions of its range represented, resulting in relatively small variance in the response. At the same time, the analysis is much less computationally expensive to generate. The LHS method also provides flexible sample size while ensuring stratified sampling, each of the input variables is sampled at n levels[73].

3.3 Random Interpolation Quadratures

A quadrature is called interpolation for a given class of functions if it is exact for any linear combination of functions. In the practical computations, since one can only perform a sample of r.v., the probability error is not zero, but it is very small. So, the random interpolation quadrature are high quality quadrature. The problem is that they have a restricted area of application: one should be sure that each integrand belongs to a given class of function presented by a linear combination of a system of orthonormal function. These quadratures could be effective for solving problems in

some areas of modern physics, where people are interested to compute a large number of multidimensional integrals with similar integrands.

Assuming that the quadrature formula for computing the integral

$$I = \int_{\Omega} f(x)\,p(x)dx\,, \Omega \subset R^{d}\ ,\ p(x) \geq 0\ ,\int_{\Omega} p(x)dx = 1 \qquad (3 - 26)$$

Is denoted by the expression

$$I \approx \sum_{j=1}^{N} c_j f(x_j) \qquad (3 - 27)$$

Where $x_1\,,...,\,x_N \in \Omega$ are nodes. Then the random quadrature formula can be written in the following form:

$$I \approx \sum_{j=1}^{N} \kappa_j f(\xi_j) \qquad (3 - 28)$$

Where $\xi_1\,,...,\,\xi_N \in \Omega$ are random nodes and $\kappa_1\,,...,\,\kappa_N$ are random weights.

All functions considered are supposed to be partially continuous and belong to the space $L_2(\Omega)$. Let $\varphi_0,\ \varphi_1\,,...,\,\varphi_m$ be a system of orthonormal functions, such that

$$\int_{\Omega} \varphi_k(x)\varphi_j(x)dx = \delta_{kj} \qquad (3 - 29)$$

Where δ_{kj} is the Kronecker function[74].

For $p(x) = \varphi_0(x)$ an approximate solution for the integral

$$I = \int_{\Omega} f(x)\varphi_0(x)dx \qquad (3 - 30)$$

Let us fix arbitrary nodes and choose the weight $c_0\,, c_1\,,...,\,c_m$ such that is exact for the system of orthonormal functions $\varphi_0,\ \varphi_1\,,...,\,\varphi_m$. In this case it is convenient to represent the quadrature formula as a ratio of two determinants

$$I \approx \frac{W_f(x_0\,, x_1\,,...,\,x_m)}{W_{\varphi_0}(x_0\,, x_1\,,...,\,x_m)} \qquad (3 - 31)$$

Where

$$W_g(x_0, x_1, ..., x_m) = \begin{vmatrix} g(x_0) & \varphi_1(x_0) & \cdots & \varphi_m(x_0) \\ g(x_1) & \varphi_1(x_1) & \cdots & \varphi_m(x_1) \\ \vdots & \vdots & \ddots & \vdots \\ g(x_m) & \varphi_1(x_m) & \cdots & \varphi_m(x_0) \end{vmatrix} \quad (3 - 32)$$

It is easy to check that if $W_{\varphi_0} \neq 0$ then the formula is exact for every linear combination of the following form: $f = a_0\varphi_0 + \cdots + a_m\varphi_m$

3.4. Iterative Monte Carlo Methods for Linear Equations

In general, Monte Carlo numerical algorithms may be divided into two classes --- direct algorithms and iterative algorithms. The direct algorithms provide an estimate of the solution of the equation in a finite number of steps, and contain only a stochastic error. However, iterative Monte Carlo algorithms deal with an approximate solution obtaining an improved solution with each step of the algorithm.

Iterative algorithms are preferred for solving integral equations and large sparse systems of algebraic equations. Such algorithms are good for diagonally dominant systems in which convergence is rapid; they are not so useful for problems involving dense matrices.

Define an iteration of degree j as

$$u^{k+1} = F_k(A, b, u^k, u^{k-1}, ..., u^{k-j+1}) \quad (3 - 33)$$

Where u^k is obtained from the k^{th} iteration. Usually the degree of j is kept small because of storage requirements. The iteration is called stationary if $F_k = F$ for all k, that is, F_k is independent of k.

The iterative Monte Carlo process is said to be linear if F_k is a linear function of $u^k, u^{k-1}, ..., u^{k-j+1}$. We shall consider iterative stationary linear Monte Carlo algorithms and will analyse both systematic and stochastic errors. Sometimes the iterative stationary linear Monte Carlo algorithms are called Power Monte Carlo algorithms. The reason is that these algorithms find an approximation of a functional of powers of linear operators. It is also known as Markov chain Monte Carlo since the statistical estimates can be considered as weights of Markov chains.

3.4.1 Iterative Monte Carlo Algorithms

Consider a general description of the iterative Monte Carlo algorithms. Let X be a Banach space of real-valued functions. Let $f = f(x) \in X$ and $u_k = u(x_k) \in X$ be defined in Rd and $L = L(u)$ be a linear operator defined on X .

Consider the sequence $u_1, u_2, ...,$ defined by the recursion formula

$$u_k = L(u_{k-1}) + f \ , k = 1, 2, ... \tag{3 - 34}$$

The formal solution of this equation is the truncated Neumann series

$$u_k = f + L(f) + \cdots + L^{k-1}(f) + L^k(u_0) \ , k > 0 \tag{3 - 35}$$

Where L^k means the k^{th} iterate of L .

As an example consider the integral iterations.

Let $u(x) \in X$, $x \in \Omega \subset R^d$ and $l(x, x')$ be a function defined for $x \in \Omega, x' \in \Omega$. The integral transformation

$L(u(x)) = \int_\Omega l(x, x')u(x')dx'$ maps the function to the function $L(u(x))$, and is called an iteration of $u(x)$ by the integral transformation kernel $l(x, x')$. The second integral iteration of $u(x)$ is denoted by

$$L(L(u(x))) = L^2(u(x)) \tag{3 - 36}$$

Obviously,

$$L^2(u(x)) = \int_\Omega \int_\Omega l(x, x')l(x', x'')dx'dx'' \tag{3 - 37}$$

In this way $L^3(u(x)), \cdots, L^i(u(x)), \cdots$ can be defined.

When the infinite series converges, the sum is an element u from the space X which satisfies the equation

$$u = L(u) + f \tag{3 - 38}$$

The truncation error is

$$u_k - u = L^k(u_0 - u) \tag{3 - 39}$$

Let $J(u_k)$ be a linear functional that is to be calculated. Consider the spaces

$$T_{i+1} = \underbrace{R^d \times R^d \times \cdots \times R^d}_{i \ \ times} \quad , i = 1, 2, \cdots, k$$

Where "$\times$" denotes the Cartesian product of spaces.

Random variables $\theta_i , i = 0,1,\cdots,k$ are defined on the respective product spaces T_{i+1} and have conditional mathematical expectations:

$$E(\theta_0) = J(u_0) , E(\theta_1/\theta_0) = J(u_1) , \cdots , E(\theta_k/\theta_0) = J(u_k) \tag{3 - 40}$$

Where $J(u)$ is a linear functional of u

The computational problem then becomes one of calculating repeated realizations of θ_k and combining them into an appropriate statistical estimator of $J(u_k)$

As an approximate value of the linear functional $J(u_k)$ is set up

$$J(u_k) \approx \frac{1}{N} \sum_{s=1}^{N} \{\theta_k\}_s \tag{3 - 41}$$

Where $\{\theta_k\}_s$ is the s^{th} realization of the random variable.

The probable error of the above equation is

$$r_N = c\sigma(\theta_k) N^{-0.5} \tag{3 - 42}$$

Where $c \approx 0.6745$ and $\sigma(\theta_k)$ is the standard deviation of the random variable θ_k

There are two approaches which are corresponding with two special cases of the operator L:

- L is a matrix, u and f are vectors;
- L is an ordinary integral transform

$$L(u) = \int_\Omega l(x, y) u(y) dy \tag{3 - 43}$$

First consider the case of an ordinary integral transform,

$$u(x) = \int_{\Omega} l(x,y)u(y)dy + f(x) \quad \text{or} \quad u = L(u) + f \tag{3 - 44}$$

Monte Carlo algorithms frequently involve the evaluation of linear functionals of the solution of the following type

$$J(u) = \int_{\Omega} h(x)u(x)dx = (u,h) \tag{3 - 45}$$

In fact, this equation defines an inner product of a given function $h(x) \in X$ with the solution of the integral equation.

Sometimes, the adjoint equation $v = L^* v + h$ will be used.

$v, h \in X^*$, $L^* \in [X \to X^*]$, where X^* is the dual functional space to X and L^* is an adjoint operator.

For some important applications $X = L_1$ and

$$\|f\|_{L_1} = \int_{\Omega} |f(x)| dx \tag{3 - 46}$$

$$\|L\|_{L_1} \le \sup_x \int_{\Omega} |l(x,x')| dx' \tag{3 - 47}$$

In this case $h(x) \in L_\infty$, hence $L_1^* \equiv L_\infty$ and

$$\|h\|_{L_\infty} = \sup |h(x)|, \; x \in \Omega \tag{3 - 48}$$

For many applications $X = X^* = L_2$. Note also, that if $h(x), u(x) \in L_2$ then the inner product is finite. In fact,

$$\left| \int_{\Omega} h(x)u(x)dx \right| \le \int_{\Omega} |h(x)u(x)| dx \le \left\{ \int_{\Omega} h^2 dx \int_{\Omega} u^2 dx \right\}^{1/2} < \infty \tag{3 - 49}$$

One can also see, that if $u(x) \in L_2$ and $l(x,x') \in L_2(\Omega \times \Omega)$ then $L(u(x)) \in L_2$:

3.4.2 Convergence and mapping

To analyse the convergence of Monte Carlo Algorithms consider the following equation

$$u = \lambda L(u) + f \tag{3 - 50}$$

Where λ is some parameter. $\lambda_1, \lambda_2, \cdots$ are the eigne values, where it is supposed that $|\lambda_1| \geq |\lambda_2| \geq \cdots$ Note that the matrices can be considered as linear operators. Define resolvent operator R_λ by the equation

$$I + \lambda R_\lambda = (I - \lambda L)^{-1} \tag{3 - 51}$$

Where I is the identity operator.

Monte Carlo algorithms are based on the representation

$$u = (I - \lambda L)^{-1} f = f + \lambda R_\lambda f \tag{3 - 52}$$

Where $R_\lambda = L + \lambda L^2 + \cdots$

The systematic error of R_λ, where m terms are used, is

$$r_s = \mathrm{O}[|\lambda/\lambda_1|^{m+1} m^{\rho-1}] \tag{3 - 53}$$

Where ρ is the multiplicity of the root λ_1. When λ is approximately equal to λ_1 the sequence and the corresponding Monte Carlo algorithm converges slowly. When $\lambda \geq \lambda_1$ the algorithm does not converge.

3.5 Morkov Chain Monte Carlo methods for Eigen-value Problem

It is known that the problem of calculating the smallest by magnitude eigen value of a matrix A is more difficult from a numerical point of view than the problem of evaluating the largest eigen-value. Nevertheless, for important application in physics and engineering it is necessary to estimate the value of the smallest by magnitude eigen value, since this usually defines the most stable state of the system described the considered matrix.

3.5.1 Formulation of Eigen-value problem

For matrices with a large size, which often appear in practice, it is not easy to find efficient algorithms for evaluating the smallest eigen value. Consider the following problem of evaluating eigen values $\lambda(A)$:

$$Ax = \lambda(A)x \tag{3 - 54}$$

It is assumed that

A is a given symmetric matrix, $a_{ij} = a_{ji}$ for all $i, j = 1, 2, \cdots, n$;

$$\lambda_{\min} = \lambda_n < \lambda_{n-1} \le \lambda_{n-2} \le \cdots \le \lambda_2 < \lambda_1 = \lambda_{\max} \tag{3 - 55}$$

We use the following presentation of matrices:

$$A = \left\{a_{ij}\right\}_{i,j=1}^{n} = (a_1, \cdots, a_i, \cdots, a_n)^T \tag{3 - 56}$$

Where $a_i = (a_{i1}, \cdots, a_{in}) \quad i = 1, \cdots, n$ and the symbol T means transposition.

The following norms of vectors

$$\|h\| = \|h\|_1 = \sum_{i=1}^{n} |h_i| \qquad \|a_i\| = \|a_i\|_1 = \sum_{j=1}^{n} |a_{ij}| \tag{3 - 57}$$

And matrices are used.

$$\|A\| = \|A\|_1 = \max_j \sum_{i=1}^{n} |a_{ij}| \tag{3 - 58}$$

In general, $\|A\| \ne \max_i \|a_i\|$

By $\overline{A}$ we denote the matrix containing the absolute values of elements of a given matrix A:

$$\overline{A} = \left\{\left|a_{ij}\right|\right\}_{i,j=1}^{n} \qquad p_k(A) = \sum_{i=0}^{k} c_i A^i \,,\ c_i \in \square \tag{3 - 59}$$

We denote matrix polynomial of degree k.

As usual, $(v,h)=\sum_{i=1}^{n} v_i h_i$ denotes the inner product of vectors v and h.

We will be interested in computing inner products of the following type:

$(v, p_k(A)h)$

The random variable ξ could be a randomly chosen component h_{α_k} of a given vector h. In this case the meaning of $E(h_{\alpha_k})$ is mathematical expectation of the value of randomly chosen element of h

$$D(\xi)=\sigma^2(\xi)=E(\xi^2)-[E(\xi)]^2 \tag{3 - 60}$$

We denote the variance of the random variable ξ. Basically, we are interested in evaluation of forms: $(v, p_k(A)h)$

In a special case of $p_k(A)=A^k$ the form $(v, p_k(A)h)$ becomes $(v, A^k h)$, $k \geq 1$

Suppose that a real symmetric matrix A is diagonalizable,

$$x^{-1}Ax = diag(\lambda_1, \cdots, \lambda_n) \tag{3 - 61}$$

If A is a symmetric matrix, then the values are real numbers, $\lambda \in \mathbb{R}$

The well-known Power method gives an estimate for the dominant eigen value λ_1. This estimate uses the so-called Rayleigh quotient $\mu_k = \dfrac{(v, A^k h)}{(v, A^{k-1} h)}$

Where $v, h \in \mathbb{R}^n$ are arbitrary vectors. The Rayleigh quotient is used to obtain an approximation to λ_1

$$\lambda_1 \approx \frac{(v, A^k h)}{(v, A^{k-1} h)} \tag{3 - 62}$$

Where k is an arbitrary large natural number.

To construct an algorithm for evaluating the eigenvalue of minimum modulus λ_n, one has to consider the following matrix of polynomial:

$$p_i(A) = \sum_{k=0}^{i} q^k C_{m+k-1}^k A^k \tag{3 - 63}$$

Where C_{m+k-1}^k are binomial coefficients, the characteristic parameter q is used as acceleration parameter of the algorithm.

If $|q|\|A\| < 1$ and $i \to \infty$, then the polynomial becomes the re-solvent matrix

$$p_\infty(A) = p(A) = \sum_{k=0}^{\infty} q^k C_{m+k-1}^k A^k = [I - qA]^{-m} = R_q^m \tag{3 - 64}$$

Where $R_q = [I - qA]^{-1}$ is the re-solvent matrix of the equation.

$$x = qAx + h \tag{3 - 65}$$

Values $q_1, q_2, \cdots$ for which the equation above is fulfilled are called characteristic values. The re-solvent operator

$$R_q = [I - qA]^{-1} = I + A + qA^2 + \cdots \tag{3 - 66}$$

Exists if the sequence converges. The systematic error of the presentation when m terms are used is

$$R_s = \mathrm{O}[|q/q_1|^{m+1} m^{\rho-1}] \tag{3 - 67}$$

Where ρ is multiplicity of the root q_1. Estimation is analogue of MC algorithm converges if $|q| < |q_1|$. When $|q| \geq |q_1|$ the algorithm does not converge for $q = q_* = 1$, but the solution of $x = qAx + h$ exists. In this case one may apply a mapping of the spectral parameter q.

One can consider the ratio:

$$\lambda = \frac{(v, Ap(A)h)}{(v, p(A)h)} = \frac{(v, AR_q^m h)}{(v, R_q^m h)} \tag{3 - 68}$$

Where $R_q^m h = \sum_{k=1}^{m} g_k^m c_k$ and g_k^m are computed. If $q < 0$, then

$$\frac{(v, AR_q^m h)}{(v, R_q^m h)} \approx \frac{1}{q}(1 - \frac{1}{\mu^k}) \approx \lambda_n \qquad (3 - 69)$$

Where $\lambda_n = \lambda_{\min}$ is the minimal by modulo eigenvalue, and μ^k is the approximation to the dominant eigenvalue of R_q.

If $|q| > 0$, then

$$\frac{(v, AR_q^m h)}{(v, R_q^m h)} \approx \lambda_1 \qquad (3 - 70)$$

Where $\lambda_1 = \lambda_{\max}$ is dominant eigen value.

The approximate equations can be used to formulate efficient Monte Carlo algorithms for evaluating both the dominant and the eigenvalue of minimum modulus of real symmetric matrices. We consider a MAO algorithm for computing bilinear forms of matrix powers, which can be also used to formulate the solution for the dominant eigenvalue problem. Assume, we considering the set, A, of algorithms, A, for calculating bilinear forms of matrix powers $(v, A^k h)$ with a probability error $R_{k,N}$ less than a given constant ε and the probability $c < 1$ is also fixed. Obviously, for fixed ε and $c < 1$ the computational cost depends linearly on the number of iterations k and on the number of Markov chains N.

3.5.2 Method for Choosing the Number of Iterations k

Assume that we wish to estimate the value of the bilinear form $(v, A^k h)$, so that with a given probability $P < 1$ the error is smaller than a given positive ε:

$$\left| (v, A^k h) - \frac{1}{N} \sum_{i=1}^{N} \theta_i^k \right| \le \varepsilon \qquad (3 - 71)$$

In the case of balanced errors,

$$R_{k,N} = R_{k,s} = \frac{\varepsilon}{2} \qquad (3 - 72)$$

When a mapping procedure is applied one may assume that there exists a positive constant $\alpha < 1$ such that

$\alpha \geq \left|g_i^k\right| \times \|A\|$ for any i and k.

Then

$$\frac{\varepsilon}{2} \leq \frac{(\left|g_i^k\right| \|A\|)^{k+1} \|h\|}{1-\left|g_i^k\right| \|A\|} \leq \frac{\alpha^{k+1} \|h\|}{1-\alpha} \tag{3 - 73}$$

And for k should be chosen the smallest natural number for which

$$k \geq \frac{|\log \delta|}{|\log \alpha|} - 1 \qquad \delta = \frac{\varepsilon(1-\alpha)}{2\|h\|} \tag{3 - 74}$$

If a mapping procedure is not applied, the corresponding Neumann series converges fast enough, then one assumes that a positive constant α, such that $\alpha \geq \|A\|$ exists. Then the number of iterations k should be chosen.

There are other possibilities to estimate the number of needed iterations k if a mapping procedure is applied. The choice of the method of estimation of k depends on the available a priori information, which comes from the concrete scientific application.

3.5.3 Method for choosing the number of chains

To estimate the computational cost $\tau(A)$ we should estimate the number N of realizations of the random variable θ^k. We assume that there exists a constant σ such that

$$\sigma \geq \sigma(\theta^k) \tag{3 - 75}$$

Then we have

$$\varepsilon = 2R_N^k = 2c_p \sigma(\theta^k) N^{-0.5} \geq 2c_p \sigma N^{-0.5} \tag{3 - 76}$$

And $N \geq \left\{\frac{2c_p\sigma}{\varepsilon}\right\}^2$

Taking into account relations $k \geq \frac{|\log \delta|}{|\log \alpha|} - 1$, $\delta = \frac{\varepsilon(1-\alpha)}{2\|h\|}$ and $N \geq \left\{ \frac{2c_p \sigma}{\varepsilon} \right\}^2$ one can get estimates of the computational cost of biased MC algorithms.

3.6 Examples

3.6.1 Importance sampling

$$\mu = \int f(x)\pi(x)dx \tag{3 - 77}$$

$f(x)$ is a measurable function and $\pi(x)$ is a probability density function.

Importance distribution function $\mathrm{g}(x)$ is used to apply a change of measure

$$\mu = \int \frac{\pi(x)}{\mathrm{g}(x)} f(x)\,\mathrm{g}(x)dx \tag{3 - 78}$$

If $\omega(\mathrm{X}_i) = \frac{\pi(\mathrm{X}_i)}{\mathrm{g}(\mathrm{X}_i)}$, $i = 1, \ldots, n$, then

$$\hat{\mu}_n^{IS} = \frac{1}{n}\sum_{i=1}^{n} \omega(\mathrm{X}_i) f(\mathrm{X}_i) \tag{3 - 79}$$

Here, we had an example of student-t distribution $\mathrm{T}(\nu, \theta, \sigma^2)$ with density

$$\pi(x) = \frac{\Gamma((\nu+1)/2)}{\sigma\sqrt{\nu\pi}\,\Gamma(\nu/2)} \left(1 + \frac{(x-\theta)^2}{\nu\sigma^2}\right)^{-(\nu+1)/2} \mathrm{I}_R(x) \qquad (\theta = 0, \sigma = 1, \nu = 12) \tag{3 - 80}$$

We choose the quantities of interest to be

$$\begin{cases} f_1(x) = \left(\dfrac{\sin(x)}{x}\right)^5 \mathrm{I}(x)_{(2.1,+\infty)} \\ f_2(x) = \sqrt{\left|\dfrac{x}{1-x}\right|} \\ f_3(x) = \dfrac{x^5}{1+(x-3)^2} \mathrm{I}(x)_{[0,+\infty)} \end{cases} \tag{3 - 81}$$

We study the performance of the importance sampling estimator $\hat{\mu}_n^{IS}$ when the following instrumental distributions are used

$\mathrm{T}(\nu^*, 0, 1)$ with $\nu^* < \nu$, $\nu^* = 7$

$\mathrm{N}(0, \nu/(\nu-2))$

$C(0,1)$

We shall note that the Cauchy distribution $C(\alpha, \beta)$ has density function

$$\pi(x) = \frac{1}{\pi\beta(1+((x-\alpha)/\beta)^2)}\mathrm{I}(x) \qquad (3 - 82)$$

Performed Monte Carlo simulation to estimate $\hat{\mu}_n^{IS}$, plot 95% and 5% quantiles and the mean of the estimator for n=1,…, 50000

Table 3 - 1 Time cost of different PDF by importance sampling method

	f1	f2	f3
Student -T	7.634	7.628	7.600
Normal	5.974	5.956	5.940
Cauchy	3.807	3.563	3.923
Exact	1.768	1.172	1.719

Table 3 - 2 Results of different PDF by importance sampling method

	f1	f2	f3
Student -T	7.705e-5	1.157	4.523
Normal	7.444e-5	1.167	4.659
Cauchy	7.984e-5	1.165	4.514
Exact	7.749e-5	1.164	4.708

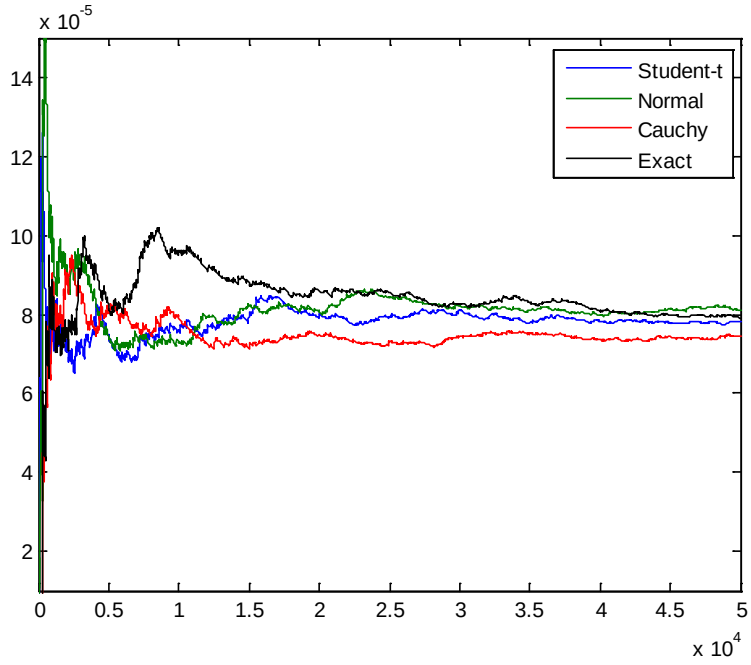

Fig 3 - 1 Convergence history of different PDF in function f1

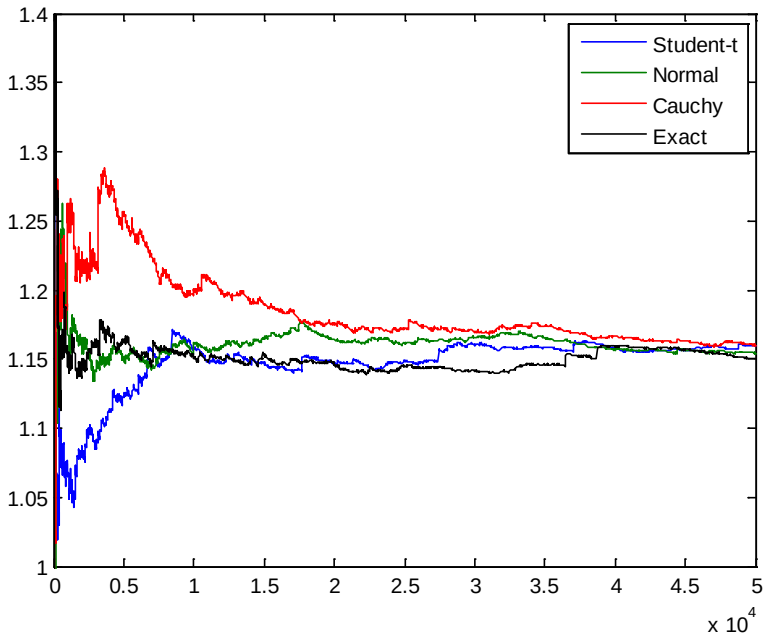

Fig 3 - 2 Convergence history of different PDF in function f2

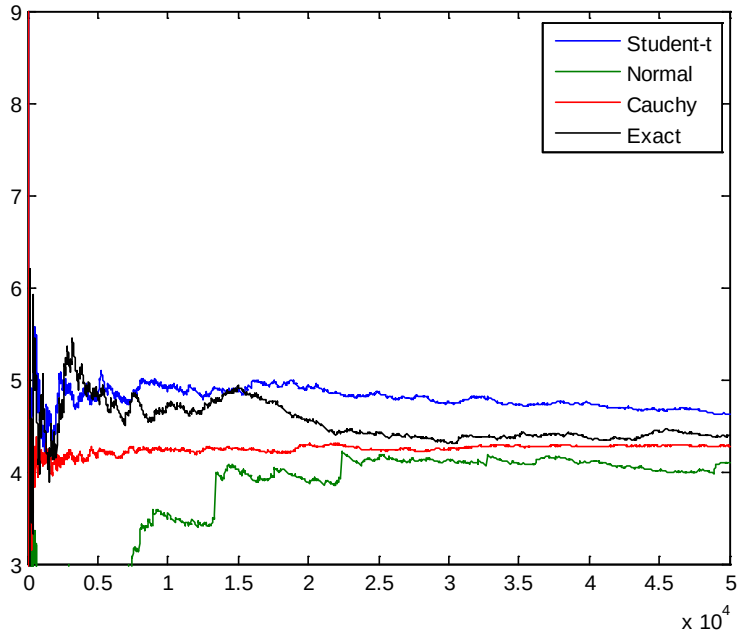

Fig 3 - 3 Convergence history of different PDF in function f3

The fundamental issue in implementing importance sampling simulation is the choice of the biased distribution which encourages the important regions of the input variables. Choosing or designing a good biased distribution is the key point of importance sampling. The rewards for a good distribution can be huge run-time savings; the penalty for a bad distribution can be longer run times than for a general Monte Carlo simulation.

In principle, the importance sampling ideas remain the same in these situations, but the design becomes much harder. A successful approach to combat this problem is essentially breaking down a simulation into several smaller, more sharply defined sub-problems. Then importance sampling strategies are used to target each of the simpler sub-problems.

In order to identify successful importance sampling techniques, it is useful to be able to quantify the run-time savings due to the use of the importance sampling approach. The performance measure commonly used is $\sigma^2_{MC}/\sigma^2_{IS}$, and this can be interpreted as the speed-up factor by which the importance sampling estimator achieves the same precision as the Monte Carlo estimator. This has to be computed empirically since the estimator variances are not likely to be analytically possible when their

mean is intractable. Other useful concepts in quantifying an importance sampling estimator are the variance bounds and the notion of asymptotic efficiency.

3.6.2 Latin Hypercube sampling in Finite element model of structure

It is useful to know the modal frequencies of a structure as it allows you to ensure that the frequency of any applied periodic loading will not coincide with a modal frequency and hence cause resonance, which leads to large oscillations. The dynamic equation can be written as,

$$[M]\{\ddot{x}\}+[C]\{\dot{x}\}+[K]\{x\}=\{F\} \tag{3 - 83}$$

Where $[M]$ is the mass matrix describing the distribution of mass, it is about the structural degree of freedom, $\{\dot{x}\}$ and $\{\ddot{x}\}$ are the first and second derivatives of the displacement with respect to time. Note that the force applied to the system is now a function of time. While mass and stiffness of a structure are measured and relatively easily derived, the mechanism whereby energy is lost through damping is less easily modeled. The viscous damping model represented by matrix $[C]$ is commonly but by no means exclusively used, being proportional to velocity. If there is no damping, the equation of motion is

$$[M]\{\ddot{x}\}+[K]\{x\}=\{F\} \tag{3 - 84}$$

For free (unforced) vibrations the following relationship is obeyed

$$[M]\{\ddot{x}\}+[K]\{x\}=0 \tag{3 - 85}$$

The solution to which can be written in the form

$$\{x\}=\{\psi\}_j e^{iw_j t} \tag{3 - 86}$$

Where ω_j are the resonant frequencies. Substituting back into the vibration equation leads to the well-known eigenvalue problem

$$[K]\{\psi\}_j=\lambda_j[M]\{\psi\}_j \tag{3 - 87}$$

Where $\lambda_j = \omega_j^2$, and $\{\psi\}_j$ can be thought of the mode shapes corresponding to the system natural frequencies $\{\omega\}_j$.

While the eigenvalues have an exact relationship with the resonant frequencies, the eigenvectors are arbitrarily scaled; it is common practice to define a uniquely scaled set of eigenvectors such that

$$[\phi]^T [M][\phi] = [I] \tag{3 - 88}$$

The result is

$$[\phi]^T [K][\phi] = diag(\lambda) \tag{3 - 89}$$

Where $[\phi]$ is the matrix of mass normalized eigen-vectors.

The natural frequency of a system is dependent only on the stiffness of the structure and the mass which participates with the structure (including self-weight). It is not dependent on the load function, as demonstrated in equation (3-87).

In this paper, our finite element model of wing structure, as presented in Fig.3-4, is constructed by ANSYS Parameter Design Language. The parameters in the original deterministic model are corresponding with geometrical properties and material properties. Where S is the parameter representing the ratio of area between the two airfoil sections, it is 0.25 as in initial. L and D as presented in the Fig.1, are 6.25 m and 1.42 m respectively. For material property, Young's module is 7e10 Pa, Poisson's ratio is 0.33, and physical density is 2700kg/m3.

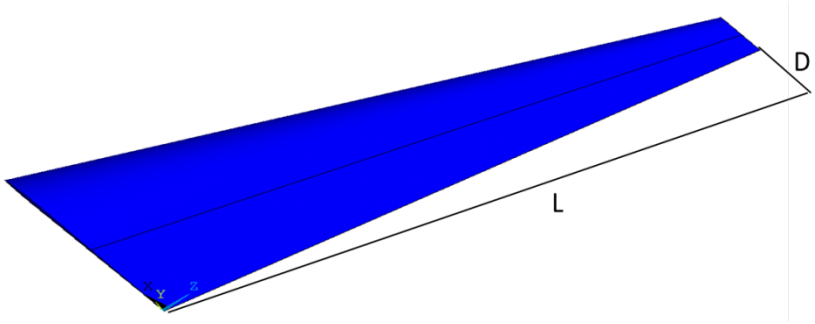

Fig 3 - 4 Finite element model of wing structure

The results of natural frequencies of wing structure in the deterministic finite element model are as presented in Table 3.3. According to each natural frequency, the wing structure has deformation and the contour of Von-Mises stress as in Fig.3-5. As discussed before, the natural frequencies of wing structure are the frequencies should be avoided in order to prevent the resonance disaster. If the distance between two neighbor frequencies are large, the domain of safety is amplified. This will be a criterion in the section of reliability analysis.

Table 3 - 3 Results of deterministic finite element model

	1	2	3	4	5
Natural frequency /Hz	61468	197798	291869	447981	578028
Minimum stress / N/M2	0.243e10	0.705e10	0.188e11	0.294e11	0.482e11
Maximum stress / N/M2	0.249e12	0.189e13	0.143e13	0.631e13	0.391e13

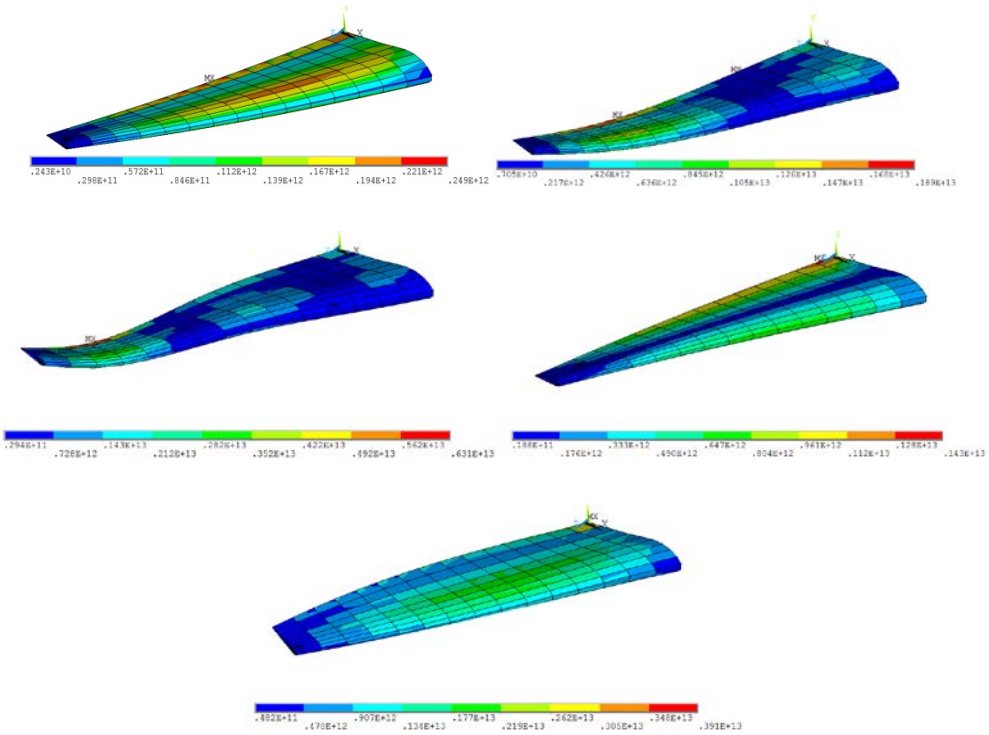

Fig 3 - 5 Contour picture of Von-Mises stress in five natural frequencies

The Monte Carlo simulation, one of the best-known probabilistic methods, consists of performing a large number of trials in order to estimate the output variability. The output stochastic data in terms of mean value, standard deviation, coefficient of variation and distribution are obtained.

To begin generating the LH sample, an interval of each feature is chosen at random. The intersection of these intervals in the multi-dimensional feature space is a small hypercube, from which a sample is taken at random. Next, type of interval is selected at random for each feature. A sample is produced at random from that small hypercube. This continues until N samples have been generated. Each interval of each parameter is sampled exactly once in the process. In contrast to random sampling, the entire range of each feature is always represented in a LH sample.

Unbiased estimates of the sample means of the outcomes are obtainable, and the mean squared errors of the estimators of the variances of model outcomes are smaller for the LH sample than for random or stratified sampling. They point out that in contrast to full or fractionalized factorial, central composite, and other fixed point strategies, LH sampling allows such estimates to be made without reliance upon the response surface itself.

Latin Hypercube sampling method is performed in the deterministic finite element model to calculate the natural frequencies. 10000 groups of sampling ensure the accuracy of the results. The parameters corresponding with geometry (S, D, L) and material property (E, P, R) are as input variables in the process of Latin Hypercube sampling method, while the natural frequencies of specific wing structure are as output variable in each sampling iteration.

Fig.3-6 provides the records of natural frequencies in the process of stochastic simulation. To be more obvious, the accumulative probabilities of five natural frequencies of wing structure are presented in Fig.3-7 as numerical statistics.

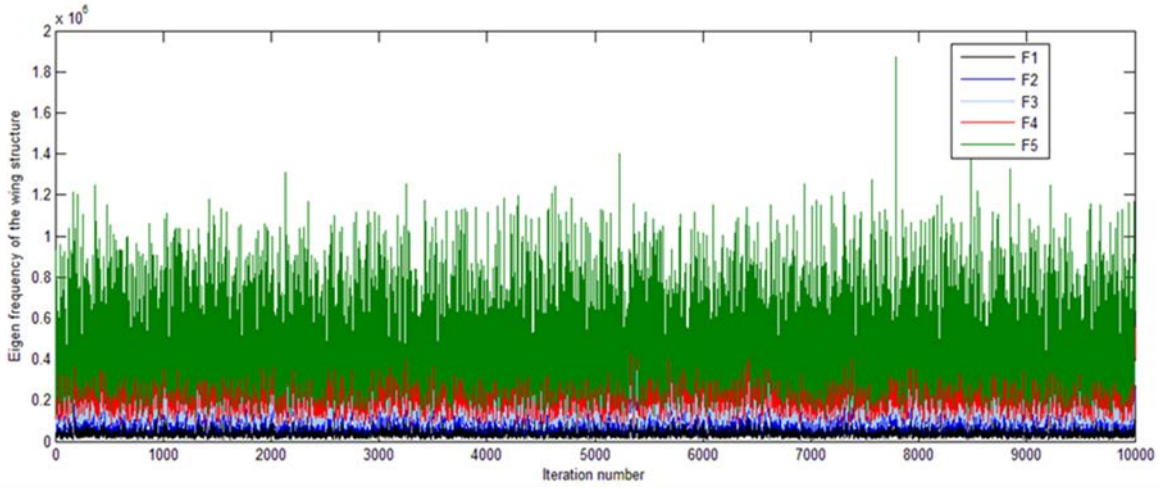

Fig 3 - 6 Records of natural frequencies in the process of Latin Hypercube sampling

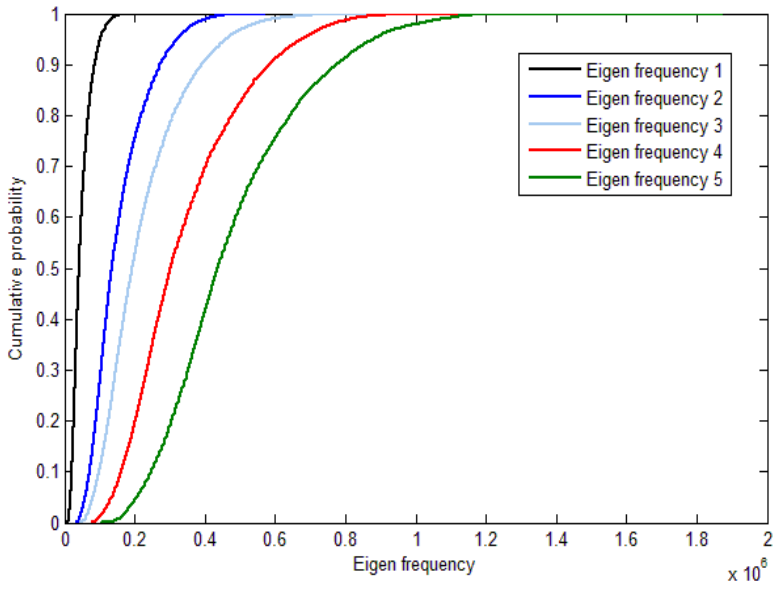

Fig 3 - 7 Cumulative probability of five natural frequencies in MCS

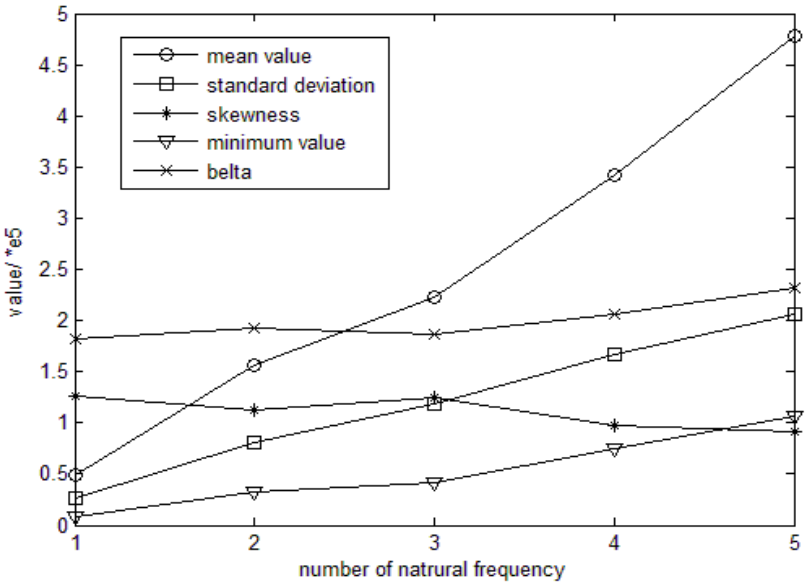

Fig 3 - 8 Numerical statistic in the stochastic simulation

The evaluation of the stochastic simulation in Latin Hypercube sampling method presented in Table 3.4. The mean value, standard deviation, skewness, and also the minimum and maximum are concluded as statistic in the sampling method, or as showed in Fig.3-8. It is evident that the natural frequency increase by the serial number. For example, the mean value of the second natural frequency is larger than that of the first natural frequency, while the Fig.3-6 also provides the evidence to it. In addition, the standard deviation and the minimum value have the same tendency with the mean value in the process of stochastic simulation. By contrast, the values of belta and skew do not have evident fluctuation and keep stable in a certain range for the five natural frequencies.

Table 3 - 4 Results of Latin Hypercube Sampling method

	F1	F2	F3	F4	F5
Mean value /*e5 Hz	0.48595	1.5632	2.2246	3.4208	4.7813
Standard deviation /*e5 Hz	0.26679	0.81028	1.1919	1.6633	2.0616
Skewness /*e5 Hz	1.2572	1.1292	1.2509	0.96708	0.91258
Minimum /*e5 Hz	0.08809	0.32320	0.41714	0.74041	1.0691
Maximum /*e5 Hz	1.9210	5.7092	9.4982	11.670	18.737
Belta	1.8215	1.9292	1.8664	2.0566	2.3192

3.7 Conclusion

The structure of this chapter is that in the first part we expressed the mathematical formulation of Monte Carlo simulation; however, to overcome the disadvatages of Monte Carlo Simulation, namely computational burden to make sure the certain level of accuracy, we discussed advanced MCS method in the second part of this chapter. After that, the discussion about random interpolation quadratures, iterative MCS for linear equations and Morkov chain MCS is also provided. In the last section of this chapter, we applied MCS methods in numerical simulation of different examples.

In the example of importance sampling method of MCS, fundamental issue is the choice of the biased distribution which encourages the important regions of the input variables. The rewards for a good distribution can be huge run-time savings; the penalty for a bad distribution can be longer run times than for a general Monte Carlo simulation.

Performing Latin hypercube sampling method in the finite element model of mechanical structure is an effective to propogate the uncertainties in a deterministic system. In this chapter, two examples of Latin hypercube sampling method in finite element models were discussed, one is a static finite element model, the other is a dynamic finite element model.

In the first model, parameters which are corresponding with the geometry property and material property of finite element model were definded as input variables in the process of Latin Hypercube sampling, while the largest stress in the whole structutre were captured by finite element model calculation and recorded as the output datas. In the second model, it is fininte element model of wing structure. Different with the first model, the output datas of Latin Hypercube sampling are the natural frequency of the certain wing structure.

Chapter 4 Stochastic Expansion for Probability analysis

One of the effective choices for uncertainty analysis is the direct use of stochastic expansion of output responses and input random variables for representing uncertainty. Stochastic expansion provides analytically appealing convergence properties based on the concept of a random process[75]. The polynomial chaos expansion can reduce computational effort of uncertainty quantification in engineering design applications where system response is computed implicitly[76].

4.1 Fundamental of PCE

The PCE stemmed from both Wiener and Ito's work on mathematical descriptions of irregularities[77]. Since Wiener introduced the concept of homogeneous chaos, the PCE has been successfully used for the uncertainty analysis in various applications. A simple definition of the PCE for a Gaussian random response $u(\theta)$ as a convergent series is as follows:

$$u(\theta) = a_0\Gamma_0 + \sum_{i=1}^{\infty} a_{i1}\Gamma_1(\xi_{i1}(\theta)) + \sum_{i_1=1}^{\infty}\sum_{i_2=1}^{i_1} a_{i_1 i_2}\Gamma_2(\xi_{i1}(\theta),\xi_{i2}(\theta)) + \cdots \quad (4\text{ - }1)$$

Where $\{\xi_i(\theta)\}_{i=1}^{\infty}$ is a set of Gaussian random variables; $\Gamma_p(\xi_{i1},\cdots,\xi_{ip})$ is the genetic element of a set of multidimensional Hermite polynomials, usually called homogeneous chaos of order p ; $a_{i1},\cdots,a_{ip}$ are deterministic constants; and θ represents an outcome in the space of possible outcomes of a random event.

PCE is convergent in the mean-square sense and the p^{th} order PCE consists of all orthogonal polynomials of order p , including any combination of $\{\xi_i(\theta)\}_{i=1}^{\infty}$; furthermore, $\Gamma_p \perp \Gamma_q$ for $p \neq q$. This orthogonality greatly simplifies the procedure of statistical calculations, such as moments. Therefore, PCE can be used to approximate non-Gaussian distributions using a least-squares scheme: for example, in order to compare the skewness and kurtosis of distributions.

The general expression to obtain the multidimensional Hermite polynomials is given by

$$\Gamma_p(\xi_{i1},\cdots,\xi_{ip}) = (-1)^n \frac{\partial^n e^{-\frac{1}{2}\vec{\xi}^T\vec{\xi}}}{\partial\xi_{i1},\cdots,\partial\xi_{ip}} e^{\frac{1}{2}\vec{\xi}^T\vec{\xi}} \qquad (4 - 2)$$

Where the vector $\vec{\xi}$ consists of n Gaussian random variables.

Then $u(\theta)$ can be written more simply as

$$u(\theta) = \sum_{i=0}^{P} b_i \Psi_i(\vec{\xi}(\theta)) \qquad (4 - 3)$$

Where b_i and $\Psi_i(\vec{\xi}(\theta))$ are one to one correspondences between the coefficients $a_{i1},\cdots,a_{ip}$ and the functions $(\xi_{i1},\cdots,\xi_{ip})$, respectively.

4.2 Stochastic approximation

One of the uses for stochastic expansion is the non-intrusive formulation to create a surrogate model of stochastic responses using PCE. The methodology is presented using a simple example. If we fit curvilinear data, the following regression model can be considered:

$$Y(\mathrm{x}) = \beta_0 F_0(\mathrm{x}) + \beta_1 F_1(\mathrm{x}) + \beta_2 F_2(\mathrm{x}) + \beta_3 F_3(\mathrm{x}) \qquad (4 - 4)$$

Where β_0 , β_1 , β_2 , β_3 represent the mean, linear, quadratic and cubic effect, respectively, of the response; Y and $F_i(\mathrm{x})$ are basis polynomials

It is obvious that the use of orthogonal polynomial can eliminate collinearity and ill-conditioned problems. The basic idea of the stochastic approximation utilizing stochastic expansion is to select an appropriate basis function to represent the response of uncertain systems. The PCE, which employs orthogonal basis functions and is mean-square convergent, is a good choice for estimating the response variability of uncertain systems.

PCE can be used to represent the response of an uncertain system in the non-intrusive formulation. The basic idea of this approach is to project the response and stochastic system operator onto the stochastic space spanned by PCE, with the

projection coefficients, b_i ,being evaluated through an efficient sampling scheme. We first define vector x at a particular point $(\xi_i, \cdots, \xi_m)$ of random variables.

The estimated response at this point is

$$y(\mathrm{x}) = \mathrm{x}^T \hat{\beta} \tag{4 - 5}$$

Where $\hat{\beta}$ is a set of undetermined coefficients of PCE.

Generally, the method of least squares is used to obtain the regression coefficients for n sample values of x and y as

$$\hat{\beta} = (\mathrm{X}^T \mathrm{X})^{-1} \mathrm{X}^T Y \tag{4 - 6}$$

Where X is a n*p matrix of the levels of the regressor variables and Y is a n*l vector of the responses.

The fitted model $\hat{Y}$ and the residuals e are

$$\hat{Y} = X\hat{\beta} \tag{4 - 7}$$

And $e = Y - \hat{Y}$

Once the analyst determines, various statistics can be obtained including the mean, variance, and confidence interval of the stochastic responses. A confidence interval indicates a range of values that likely contains the analysis results. Generally, the confidence interval of any parameter includes two parts: the confidence level and margin of error.

The confidence level denotes the probability with which the interval contains the true parameter value. The margin of error represents how accurate our guess of the true parameter value is. Where x_0 is the vector at a particular point $(\xi_i, \cdots, \xi_m)$ of random variables. Then, the estimated mean response at this point is

$$\hat{y}(\mathrm{x}_0) = x_0^T \hat{\beta} \tag{4 - 8}$$

Where $\hat{\beta}$ is a set of undetermined coefficients of PCE. A $100(1-\alpha)$ percent confidence interval at the particular point x_0 is

$$\hat{y}(\mathrm{x}_0) - \mathrm{t}_{\frac{\alpha}{2},\mathrm{v}} \sqrt{\sigma^2 x_0^T (\mathrm{X}^T \mathrm{X})^{-1} x_0} \;\le\; \mu \;\le\; \hat{y}(\mathrm{x}_0) + \mathrm{t}_{\frac{\alpha}{2},\mathrm{v}} \sqrt{\sigma^2 x_0^T (\mathrm{X}^T \mathrm{X})^{-1} x_0} \qquad (4 - 9)$$

Where σ^2 is variance, v is degree of freedom and α indicates the $100(1-\alpha)$ th percentile of the t distribution. The point x_0 is not limited to one of the sampling points used, since the interval includes the results of random samples from the given population with mean μ.

Gamma distribution or exponential distributions, which are widely used in engineering and science disciplines, should be represented by normal probability distribution.

Table 4 - 1 Representation of various distributions as functionals of normal random variables

Distribution Type	Transformation
Normal (μ,σ)	$\mu+\sigma\xi$
Lognormal (μ,σ)	$\exp(\mu+\sigma\xi)$
Uniform (a,b)	$a+(\mathrm{b}-\mathrm{a})\left(\frac{1}{2}+\frac{1}{2}erf(\frac{\xi}{\sqrt{2}})\right)$
Exponential (λ)	$-\frac{1}{\lambda}\log\left(\frac{1}{2}+\frac{1}{2}erf(\frac{\xi}{\sqrt{2}})\right)$
Gamma (a,b)	$ab\left(\xi\sqrt{\frac{1}{9a}}+1-\frac{1}{9a}\right)^3$

4.3 Hermite Polynomials and Gram-Charlier Series

Before beginning the topic of the KL transform, it is useful to see several properties of the Hermite polynomial, which is the basis of the PCE. The construction of Hermite Polynomial was described by Pafnuty Chebyshev and Charles Hermite. The second-order differential equation is given by

$$\frac{d^2y}{dx^2} - x\frac{dy}{dx} + ny = 0 \quad \text{Or} \quad \frac{d^2y}{dx^2} - 2x\frac{dy}{dx} + 2ny = 0 \qquad (4 - 10)$$

Where n is a positive integer. The corresponding possible solutions are

$$H_n(\mathrm{x}) = (-1)^n e^{x^2/2} \frac{d^n e^{-x^2/2}}{dx^n}$$

$$\text{Or} \quad H_n(\mathrm{x}) = (-1)^n e^{x^2} \frac{d^n e^{-x^2}}{dx^n} \tag{4 - 11}$$

These polynomials are called the Hermite polynomials. Although these two equations are not equivalent, the first is a linear rescaling of the domain of the second. Since the n^{th} derivative of the normal density function, $\varphi(\mathrm{x}) = 1/\sqrt{2\pi}\, e^{-x^2/2}$ is included in this equation, the definition of Equation is often used in probabilistic analysis.

The orthogonal properties of the Hermite polynomials are given in the interval $[-\infty, +\infty]$ with respect to the weight function of $e^{-x^2/2}$ or e^{-x^2}:

$$\int_{-\infty}^{\infty} e^{-x^2/2} H_n(\mathrm{x}) H_m(\mathrm{x}) dx = n!\sqrt{2\pi}\delta_{nm} \tag{4 - 12}$$

And $\int_{-\infty}^{\infty} e^{-x^2} H_n(\mathrm{x}) H_m(\mathrm{x}) dx = 2^n n!\sqrt{\pi}\delta_{nm}$

It implies that the Hermite polynomials are orthogonal with respect to the Gaussian distribution. Also, notice that the weight functions, $e^{-x^2/2}$ or e^{-x^2}, help keep the integral from reaching infinity over the interval from $-\infty$ to ∞, since the exponential functions converge to zero much faster than the polynomials blow up when x is large.

$$H_n(x) = (-1)^n e^{x^2/2} \frac{d^n}{dx^n} e^{-x^2/2} \tag{4 - 13}$$

$$\begin{cases} H_0(x) = 1 \\ H_1(x) = x \\ H_2(x) = x^2 - 1 \\ H_3(x) = x^3 - 3x \\ H_4(x) = x^4 - 6x^2 + 3 \\ H_5(x) = x^5 - 10x^3 + 15x \end{cases} \tag{4 - 14}$$

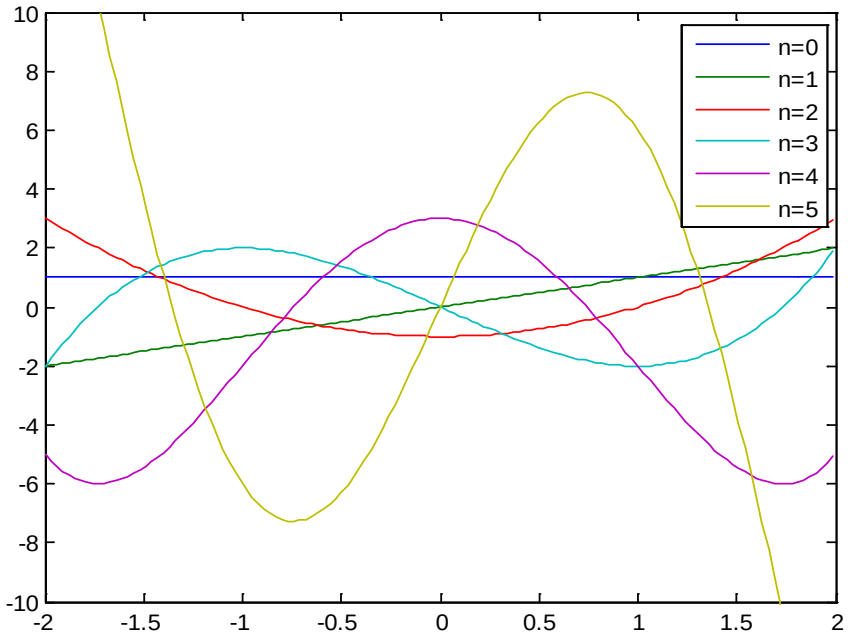

Fig 4 - 1 Hermite polynomials

When this orthogonal property of the Hermite polynomials is used to estimate the probability density function, the procedure is known as the Gram-Charlier method. The basic idea of Gram-Charlier method is that the density function of the Gaussian distribution and its derivatives provide a series expansion to represent an arbitrary density function. The Gram-Charlier series is given by

$$f(\mathrm{x}) = \mathrm{b}_0\,\varphi(\mathrm{x}) + \mathrm{b}_1\,\varphi'(\mathrm{x}) + \mathrm{b}_2\,\varphi''(\mathrm{x}) + \cdots \tag{4 - 15}$$

Where $f(\mathrm{x})$ denotes the unknown probability density function, and $\varphi^{n}(\mathrm{x})$ is the n^{th} derivative of the normal density function, $\varphi(\mathrm{x}) = 1/\sqrt{2\pi}\,e^{-x^2/2}$

$$H_n(\mathrm{x}) = (-1)^n \frac{\varphi^{(\mathrm{n})}(\mathrm{x})}{\varphi(\mathrm{x})} \tag{4 - 16}$$

$$\varphi^{(\mathrm{n})}(\mathrm{x}) = (-1)^n \varphi(\mathrm{x}) H_n(\mathrm{x}) \tag{4 - 17}$$

Then

$$\begin{aligned} f(\mathrm{x}) &= \varphi(\mathrm{x})\left[b_0 H_0(\mathrm{x}) - b_1 H_1(\mathrm{x}) + b_2 H_2(\mathrm{x}) + \cdots\right] \\ &= \varphi(\mathrm{x}) \sum_{m=0}^{\infty} (-1)^m b_m H_m(\mathrm{x}) \end{aligned} \tag{4 - 18}$$

To find the b_i coefficient, multiply both sides by $H_n(\mathrm{x})$ and integrate from $-\infty$ to ∞. The result is

$$\int_{-\infty}^{\infty} f(\mathrm{x}) H_n(\mathrm{x}) dx = \sum_{m=0}^{\infty} (-1)^m b_m \int_{-\infty}^{\infty} \varphi(\mathrm{x}) H_n(\mathrm{x}) H_m(\mathrm{x}) dx \qquad (4 - 19)$$

Because of the orthogonal property of the Hermite polynomials

$$\int_{-\infty}^{\infty} \varphi(\mathrm{x}) H_n(\mathrm{x}) H_m(\mathrm{x}) dx = \begin{cases} n! & for \ \ \mathrm{n} = \mathrm{m} \\ 0 & for \ \ n \neq m \end{cases} \qquad (4 - 20)$$

This property can be used to compute the coefficient,

$$\mathrm{b}_n = \frac{(-1)^n}{n!} \int_{-\infty}^{\infty} f(\mathrm{x}) H_n(\mathrm{x}) dx \qquad (4 - 21)$$

4.4 Karhunen-Loeve (KL) Transform

The primary challenge of a stochastic analysis is to discover effective ways to represent the various types of uncertainty information and to use the information to evaluate the safety of structural systems in such a way that the computational effort of the analysis is minimized. Many engineering properties in structural analysis are distributed in space and time domains. For example, material properties, like Young's modulus and distributed dynamic loads, vary over the space or time domain of the structure. The description of such space-and –time-varying quantities can be represented by the concept of the random field. This section presents an efficient way of handling spatially-correlated data and dimensionality reduction of the random variables by using the KL transform.

Due to the simplicity of its procedure, the most widely used method of multivariate data analysis is the orthogonal transform method. The KL transform is a viable tool with multiple uses for uncertainty analysis because it can generate correlated random variables and effectively reduce the dimensionality of the correlated data set.

The KL expansion can be viewed as part of a general orthogonal series expansion. Consider a general series expansion of $f(\mathrm{x})$ with a complete set of orthogonal and normalized base functions $\phi_i(\mathrm{x})$:

$$f(\mathrm{x}) = \sum_{i=1}^{N} \mathrm{b}_i \phi_i(\mathrm{x}) \tag{4 - 22}$$

Where the coefficients b_i represent the projection of $f(\mathrm{x})$ on the basis function $\phi_i(\mathrm{x})$ and b_i are obtained by

$$\mathrm{b}_i = \int f(\mathrm{x})\phi_i(\mathrm{x})dx \tag{4 - 23}$$

The condition of uncorrelated coefficients yields

$$\left\langle (\mathrm{b}_i - \mu_i)(\mathrm{b}_j - \mu_j) \right\rangle = \lambda_j \delta_{ij} \tag{4 - 24}$$

Where $\langle \bullet \rangle$ indicates the expected value operation, δ_{ij} is the Kronecker delta, and μ is the mean of the coefficients b. This restriction results in the following eigenvalue analysis of the covariance function

$$\lambda_i \phi_i(\mathrm{x}) = \int K(\mathrm{x}, \mathrm{y})\phi_i(\mathrm{y})\,\mathrm{dy} \tag{4 - 25}$$

Where $\phi_i(\mathrm{x})$ and λ_i denote the eigen-functions and eigen-values of the covariance function $K(\mathrm{x}, \mathrm{y})$, respectively, and x and y are the temporal or spatial coordinates:

$$K(\mathrm{x}, \mathrm{y}) = \left\langle (\mathrm{b}(\mathrm{x}) - \mu(\mathrm{x}))(\mathrm{b}(\mathrm{y}) - \mu(\mathrm{y})) \right\rangle \tag{4 - 26}$$

Where $\mu(\mathrm{x})$ is the mean of the coefficients $\mathrm{b}(\mathrm{x})$.

The series of the eigen functions and the eigen values forms the KL expansion:

$$w(\mathrm{x}) = \sum_{i=1}^{\infty} \sqrt{\lambda_i}\, \xi_i \phi_i(\mathrm{x}) \tag{4 - 27}$$

Where ξ_i is a set of uncorrelated random variables, and this expansion expresses the projection of the random process $w(\mathrm{x})$.

In the discrete case

$$[P][\Lambda] = [K][P] \tag{4 - 28}$$

Where the covariance matrix $[K]$ is a symmetric and nonnegative definite matrix, and $[P]$ and $[\Lambda]$ are the orthogonal eigenvector matrix and the eigenvalue matrix, respectively.

Consequently, the orthogonal decomposition of the covariance matrix provides the product of the matrices of eigen vectors and eigen values:

$$[K]=[P][\Lambda][P]^T \tag{4 - 29}$$

Or $[K]=[A][A]^T$

Where $[A]$ is the transform matrix chosen as $[A]=[P][\Lambda]^{1/2}$.

The transform matrix $[A]$ can be employed to yield the correlated random vector T:

$$[T]=[A][X] \tag{4 - 30}$$

Where $[X]$ is the (n*1) matrix of uncorrelated random variables $X_j, (\mathrm{j}=1,\cdots,\mathrm{n})$, and the transformed matrix, $[T]$, possesses a given covariance matrix $[K]$.

In addition to generating the dependent random variables, T, the KL transform can be used to reduce the dimension of the random variables. The main advantage of this procedure is to permit significant reduction in the number of uncorrelated random variables that represent random fields, especially for high levels of correlation.

4.5 KL Expansion to solve Eigen value problem

The KL expansion can be derived based on the analytical properties of its covariance function. Let the covariance function be specified by the exponential covariance with a variance of C_0, correlation length of $1/h$, and two different location of x_1 and x_2 defined in $[-a \le x_1, x_2 \le a]$:

$$K(x_1, x_2)=\mathrm{C}_0\, e^{-h|x_1-x_2|}, \quad -a \le x_1, x_2 \le a \tag{4 - 31}$$

Then $\lambda_i\phi_i(\mathrm{x})=\int K(\mathrm{x},\mathrm{y})\phi_i(\mathrm{y})\,\mathrm{dy}$ can be written as

$$\lambda\phi(x_1) = \int_{-a}^{a} \mathrm{C}_0\, e^{-h|x_1 - x_2|}\phi(x_2)\,\mathrm{d}\,x_2 \qquad (4 - 32)$$

We need to solve the above equation by converting the integral equation to a differential equation, and then substituting the solution back into the integral equation. To eliminate the absolute magnitude sign,

$$\lambda\phi(x_1) = \int_{-a}^{x_1} \mathrm{C}_0\, e^{-h(x_1 - x_2)}\phi(x_2)\,\mathrm{d}\,x_2 + \int_{x_1}^{a} \mathrm{C}_0\, e^{h(x_1 - x_2)}\phi(x_2)\,\mathrm{d}\,x_2 \qquad (4 - 33)$$

Defining $\omega = (2C_0 h - h^2\lambda)/\lambda$

$$\phi''(x_1) + \omega^2\phi(x_1) = 0 \qquad -a \le x_1 \le a \qquad (4 - 34)$$

Letting $x_1 = t$

$$\phi(t) = c_1 e^{j\omega t} + c_2 e^{j\omega t},\ \omega^2 \ge 0 \qquad (4 - 35)$$

Where, c_1 and c_2 are constants.

Applying the boundary condition, yields

$$(\mathrm{h} - \omega\tan(\omega\,\mathrm{a}))(\omega + h\tan(\omega\,\mathrm{a})) = 0$$

$$\mathrm{h} - \omega\tan(\omega\,\mathrm{a}) = 0 \text{ or } \omega + h\tan(\omega\,\mathrm{a}) = 0$$

The values of ω can be determined graphically or numerically, and the corresponding eigen values are

$$\lambda_i = \frac{2\,\mathrm{C}_0\, h}{h^2 + \omega_i^2} \ ,\ \text{i=1,2,3,…..,n} \qquad (4 - 36)$$

The resulting eigen function are

$$\phi_i(t) = \frac{\cos\omega_i t}{\sqrt{a + \dfrac{\sin(2\omega_i a)}{2\omega_i}}} \quad \text{(for, i=odd)},\ -a \le t \le a \qquad (4 - 37)$$

$$\phi_i(t) = \frac{\sin\omega_i t}{\sqrt{a - \dfrac{\sin(2\omega_i a)}{2\omega_i}}} \quad \text{(for, i=even)},\ -a \le t \le a \qquad (4 - 38)$$

After graphical or numerical solution of transcendental equations for ω_i , the eign functions can be given as a set of periodic sines and cosines at approximately $(\mathrm{i}-1)\pi/2$

4.6 Spectral Stochastic Finite Element Method

PCE is used to represent stochastic responses, and the KL expansion is used to represent the input of random fields in the intrusive formulation procedure. This method is also known as the SSFEM and yields appropriate results for a wide range of random fluctuations[78].

4.6.1 Role of KL expansion in SSFEM

Recall that in the KL expansion a series of eigen functions and eigen values with a set of random variables ξ_i represent the random process. The eigen values and eigen functions can be obtained. Let $w(\mathrm{x},\theta)$ denote a random process, so that the function can be expanded in the following form, truncated to M terms:

$$w(\mathrm{x},\theta) = \bar{\mathrm{w}}(\mathrm{x}) + \sum_{i=1}^{M} \sqrt{\lambda_i}\,\xi_i(\theta)\phi_i(\mathrm{x}) \qquad (4\text{ - }39)$$

Where $\bar{\mathrm{w}}(\mathrm{x})$ denotes the expected value of the random process, and θ represents an outcome in the space of possible outcomes of a random event.

Suppose the Young's modulus is a Gaussian random field. Then, the elasticity matrix D can be written as

$$D(\mathrm{x},\theta) = w(\mathrm{x},\theta)D_0 \qquad (4\text{ - }40)$$

Where D_0 is a constant matrix similar to the one in deterministic finite element analysis.

The element stiffness matrix is

$$K^e(\theta) = \mathrm{K}_0^{(\mathrm{e})} + \sum_{i=1}^{M} \mathrm{K}_i^{(\mathrm{e})}\,\xi_i(\theta) \qquad (4\text{ - }41)$$

Where $\mathrm{K}_0^{(\mathrm{e})}$ is the mean element stiffness matrix and

$$\mathrm{K}_i^{(\mathrm{e})} = \sqrt{\lambda_i} \int_{\Omega_e} \phi(\mathrm{x})\, \mathrm{B}_e^T D_0 B_e d\Omega^e \tag{4 - 42}$$

Where B_e is the matrix determined from the shape functions and geometric condition of the finite element.

Assembling the above element contributions in the finite element analysis procedure eventually gives

$$\left[K_0 + \sum_{i=1}^{M} K_i \xi_i(\theta) \right] u(\theta) = \mathrm{f} \tag{4 - 43}$$

$$K_0 \left[I + \sum_{i=1}^{M} K_0^{-1} K_i \xi_i(\theta) \right] u(\theta) = \mathrm{f} \tag{4 - 44}$$

$$\left[I + \sum_{i=1}^{M} K_0^{-1} K_i \xi_i(\theta) \right] u(\theta) = u_0 = K_0^{-1} f \tag{4 - 45}$$

It leads to

$$u(\theta) = \left[I + \sum_{i=1}^{M} K_0^{-1} K_i \xi_i(\theta) \right]^{-1} u_0 \tag{4 - 46}$$

Now, the displacement vector can be obtained by the Neumann series

$$u(\theta) = \sum_{i=0}^{\infty} (-1)^i \left(\sum_{n=1}^{M} K_0^{-1} K_n \xi_n(\theta) \right)^i u_0 \tag{4 - 47}$$

Applying the expected value operator, the mean of the response yields

$$E[u] = \sum_{i=0}^{\infty} (-1)^i E\left[\left(\sum_{n=1}^{M} K_0^{-1} K_n \xi_n(\theta) \right)^i u_0 \right] \tag{4 - 48}$$

In a general case, the covariance matrix yields

$$Cov[u,u] = \sum_{i=0}^{\infty} \sum_{j=0}^{\infty} (-1)^{i+j} E\left[\left(\sum_{n=1}^{M} K_0^{-1} K_n \xi_n \right)^i K_0^{-1} f \times f^T K_0^{-T} \left(\sum_{m=1}^{M} K_m^T K_0^{-T} \xi_m \right)^j \right] \tag{4 - 49}$$

Obviously, the KL expansion requires known covariance functions to obtain the eigen values and eigen functions. Since the covariance function of stochastic responses often is not known, PCE is used to represent stochastic responses in SSFEM.

4.6.2 Role of PCE in SSFEM

Recalling the definition of PCE, $u(\theta)$ can be projected on the expansion

$$u(\theta) = \sum_{j=0}^{\infty} b_j \psi_j(\theta) \tag{4 - 50}$$

Then in finite element model

$$\left(\sum_{i=1}^{\infty} K_i \xi_i(\theta) \right) \left(\sum_{j=0}^{\infty} b_j \psi_j(\theta) \right) = f \tag{4 - 51}$$

Truncating the KL expansion after M terms and PCE after P terms results in

$$\sum_{i=0}^{M} \sum_{j=0}^{P} \xi_i(\theta) \psi_j(\theta) K_i b_j - f = \varepsilon \tag{4 - 52}$$

Minimization of the residual leads to an accurate approximation of the solution $u(\theta)$. This requires the residual to be orthogonal to the approximating space spanned by the PCE. Orthogonality requires the inner product be equal to zero, namely,

$$E\left[\varepsilon \cdot \Psi_k\right] = 0 \tag{4 - 53}$$

Thus, the expected value of $\sum_{i=0}^{M} \sum_{j=0}^{P} \xi_i(\theta) \psi_j(\theta) K_i b_j - f = \varepsilon$ become

$$\sum_{i=0}^{M} \sum_{j=0}^{P} E\left[\xi_i(\theta) \Psi_j(\theta) \Psi_k(\theta) \right] K_i b_j = E\left[f \Psi_k(\theta) \right] \quad k = 0, \cdots, P \tag{4 - 54}$$

Which can be rewritten as

$$\sum_{j=0}^{P} K_{jk} b_j = f_k \tag{4 - 55}$$

Where

$$K_{jk} = \sum_{i=0}^{M} C_{ijk} K_i \tag{4 - 56}$$

$$C_{ijk} = E\left[\xi_i(\theta)\Psi_j(\theta)\Psi_k(\theta)\right] \tag{4 - 57}$$

$$f_k = E\left[f\,\Psi_k(\theta)\right] \tag{4 - 58}$$

In matrix, we can rewrite as

$$\begin{bmatrix} K^{(0,0)} & K^{(0,1)} & \cdots & K^{(0,\mathrm{P})} \\ K^{(1,0)} & K^{(1,1)} & \cdots & K^{(1,\mathrm{P})} \\ \vdots & \vdots & \ddots & \vdots \\ K^{(\mathrm{P},0)} & K^{(\mathrm{P},1)} & \cdots & K^{(\mathrm{P},\mathrm{P})} \end{bmatrix} \begin{Bmatrix} b^{(0)} \\ b^{(1)} \\ \vdots \\ b^{(\mathrm{P})} \end{Bmatrix} = \begin{Bmatrix} f^{(0)} \\ f^{(1)} \\ \vdots \\ f^{(\mathrm{P})} \end{Bmatrix} \tag{4 - 59}$$

There is a P+1 dimensional matrix

Once the system is computed with the coefficient vectors b_j, the statistics of the solution can be readily obtained. The mean and covariance matrix of $u(\theta)$ can be obtained as

$$E\left[u(\theta)\right] = b_0 \tag{4 - 60}$$

$$Cov\left[u,u\right] = E\left[(\mathrm{u}-\mathrm{u}_0)(\mathrm{u}-\mathrm{u}_0)^T\right] = \sum_{j=1}^{P} E\left[\Psi_j^2\right] b_j b_j^T \tag{4 - 61}$$

Multi-dimensional Hermite orthogonal polynomials are firstly proposed to represent Gaussian stochastic process by Wiener, based on which a spectral stochastic finite element method is developed by Ghanem and Spanos and widely used in various applications, including structural mechanics, fluid flow, etc[79].

The efficient method for UA aims to reduce the time for a single reliability analysis or moment evaluation procedure, and the advanced formulation is to reduce the number of UA. Establish an explicit relation between the probability of failure/moments and the design variables.

- Sequential quadratic programming (SQP) method is one of the most used methods, a standard mathematical programming algorithm for solving non-linear programming optimization problems. This method can assure a local optimum but not a global one. This shortcoming may be avoided by multiple initial design (evolutionary algorithm, genetic algorithm these approaches no gradient information is needed)

- Perturbation method is based on Taylor series expansion in terms of a set of zero mean random variables. It can be used advantageously in cased where the random fluctuations are small compared with the nominal structure, such that terms of order two or higher are negligible. The perturbation method has the capability to determine the uncertainties without large dispersion, especially for moment evaluations of the random response. There is less applications of such method to reliability analysis.
- Polynimial chaos expansion method. In the framework of the polynomial chaos expansion, the random response can be approximated with an acceptable accuracy.

The main advantage of the PCE compared to the K-L expansion is that the covariance structure is not required.

PCE, from the efficiency point of view, is more applicable for problems with small number of random inputs. This situation is more involved with static problems rather than dynamic ones since the stochastic excitation is discretized by a uncertainty sequence with high dimension.

4.7 Examples

4.7.1 Orthogonal polynomial

In the one-dimensional case, we can expand the random response u using orthogonal polynomials in ξ, which has a known probability distribution such as unit normal, $N[0,1]$. If u is a function of a normally distributed random variable x, which has the known mean μ_x and variance σ_x^2, ξ is a normalized variable:

$$\xi = \frac{x - \mu_x}{\sigma_x} \tag{4 - 62}$$

Generally, the one-dimensional Hermite polynomials are defined by

$$\Psi_n(\xi) = (-1)^n \frac{\varphi^n(\xi)}{\varphi(\xi)} \tag{4 - 63}$$

Where $\varphi^n(\xi)$ is the n^{th} derivative of the normal density function, $\varphi(\xi) = 1/\sqrt{2\pi} e^{-\xi^2/2}$.

This is simply the single-variable version

$$\{\Psi_i\} = \{1,\ \xi,\ \xi^2 - 1,\ \xi^3 - 3\xi,\ \xi^4 - 6\xi^2 + 3,\ \xi^5 - 10\xi^3 + 15\xi,\ \cdots\} \quad (4 - 64)$$

Thus, a second-order , 2-D PCE is given by

$$u(\theta) = b_0 + b_1\xi_1(\theta) + b_2\xi_2(\theta) + b_3(\xi_1^2(\theta) - 1) + b_4\xi_1(\theta)\xi_2(\theta) + b_5(\xi_2^2(\theta) - 1) \quad (4 - 65)$$

Where $\xi_1(\theta)$ and $\xi_2(\theta)$ are two independent random variables.

Suppose we have a random variable x that is normally/non-normally distributed. This random variable x can be approximated by the first four terms of the PCE as follows:

$$x \approx z(\xi) = b_0 + b_1\xi + b_2(\xi^2 - 1) + b_3(\xi^3 - 3\xi) \quad (4 - 66)$$

Calculate the first four central moments of z in terms of the coefficients b_i.

The standard normal random variable ξ and orthogonal polynomials Ψ_i satisfy

$$\Psi_0 = 1,\ \ E[\Psi_i] = 0 \quad (4 - 67)$$

$$E[\Psi_i\Psi_j] = E[\Psi_i^2]\delta_{ij}\ ,\ \delta_{ij} = \begin{cases} 1, & i = j \\ 0, & i \neq j \end{cases} \quad (4 - 68)$$

Where δ_{ij} is the Kronecker delta.

Suppose the first four moments of a random variable, x, are given by $m_x^1 = 2$, $m_x^2 = 3.2$, $m_x^3 = 7.5$, $m_x^4 = 45$. Estimate the coefficients b_i of z by using the least-square criterion:

Minimize $\sum_{j=1}^{4} f_j^2(b_i)$ $\quad (\mathrm{i} = 1, 2, 3)$

Where $f_1(b_i) = m_z^1 - m_x^1 = 0$

$f_2(b_i) = m_z^2(b_i) - m_x^2$

$f_3(b_i) = m_z^3(b_i) - m_x^3$

$f_4(b_i) = m_z^4(b_i) - m_x^4$

Then we can perform optimization to have solution of coefficients b_i and make sure minimize $\sum_{j=1}^{4} f_j^2(b_i)$

$$E\left[\xi^k\right]=0 \quad \forall k \ \ odd$$

$$E\left[\xi^0\right]=1,\ E\left[\xi^2\right]=1,\ E\left[\xi^4\right]=3,\ E\left[\xi^6\right]=15\ldots$$

$$m_z = b_0$$

$$m_z^2 = E\left[(\mathrm{z}-\mathrm{b}_0)^2\right] = b_1^2 + 2b_2^2 + 6b_3^2$$

$$m_z^3 = E\left[(\mathrm{z}-\mathrm{b}_0)^3\right] = 6b_1^2 b_2 + 8b_2^3 + 36b_1 b_2 b_3 + 108 b_2 b_3^2$$

$$m_z^4 = E\left[(\mathrm{z}-\mathrm{b}_0)^4\right] = 3b_1^4 + 60b_2^4 + 3384b_3^4 + 24b_1^3 b_3 + 60b_1^2 b_2^2 + 252 b_1^2 b_3^2 + 576 b_1 b_2^2 b_3 + 1296 b_1 b_3^3 + 2232 b_2^2 b_3^2$$

Then $b_0 = 2,\ b_1 = -1.545,\ b_2 = 0.628,\ b_3 = 0.141$

$$x \approx z(\xi) = 2 - 1.545\xi + 0.628(\xi^2 - 1) + 0.141(\xi^3 - 3\xi)$$

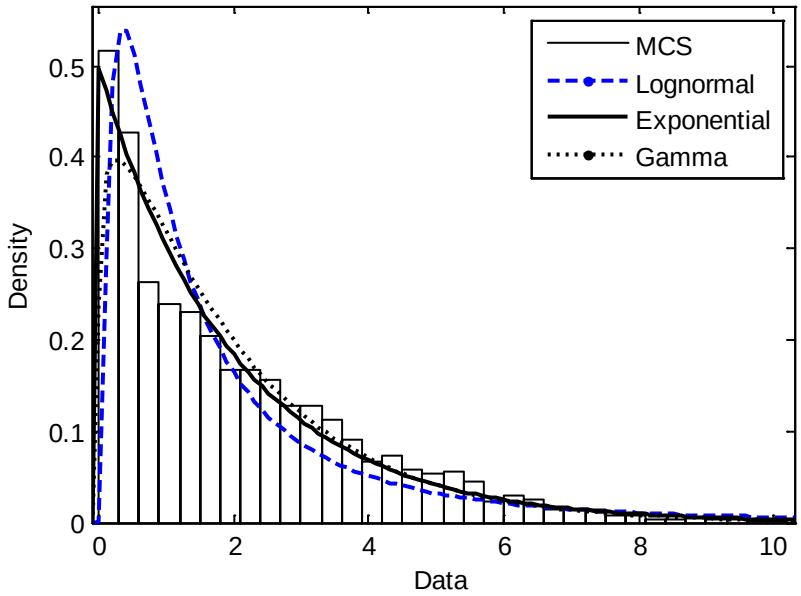

Fig 4 - 2 5000 Gaussian sampling points are generated in the Monte Carlo simulation

$$m^1 = 2.0049,\ m^2 = 3.2364,\ m^3 = 7.0124,\ m^4 = 43.2743$$

4.7.2 Gram-Charlier series

Specify the first seven coefficients of the Gram-Charlier series

$$b_0 = \int_{-\infty}^{+\infty} f(x)dx, \tag{4 - 69}$$

$$b_1 = -\int_{-\infty}^{+\infty} f(x)xdx, \tag{4 - 70}$$

$$b_2 = \frac{1}{2}\int_{-\infty}^{+\infty} f(x)(x^2 - 1)dx, \tag{4 - 71}$$

$$b_3 = -\frac{1}{6}\int_{-\infty}^{+\infty} f(x)(x^3 - 3x)dx, \tag{4 - 72}$$

$$b_4 = \frac{1}{24}\int_{-\infty}^{+\infty} f(x)(x^4 - 6x^2 + 3)dx, \tag{4 - 73}$$

$$b_5 = -\frac{1}{120}\int_{-\infty}^{+\infty} f(x)(x^5 - 10x^3 + 15x)dx, \tag{4 - 74}$$

$$b_6 = \frac{1}{720}\int_{-\infty}^{+\infty} f(x)(x^6 - 15x^4 + 45x^2 - 15)dx, \tag{4 - 75}$$

The n^{th} order central moment can be given by

$$m_x^n = E\left[(\mathrm{X} - \mu_x)^n\right] = \int_{-\infty}^{+\infty} (X - \mu_x)^n f_X(x)dx \tag{4 - 76}$$

Let the first moment be zero $\mu_x = m^1 = 0$

Then

$$b_0 = 1,\ b_1 = 0,\ b_2 = \frac{1}{2}(m^2 - 1),\ \mathrm{b}_3 = -\frac{1}{6}(m^3 - 3m^1)$$

$$\mathrm{b}_4 = \frac{1}{24}(m^4 - 6m^2 + 3),\ b_5 = -\frac{1}{120}(m^5 - 10m^3 + 15m^1),\ b_6 = \frac{1}{720}(m^6 - 15m^4 + 45m^2 - 15)$$

The coefficients of Gram-Charlier series can be expressed by Hermite polynomials in terms of central moments.

Suppose a target covariance matrix is given by

$$[C]=\begin{bmatrix} 1 & 0.63 & 0.75 & 0.92 \\ 0.63 & 1 & 0.96 & 0.84 \\ 0.75 & 0.96 & 1 & 0.72 \\ 0.92 & 0.84 & 0.72 & 1 \end{bmatrix}$$

Generate the correlated random variables (normal distribution), and compare the sample covariance matrix $[\tilde{C}]$

$$P=\begin{bmatrix} 0.4320 & -0.4475 & 0.6166 & 0.4827 \\ 0.5744 & 0.3822 & -0.5195 & 0.5040 \\ -0.4851 & -0.5522 & -0.4547 & 0.5030 \\ -0.4981 & 0.5905 & 0.3784 & 0.5099 \end{bmatrix}$$

$$\Lambda=\begin{bmatrix} -0.0653 & 0 & 0 & 0 \\ 0 & 0.1733 & 0 & 0 \\ 0 & 0 & 0.4807 & 0 \\ 0 & 0 & 0 & 3.4114 \end{bmatrix}$$

$$[A]=[P][\Lambda]^{1/2}=\begin{bmatrix} 0 & -0.1863 & 0.4275 & 0.8915 \\ 0 & 0.1591 & -0.3602 & 0.9309 \\ 0 & -0.2299 & -0.3152 & 0.9291 \\ 0 & 0.2458 & 0.2623 & 0.9418 \end{bmatrix}$$

$$[\tilde{C}_{500}]=\begin{bmatrix} 1.1109 & 0.7590 & 0.8411 & 0.9690 \\ 0.7590 & 1.0681 & 0.9923 & 0.8565 \\ 0.8411 & 0.9923 & 1.1375 & 0.8227 \\ 0.9690 & 0.8565 & 0.8227 & 1.0850 \end{bmatrix}$$

4.7.3 Surrogate model for reliability analysis

The example of Latin hypercube sampling ub finite element model of wing structure in Chapter 3, will be applied here for stochastic expansion in probabilistic analysis. The direct use of stochastic expansions is an efficient choice for representing uncertain parameters because they provide analytically appealing convergence properties.

Effective methods for model updating are generally based on a sensitivity formulation, using a truncated Taylor series expansion[80] [10]. The resulting matrix equation is of the form

$$\{\Delta R\}=[S]\{\Delta P\} \qquad (4 - 77)$$

Where the elements of $\{\Delta P\}$ are the unknown adjustments to design variables that are required to produce the changes $\{\Delta R\}$ between the reference response vector and the actual system responses. The sensitivity matrix $[S]$ contains the gradients of responses with respect to design variables:

$$[S] = S_{ij} = \frac{\partial R_i}{\partial P_j} \tag{4 - 78}$$

These sensitivities can be computed for all physical element properties (material properties; geometrical properties, boundary conditions, mass and spring stiffness) by using direct derivation or perturbation techniques depending on whether mass and stiffness show a proportional or non-proportional behavior with respect to the property.

The most general estimation procedure is the Bayesian parameter estimation algorithm in which relative confidences in initial estimates of the parameters are taken into account together with confidences in the test data[81] [11]. The Bayesian view originates from statistical parameter estimation methods: the responses, as well as the model parameters, are not considered as deterministic values, but as stochastic variables with a certain probability to have the correct value. The confidences in the different measured test values and the confidences in initial parameter estimation can be expressed with weighting matrices for both the response and parameter vectors[82] [12].

In a Bayesian parameter estimation procedure, the discrepancy between initial model predictions[83] [13] and the test data is resolved by minimizing a weighted error

$$E = (\{R\} - \{R^e\})^T [C_R] (\{R\} - \{R^e\}) + (\{P\} - \{P^0\})^T [C_P] (\{P\} - \{P^0\}) \tag{4 - 79}$$

With $\{R\}, \{R^e\}$ are the analytical response and test data vectors respectively;

$\{P\}, \{P^0\}$ are the parameter vector of the final and original model;

$[C_R], [C_P]$ are the weighting matrices expressing confidences in test data and model parameters.

This error can be minimized by taking the partial derivative of Eq.(9) with respect to P_j equal to zero. This leads to:

$$\{P\} = \{P^0\} + [G](\{R^e\} - \{R\}) \tag{4 - 80}$$

With $[G]$ the gain matrix computed as:

$$[G] = [C_P][S]^T([C'_R] + [S][C_P][S]^T)^{-1} \tag{4 - 81}$$

In an iterative procedure, an error function is verified to control convergence. A general form of such error function can be,

$$E = \frac{1}{N}\sum_{i=1}^{N}\frac{|\Delta R_i|}{R_i} \tag{4 - 82}$$

Table 4 - 2 Results of sensitivity anlysis for input variables

	S	D	L	E	P	R
F1	-0.268	-0.103	-0.777	0.513	0.032	0.001
F2	0.013	-0.104	-0.806	0.542	0.028	0.005
F3	-0.260	-0.144	-0.764	0.528	0.026	0.002
F4	0.114	-0.089	-0.783	0.565	0.009	0.005
F5	-0.204	-0.050	-0.688	0.641	-0.053	0.001

The sensitivity of variables are usually expressed as systems of differential equations and analyzed by calculation of partial derivatives of outcome or system variables with respect to the input parameters. Table 4.2 presents the results of sensitivity analysis for the input variables, namely S, D, L corresponding with the geometry of the wing structure and E, P, R, Young's module, Poission ratio and physical density respectively according to the specific material. The results point out that the natural frequencies are very sensitive to the change of length of the wing, additionally Young's module also play an important role to the output variable. In the other hands, the effect of Poisson ratio and physical density is not deserved to pay attention, which will be neglected in the following section. Therefore, S, D, L, E are chosen as the more sensitive parameters to natural frequencies.

The polynomial regression models are used to approximate a structural response or the complete limit state function $G(x)$ of the reliability problem. The limit state function defines the failure domain $D_f = \{x : G(x) \le 0\}$, and the safe domain $D_s = \{x : G(x) > 0\}$ as a function of a vector $x = \{x_1, x_2, ..., x_n\}^T$ of n basic random variables that describe the uncertain quantities of the structural system

A regression model[84] [14] for $G(x)$ can be written as:

$$G(x) = F(\beta : x) + \varepsilon(x) \tag{4 - 83}$$

With

$$F(\beta : x) = \beta_0 + \sum_{i=1}^{n} \beta_i x_i \tag{4 - 84}$$

A polynomial regression model and $\varepsilon(x)$ a random error term that represents the difference between the true limit state function values and the approximate values predicted by Eq.4-84. These random errors are assumed to be independent and normally distributed with zero mean and constant variance.

Where β_0 is the value of the model at the origin of the space of basic random variables, β_i can be interpreted as the gradient in the direction x_i . The total number of regression coefficients to be estimated in this model is p=n+1.

Second-order polynomials of the form,

$$F(\beta : x) = \beta_0 + \sum_{i=1}^{n} \beta_i x_i + \sum_{i=1}^{n} \sum_{j=1}^{n} \beta_{ij} x_i x_j \tag{4 - 85}$$

The regression model parameters β are estimated by fitting the model to a sample of support points.

These models re frequently described in the literature as the realization of a stochastic field. Based on this idealization, the limit state function[85] [15] can be written as

$$G(x) = F(\beta : x) + z(x) \tag{4 - 86}$$

Where $F(\beta:x)$ is a deterministic component defined by a regression model that gives an approximation to $G(x)$ in mean value and $z(x)$ is a stationary Gaussian process with zero mean and covariance ,

$$Cov[z(x), z(x')] = \sigma^2 R(\theta : x, x') \tag{4 - 87}$$

That interpolates the errors between the regression model predictions $F(\beta:x)$ and the true limit state function values $G(x)$ at the m realizations of the vector of basic random variables x, with σ^2 the constant process variance and R is a prescribed correlation function.

Several correlation functions are available, such as the exponential, linear and Gaussian correlation functions, the most widely used correlation function for structural reliability problems is the anisotropic Gaussian correlation function

$$R(\theta : x, x') = \prod_{i=1}^{n} \exp(-\theta_i d_i^2) \tag{4 - 88}$$

With $d_i = x_i - x_i'$ the distance between the evaluation point x and the reference point x' in the ith direction of the basic random variables space and $\theta = [\theta_1, \ldots, \theta_n]^T$ a vector of parameters that define the inverse of the correlation length in each direction.

A kriging interpolation model is completely defined by a vector of regression coefficients β, a vector of correlation parameter θ and the variance σ^2 of the stationary Gaussian process. These parameters are estimated by fitting the Kriging model to a sample of support points.

Where F is the regression matrix and y is the vector of true limit state function values. A 0-order polynomial or first- and second –order polynomials are adopted as regression models $F(\beta:x)$. The matrix R defines the correlation between each pair of support points according to the prescribed correlation function.

The vector of correlation coefficients β and the process variance σ^2 depend on the vector of correlation parameters θ through the correlation matrix R, and therefore θ has to be first estimated using the method of maximum likelihood:

$$\hat{\theta} = \arg\min_{\theta} \{ L(\theta) \} \tag{4 - 89}$$

$$L(\theta) = \left| R(\theta) \right|^{1/m} \sigma^2(\theta) \tag{4 - 90}$$

Its prediction at a given point of the space of basic random variables can be obtained,

$$\hat{G}(x) = f(x)^T \hat{\beta} + r(x)^T \hat{\gamma} \tag{4 - 91}$$

$$\hat{\gamma} = R^{-1}(y - F\hat{\beta}) \tag{4 - 92}$$

$$r(x)^T = [R(\theta : x, x^{(1)}), \ldots, R(\theta : x, x^{(m)})] \tag{4 - 93}$$

A vector with the correlations between the prediction point and the m realizations $x^{(k)}$ $(k = 1, \ldots, m)$ of the vector of basic random variables used in the Kriging model fitting corresponds to the expected or mean value of the Kriging model prediction, an estimate for the variance or uncertainty associated with the model predictions can be given by:

$$\sigma_G^2 = \sigma^2 \left[1 + u(x)^T (F^T R^{-1} F)^{-1} u(x) - r(x)^T R^{-1} r(x) \right] \tag{4 - 94}$$

$$u(x) = F^T R^{-1} r(x) - f(x) \tag{4 - 95}$$

σ_G^2 provides an important index to quantify the uncertainty of predictions and to further adjudge the fitting accuracy. Its existence supplies an approach to improve the design of experiment and to make Kriging more precise.

To compare the results of Kriging model with Latin Hypercube method, probability density of first natural frequency in each method is calculated to demonstrate the accuracy and stability of this surrogate model. Fig 4-3 and Fig 4-4 are the results of different regression in Kriging model by fitting 1000 and 2000 groups of results of Latin Hypercube sampling method. In Fig 4-3, we can find the results of 0 order regression and first order regression are not satisfied, far from the exact probability density of 10000 groups of sampling in Latin Hypercube sampling, especially, the result of 0 order regression in Kriging model is even worse. Fig 4-4 proves the same situation. In the other hand, the results of second order regression in Kriging model are closer to the exact advanced MCS. However, the peak of probability density

curve of Kriging model in our model is lower than that of Latin Hypercube sampling method. A certain point can be found, in the range of smaller than this certain point the probability and probability density of Kriging model is lower than that of Latin Hypercube sampling method. Fig 4-3 , Fig 4-4 also present the advantage of Latin Hypercube sampling method as mentioned in the stochastic simulation, the result of probability distribution of 1000, 2000, and 10000 groups of sampling is convergent and close. Therefore, the second order regression in Kriging model will be applied in the next section while the results of 1000 groups of sampling by Latin Hypercube method are settled as reference.

The discussion of convergence for Kriging model (second order regression) by fitting different amount of sampling groups is concluded in Fig 4-5. It is obvious that the fitting results of 1000, 2000, 5000 groups of sampling are convergent. To make sure the integrity of the sample space, the results of 1000, 2000, 5000 Latin Hypercube sampling are independently performed in stochastic simulation. The results of natural frequencies are calculated in finite element model for each certain sampling iteration. Kriging model as a surrogate model, in it, the second order regression provides convergent and accurate results. In addition, the advantages of Kriging model are not only at their convergence and accuracy, but also reflect at time-saving process. The 5000 Latin Hypercube sampling and performing calculation of natural frequencies of wing structure in the finite element model costs 1955.491 s, and if 1000 sampling, it also cost 371.237 s; while in the surrogate model, fitting 1000 groups of sampling in second order regression only 9.632 s, and predict the corresponding result of 1000 random sampling groups, it costs 10.713 s. The advantage of time-saving is very competitive as a surrogate model.

To test the stability of Kriging model, we applied the Kriging model by second order regression of fitting 1000 groups of Latin Hypercube sampling. In this model, the random sampling spaces are same with the original model and the samples are taken by same probability distribution as in Latin Hypercube method. Fig 4-6 shows the results, the result of 500 groups sampling is not sufficiently satisfied the accuracy, while the results of 1000 groups sampling and 2000 groups are close and convergent.

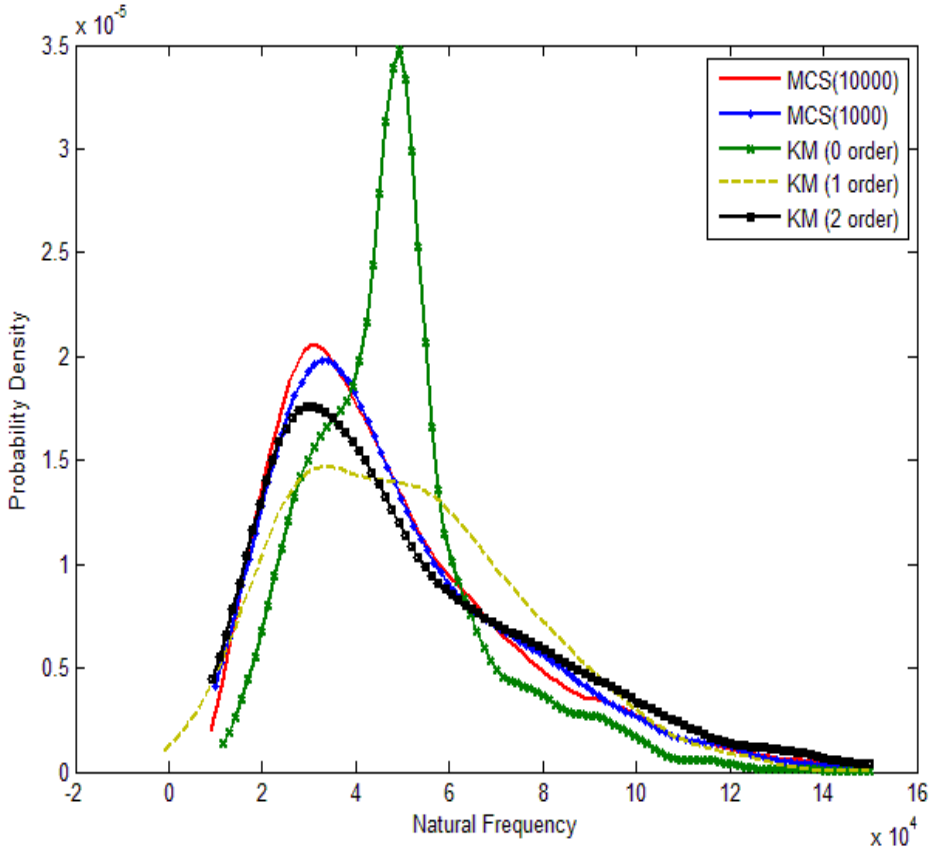

Fig 4 - 3 Kriging model 1000 points fitting result

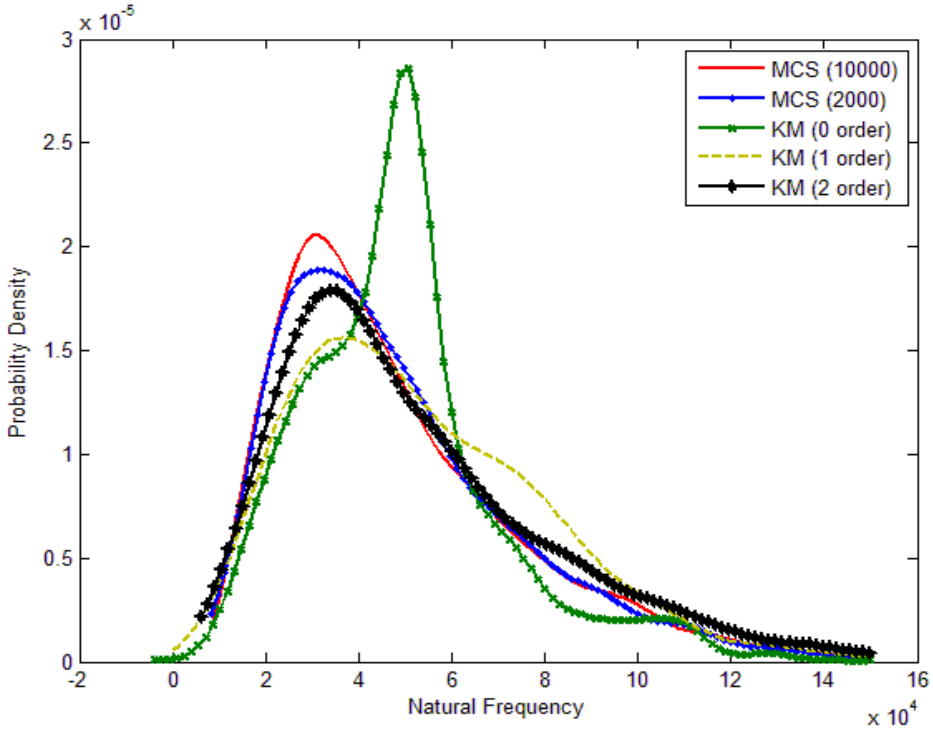

Fig 4 - 4 Kriging model 2000 points fitting results

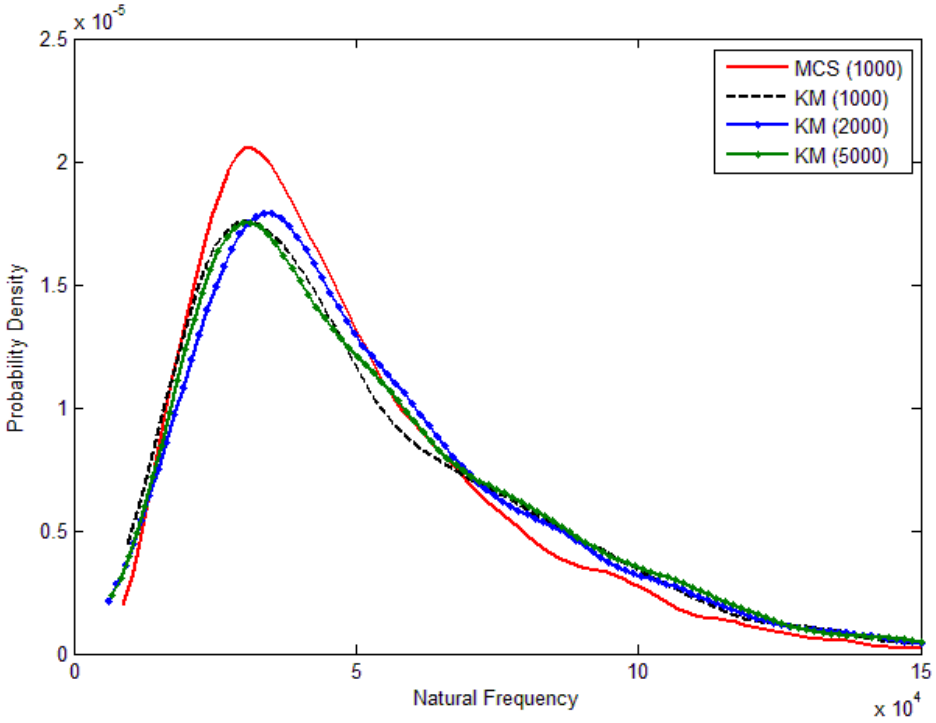

Fig 4 - 5 Second order Kriging model fitting results

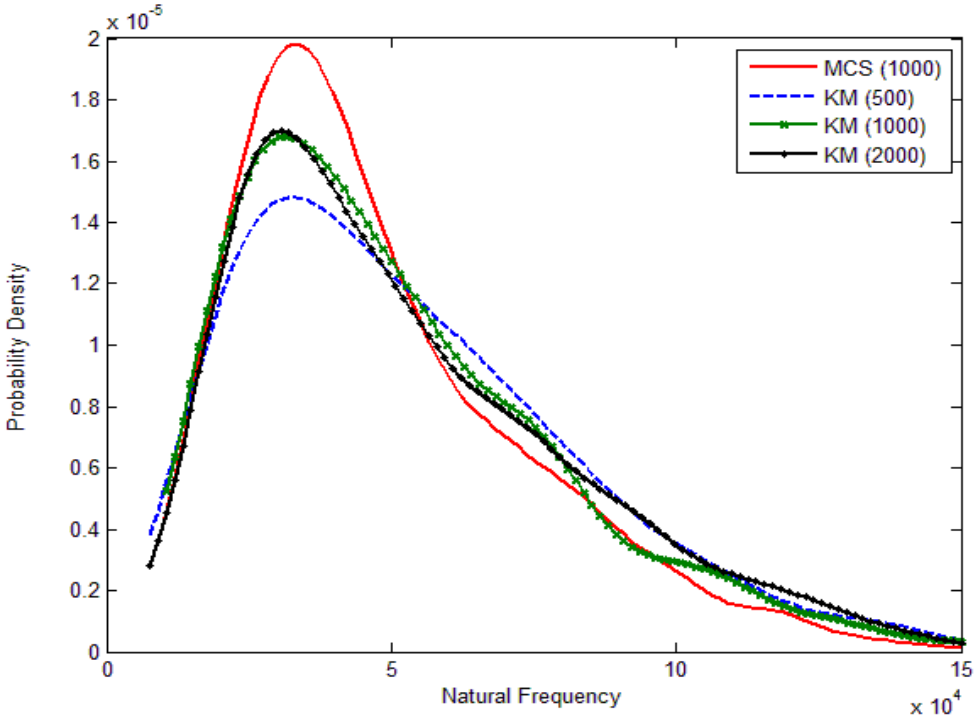

Fig 4 - 6 Stability of results in Kriging model

The results of Monte Carlo simulation are discrete, the disordered arrays are not explicit to the following reliability analysis, Kriging model provides a method to predict

the results in the continuous space. The parameters S, D, L, and E are supposed to be uncertain and fluctuate in a specific range in order to simulate the uncertainties in the real situation. To be general, the type of probability distribution is chosen to be Gaussian distribution, as $(\mu_S, \sigma_S), (\mu_D, \sigma_D), (\mu_L, \sigma_L)$ and (μ_E, σ_E) for the parameters respectively. The mean value of each parameter is searched and discussed to find the relationships between them and the natural frequencies of wing structure. The standard deviation of each parameter is settled by 10% of the scope of each parameter to simulate the fluctuation.

Since the number of the input variables in the Kriging model is 4, it means our problem is beyond 3 dimension. To explicitly present the relationship between the input variables and the output variables (natural frequencies of wing structure), we suppose a function $\mathrm{F}(\mu_S, \mu_D, \mu_L, \mu_E)$, which combine the four parameters together, each of them is independent to the others.

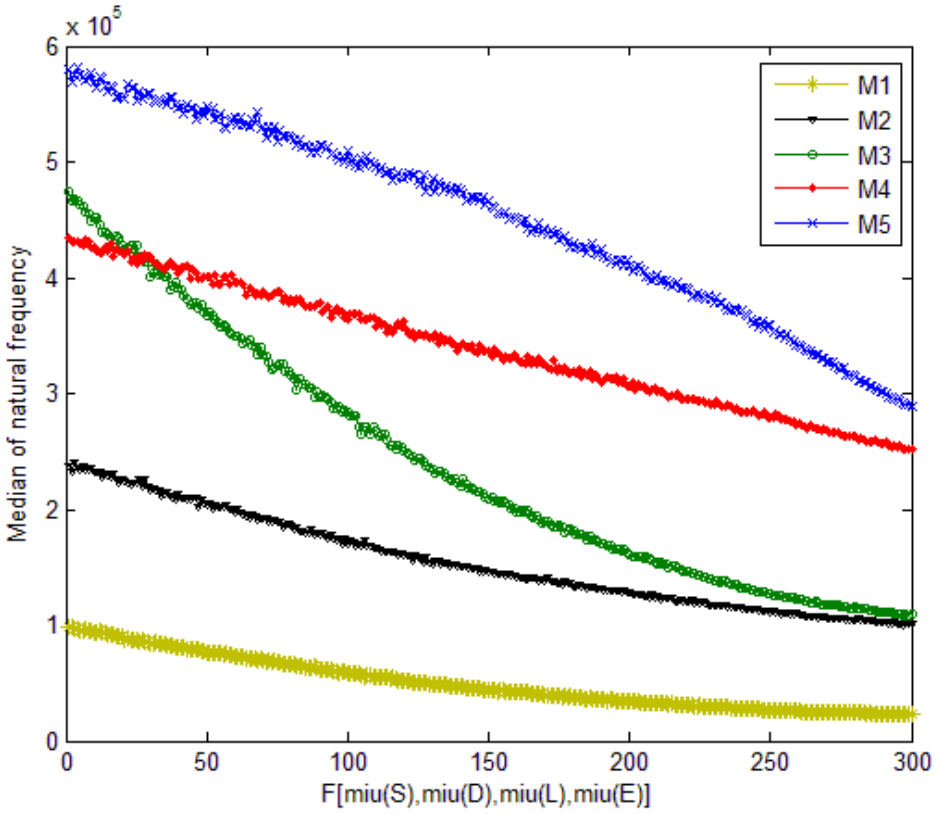

Fig 4 - 7 Results of median value of natural frequency

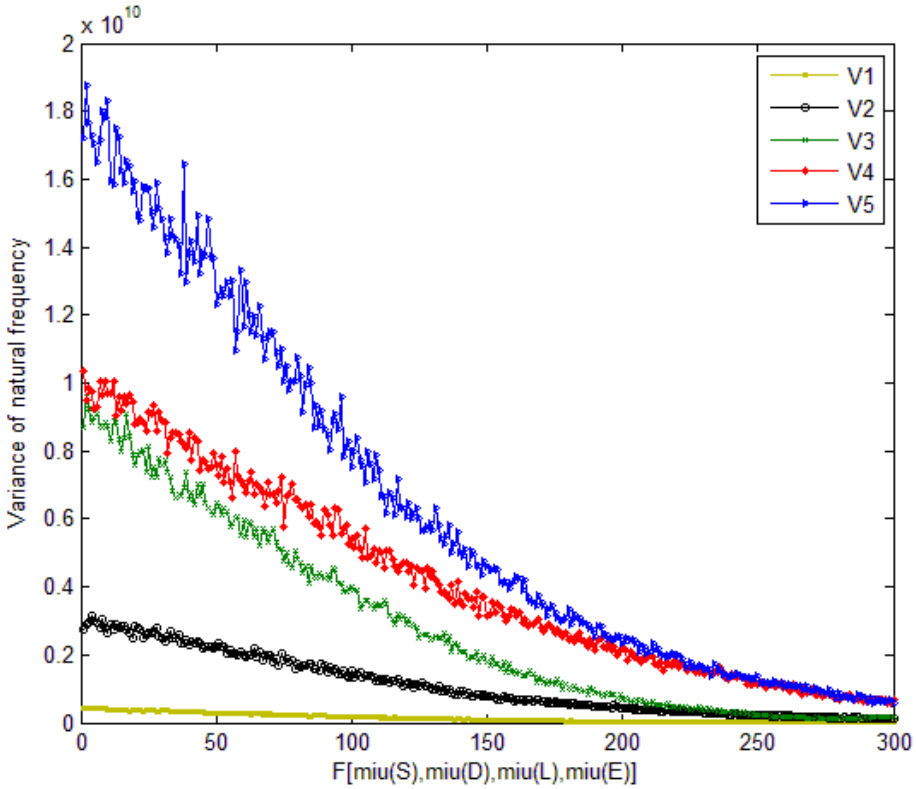

Fig 4 - 8 Results of variance of natural frequency

Fig 4-7 and Fig 4-8 are the results of median value and variance of natural frequency in wing structure respectively. Fig 4-7 presents that according to the increase of μ_S, μ_D, μ_L, μ_E, the median value of natural frequency will reduce, and the third natural frequency has the steepest gradient. The variance of natural frequency in Fig 4-8 has the same tendency, when the $\mathrm{F}(\mu_S, \mu_D, \mu_L, \mu_E)$ increases, the variance of natural frequency will become smaller

In the point of opinion, the variance of natural frequency is smaller, and the difference between two neighbour natural frequencies is larger, the wing structure is safer from the resonance disaster. Fig 4-9 provides important information that the difference of median value between the second and first natural frequency, that between the third and the second natural frequency, and that between the fifth and the forth natural frequency has the same tendency, that have negative gradient with $\mathrm{F}(\mu_S, \mu_D, \mu_L, \mu_E)$. In contrary, the difference of median value between the fourth and the third natural frequency has positive gradient, namely if $\mathrm{F}(\mu_S, \mu_D, \mu_L, \mu_E)$ become larger, m43 will amplify. Fig 4-10 presents the results of belta of natural frequency in wing structure.

The five natural frequencies have the same tendency, belta of them grows when $F(\mu_S, \mu_D, \mu_L, \mu_E)$ increases.

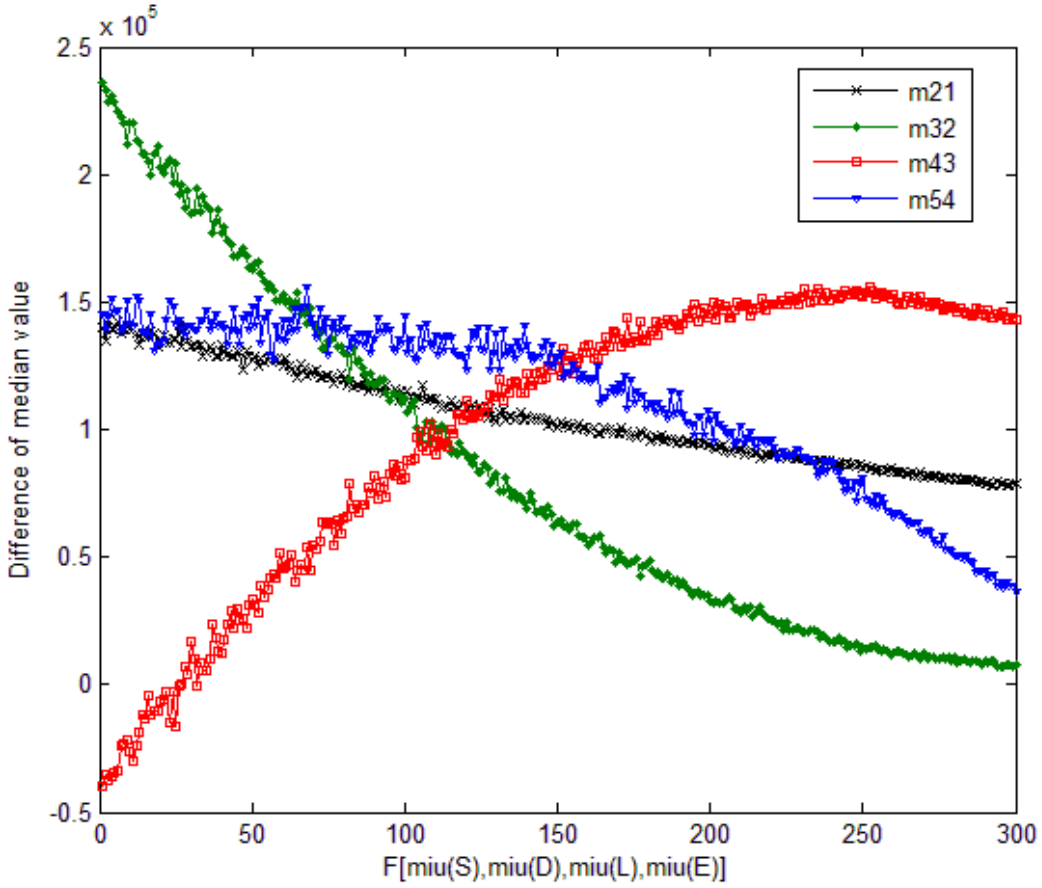

Fig 4 - 9 Difference of median value between two neighbour natural frequencies

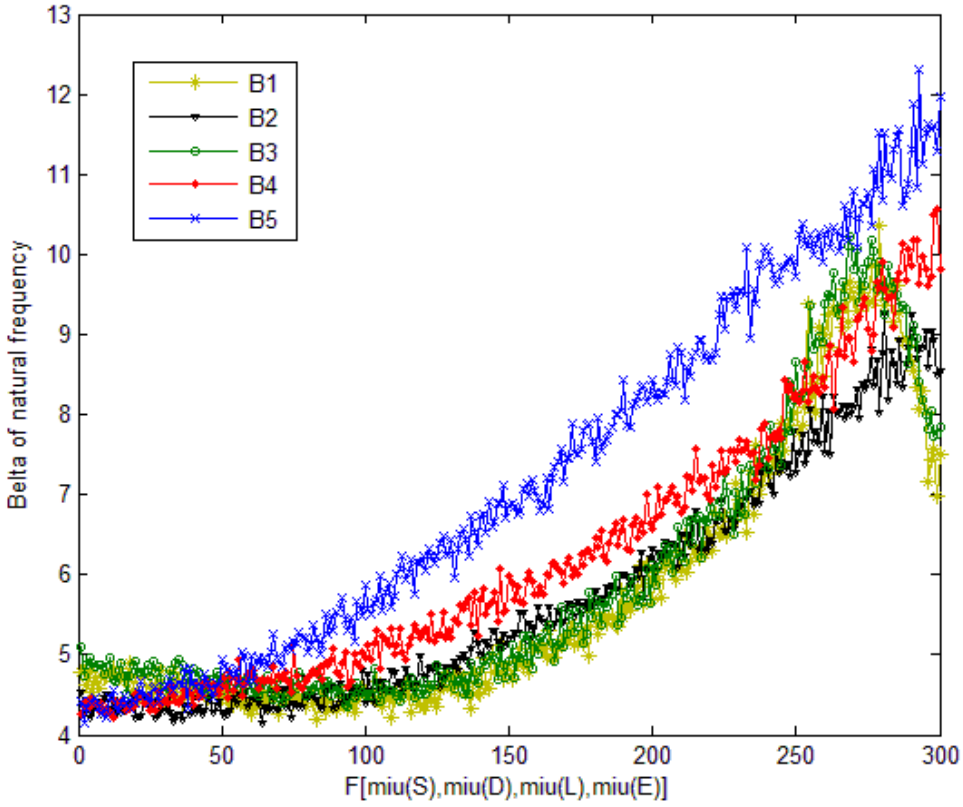

Fig 4 - 10 Results of belta of natural frequency in wing structure

We built a deterministic finite element model to calculate the natural frequencies of wing structure. Latin Hypercube sampling method was applied to propagate the uncertainties in the parameters which corresponding with geometry property and material property. Sensitivity analysis pointed out the more important parameters in the stochastic simulation process. Kriging model as a surrogate model of the stochastic simulation sharply reduce the calculation expense, and also has good accuracy and convergence as discussed. We used the Kriging model in reliability analysis to find the influence of uncertainties in input variables to the natural frequency of wing structure, which should be taken care in order to prevent resonance disaster.

4.8 Conclusion

In this chapter, stochastic expansion for probability analysis is presented. Hermite pomynomial and Gram – Charlier series are introduced and applied in the examples. Karhunen – Loeve expansion and polynomial chaos expansion are important methods in spectral stochastic finite element method as demonstrated. In the example of surrogate model for reliability analysis, we take consideration of natural

frequency of wing structure. Usually, researchers and designers identify the basic natural frequencies of a specific structural system and avoid the periodic loading coincide with them in order to prevent the damage or failure of resonance. In the process of identification of natural frequencies for a structure, the deterministic model is not sufficient because of ignoring the uncertainties and complexities in the real operation situation. Probability method is an effective way to propagate and quantify the uncertainties. We applied advanced Monte Carlo Simulation (Latin Hypercube sampling approach) to perform the parameter fluctuation of the input variables, such as geometrical and material properties as in Chapter 3. Based on the results of MCS, Kriging model is built to reduce the computation burden and provide the continuous model for the following reliability analysis. To relief the heavy computational burden in the simulation process, the sensitivity analysis also was applied and effectively point out the most important parameters which evidently influence the output variables, namely natural frequencies in our research. Second order regression in Kriging model has good accuracy and convergence. In the process of predicting the results of natural frequency of wing structure, Kriging model has satisfied stability. Reliabilty analysis based on Kriging model offers the useful information in preventing as resonance disaster in wing structure.

Chapter 5 Reliability based design optimization

In the field of mechanics, variation in systems, such as loading condition, material properties, geometry, boundary condition, etc. is considered by introducing simplifying hypotheses. These hypotheses are formulated based on past experiences and engineering judgment, by introducing extreme or mean values and/or application of safety factors in the designing process to simplify the problems. However, the traditional approaches of deterministic models are not appropriate because of neglecting the uncertainties and simplifying the problem for analysis. Hence, a proper design procedure must explicitly consider these types of uncertainties, as they may cause significant changes in the performance and reliability of final designs.

Despite of the fact that an adequate level of reliability is a basic objective when designing a system, other design goals may be important as well, there is an increasing demand for structures which are safer and at the same time more economical. In consequence, engineering practice expects to have optimization procedures available which take into account the effects of uncertainty.

Procedures which deal with optimization considering uncertainties are significantly more involved than their deterministic counterparts. Optimization processes requires the evaluation of costly objective and constraint functions numerous times. The associated computation costs are usually prohibitive, especially under uncertain condition, when the system is represented by means of a large and detailed finite element model or when the representation of the loading acting on a structure requires a numerically involved model. Therefore, special procedures must be applied in order to make the design problem tractable. Such procedures include:

1. Application of efficient optimization techniques which require less function calls. These techniques can take advantage of special characteristics of the problem by introducing sequential approximations for representations of the objective function and constraints by reciprocal and/or hybrid variable.
2. Introduction of approximation concepts at different levels of the optimization process.
3. Performing simulation that allowing treat realistic uncertainty models involving

uncertain parameters in an efficient manner.

4. An appropriate computational implementation, computational aspects play a key role, as the systems and structures are large and require detailed modeling. In this regard, parallel computing has become a tool which is steadily gaining interest among researchers and engineers.

5.1 General remarks of RBDO

The fundamental goal in engineering disciplines is to design and construct systems or components that satisfy certain performance objectives during their lifetime. Such objectives cover a wide range of possibilities, control of vibrations induced by uncertainty, or minimization of the effects of multi-site damage. In practical design situation, it is impossible to comply with the performance objectives deterministically because of the inherent random nature of loading conditions, structural parameters and conditions of operation of the structures. Hence, the fulfillment of the performance objectives should be accomplished by probabilistic means, with an associated reliability.

In fact, high levels of reliability are usually associated with large economical costs. Obviously, the enhanced reliability requires increased amount of construction material, more sophisticated construction procedures, thorough maintenance, etc. An adequate design procedure should offer an appropriate trade-off between an acceptable reliability level and economical design of the structure. RBDO provides the means for achieving such trade-off offering an optimal design solution taking into account the effects of uncertainties.

The RBDO allows determining the best design according to some predefined criterion. The formulation of an RBDO problem requires the identification and definition of a number of items, namely the input variables of the system (design variables and uncertain parameters), the failure events of the system (violation of target performance), the constraints of the design problem and the objective function that allows identifying the most convenient design. Clearly as following,

1 Definition of the design variables
2 Identification of the uncertain parameters
3 Formulation of the failure (or critical) events associated with the performance of the system

4 Definition of the constraints of the design problem.

5 Statement of an objective function

Design variables, the parameters that need to be determined to obtain the desired structural performance under some constraints, they can be geometry parameters like beam length, plate thickness and cross section, as well as material properties including reinforcement distribution.

State variables are the parameters representing responses of the structure. A typical response refers to displacement, velocity, acceleration, stress, strain and so on. In practical application, the state variables are mostly implicit functions of design variables and available in numerical way.

Objective function is the function to evaluate the merit of a design. Frequently, one objective function can measure weight, stiffness, displacement in a given direction, or simple costs. The objective function is commonly formulated by a minimization problem.

Deterministic constraint is the restriction that must be satisfied in a structural design optimization corresponding some critical failure mechanism. Side constraints provide the lower bound and upper bound of the design variables.

5.1.1 Single Objective Optimization Description

A single objective optimization problem consists of optimizing function:

Opt (F(x))

Where $x = (x_1, x_2, ..., x_n)^t$

Subject to:

$$\begin{aligned} &g_j(x) \le 0,\ j = 1, 2, ..., q, \\ &h_j(x) = 0,\ j = 1, 2, ..., r, (q + r = m) \end{aligned} \qquad (5 - 1)$$

There are several types of single optimization problems.

Type 1 (component reliability):

Minimize a system cost function $C_S = C(R_i, x_i)$

Subject to

$$R_{i,\min} \le R_i \le R_{i,\max}, i = 1, 2, ..., n; \\ R_{S,\min} \le R_S \le R_{S,\max} \quad (5 - 2)$$

Type 2 (redundancy allocation):

Find the optimal $x_i, i = 1, 2, ..., n,$ which Max $R_S = f(R_i, x_i)$

Subject to: $g_j(x_1, x_2, ..., x_n) \le 0, j = 1, 2, ..., m,$ in this problem R_i is fixed and x_i can vary.

Type 3 (component reliability and redundancy allocation):

Maximize $R_S = f(R_i, x_i), i = 1, 2, ..., n,$

Subject to:

$$g_j(x_1, R_1, x_2, R_2, ..., x_n, R_n) \le 0, j = 1, 2, ..., m, \quad (5 - 3)$$

$$0 \le R_i \le 1, i = 1, 2, ..., n; \; x_i \ge 1$$

For both type 2 and 3 problems the function $f(R_i, x_i)$ can be any expression. For example, in the cases to be analyzed in series-parallel systems, the expression for $f(R_i, x_i)$ is

$$f(R_i, x_i) = \prod_{i=1}^{n} \left[1 - (1 - R_i)^{x_i} \right] \quad (5 - 4)$$

Within these single optimization problems, the constraints g_j are usually associated with system weight, volume and cost and are often defined or assumed, for the purpose of simplicity, as linear functions.

As examples of such constraints we have:

$$g_1 = \sum_{i=1}^{n} P_i x_i^2 \le P \quad (5 - 5)$$

$$g_2 = \sum_{i=1}^{n} C_i \left[x_i + \exp(k_i x_i) \right] \le C \quad (5 - 6)$$

$$g_3 = \sum_{i=1}^{n} W_i \left[x_i * \exp(k_i x_i) \right] \le W \qquad (5 - 7)$$

Constraint Eq. (5-5) is a combination of weight and volume: P_i is the product of weight per unit and volume per unit. Constraint Eq. (5-6) is a cost constraint. The term $\exp(k_i x_i)$ is the additional cost for interconnecting parallel units while Eq. (5-7) is a weight constraint: the weight of a single unit is increased by the factor $\exp(k_i x_i)$ due to the weight of the interconnecting links.

Note that in these formulations, only a single objective function is considered. The other objectives (reliability, cost, weight, or volume) are modeled as constraints. That means that the designers consider all individual targets separately.

5.1.2 Multiple-Objective Optimization description

A multi-objective optimization problem consists of optimizing a vector of functions:

$$\text{Opt } \left(\mathrm{F}(\mathrm{x}) \right) = (f_1(x), f_2(x), ..., f_k(x)) \qquad (5 - 8)$$

Subject to:

$$\begin{aligned} & g_j(x) \le 0,\ j = 1, 2, ..., q, \\ & h_j(x) = 0,\ j = 1, 2, ..., r, (q + r = m) \end{aligned} \qquad (5 - 9)$$

Where $x = (x_1, x_2, ..., x_n)^t \in X$ is a solution vector, or vector of decision variables, and X is the feasible domain.

The concept of optimality in single objective is not directly applicable in multiple-objective problems. For this reason a classification of the solutions is introduced in terms of Pareto optimality, according to the following definitions:

In terms of minimization:

Definition 1. Pareto optimal: A solution vector $x^* \in X$ is Pareto optimal solution iff

$$\neg \exists x \in X : f_i(x) \le f_i(x^*) \wedge f_i(x) \ne f_i(x^*); \forall i = \{1, 2, ..., k\}. \qquad (5 - 10)$$

These solutions are also called true Pareto solutions.

Definition 2. Pareto dominance: A solution x^1 dominates x^2, denoted as $x^1 \succ x^2$ iff

$$f_i(x^1) \le f_i(x^2) \wedge \exists j : f_j(x) < f_j(x^2); i, j = \{1, 2, ..., k\} \qquad (5 - 11)$$

If there are no solutions which dominate x^1, then x^1 is non-dominated.

Definition 3. Pareto set: A set of non-dominated solutions $\left\{ x^* \middle| \neg \exists x : x \succ x^* \right\}$ is said to be a Pareto set.

Definition 4. Pareto front: the set of vectors in the objective space that ate image of a Pareto set, $\left\{ F(x^*) \middle| \neg \exists x : x \succ x^* \right\}$

The reliability optimization problems presented in single objective problem can be formulated as multi-objective problem, transforming one or more constraints into one or more objectives. For example, we define the following multi-objective problems:

MOP Type 1 (component reliability):

Maximize the system reliability R_S and minimize a cost function C_S subject to

$R_{i,\min} \le R_i \le R_{i,\max}$, $i = 1, 2, ..., n.$

MOP Type 2 (redundancy allocation):

Find the optimal x_i, $i = 1, 2, ..., n.$ which maximize $R_S = f(R_i, x_i)$ and minimize a cost function C_S

Subject to: $g_j(x_1, x_2, ..., x_n) \le 0, j = 1, 2, ..., m.$

MOP Type 3 (component reliability and redundancy allocation):

Maximize $R_S = f(R_i, x_i), i = 1, 2, ..., n.$ and minimize a cost function C_S

Subject to: $g_j(x_1, R_1, x_2, R_2, ..., x_n, R_n) \le 0, j = 1, 2, ..., m;$

$0 \le R_i \le 1, i = 1, 2, ..., n; x_i \ge 1$ (integer).

Within these problems, we will consider that the cost function to be minimized corresponds to the previously defined cost constraint g_2 in the single objective formulation.

Notice that even if the two objectives considered in these MOP types are reliability and cost, the MOP approach is general and can be used for any type and number of objectives. The selection of such objectives clearly depends on the problem under study and the design maker criteria.

5.2 First –order reliability method

When a structure exceeds a specific limit causes it is unable to perform as requires, this specific limit is called a limit-state. The structure will be considered unreliable if the failure probability of the structure limit-state exceeds the required value. For most structures, the limit-state can be divided into two categories:

- Ultimate limit-states are related to a structural collapse of part or all of the structure. Examples of the most common ultimate limit-states are corrosion, fatigue, deterioration, fire, plastic mechanism, progressive collapse, fracture, etc. Such a limit-state should have a very low probability of occurrence, since it may risk the loss of life and major financial losses.

- Serviceability limit-states are related to disruption of the normal use of the structures, typical examples are excessive deflection, excessive vibration, drainage, leakage, local damage, etc. A higher probability of occurrence may be tolerated in such limit-states.

The probabilistic methods include the stochastic finite element method, the first- and second-order reliability method, sampling methods, the utilization of stochastic expansion based on the random process concept, etc.

Due to the curse of dimensionality in the probability-of-failure calculation, numerous methods are used to simplify the numerical treatment of the integration process. The Taylor series expansion is often used to linearize the limit-state. In this approach, the first- or second-order Taylor series expansion is used to estimate reliability. FOSM is also referred to as the Mean Value First Order Second Moment method (MVFOSM), since it is a point expansion method at the mean point and the second moment is the highest-order statistical result used in this analysis.

Although the implementation of FOSM is simple, it has been shown that the accuracy is not acceptable for low probability of failure or for highly nonlinear responses [1]. In SOSM, the addition of a second-order term increases computational effort significantly, yet the improvement in accuracy is often minimal.

The safety index approach to reliability analysis is actually a mathematical optimization problem for finding the point on the structural response surface that has the shortest distance from the origin to the surface in the standard normal space.

The FOSM method, as implied, inputs and outputs are expressed as the mean and standard deviation. Higher moments, which might describe skew and flatness of the distribution, are ignored.

5.2.1 First – order second moment method

In mean value first order second moment method (MVFOSM), the limit-state function is represented as the first-order Taylor series expansion at the mean value point. Assuming that the variables X are statistically independent, the approximate limit-state function at the mean is written as

$$\tilde{g}(X) \approx g(\mu_X) + \nabla g(\mu_X)^T (X_i - \mu_{X_i}) \tag{5 - 12}$$

Where, $\mu_X = \left\{ \mu_{x_1}, \mu_{x_2}, ... \mu_{x_n} \right\}^T$ and $\nabla g(\mu_X)$ is the gradient of g evaluated at μ_X,

$$\nabla g(\mu_X) = \left\{ \frac{\partial g(\mu_X)}{\partial x_1}, \frac{\partial g(\mu_X)}{\partial x_2}, ... \frac{\partial g(\mu_X)}{\partial x_n} \right\}^T \tag{5 - 13}$$

The mean value of the approximate limit-state function $\tilde{g}(X)$ is

$$\mu_{\tilde{g}} \approx E\left[g(\mu_X) \right] = g(\mu_X) \tag{5 - 14}$$

Because

$$Var\left[g(\mu_X) \right] = 0 \qquad Var\left[\nabla g(\mu_X) \right] = 0 \tag{5 - 15}$$

$$\begin{aligned} Var\left[\nabla g(\mu_X)^T (X - \mu_X) \right] &= Var\left[\nabla g(\mu_X)^T X \right] - \mu_X Var\left[\nabla g(\mu_X) \right] \\ &= Var\left[\nabla g(\mu_X)^T X \right] = \left[\nabla g(\mu_X)^T \right]^2 Var(X) \end{aligned} \tag{5 - 16}$$

The variance of the approximate limit-state function $\tilde{g}(X)$ is

$$Var\left[\tilde{g}(X)\right] \approx Var\left[g(\mu_X)\right] + Var\left[\nabla g(\mu_X)^T (X - \mu_X)\right] \tag{5 - 17}$$

Therefore, the standard deviation of the approximate limit-state function is

$$\sigma_{\tilde{g}} = \sqrt{Var\left[\tilde{g}(X)\right]} = \sqrt{\left[\nabla g(\mu_X)^T\right]^2 Var(X)} = \left[\sum_{i=1}^{n}\left(\frac{\partial g(\mu_X)}{\partial x_i}\right)^2 \sigma_{x_i}^2\right]^{\frac{1}{2}} \tag{5 - 18}$$

The reliability index β is computed as:

$$\beta = \frac{\mu_{\tilde{g}}}{\sigma_{\tilde{g}}} \tag{5 - 19}$$

If the limit-state function is nonlinear, the approximate limit-state surface is obtained by linearizing the original limit-state function at the mean value point. In a general case with independent variables of n-dimensional space, the failure surface is a hyper-plane and can be defined as a linear-failure function:

$$\tilde{g}(X) = c_0 + \sum_{i=1}^{n} c_i x_i \tag{5 - 20}$$

The MVFOSM reliability index can still be used for this n-dimensional case, in which

$$\mu_{\tilde{g}} = c_0 + c_1\mu_{x_1} + c_2\mu_{x_2} + ... + c_n\mu_{x_n} \tag{5 - 21}$$

$$\sigma_{\tilde{g}} = \sqrt{\sum_{i=1}^{n} c_i^2 \sigma_{x_i}^2} \tag{5 - 22}$$

The MVFOSM method changes the original complex probability problem into a simple problem. This method directly establishes the relationship between the reliability index and the basic parameters (mean and standard deviation) of the random variables. However, there are two serious drawbacks in the MVFOSM method:

(1) Evaluation of reliability by linearizing the limit-state function about the mean values leads to erroneous estimates for performance functions with high nonlinearity, or for large coefficients of variation.

This can be seen from the following mean valued calculation of $\tilde{g}(X)$, which assumes that truncation of the Taylor series expansion for a case of only one random variable at the first three terms is

$$\tilde{g}(X) \approx g(\mu_X) + (X - \mu_X)\nabla g(\mu_X) + \frac{(X - \mu_X)^2}{2}\nabla g^2(\mu_X) \tag{5 - 23}$$

The mean value of the approximate limit-state function $\tilde{g}(X)$ can be calculated as

$$\mu_{\tilde{g}} \approx E\left[g(\mu_X)\right] + E\left[(X - \mu_X)\nabla g(\mu_X)\right] + E\left[\frac{(X - \mu_X)^2}{2}\nabla g^2(\mu_X)\right] \tag{5 - 24}$$

Because

$$E\left[g(\mu_X)\right] = g(\mu_X) \tag{5 - 25}$$

$$\begin{aligned} E\left[(X - \mu_X)\nabla g(\mu_X)\right] &= E\left[X\nabla g(\mu_X)\right] - E\left[\mu_X \nabla g(\mu_X)\right] \\ &= \nabla g(\mu_X)E(X) - \mu_X \nabla g(\mu_X) = 0 \end{aligned} \tag{5 - 26}$$

$$\begin{aligned} E\left[\frac{(X - \mu_X)^2}{2}\nabla g^2(\mu_X)\right] &= \frac{1}{2}\nabla^2 g(\mu_X)E\left[(X - \mu_X)^2\right] \\ &= \frac{1}{2}\nabla^2 g(\mu_X)Var(X) \end{aligned} \tag{5 - 27}$$

It is obvious that the third term on the right side depends on the variance of X and the second-order gradients of the limit-state function. If the variance of X is small or the limit-state function is closed to linear, the third term can be ignored and the mean value of $\tilde{g}(X)$ is the same as $\mu_{\tilde{g}} \approx E\left[g(\mu_X)\right] = g(\mu_X)$ Otherwise, large errors in the mean value estimation will result.

(2) The MVFORM method fails to be invariant with different mathematically equivalent formulations of the same problem. This is a problem not only for nonlinear form of limit-state, but also for certain linear forms.

5.2.2 Hasofer and lind safety-index

Searching for the MPP on the limit-state surface is a key step in the HL method. The improvement of the HL method compared with the MVFOSM also comes from

changing the expansion point from the mean value point to the MPP. Hasofer and Lind proposed a linear mapping of the basic variables into a set of normalized and independent variables u_i.

Any orthogonal distribution of standard normally distributed variables $U = \{u_1, u_2, ..., u_n\}^T$ results in a new set of normalized and uncorrelated variables. Therefore, the distributions of U are rotationally symmetric with respect to second moment distribution. Based on the transformation, the mean value point in the original space is mapped into the origin of the normal space. The failure surface $g(X) = 0$ in X-space is mapped into the corresponding failure surface $g(U) = 0$ in U-space. Due to rotational symmetry of the second-moment representation of U, the geometrical distance from the origin in U-space to any point on $g(U) = 0$ is simply the number of standard deviations from the mean value point in X-space to the corresponding point on $g(X) = 0$. The distance to the failure surface can then be measured by the safety-index function:

$$\beta(U) = (U^T U)^{1/2} = \|U\|_2 , U \in g(U) = 0 \qquad (5 - 28)$$

The safety-index β is the shortest distance from the origin to the failure surface $g(U) = 0$

$$\beta = \min_{U \in g(U)=0} (U^T U)^{1/2} \qquad (5 - 29)$$

The point $U^* \left(u_1^*, u_2^*, ..., u_n^*\right)$ on $g(U) = 0$ is the design point. The values-of-safety indices are the same when the failure surface is a hyper-plane. The value of β_{HL} is the same for the true failure surface as well as for the approximate tangent hyper-plane at the design point. The ambiguity in the value of the first-order reliability index is thus resolved when the design point is taken as the linearization point. The resultant reliability index is a sensible measure for the distance to the failure surface.

β_{HL} is the solution of a constrained optimization problem in the standard normal space.

Minimize: $\beta(U) = (U^T U)^{1/2}$

Subject to : $g(U) = 0$

There are many algorithms available that can solve this problem, such as mathematical optimization schemes or other iteration algorithms. Several constrained optimization methods were used, including primal methods (feasible directions, gradient, projection, reduced gradient), penalty methods, dual methods, and Lagrange multiplier methods. Each method had its advantages and disadvantages, depending upon the attributes of the method and the nature of the problem.

The HL method was proposed by Hasofer and Lind. Rachwitz and Fiessler extended the HL method to include random variable distribution information, calling their extended method the HL-RF method. Assuming that the limit-state surface with n-dimensional normally distributed and independent random variables X is

$$g(X) = g(\{x_1, x_2, ...x_n\}^T) = 0 \tag{5 - 30}$$

This limit-state function can be linear or nonlinear. Based on the transformation, the limit-state function is transformed into

$$g(U) = g(\{\sigma_{x_1} u_1 + \mu_{x_1}, \sigma_{x_2} u_2 + \mu_{x_2}, ..., \sigma_{x_n} u_n + \mu_{x_n}\}^T) = 0 \tag{5 - 31}$$

The normal vector from the origin $\widehat{O}$ to the limit-state surface $g(U)$ generates an intersection point P^*. The distance from the origin to the MPP is the safety-index β. The first-order Taylor series of expansion of $g(U)$ at the MPP U^* is

$$\tilde{g}(U) \approx g(U^*) + \sum_{i=1}^{n} \frac{\partial g(U^*)}{\partial U_i}(u_i - u_i^*) \tag{5 - 32}$$

From the transformation

$$\frac{\partial \hat{g}(U)}{\partial u_i} = \frac{\partial g(X)}{\partial x_i}\sigma_{x_i} \tag{5 - 33}$$

The shortest distance from the origin to the above approximate failure surface

$$\widehat{OP}^* = \beta = \frac{g(U^*) - \sum_{i=1}^{n} \frac{\partial g(U^*)}{\partial x_i} \sigma_{x_i} u_i^*}{\sqrt{\sum_{i=1}^{n} \left(\frac{\partial g(U^*)}{\partial x_i} \sigma_{x_i}\right)^2}} \tag{5 - 34}$$

The direction cosine of the unit outward normal vector is given as

$$\cos\theta_{x_i} = \cos\theta_{u_i} = -\frac{\frac{\partial g(U^*)}{\partial u_i}}{\left|\nabla g(U^*)\right|} = -\frac{\frac{\partial g(X^*)}{\partial x_i}\sigma_{x_i}}{\left[\sum_{i=1}^{n} \left(\frac{\partial g(X^*)}{\partial x_i}\sigma_{x_i}\right)^2\right]^{1/2}} = \alpha_i \tag{5 - 35}$$

Where α_i expresses the relative effect of the corresponding random variable on the total variation. Thus, it is called the sensitivity factor.

The coordinates of the point P^* are computed as

$$u_i^* = \frac{x_i^* - \mu_{x_i}}{\sigma_{x_i}} = \widehat{OP}^* \cos\theta_{x_i} = \beta \cos\theta_{x_i} \tag{5 - 36}$$

The coordinates corresponding to P^* in the original space are

$$x_i^* = \mu_{x_i} + \beta\sigma_{x_i} \cos\theta_{x_i} \ , \ (i = 1, 2, ..., n) \tag{5 - 37}$$

Since P^* is a point on the limit-sate surface,

$$g(\{x_1, x_2, ...x_n\}^T) = 0 \tag{5 - 38}$$

The direction cosine of the unit outward normal vector of the limit-state function α_i is defined as the sensitivity factor, which shows the relative importance of each random variable to the failure probability. The sensitivity of the failure probability or the safety index to small changes in the random variables can be examined, which usually provides information useful to studying the statistical variation of the response.

The physical meaning of α_i implies the relative contribution of each random variable to the failure probability. For example, the larger the α_i value is, the higher the contribution towards the failure probability. This is due to

$$\alpha_1^2 + \alpha_2^2 + ... + \alpha_n^2 = 1 \tag{5 - 39}$$

In fact, α_i is the sensitivity of the safety-index β at the MPP. From the definition of β as the distance from the origin to the limit-state surface, $g(U) = 0$, it follows that

$$\frac{\partial \beta}{\partial u_i} = \frac{\partial}{\partial u_i}\sqrt{u_1^2 + u_2^2 + ... + u_n^2} = \frac{u_i}{\beta} = \alpha_i \text{ , } (i = 1, 2, ..., n) \tag{5 - 40}$$

The sensitivity factors for the failure probability P_f are

$$\frac{\partial \beta}{\partial u_i} = \frac{\partial}{\partial u_i}\phi(-\beta) = \phi(-\beta)\frac{\partial \beta}{\partial u_i} \tag{5 - 41}$$

In some cases, the failure surface may contain several points corresponding to stationary values of the reliability-index function. Therefore, it may be necessary to use several starting points to find all the stationary values $\beta_1, \beta_2, ..., \beta_m$. This is called a multiple MPP problem.

The HL safety-index is

$$\beta_{HL} = \min\left\{\beta_1, \beta_2, ..., \beta_m\right\} \tag{5 - 42}$$

The difference between the MVFOSM method and the HL method is that the HL method approximates the limit-state function using the first-order Taylor expansion at the design point $X^{(k)}$ or $U^{(k)}$ instead of the mean value point μ_X ; Also, the MVFOSM method does not require iterations, while the HL method needs several iterations to converge for nonlinear problems. The HL method usually provided better results than the mean-value method for nonlinear problems. How well a linearized limit-state function, $\tilde{g}(U) = 0$, approximates a nonlinear function $g(U)$ in terms of the failure probability P_f depends on the shape of $g(U) = 0$. If it is concave towards the origin, P_f is underestimated by the hyper-plane approximation. Similarly, a convex function implies overestimation. However, there is no guarantee that the HL algorithm converges in all situations. Furthermore, the HL method only considers normally distributed random variables, so it cannot be used for non-Gaussian random variables.

5.2.3 Hasofer Lind- Rackwitz Fiessler (HL-RF) Method

In the Hasofer Lind method, the random variables X are assumed to be normally distributed. In non-gaussian cases, even when the limit-state function $g(X)$ is linear, the structural probability calculation is inappropriate. However, many structural reliability problems involve non-Gaussian random variables. It is necessary to find a way to solve the non-Gaussian problems. There are many methods available for conducting the transformations, such as Rosenblatt, and Hohenbichler and Rachwitz. A simple, approximate transformation called the equivalent normal distribution, or the normal tail approximation, is described below. The main advantages of this transformation are:

(1) It does not require the multi-dimensional integration
(2) Transformation of non-Gaussian variables into equivalent normal variables has been accomplished prior to the solution.
(3) Calculation of the structural probability is retained
(4) It often yields excellent agreement with the exact solution of the multi-dimensional integral of probability formula

When the variables are mutually independent, the transformation is given as

$$u_i = \Phi^{-1}\left[F_{x_i}(x_i)\right] \tag{5 - 43}$$

Where Φ^{-1} is the inverse of Φ

One way to get the equivalent normal distribution is to use the Taylor series expansion of transformation at the MPP X^*, neglecting nonlinear terms

$$u_i = \Phi^{-1}\left[F_{x_i}(x_i^*)\right] + \frac{\partial}{\partial x_i}\left(\left[\Phi^{-1}F_{x_i}(x_i)\right]\right)\Big|_{x_i^*}(x_i - x_i^*) \tag{5 - 44}$$

Where

$$\frac{\partial}{\partial x_i}\Phi^{-1}\left[F_{x_i}(x_i)\right] = \frac{f_{x_i}(x_i)}{\phi(\Phi^{-1}\left[F_{x_i}(x_i)\right])} \tag{5 - 45}$$

$$u_i = \frac{x_i - \left[x_i^* - \Phi^{-1}\left[F_{x_i}(x_i^*)\right]\phi(\Phi^{-1}\left[F_{x_i}(x_i^*)\right])/f_{x_i}(x_i^*)\right]}{\phi(\Phi^{-1}\left[F_{x_i}(x_i^*)\right])/f_{x_i}(x_i^*)} \tag{5 - 46}$$

Which can be written as,

$$u_i = \frac{x_i - \mu_{x_i'}}{\sigma_{x_i'}} \tag{5 - 47}$$

Where $F_{x_i}(x_i)$ is the marginal cumulative distribution function, $f_{x_i}(x_i)$ is the probability density function, and $\mu_{x_i'}$ and $\sigma_{x_i'}$ are the equivalent means and standard deviation of the approximate normal distributions, and which are given as

$$\sigma_{x_i'} = \frac{\phi(\Phi^{-1}\left[F_{x_i}(x_i^*)\right])}{f_{x_i}(x_i^*)} \tag{5 - 48}$$

$$\mu_{x_i'} = x_i^* - \Phi^{-1}\left[F_{x_i}(x_i^*)\right]\sigma_{x_i'} \tag{5 - 49}$$

Another way to get equivalent normal distributions is to match the cumulative distribution functions and probability density function of the original, non-normal random variable distribution, and the approximate or equivalent normal random variable distribution at the MPP. Assuming that x_i' is an equivalent normally distributed random variable, the cumulative distribution function values of x_i and x_i' are equal:

$$F_{x_i}(x_i^*) = F_{x_i'}(x_i^*) \tag{5 - 50}$$

Or

$$F_{x_i}(x_i^*) = \Phi\left(\frac{x_i^* - \mu_{x_i'}}{\sigma_{x_i'}}\right) \tag{5 - 51}$$

So

$$\mu_{x_i'} = x_i^* - \Phi^{-1}\left[F_{x_i}(x_i^*)\right]\sigma_{x_i'} \tag{5 - 52}$$

The probability density function value of x and x_i^* are equal:

$$f_{x_i}(x_i^*) = f_{x_i'}(x_i^*) \tag{5 - 53}$$

$$f_{x_i}(x_i^*)=\frac{1}{\sigma_{x_i'}}\phi\left(\frac{x_i^*-\mu_{x_i'}}{\sigma_{x_i'}}\right) \tag{5 - 54}$$

5.2.4 FORM with adaptive approximations

In the previous algorithms, the limit-state function, $g(U)$ was approximated by the first-order Taylor expansion at the MPP. For nonlinear problems, this approach is only an approximation, and several iterations are usually required. How fast the algorithm converges depends on how well the linearized limit-state function approximates the nonlinear function $g(U)$.

The limit-state function could be approximated by other functions, such as the Two-point Adaptive Nonlinear Approximations (TANA), including TANA and TANA2. This new class of approximations is constructed by using Taylor series expansion in terms of adaptive intervening variables. The nonlinearity of the adaptive approximations is automatically changed by using the known information generated during the iteration process. TANA2 also has a correction term for second-order terms.

To compute the approximate U-space limit-state surface $\tilde{g}(U)$ using TANA, we must first obtain the adaptive approximate limit-state surface in X-space. Two possible methods,

TANA:

$$\tilde{g}(\mathrm{X})=\mathrm{g}(\mathrm{X}_k)+\frac{1}{r}\sum_{i=1}^{n}x_{i,k}^{1-r}\frac{\partial \mathrm{g}(\mathrm{X}_k)}{\partial x_i}(x_i^r-x_{i,k}^r) \tag{5 - 55}$$

Where $x_{i,k}$ is the i^{th} element in the vector X_k of the k^{th} point/ iteration. The comma notation does not signify differentiation.

The nonlinear index r can be determined from

$$\mathrm{g}(\mathrm{X}_{k-1})-\left\{\mathrm{g}(\mathrm{X}_k)+\frac{1}{r}\sum_{i=1}^{n}x_{i,k}^{1-r}\frac{\partial \mathrm{g}(\mathrm{X}_k)}{\partial x_i}(x_{i,k-1}^r-x_{i,k}^r)\right\}=0 \tag{5 - 56}$$

TANA2:

$$\tilde{g}(\mathrm{X})=\mathrm{g}(\mathrm{X}_k)+\sum_{i=1}^{2}\frac{\partial \mathrm{g}(\mathrm{X}_k)}{\partial x_i}\frac{(x_{i,k})^{1-p_i}}{p_i}(x_i^{p_i}-(x_{i,k})^{p_i})+\frac{1}{2}\varepsilon_2\sum_{i=1}^{2}(x_i^{p_i}-(x_{i,k})^{p_i})^2 \qquad (5\text{ - }57)$$

Then,

$$\frac{\partial \mathrm{g}(\mathrm{X}_{k-1})}{\partial x_i}=(\frac{x_{i,k-1}}{x_{i,k}})^{p_{i-1}}\frac{\partial \mathrm{g}(\mathrm{X}_k)}{\partial x_i}+\varepsilon_2(x_{i,k-1}^{p_i}-x_{i,k}^{p_i})x_{i,k-1}^{p_{i-1}}p_i \qquad (5\text{ - }58)$$

$$\mathrm{g}(\mathrm{X}_{k-1})=\mathrm{g}(\mathrm{X}_k)+\sum_{i=1}^{n}\frac{\partial \mathrm{g}(\mathrm{X}_k)}{\partial x_i}\frac{(x_{i,k})^{1-p_i}}{p_i}(x_i^{p_i}-(x_{i,k})^{p_i})+\frac{1}{2}\varepsilon_2\sum_{i=1}^{n}(x_{i,k-1}^{p_i}-(x_{i,k})^{p_i})^2 \qquad (5\text{ - }59)$$

$(i=1,2,....,n)$

To map $\tilde{g}(\mathrm{X})$ into $\tilde{g}(\mathrm{U})$ by using the standard normal or equivalent normal transformations:

$$\tilde{g}(\mathrm{X})=\tilde{g}(\sigma_{x_1'}\mathrm{u}_1+\mu_{x_1'},\sigma_{x_2'}\mathrm{u}_2+\mu_{x_2'},....,\sigma_{x_n'}\mathrm{u}_n+\mu_{x_n'}) \qquad (5\text{ - }60)$$

The nonlinear index, r, is numerically calculated by minimizing the difference between the exact and the approximate limit-state functions at the previous point X_{k-1}. In theory, r can be any positive or negative number. In practice, r can be restricted from, say, -5 to 5, for the X-space iterations to avoid numerical difficulties associated with higher order polynominals.

Usually, the adaptive safety-index algorithm is better than the HL-RF method, because the nonlinear index r is determined by comparing linear approximations and minimizing the difference between exact and approximate limit-state functions. In the process of searching for r, the nonlinear index will automatically become 1 if other values of r cannot provide any improvement over the linear approximation.

5.3 Second-order Reliability Method (SORM)

FORM usually works well when the limit-state surface has only one minimal distance point and the function is nearly linear in the neighborhood of the design point. However, the failure probability estimated by FORM using the safety-index β may give unreasonable and inaccurate results, if the failure surface has large curvatures (high nonlinearity). To resolve this problem, the second-order Taylor series is

considered. Various nonlinear approximate methods have been proposed in the literature.

5.3.1 First- and Second-order Approximation of Limit-state Function

To facilitate the integration, the standard normal Y-space instead of U-space can be considered in most failure probability calculations. To conduct the rotation from the standard normal U-space to the Y-space, an orthogonal matrix H need to be generated in which the n^{th} row of H is the unit normal of the limit-state function at the MPP. To generate H, first, an initial matrix is selected as follows:

$$\begin{pmatrix} \dfrac{-\partial g(U^*)/\partial U_1}{\left|\nabla g(U^*)\right|} & \dfrac{-\partial g(U^*)/\partial U_2}{\left|\nabla g(U^*)\right|} & \cdots & \dfrac{-\partial g(U^*)/\partial U_n}{\left|\nabla g(U^*)\right|} \\ 0 & 1 & \cdots & 0 \\ 0 & 0 & \cdots & 0 \\ \vdots & \vdots & \ddots & \vdots \\ 0 & 0 & \cdots & 1 \end{pmatrix} \tag{5 - 61}$$

Where the last n-1 row consist of zeros and unity on the diagonal. The Gram-Schmidt algorithm is used to orthogonalize the above matrix to obtain an orthogonal matrix. First,

$$f_1 = \left\{ \frac{-\partial g(U^*)/\partial U_1}{\left|\nabla g(U^*)\right|}, \frac{-\partial g(U^*)/\partial U_2}{\left|\nabla g(U^*)\right|}, ..., \frac{-\partial g(U^*)/\partial U_n}{\left|\nabla g(U^*)\right|} \right\}^T \tag{5 - 62}$$

$$f_2 = \{0,1,0,....,0\}^T \tag{5 - 63}$$

$$f_n = \{0,0,0,....,1\}^T \tag{5 - 64}$$

Set

$$D_1 = (f_1, f_1)^{\frac{1}{2}} \ , \ e_{11} = \frac{1}{D_1} \ , \ \gamma_1 = e_{11} f_1 \tag{5 - 65}$$

$$D_2 = \left[(f_2, f_2) - \left|(f_2, \gamma_1)\right|^2 \right]^{\frac{1}{2}} \tag{5 - 66}$$

$$e_{12} = -\frac{(f_2, \gamma_1)}{D_2} \tag{5 - 67}$$

$$e_{22} = \frac{1}{D_2}\ ,\ \gamma_2 = e_{12}\gamma_1 + e_{22} f_2 \tag{5 - 68}$$

And in general,

$$D_k = \left[(f_k, f_k) - \left|(f_k, \gamma_1)\right|^2 - \left|(f_k, \gamma_2)\right|^2 - ,..., - - \left|(f_k, \gamma_{k-1})\right|^2 \right]^{\frac{1}{2}} \tag{5 - 69}$$

$$e_{1k} = -\frac{(f_k, \gamma_1)}{D_k},\quad e_{2k} = -\frac{(f_k, \gamma_2)}{D_k}\ ,....,\quad e_{k-1,k} = -\frac{(f_k, \gamma_{k-1})}{D_k} \tag{5 - 70}$$

$$e_{kk} = \frac{1}{D_k},\ \gamma_k = e_{1k}\gamma_1 + e_{2k}\gamma_2 + ,..., e_{k-1,k}\gamma_{k-1} + e_{kk} f_k \tag{5 - 71}$$

Where (f, f) and (f, γ) represent the scalar product of two vectors. It can be verified that the generated vectors $\gamma_1, \gamma_2, \ldots, \gamma_n$ are orthogonalized. The generated orthogonal matrix H_0 is $H_0^T = \left\{\gamma_1^T, \gamma_2^T, \ldots, \gamma_n^T\right\}$.

$$H^T = \left\{\gamma_2^T, \gamma_3^T, \ldots, \gamma_n^T, \gamma_1^T\right\} \tag{5 - 72}$$

First-order approximation: assuming the most probable failure point (MPP) in U-space to be

$$\tilde{g}(U) \approx g(U^*) + \nabla g(U^*)(U - U^*) = 0 \tag{5 - 73}$$

In this equation, $g(U^*)$ equals 0 because U^* point is on the response surface. Dividing by $\left|\nabla g(U^*)\right|$,

$$\tilde{g}(U) \approx \frac{\nabla g(U^*)}{\left|\nabla g(U^*)\right|}(U - U^*) \tag{5 - 74}$$

$$\beta = -\frac{\nabla g(U^*)U^*}{\left|\nabla g(U^*)\right|} \tag{5 - 75}$$

Substituting this equation, we obtain

$$\tilde{g}(U) \approx \frac{\nabla g(U^*)}{\left|\nabla g(U^*)\right|}U + \beta = 0 \tag{5 - 76}$$

By a rotation of U into a new set of mutually independent standard normal random variables Y using the orthogonal matrix H

$$Y = HU \tag{5 - 77}$$

And the approximate response surface becomes

$$\tilde{g}(U) \approx -y_n + \beta = 0 \tag{5 - 78}$$

Or $y_n = \beta$

If the limit-state functions of the practical problems are linear or close to linear, this approximation closely or exactly represents the response surface. Otherwise, the truncation errors from the first-order Taylor approximation might be large and more accurate approximations need to be employed.

The second-order approximation of the response surface $g(U) = 0$ is given by the second-order Taylor series expansion at the MPP:

$$\tilde{g}(U) \approx g(U^*) + \nabla g(U^*)^T (U - U^*) + \frac{1}{2}(U - U^*)^T \nabla^2 g(U^*)(U - U^*) \tag{5 - 79}$$

Where $\nabla^2 g(U^*)$ represents the symmetric matrix of the second derivative of the limit-state function:

$$\nabla^2 g(U^*)_{ij} = \frac{\nabla^2 g(U^*)}{\partial u_i \partial u_j} \tag{5 - 80}$$

Dividing by $\left|\nabla g(U^*)\right|$ and considering $g(U^*) = 0$, we obtain

$$\tilde{g}(U) \approx \alpha^T (U - U^*) + \frac{1}{2}(U - U^*)^T B(U - U^*) \tag{5 - 81}$$

Where $\alpha = \dfrac{\nabla g(U^*)}{\left|\nabla g(U^*)\right|}$ and $B = \dfrac{\nabla^2 g(U^*)}{\left|\nabla g(U^*)\right|}$

$$\tilde{g}(Y) \approx -y_n + \beta + \frac{1}{2}(H^{-1}Y - H^{-1}Y^*)^T B(H^{-1}Y - H^{-1}Y^*) \tag{5 - 82}$$

Where Y^* is the Y-space MPP, corresponding to the U-space MPP U^*. In Y-space, the y_n axis is in coincidence with the β vector.

Since the H matrix is an orthogonal matrix,

$$H^{-1} = H^T \tag{5 - 83}$$

Substituting this equation into

$$\tilde{g}(Y) \approx -y_n + \beta + \frac{1}{2}(Y - Y^*)^T HBH^T (Y - Y^*) \tag{5 - 84}$$

By a series of orthogonal transformations, H_1 , H_2 ,...., H_m , for the first n-1 variables,

$$\overline{Y} = \{y_1, y_2, ..., y_{n-1}\}^T \tag{5 - 85}$$

$$\overline{Y}' = H_1\, H_2\, ..., H_m \overline{Y} \tag{5 - 86}$$

Quantities associated with n-1 variables are denoted with a bar. Finally, the first $(n-1)\times(n-1)$ order matrix of HBH^T becomes a diagonal matrix:

$$\overline{H}\overline{B}\overline{H}^T = \begin{bmatrix} k_1 & 0 & \cdots & 0 \\ 0 & k_2 & \cdots & 0 \\ 0 & 0 & \cdots & 0 \\ \vdots & \vdots & \ddots & 0 \\ 0 & 0 & \cdots & k_{n-1} \end{bmatrix} \tag{5 - 87}$$

$$y_n = \beta + \frac{1}{2}\sum_{i=1}^{n-1} k_i y_i'^2 \tag{5 - 88}$$

In fact, the above procedure for finding the diagonal matrix can be treated as an eigenvalue problem. So, k are given by $k_{ij} = (\overline{H}\overline{B}\overline{H}^T)_{ij}$, $(i, j = 1, 2, ..., n-1)$

Where k_{ij} represents the curvature of the response surface at the MPP.

The major computational cost is in computing the second derivatives B of the limit-state function at the MPP. The exact second-order derivatives of $g(U)$ require additional $n(n+1)/2$ limit-state function simulations for a finite difference scheme. For

problems having a large number of random variables, this calculation is extremely computer intensive. From this procedure, it is clear that one has to increase computational efficiency in calculating the curvature matrix and second-order function derivatives. Then, it enables an accelerated and cost-effective procedure to perform the second-order probability analysis, particularly when finite element-based structural analysis tools are used.

5.3.2 Breitung's Formulation

In Breitung formulation, first, a Laplace method for the asymptotic approximation of multidimensional integrals is needed, define as

$$I(\beta) = \int_{g(Y)<0} \exp(\frac{-\beta^2 |Y|^2}{2}) dY \qquad (5 - 89)$$

Where $I(\beta)$ is an integral over a fixed domain whose integrand is an exponential function depending linearly on the parameter β^2.

$$I(\beta) \sim (2\pi)^{(n-1)/2} \exp(\frac{-\beta^2}{2}) \beta^{-(n+1)} |J|^{-1/2}, \ \beta \to \infty \qquad (5 - 90)$$

Where J is a quantity independent of β, depending only on the first and second derivatives of the failure surface at the MPP.

In the case of independent standard normal random variables, the joint probability density function (PDF) is given by

$$P_f = (2\pi)^{-n/2} \int_{g(U)<0} \exp(\frac{-|U|^2}{2}) dU \qquad (5 - 91)$$

Substituting $(x_1, x_2, ..., x_n) \to (y_1, y_2, ..., y_n)$ with $y_i = \beta^{-1} u_i$

$$P_f = (2\pi)^{-n/2} \beta^n \int_{g(Y)<0} \exp(\frac{-\beta^2 |Y|^2}{2}) dY \qquad (5 - 92)$$

$$P_f \sim (2\pi)^{-1/2} \beta^{-1} \exp(\frac{-\beta^2}{2}) |J|^{-1/2}, \ \beta \to \infty \qquad (5 - 93)$$

Since the failure surface is approximated by the quadratic Taylor series expansion at the MPP

$$\left|J\right| = \sum_{i=1}^{p} \left|J_i\right| = \sum_{i=1}^{n} \prod_{j=1}^{n-1} (1 + k_{ij}\beta) \tag{5 - 94}$$

Where p is the number of points on $g(U) = 0$ with the shortest distance β from the origin to the failure surface, and k_{ij} is the main curvature of the failure surface at the MPP. If there is only one MPP on the surface, considering Mill's ratio

$$\Phi(-Y) \approx (2\pi)^{-1/2} Y^{-1} \exp(\frac{-Y^2}{2}) \tag{5 - 95}$$

$$P_f \approx \Phi(-\beta) \prod_{j=1}^{n-1} (1 + k_j\beta)^{-1/2} \tag{5 - 96}$$

5.3.3 Tvedt's Formulation

Based on the second-order approximation of the failure surface, the approximate failure region Ω is defined as

$$\Omega = \left\{ Y \left| y_n - (\beta + \frac{1}{2} \sum_{i=1}^{n-1} k_i y_i'^2) \right| > 0 \right\} \tag{5 - 97}$$

The failure probability can be computed from a formulation in Y-space:

$$P_f = 1 - \int_{-\infty}^{+\infty} \cdots \int_{-\infty}^{+\infty} \phi(y_1) \cdots \phi(y_{n-1}) \int_{\beta + \frac{1}{2}\sum_{i=1}^{n-1} k_i y_i'^2}^{\infty} \phi(y_n) dy_n dy_{n-1} \cdots dy_1 \tag{5 - 98}$$

Tvedt has derived a three-term approximation for this equation by a power series expansion in terms of $\frac{1}{2}\sum_{i=1}^{n-1} k_i y_i'^2$, ignoring terms of orders higher than two. The resulting approximation for P_f is

$$A_1 = \Phi(-\beta) \prod_{i=1}^{n-1} (1 + k_i\beta)^{-1/2} \tag{5 - 99}$$

$$A_2 = \left[\beta\Phi(-\beta) - \phi(\beta)\right] \left\{ \prod_{i=1}^{n-1} (1 + k_i\beta)^{-1/2} - \prod_{i=1}^{n-1} (1 + k_i(\beta + 1))^{-1/2} \right\} \tag{5 - 100}$$

$$A_3 = (\beta+1)\left[\beta\Phi(-\beta)-\phi(\beta)\right]\left\{\prod_{i=1}^{n-1}(1+k_i\beta)^{-1/2}\right\} - \mathrm{Re}\left\{\prod_{i=1}^{n-1}(1+k_i(\beta+1))^{-1/2}\right\} \qquad (5\text{ - }101)$$

$$P_f = A_1 + A_2 + A_3 \qquad (5\text{ - }102)$$

The first term, A_1 is the Breitung formula. Re denotes the real part. This method has been found to give very good approximation in most cases. The asymptotic behavior of the three terms can be compared in the asymptotic sense. It may be shown that the ratio of the second term to the first term is

$$\frac{A_2}{A_1} \approx \frac{1}{2\beta^2}\sum_{i=1}^{n-1}\frac{k_i\beta}{1-k_i\beta} \quad ,\beta\to\infty \qquad (5\text{ - }103)$$

Similarly,

$$\frac{A_3}{A_1} \approx -\frac{3}{8\beta^2}\sum_{i=1}^{n-1}\left(\frac{k_i\beta}{1-k_i\beta}\right)^2 - \frac{1}{2\beta^2}\sum_{i=1}^{n-1}\sum_{m=i+1}^{n-1}\frac{\beta^2 k_i k_m}{(1-k_i\beta)(1-k_m\beta)} \quad ,\beta\to\infty \qquad (5\text{ - }104)$$

5.3.4 SORM with adaptive approximations

Wang and Grandhi suggest an adaptive approximation method for SORM. In this method, Breitung's and Tvedt's formulas are used to perform the failure probability calculations. However, the main curvatures are calculated for the nonlinear approximation developed during the safety-index calculations. The second-order derivatives for the closed-form adaptive model representing the original limit-state can be given as

$$\begin{aligned}\nabla^2\tilde{g}(U^*)_{ij} &= \frac{\partial^2\tilde{g}(U^*)}{\partial u_i\partial u_j}\\ &= (r-1)\sum_i^n\left(u_{i,k}+\frac{\overline{x}_i}{\sigma_i}s\right)^{(1-r)}\frac{\partial g(Y_k)}{\partial u_i}\left(u_i+\frac{\overline{x}_i}{\sigma_i}s\right)^{(r-2)}\nabla^2\tilde{g}(U^*)_{ij} \qquad (5\text{ - }105)\\ &= 0 \quad (i\neq j)\end{aligned}$$

5.4 Mathematical Formulation of RBDO

RBDO is a methodology for finding optimized designs that are characterized with a low probability of failure. Mathematically, a basic formulation is described as

Find d

Minimize f(d)

Subject to

$$P(G_j(X) \le 0) - R_j \ge 0,\ j = 1, 2, ..., N$$
$$d_i^l \le d_i \le d_i^u, i = 1, 2, ..., ND;\ X_k, k = 1, 2, ...NR$$

(5 - 106)

Where f and G_j are the objective and constraint functions, respectively, X is the random design vector, d is the mean of X, N is the number of probabilistic constraints, ND is the number of design parameters, NR is the number of random parameters, R_j is the desired reliability, and the probabilistic constraints are described by the performance function $G_j(X)$, where $G_j(X) \ge 0$ indicates failure. This expression can be rewritten as:

Minimize f(d)

Subject to

$$P(G_j(X) \ge 0) - \phi(-\beta_j) \le 0,\ j = 1, 2, ..., N$$
$$d_i^l \le d_i \le d_i^u, i = 1, 2, ..., ND$$

(5 - 107)

Where ϕ represents the cumulative distribution function for the standard normal distribution, and β_j is the prescribed target reliability for the j^{th} constraint.

The probability of failure is statistically defined by a cumulative distribution function $F_{G_j}(0)$ as

$$P(G_j(X) \ge 0) = F_{G_j}(0)$$
$$= \int_{G_j(X) \le 0} ..... \int f_X(X) dX \le \phi(-\beta_{tj}) \qquad (5 - 108)$$

Where $f_X(X)$ is a joint probability density function, which needs to be integrated. To integrate, a dependent standard normal vector u through Rosenblatt transformation. In u-space, the most probable point for failure is found by locating the minimum distance between the origin and the limit-state or constraint function. The minimum

distance is defined as β. Approximate probability integration method, the first-order reliability method (FORM), has been widely used to provide efficient and adequately accurate solutions.

Through an inverse transformation with $\phi^{-1}(\bullet)$ and $F_g^{-1}(\bullet)$, the probabilistic constraint can be further expressed in two different form as:

$$\beta_{Sj} = -\phi^{-1}(F_{Gj}(0)) \geq \beta_{tj}, \tag{5 - 109}$$

$$G_{Pj} = F_{Gj}^{-1}(\phi(-\beta_{tj})) \geq 0, \tag{5 - 110}$$

Where β_{Sj} and G_{Pj} are the achieved safety reliability index and the achieved probabilistic performance measure for the j^{th} probabilistic constraint, respectively. The reliability index approach (RIA) G_{pj}^{RIA} uses the reliability index to describe the probabilistic constraint. It is also referred to as the performance measure approach (PMA) G_{pj}^{PMA}, if the probabilistic performance measure replaces the probabilistic constraint.

5.4.1 RIA based RBDO

RIA based RBDO is expressed as

Find d

Minimize f(d)

Subject to
$$\begin{aligned} &-\beta_i(d,\Theta) + \beta_{t,i} \leq 0, i = 1,2,....,N_g \\ &-h_j(d) \leq 0,\ j = 1,2,.....,N_h \\ &d^L \leq d \leq d^U \end{aligned}$$

(5 - 111)

5.4.2 PMA based RBDO

PMA based RBDO

Find d

Minimize f(d)

Subject to

$$-g_i(d,\Theta) \le 0, i = 1,2,....,N_g$$
$$-h_j(d) \le 0,\ j = 1,2,.....,N_h$$
$$d^L \le d \le d^U$$

(5 - 112)

Solving RBDO by the PMA formulation is usually more efficient and robust than the RIA one where the reliability analysis is executed directly. The efficiency lies in the fact that the search for the most probable point (MPP) of an inverse reliability problem is easier to realize than the search for the MPP corresponding to an actual reliability. Moreover, the RIA based RBDO fails to converge for distributions with bound and extreme type distribution. Hence, the PMA based RBDO is more frequently used than the RIA based RBDO.

However, when sensitivity information or closed form limit state function is not available, the PMA family may not be efficient enough. To attain this objective, a new RBDO methodology is developed to integrated the PMA method with a new RSM.

5.5 Robust design optimization

The aim of RDO is to improve the quality of a product through minimizing the effect of variation without eliminating the causes, less sensitive to system variation. RDO is to reduce the variability of the system performances.

Basically, robust design addresses both the design objective robustness and the design feasibility robustness. The former is realized by minimizing the variability of the objective function, whereas the latter is guaranteed by satisfying the uncertain constraints. To achieve these targets, unlike RBDO, there is not a unified mathematical formulation in the literatures.

Design objective robustness

Nominal –the- best type

Minimize $$f(d,\Theta) = w_1\left(\frac{\mu_f(d,\Theta) - f_t}{\mu^0 - f^0}\right)^2 + w_2\left(\frac{\sigma_f(d,\Theta)}{\sigma^0}\right)^2$$

(5 - 113)

Smaller-the better type

Minimize $$f(d,\Theta) = w_1 \operatorname{sgn}(\mu_f(d,\Theta))\left(\frac{\mu_f(d,\Theta)}{\mu^0}\right)^2 + w_2\left(\frac{\sigma_f(d,\Theta)}{\sigma^0}\right)^2$$

(5 - 114)

Larger-the-better type

Minimize $$f(d,\Theta) = w_1 \operatorname{sgn}(\mu_f(d,\Theta))(\frac{\mu^0}{\mu_f(d,\Theta)})^2 + w_2(\frac{\sigma_f(d,\Theta)}{\sigma^0})^2$$

(5 - 115)

Considering the high computational burden, several alternatives with low computational expense have been developed: such as moment approach, worst case approach, corner space evaluation approach, moment approach, first and second moment method. The mean and standard deviation can be evaluated efficiently by approximate method, such as the perturbation method and the first order Taylor's series. The associated uncertain constraint is replaced by the probabilistic constraint

5.6 Reliability based optimization in surrogate model

MCS can keep a certain level of accuracy unless a very large number of iterations are performed. It is obvious that MCS methods is computational prohibitive when simulation model is complex. To be more efficient than the random sampling method, several improved MCS methods with different sampling techniques have been developed and proved. Importance sampling (weighted sampling), is expected to reduce error to zero if probability density function is correctly selected[86]. The first-order sensitivity method, as a variance reduction technique, is also utilized to accelerate MCS estimation convergence[87]. The variance reduction techniques are especially important when MCS is applied to estimate small failure probability[88].

A compromise method of advanced MCS is Latin hypercube sampling (LHS) approach. This approach divides the range of each variable into disjoint intervals of equal probability, and one value is randomly selected from each interval[89]. It improves MCS stability and also maintains the tractability of random sampling.

To propagate uncertainty in the parameters of the Finite Element Model (FEM), we first create a deterministic FEM in the professional mechanical software ANSYS by parameter design language. In this paper, our example is a typical structure as presented in Fig 5-1, corresponding parameters were showed in Table 5.1. Among

them, there were certain parameters to describe deterministic FEM. There were also ranges of variables in Latin Hypercube sampling. In the program of mechanical analysis for FEM, we can capture plenty of information about the displacement and deformation of the structure as showed in Fig 5-1. To record the situation of the whole structure, we captured and recorded the maximum stress of the structure in each loop of sampling.

Table 5 - 1 Parameters of material and geometrical properties

Material and geometrical properties		
Certain parameters		
L	Length of the structure	10 m
E	Young's Module	2*10^5 MPa
P	Physical density	7000 kg/m^3
V	Poission ratio	0.3
Variables in Latin Hypercube sampling methods		
R1	Radius in the bottom	0.1 ~3 m
R2	Radius in the top	0.1~3 m
T1	Ratio of ring thickness	0.01~0.99
PP1	Pressure in the half surface	0~240
PP2	Force in the top	0~10^5 N

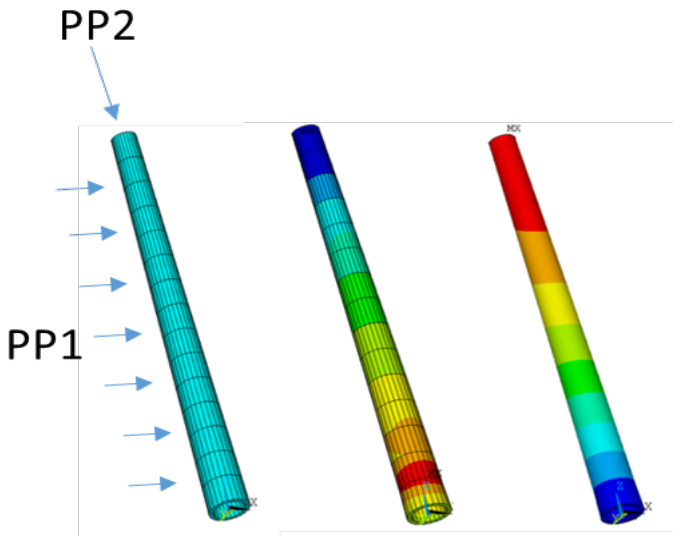

Fig 5 - 1 Finite element model and results of mechanical analysis

In Latin Hypercube sampling method, the input variables were parameters described in Table5.1.The output parameter was the maximum stress of the structure in each certain iteration of mechanical analysis. To test the stability of Latin Hypercube sampling method, different numbers of samples were attempted in our program. As presented in Fig 5-2, scatter results of Latin Hypercube sampling.

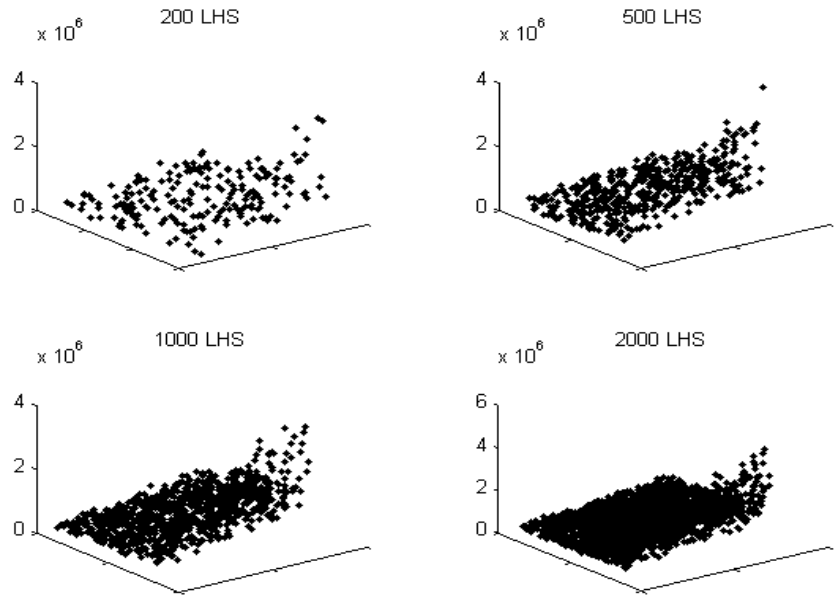

Fig 5 - 2 Scatter results of Latin Hypercube sampling method

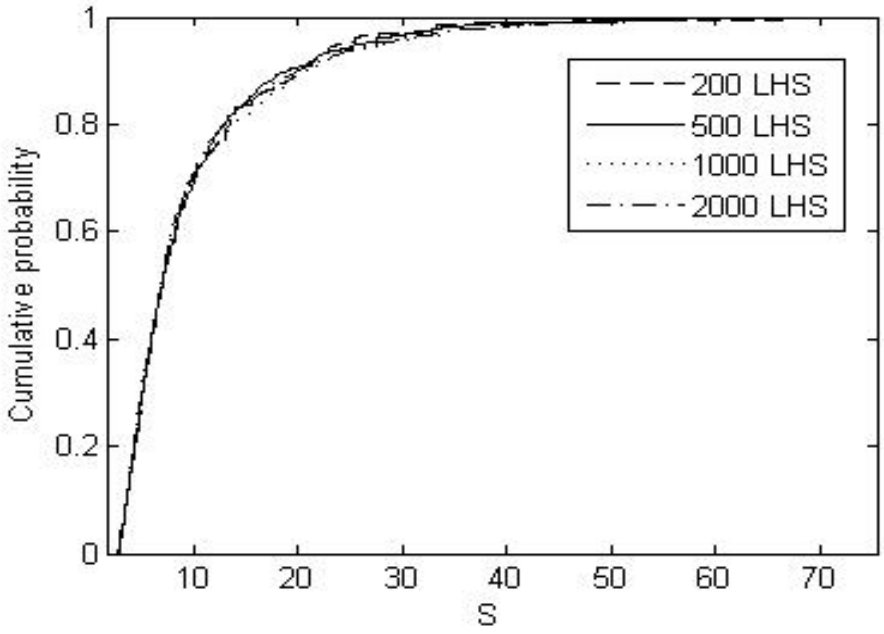

Fig 5 - 3 Cumulative probability of maximum stress

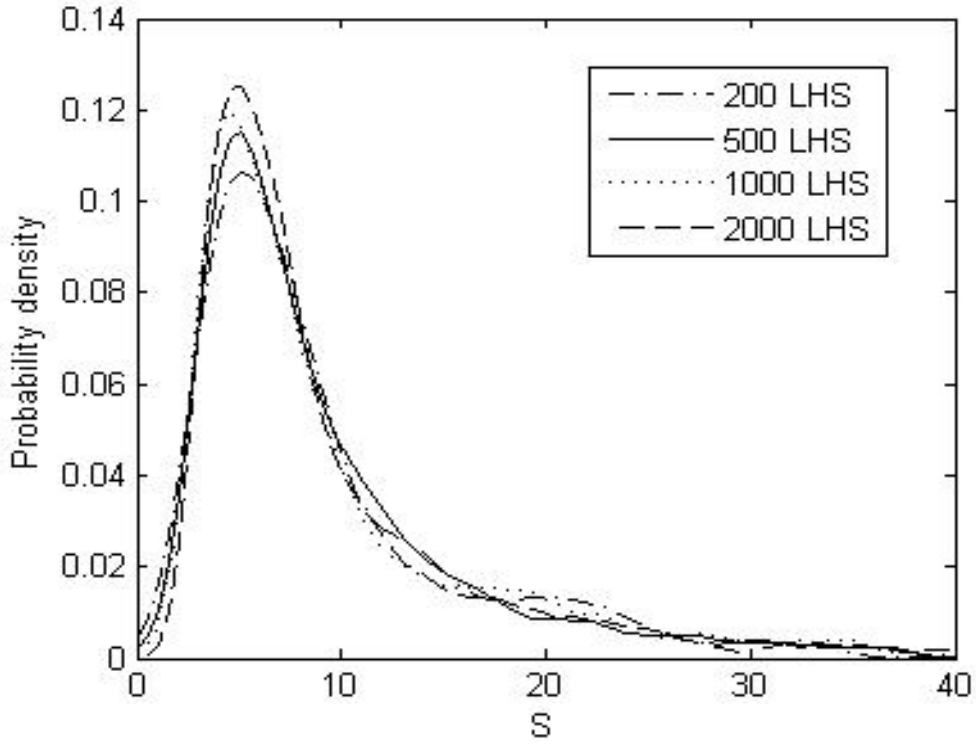

Fig 5 - 4 Probability density of maximum stress

To compare the results of Latin Hypercube -sampling with different numbers of samples, we calculated cumulative probability and probability density of output parameter in the program, as presented in Fig 5-3 and Fig 5-4. The probability of maximum stress of 200, 500, 1000, 2000 LHS is approximated to each other, the difference is not evident. It is obvious that LHS method is very stable and has good convergence. In the further discussion, we find that the results of probability density of maximum stress in different numbers of LHS are also close to each other, except in the peak of the curve. In this structural, larger number of sampling will contribute to higher peak in probability density of maximum stress.

A surrogate model can be thought of as a regression to a set of data, where the data is a set of input-output pairing obtained by evaluating a black-box model of the complex system[90]. Here, the black-box model is the system of performing Latin Hypercube sampling repeatedly in Finite Element Model.

In the other hand, a global surrogate model is a function that approximates the system across the design space. Kriging interpolators fit a spatial correlation function

to a data set consisting of input-output pairs obtained by evaluating the underlying function.

$$G(x) = F(\beta : x) + z(x) \tag{5 - 116}$$

Where $F(\beta : x)$ is a deterministic component defined by a regression model that gives an approximation to $G(x)$ in mean value and $z(x)$ is a stationary Gaussian process with zero mean and covariance .

In the other hand, we also considered non-linear fitting as a reference. It can be written as,

$$F\left(\beta : x\right) = \beta_0 \prod_{i=1}^{n} x_i^{\beta_i} \tag{5 - 117}$$

Table 5 - 2 Comparison of results of surrogate model

	Correlation coefficient	D
Non-linear fitting	0.9933	1.0585
1-order regression	0.8002	23.7895
2-order regression	0.9471	6.8092
KM(0-order)	1	5.9341e-17
KM(1-order)	1	1.6060e-19
KM(2-order)	1	3.5514e-21

To compared the results of these three surrogate model, namely non-linear fitting, response surface method (first order regression and second order regression) and Kriging model, correlation coefficient of prediction and original database and difference was calculated as in Eq (5-116)and Eq (5-117) and concluded in Table.2.

$$c = \frac{\sum_{i=1}^{n}\left(y_i - y_{av}\right)\left(\hat{y}_i - \hat{y}_{av}\right)}{\sqrt{\sum_{i=1}^{n}\left(y_i - y_{av}\right)^2}\sqrt{\sum_{i=1}^{n}\left(\hat{y}_i - \hat{y}_{av}\right)^2}} \tag{5 - 118}$$

$$D = \frac{1}{n}\sum_{i=1}^{n}\left(y_i - \hat{y}_i\right)^2 \tag{5 - 119}$$

From Tabel 5.2 we can find, firstly, the results of surface response method are not satisfied when fitting a huge amount database of random sampling space like LHS in this paper. The correlation coefficient of prediction and original database is far from 1, and the differences are also very large. Secondly, the result of non-linear fitting is a little better than surface response method. We will choose it in the following analysis as a reference in comparison. Lastly, the results of Kriging model have absolutely advantage when compared with the others. The difference of the prediction of Kriging model with the original database is extremely small and almost close to zero. In addition, in the structural example of this paper, from the results of D, second order Kriging model has a higher accuracy than first order Kriging model and zero order Kriging model. Therefore, Kriging models are more competitive in fitting huge amount of database.

To be clearer, predictions of surrogate models in cumulative probability and probability density were presented in Fig5-5 and Fig5-6 respectively. Because the results of Kriging model (zero order, first order and second order) are approximated to each other, here we put first order Kriging model in the group to compare with other surrogated model. The prediction of Kriging model is loyal to the original database in the whole predictive field. While the results of response surface method in cumulative probability and probability density are far from the original database.

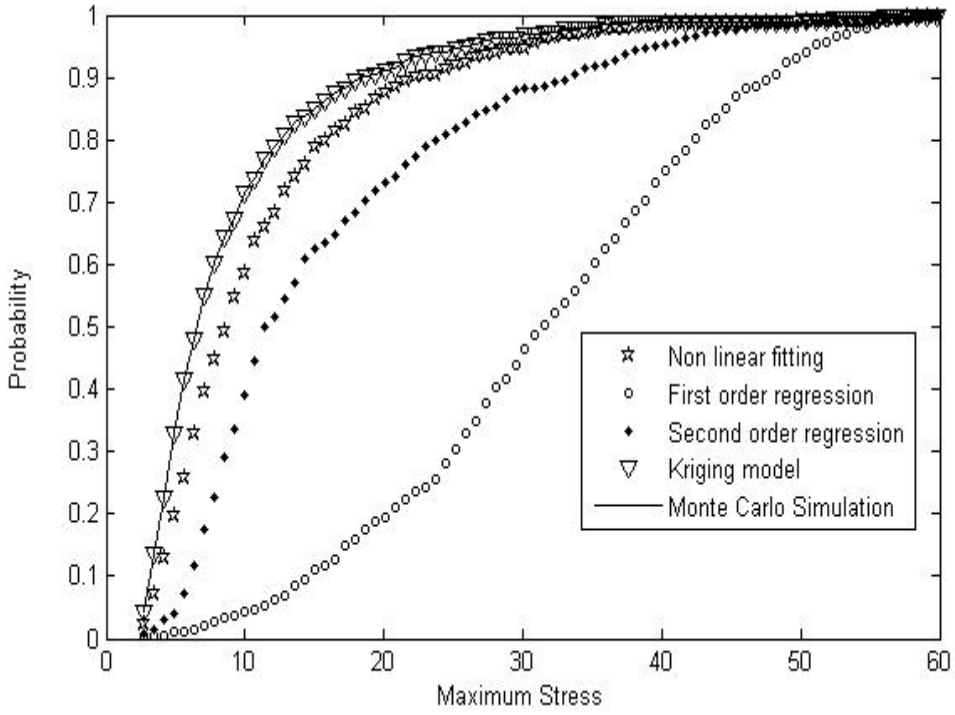

Fig 5 - 5 Prediction of surrogate models in cumulative probability

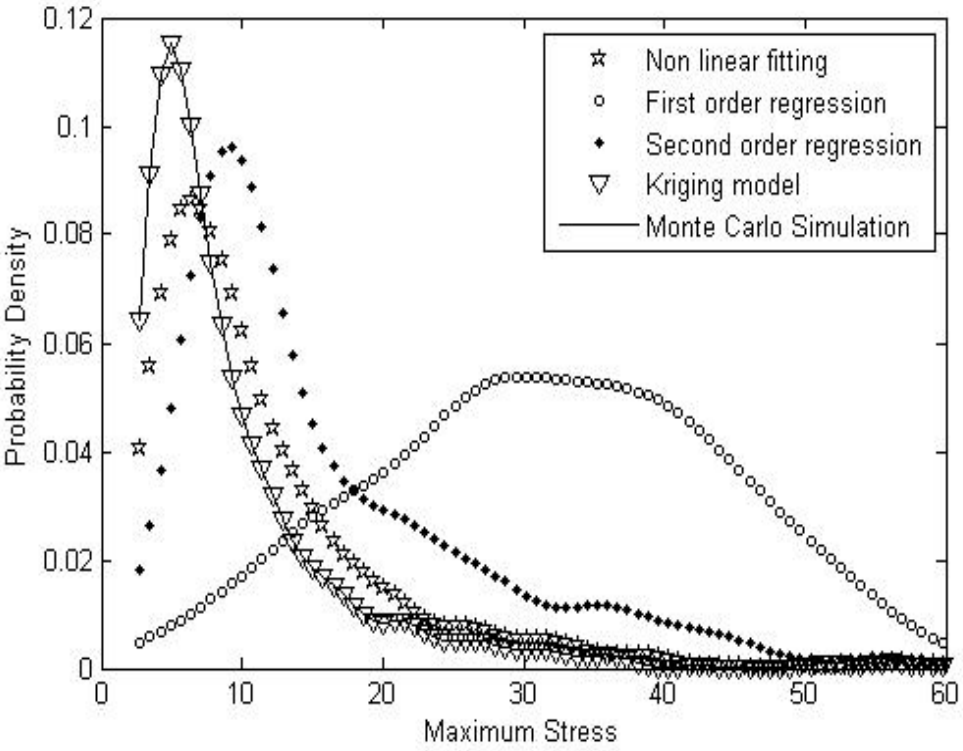

Fig 5 - 6 Prediction of surrogate models in probability density

Therefore, Kriging model will be used to construct the approximated functional relationship between design variables and corresponding response to replace mechanical analysis in FEM.

The surrogate models discussed can be presented in flowchart as in Fig5-7. In this section, reliability based optimization will be performed in surrogate model.

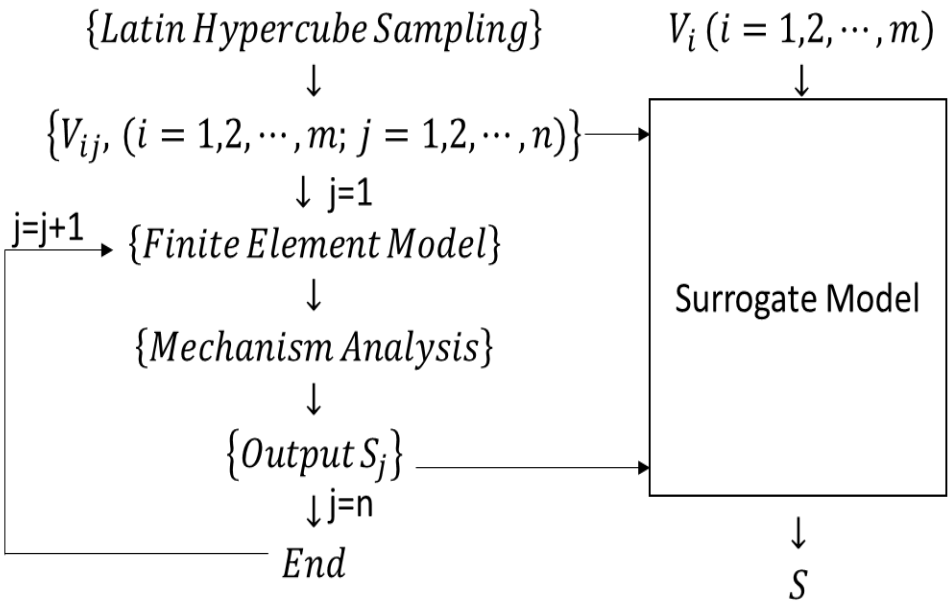

Fig 5 - 7 Flowchart of surrogate model

The reliability based optimization has been proposed for optimization which concerns with the inherent randomness in physical quantities, such as element dimensions, material properties and external loads. It can be divided into three categories: two-level methods, single loop methods and decoupled methods[91].

In two-level methods, there are reliability analysis loop and optimization loop as two nested loops. Reliability index approach (RIA) and the performance measure approach (PMA) are widely used methods in reliability assessment analysis[92]. However, when concave performance measure functions are involved, the difficulties in convergence will be suffered. Single loop approach transforms the nested optimization into single loop process by replacing the reliability constraints by Karush-Kuhn-Tucker optimality conditions[93]. It requires the explicit implementation of the probabilistic transformation and the calculation of the second order derivatives.

The decoupling approach is to transform the reliability based optimization problem into a deterministic one by explicitly approximating the failure probability as a function of the design variables[94]. One possible way of constructing the approximation is to

adopt the predefined function and select some predefined interpolation points in the space of the design variables, in this paper, as mentioned in above, Kriging model as a surrogate model will play a very important role in this step.

According to the sampling points extracted from the Latin Hypercube sampling method in Finite Element Model, we can construct the Kriging model which approximately describes the relationship between input and output. The optimization formulation can be expressed as,

$$\text{Minimum} \quad \begin{matrix} V = V(\mathrm{R}1, \mathrm{R}2, T) \\ \mathrm{P} = P\left(F_M > F_s\right) \end{matrix} \tag{5 - 120}$$

$$\text{Subject to} \quad \begin{matrix} V_{i,\min} \le V_i \le V_{i,\max}, \ i = 1,2,3; \\ V_1 = R1, V_2 = R2, V_3 = T \end{matrix} \tag{5 - 121}$$

Where V is the volume of the structure, it is linearly correlated with the weight and cost of the structure, here we make it as one of the objectives and to find small value for it. P is equal to $P\left(F_M > F_s\right)$, it is the probability of the situation when maximum stress in the whole structure is larger than yield strength of certain material chosen in the structure. $PP1$ and $PP2$ are mentioned in Table 5.1, in order to simulate uncertainties of the complicated operation environment of the structure, specific probability distribution function will be chosen and settled in certain value according to the real practical situation.

For the optimization algorithm, two heuristic algorithms were attempted in this paper. GA is a class of adaptive stochastic optimization algorithms that inspired by the principles of natural evolution to perform search and optimization[95]. The basic idea of SA is adopted from the "annealing" process used in the metallurgical industry, by which slow cooling is applied to metals to produce better aligned, low energy-state crystallization[96]. It is not to restrict the search to those solutions that decrease the objective function value, but also allow moves that increase the objective function value. This mechanism may avoid the procedure being trapped prematurely in a local minimum[97].

In GA, the variables V_i were given specific ranges according to practical situation, as $V_{i,\min} \le V_i \le V_{i,\max}$ $(i = 1,2,3)$. GA starts from a random initial solution. Every individual

or chromosome is encoded into a structure which represents its properties. The chromosomes evolve through successive iterations of generations. During each generation, the chromosomes are evaluated using some measures of fitness. In this paper, the objective of optimization as the fitness in the procedure of the GA is to find minimum $V(\mathrm{R}1, \mathrm{R}2, T)$, $P\left(F_M > F_s\right)$. In this way, we want to find a solution of the structure design, make it more economic in material cost that is minimum the volume of the structure $V = V(\mathrm{R}1, \mathrm{R}, T)$, in the same time, the reliability and safety of the structure should also been taken into consideration that is minimum the probability of failure $\mathrm{P} = P\left(F_M > F_s\right)$. To deal with multiple objectives in the optimization, $\Phi = V + P$, to keep a specific level of reliability of the structure, if $P(F_M > F_s) > 0.1$, P equals to infinitely large value to exclude this sample in the search iterations. It is an effective way to transform the constraints into objective function.

In SA, we have the same problem formation of reliability based optimization. For the algorithm of SA, a new solution is taken from the predefined neighbor-hood of the current solution. The search process proceeds by comparing with the objective function value of the current best solution. If the objective function value of the new solution is better, it becomes the current solution, the search iteration will continue until stopping criteria is met.

Table 5 - 3 Results of reliability based optimization

	GA(KM)	GA(NF)	SA(KM)	SA(NF)
R1	1.1879	0.3532	1.1063	0.3399
R2	0.1092	0.1175	0.1022	0.1001
T	0.9887	0.9896	0.9872	0.9900
P	0.0100	0	0.0320	0
V	0.0349	0.0037	0.0342	0.0032
Time	2619	1.104	2244	4.436

Table 5.3 presents the results of reliability based optimization of genetic algorithm and simulated annealing in two surrogate models, namely Kriging model and non-linear fitting model. According to observation of Table 5.3, we can find results can be divided into two groups by surrogate model. In the same surrogate model, the two

heuristic algorithms have close results. Another thing that is valuable to mention is that the computational expenses in two surrogate model is evidently different. The nonlinear fitting surrogate model sharply reduce the heavy computational burden. However, the results should be tested in finite element model of structure by performing Latin Hypercube sampling again to propagate uncertainties in the operation environment.

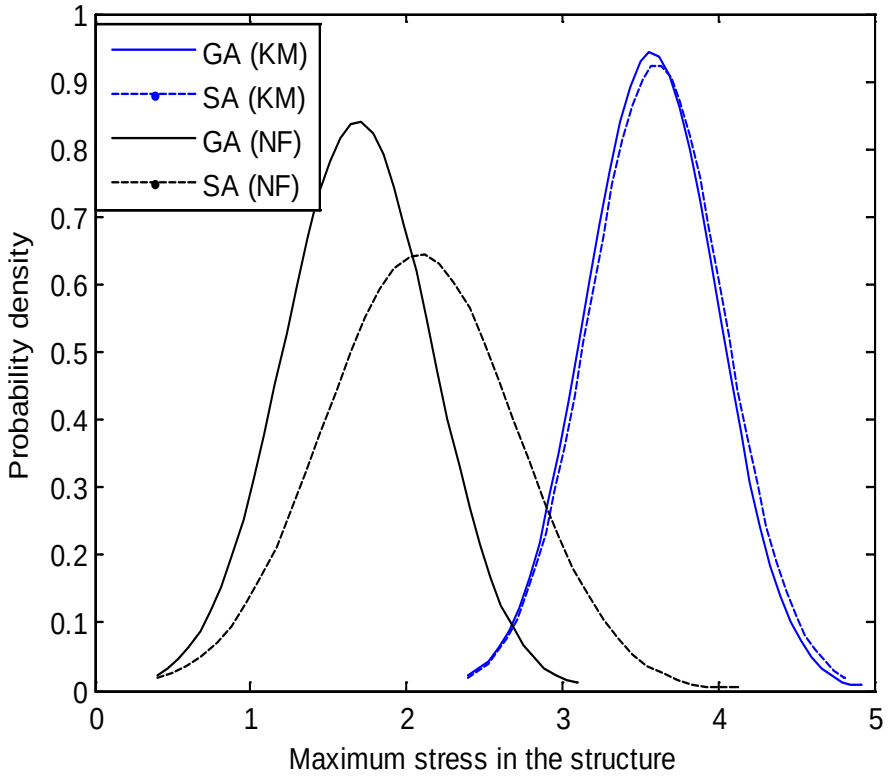

Fig 5 - 8 Probability density of Latin Hypercube sampling

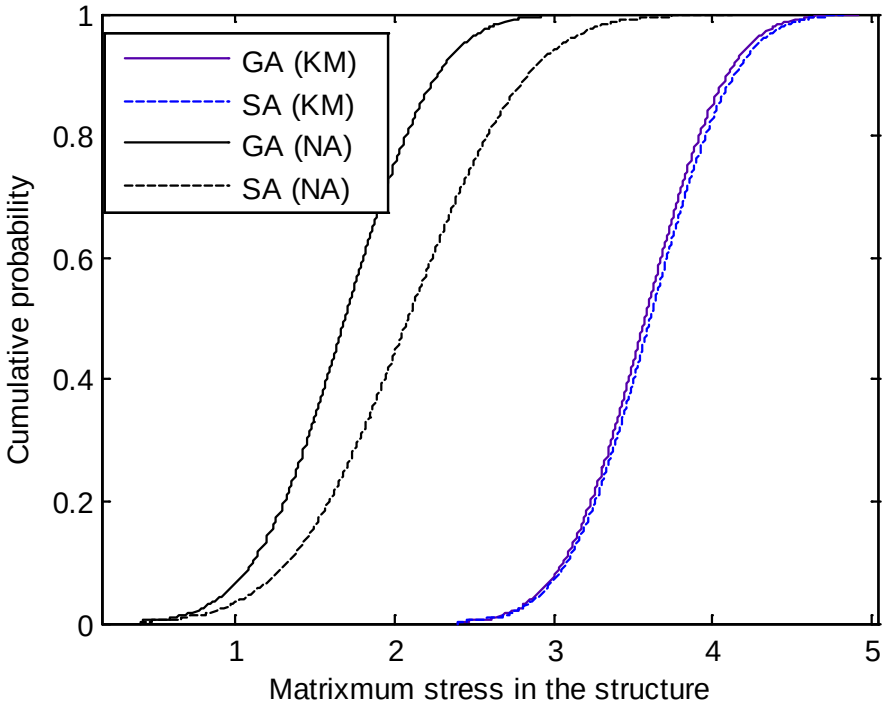

Fig 5 - 9 Cumulative probability of Latin Hypercube sampling

Fig5-8 and Fig5-9 are the results of Latin Hypercube sampling in probability density and cumulative probability respectively. In the figures, 2 in the x axe is relative to F_s. Then we can find that, firstly even though nonlinear fitting surrogate model is economic in computational expense, it is not precise in the process of prediction and is not suitable to apply in reliability optimization. In its prediction, $P(F_M > F_s) = 0$, however, when structure model takes the reliability optimization results of GA and SA in nonlinear fitting model and performs Latin Hypercube sampling, the probability of failure is far more large than 0, therefore nonlinear fitting surrogate model has the problem of distortion in prediction. Secondly, by applying nonlinear fitting surrogate model, SA obtained better result than GA, its result is safer in structural reliability and more material saving in cost. The disadvantage of SA in this group is that it spent longer time in reliability optimization program. Thirdly, Kriging model is more suitable than nonlinear fitting model as surrogate model. The results of Kriging model in two heuristic algorithms are completely satisfied to the safety criteria $P(F_M > F_s) \le 0.1$. In this group, SA also has small superiority than GA, a little more saving in material cost and safer in structure reliability. In computational cost, it also keep advantage. To improve the property of these two algorithms, we still have a lot of work to do in the future.

5.7 Conclusion

Traditional reliability-based design optimization requires a double loop iteration process. The inner optimization loop is to find the most MPP, and the outer is the regular optimization to optimize the RBDO problem with reliability objective or constraints. The computation can be prohibitive when the associated function evaluation is expensive. As a result, many approximate RBDO methods, which convert the double loop to a single loop, have been developed. In the example of this chapter, we propose an effective method to decouple the loops of reliability assessment analysis and optimization by creating surrogate models. Latin Hypercube sampling approach is performed in finite element model of structure to obtain a huge size of database for surrogate models. In surrogate models, Kriging model is more competitive than response surface model and nonlinear fitting method. Heuristic algorithms for optimization were chosen in order to prevent the premature convergence in the process optimization. The results of genetic algorithm and simulated annealing algorithm in Kriging model for reliability based optimization were tested in finite element model of the structure again. They are completely satisfied the reliability criteria and also material saving. The method proposed is constructive in reliability based optimization in structure design and engineering research.

Chapter 6 Examples

6.1 Cumulative Damage Analysis of Wing Structure by Stochastic Simulation

6.1.1 Stochastic simulation in Finite Element Model

When sampling a function of N variables, the range of each variable is divided into M equally probable intervals. M sampling points are then placed to satisfy the Latin hypercube requirements; note that this forces the number of divisions, M , to be equal for each variable. Also note that this sampling scheme does not require more samples for more dimensions (variables); this independence is one of the main advantages of this sampling scheme. Another advantage is that random samples can be taken one at a time, remembering which samples were taken so far.

The maximum number of combinations for a Latin Hypercube of M divisions and N variables (i.e., dimensions) can be computed with the following formula:

$$\left(\prod_{n=0}^{M-1}(M-n)\right)^{N-1} = (M!)^{N-1} \qquad (6 - 1)$$

The regularity of probability intervals on the probability distribution function ensures that each of the input variables has all portions of its range represented, resulting in relatively small variance in the response. At the same time, the analysis is much less computationally expensive to generate. The LHS method also provides flexible sample size while ensuring stratified sampling.

According to the advantages of LHS, it is chosen to perform Monte Carlo Simulation in order to propagate the uncertainties of stochastic process. As present in the flowchart, the parameters corresponding with description of geometry model and random loading are defined as input random variables. The maximum stress in the whole structure of wing is searched each time when calculation of FEM was performed, and it is also exported for the following procedure.

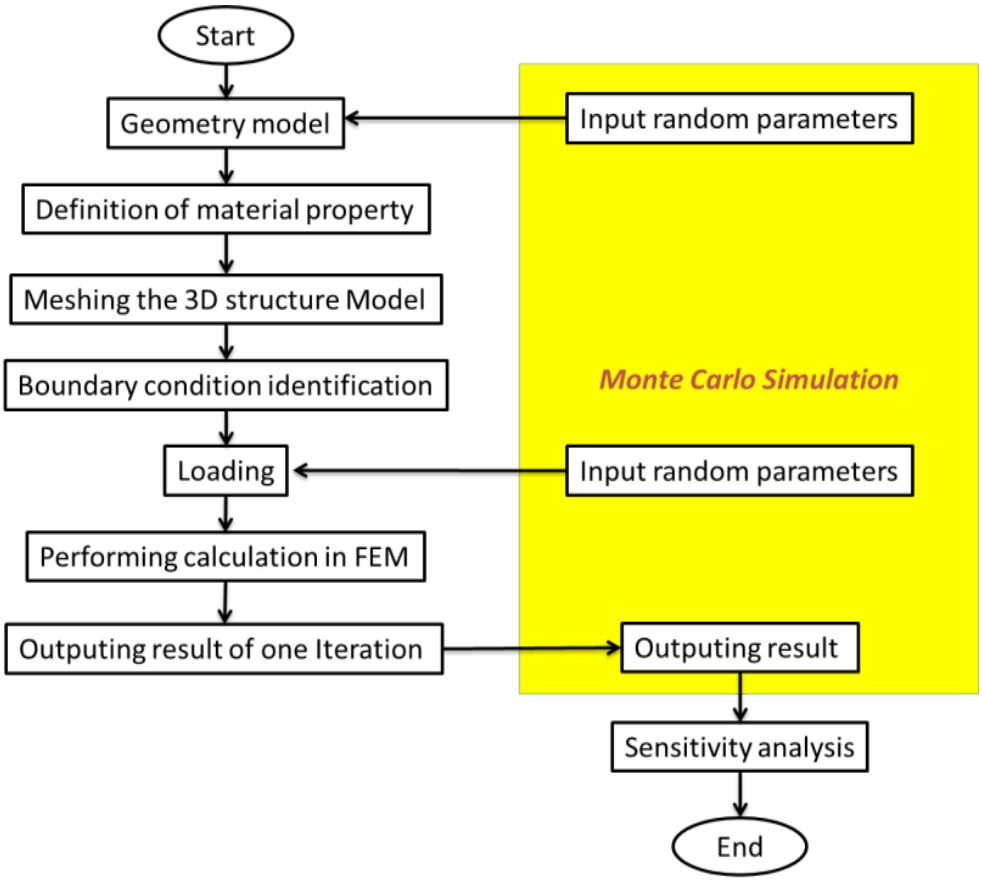

Fig 6 - 1 Flowchart of Stochastic simulation in Finite Element Model

The deterministic Finite Element Model of wing structure was created by ANSYS parameter design language as in Fig 6-1. The corresponding parameters are presented in Table 6.1. Among them, I_k $(k=1,2,\ldots,8)$ are the input random variables representing geometry uncertainties of airfoil, in the same time, P_j $(j=1,2,\ldots,24)$ are also defined as input random variables, which represent random loading in order to simulate the complicated operation environment of aircraft.

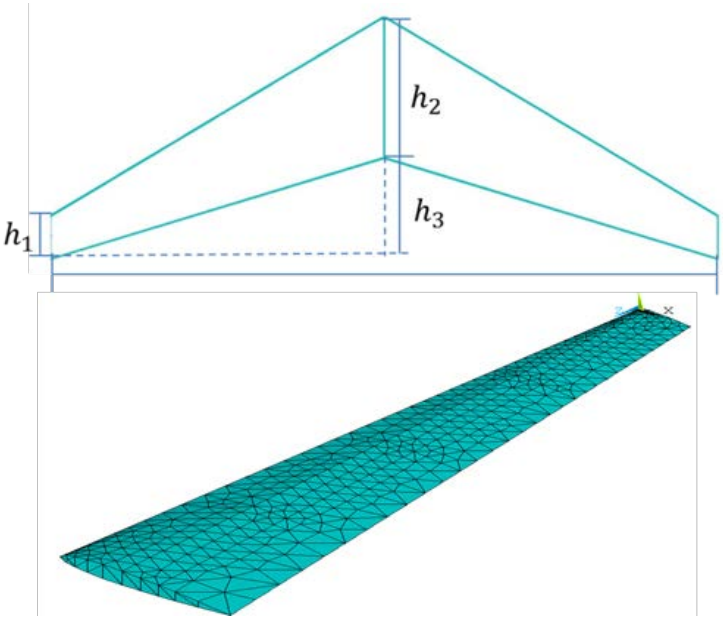

Fig 6 - 2 Finite Element Model of wing structure in ANSYS

Table 6 - 1 Parameters of Finite Element Model

Length	h_1 = 3.2 m h_2 = 10.5 m h_3 = 7.5 m l = 80 m
Airfoil	I_k $(k = 1, 2, \ldots, 8)$
Loading	P_j $(j = 1, 2, \ldots, 24)$
Material property	Physical density = 2800kg/m3 Young's module = 7e^10 Pa Poisson's ratio = 0.33

In consideration of the convergence of sampling method as present in Fig .3, in this paper, we performed 3000 random sampling for each random input variable in LHS. The maximum stress in the whole structure of wing was captured and recorded to observe the situation of the structure in stochastic simulation. The record of maximum stress in the whole structure in 3000 iterations is as in Fig6-2, Fig 6-3 presents the more obvious representation for stochastic simulation. From histogram of maximum stress, we can find the probability frequency of the stress.

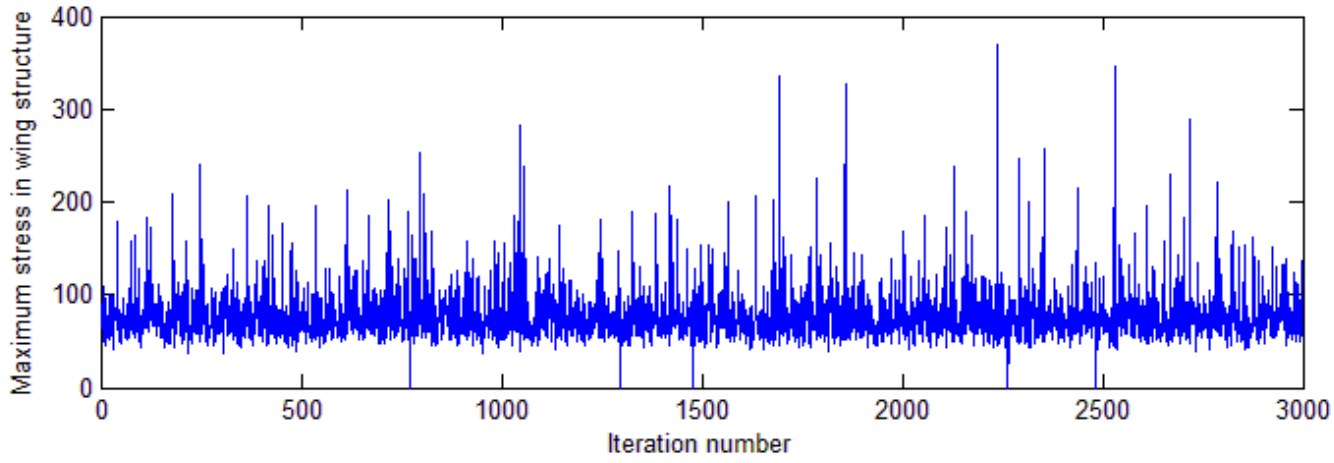

Fig 6 - 3 Record of maximum stress in the whole structure of the wing in LHS

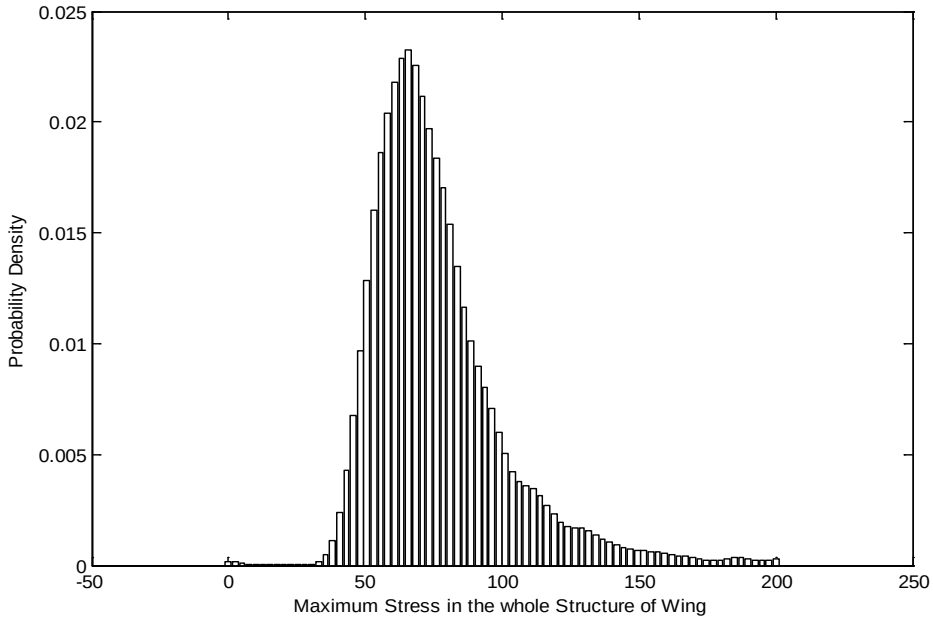

Fig 6 - 4 Histogram of maximum stress in LHS

6.1.2 Fatigue Analysis

The Palmgren-Miner rule is commonly used to predict the damage accumulation due to fatigue [98][7]. According to this rule, a linear damage accumulation law at a point in the structure subjected to variable amplitude stress time history is defined as in the formula

$$D = \sum_{i}^{m} \frac{n_i}{N_i} \tag{6 - 2}$$

Where n_i is the number of cycles at a stress level σ_i, N_i is the number of cycles required for failure at a stress level σ_i, and m is the number of stress levels identified in a stress time history at the corresponding structural point. Available S-N fatigue curves, obtained from laboratory experiments on simple specimens that are subjected to constant amplitude loads, are used to describe the number of cycles N_i required for failure in terms of the stress level σ_i. For linear systems excited by time-varying loads that can be modeled by stationary stochastic processes, these power spectral densities can be straightforwardly computed using available random vibration results.

If we know probability density function of stress range, as be calculated then equation can be expressed

$$D = \int_0^{\infty} \frac{n_T f(\Delta\sigma)}{N(\Delta\sigma)} d\Delta\sigma \tag{6 - 3}$$

Where n_T is total number of stress range $\Delta\sigma$ and $f(\Delta\sigma)$ is stress rang PDF. The n_T value can be calculated from design life multiplied by $E[\Delta\sigma]$, expected rate of stress range occurrence, and $N(\Delta\sigma)$ is number of cycles at $\Delta\sigma$ as given in S-N curve:

$$N(\Delta\sigma)^m = C \tag{6 - 4}$$

Where m and C are material constants.

Sensitivity analysis plays an important role in identification of key model features, effects of uncertainty, unnecessary model detail and database collection[99] [5]. The application of sensitivity analyses is involved in prediction of outcomes for parameter

sets and parameter modifications leads to optimal or desired simulated outcomes. When the amount of parameters in a mathematical model is large, the importance of sensitivity analyses is essential as model complexity growing, problems about validity and interpretation increasing. Fig 6-4 presents results of sensitivity analysis for the random input variables in ANSYS Probabilistic Design System. It is reasonable to pick out the most important input random variables and find the relationship between the input random variables and the output variable (maximum stress in the wing structure).

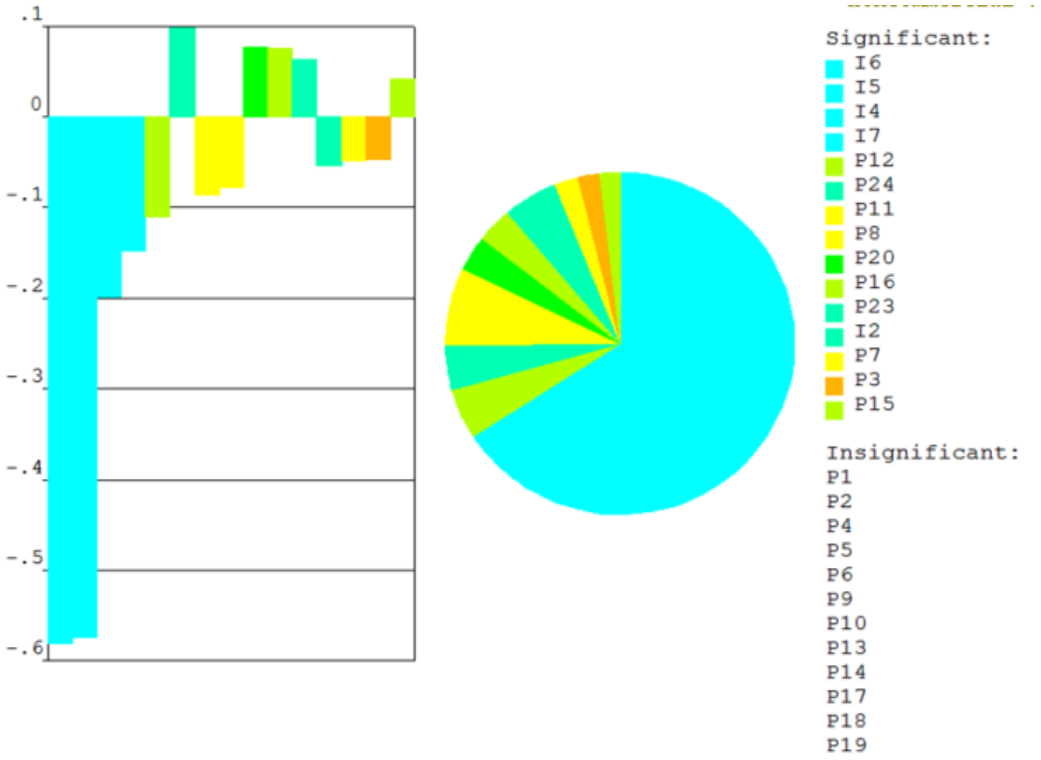

Fig 6 - 5 Result of sensitivity analysis of random input variables

In the work, we only pick out four most important input variables and expressed in the equation. Logically, the larger the amount of input random variables are picked out, more precise the polynomial to express the output variables. However, it is a trade-off between accuracy and computation burden. Our results are satisfactory in the following discussion. Since 3000 iterations of the repeating sampling are numerous, in the regression process to find the coefficient in the polynomial, we divide them into 6 groups. Each group includes 500 iterations.Table 6.2 provides the results of coefficients in the polynomial equation by linear regression method.

$$S_{\max} = c_0 + c_1 x_4 + c_2 x_5 + c_3 x_6 + c_4 x_7 + c_5 {x_4}^2 + c_6 x_4 x_5 + c_7 x_4 x_6 + c_8 x_4 x_7 + c_9 {x_5}^2 + c_{10} x_5 x_6 + c_{11} x_5 x_7 + c_{12} {x_6}^2 + c_{13} x_6 x_7 + c_{14} {x_7}^2 \quad (6-5)$$

Table 6 - 2 Results of coefficient in the polynomial expression

	1	2	3	4	5	6	Average
C0	2.4184	2.3443	2.2619	2.5146	2.4276	2.8556	2.4704
C1	-1.5756	-0.8042	-0.2494	-1.6337	-0.5776	-1.9854	-1.1376
C2	-4.1768	-4.0053	-3.9237	-4.753	-4.2908	-6.0758	-4.5376
C3	-4.374	-4.9596	-4.7479	-5.0046	-5.5037	-4.8319	-4.9036
C4	-0.28	-0.3157	-0.6375	0.0775	-0.1375	-0.8884	-0.3600
C5	1.2423	0.7418	1.0502	2.1566	0.438	1.21	1.13982
C6	-0.5483	-1.1544	-2.2422	-0.3489	-1.933	0.9374	-0.8816
C7	0.6886	1.0282	-0.6858	0.2574	0.3405	0.7263	0.39253
C8	1.7323	0.5758	0.8964	0.8691	1.9482	1.8868	1.3181
C9	3.246	3.3491	3.1617	4.1428	3.8912	5.3302	3.8535
C10	5.7342	6.7796	6.3527	6.8503	7.0194	6.6274	6.5606
C11	-0.3678	-1.5251	-0.1858	-1.7806	-1.6474	-0.0055	-0.9187
C12	3.1091	3.53	3.8684	3.9861	4.5659	3.1202	3.69662
C13	-0.6524	-0.762	0.3015	-1.0879	-0.7102	0.0215	-0.4816
C14	-0.1657	1.1731	0.3854	0.5887	0.2194	0.3075	0.41807

6.1.3 Probability density

Identification of an appropriate probability density function for uncertainty analysis in probability theory is a difficult problem and big challenge to designers and researchers. Gaussian distribution, Rayleigh distribution, and Weibull distribution, which are often applied in fatigue analysis. However, they are not precise to simulate the specific problems or satisfy the accuracy in the particular situation. In this paper, we attempted to calculate probability density of maximum stress in wing structure in the polynomial expression by Dirac's delta.

Dirac's delta may be seen as a probability[100][6], assume that P is a probability defined on Ω, such that, for any $S \subset \Omega$: $P(S)=1$, if $x_0 \in S$; $P(S)=0$. In other words, the single point of non-null probability is x_0: $P(\{x_0\})=1$, while $P(\Omega-\{x_0\})=0$. In this case, the mean of an element $\varphi \in D(\Omega)$ is

$$E(\varphi)=\varphi(x_0)=\delta_{x_0}(\varphi) \quad (6-6)$$

Thus, δ_{x_0} may be interpreted as the density of probability associated to the point x_0.

The following notations are often used in order to recall this property:

$$\varphi(x) = \int \delta(y-x)\varphi(y)dy = \int \delta_x(y)\varphi(y)dy \qquad (6\text{ - }7)$$

In these notations, Dirac's delta appears as a probability density. Then the probability density in the polynomial expression can be calculated. Fig 6-5 shows out the probability density of each group by the method of Dirac's delta.

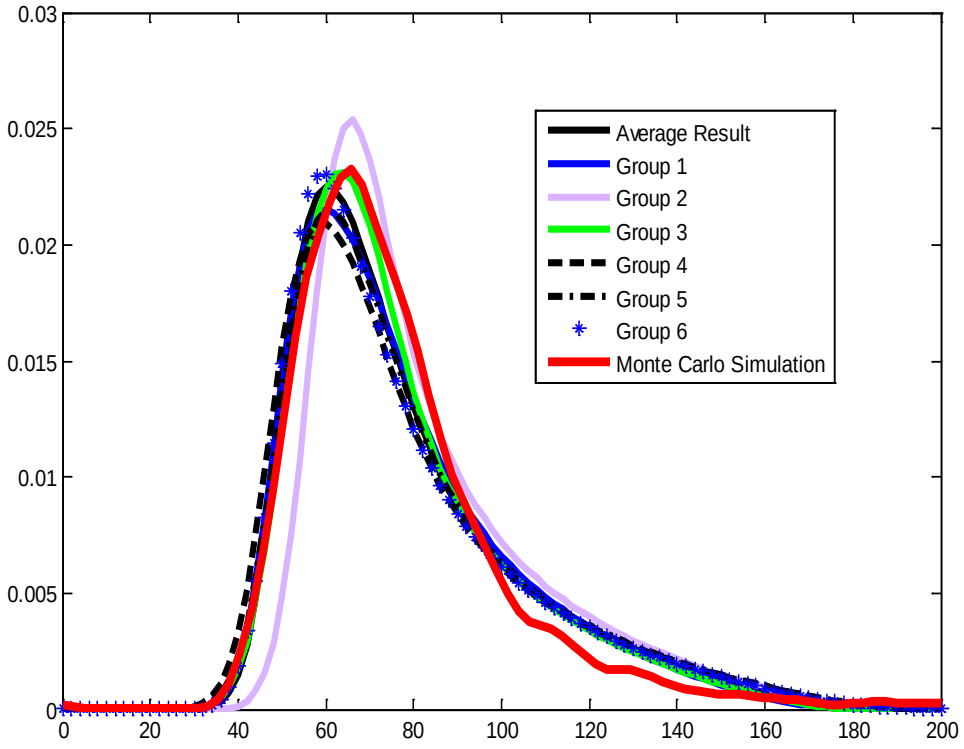

Fig 6 - 6 Probability density of polynomial equation

For Gaussian distribution $f_G(x,\mu,\sigma)$ and Weibull distribution $f_W(x,k,\lambda)$ there are two variables to be identified respectively. Rayleigh distribution $f_R(x,\sigma)$ has only one. Here, we performed optimization to identify the parameters in order to make sure they are the most precise ones. The objective of optimization process is to find the according parameters in each probability density function and the differences with the result of Monte Carlo Simulation are minimized.

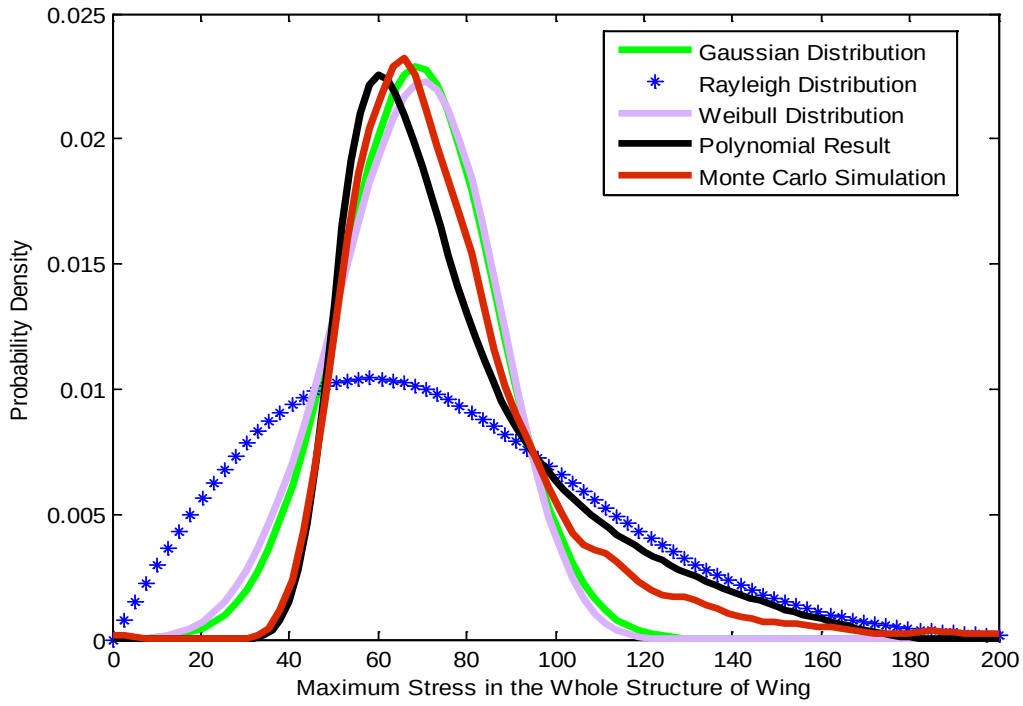

Fig 6 - 7 Probability density of different method

Fig 6-6 compares the results of classical probability density function (Gaussian, Weibull, and Rayleigh distribution), polynomial equation (by the method of Dirac's delta) and Monte Carlo Simulation. For probability density, the result of polynomial equation is close to the result of Monte Carlo Simulation. The results of Gaussian and Weibull distribution are approached and both are better than that of Rayleigh distribution. It seems the Rayleigh distribution is far than the result of Monte Carlo Simulation. Since in this kind of distribution, there is only one parameter to be identified in order to approach the result of Monte Carlo Simulation. It is evident that Rayleigh distribution does not have absolute advantages when to simulate complicated situation.

Since the probability density of the maximum stress in the wing structured is captured and expressed by several methods, the accumulative damage in Palmgren-Miner rule can be calculated. The statistic results of accumulative damage are obtained, as demonstrated in Fig 6-7 and Fig 6-8. In Fig 6-7, the results of Monte Carlo, Gaussian, Rayleigh, Weibull distribution and the result of polynomial expression are very approach when m is not larger than 1. Among them, the result of polynomial

expression is larger than that of Monte Carlo Simulation, while the results of other classical probability distributions are smaller than result of Monte Carlo Simulation.

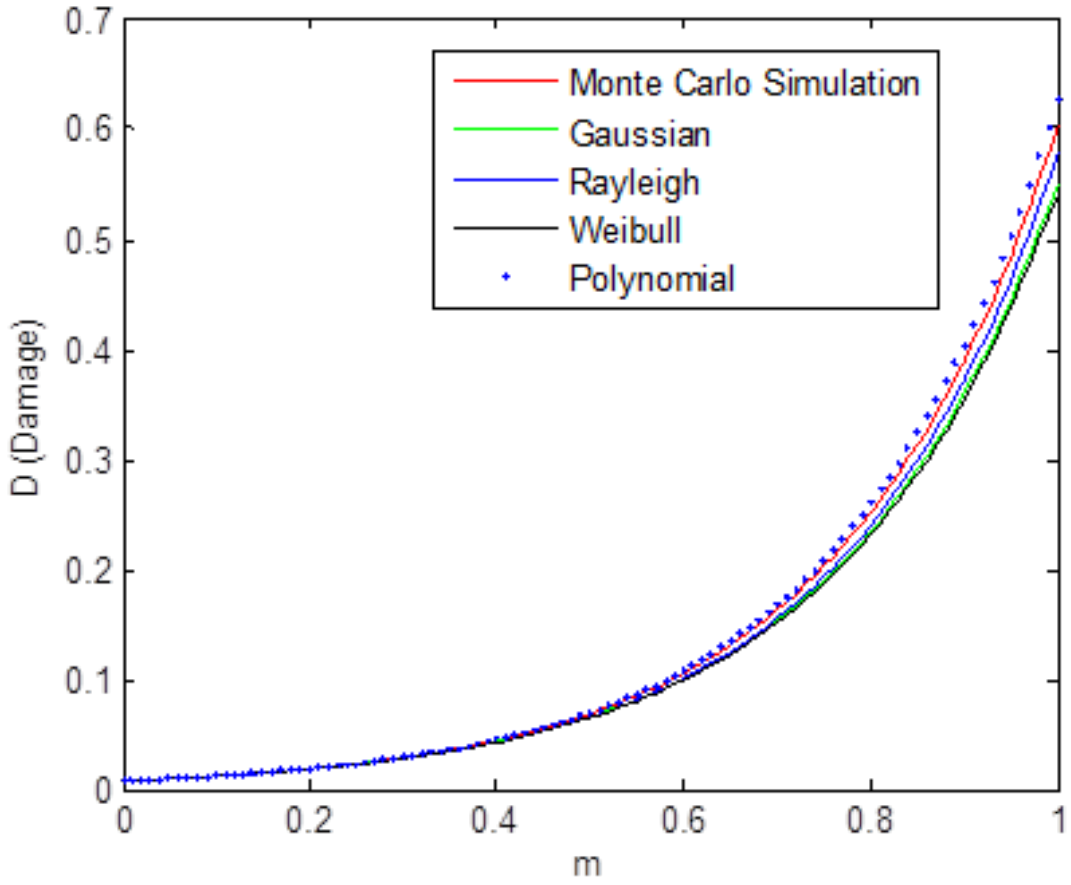

Fig 6 - 8 Results of accumulative damage in different method

To compare the results of them in details, Fig 6-8 presents the relation between the ratio and m, where ratio is the results of D/Dsmc. It is obvious that the result of polynomial equation is the closest to the result of Monte Carlo Simulation. In addition, it is also very stable, does not change when m amplify. In the other hand, the situations of the existing probability density distribution are more complicated. The results of Gaussian and Weibull are similar to each other. When m is small, they can provide the precise result, while when m become larger, the results of them far smaller than that of Monte Carlo Simulation. Different with them, the result of Rayleigh distribution will smaller than that of Monte Carlo Simulation when m is smaller than a specific value. After that, the result of Rayleigh distribution will larger than that of Monte Carlo Simulation. In a sense, the result of Rayleigh distribution is better than that of Gaussian and Weibull distribution.

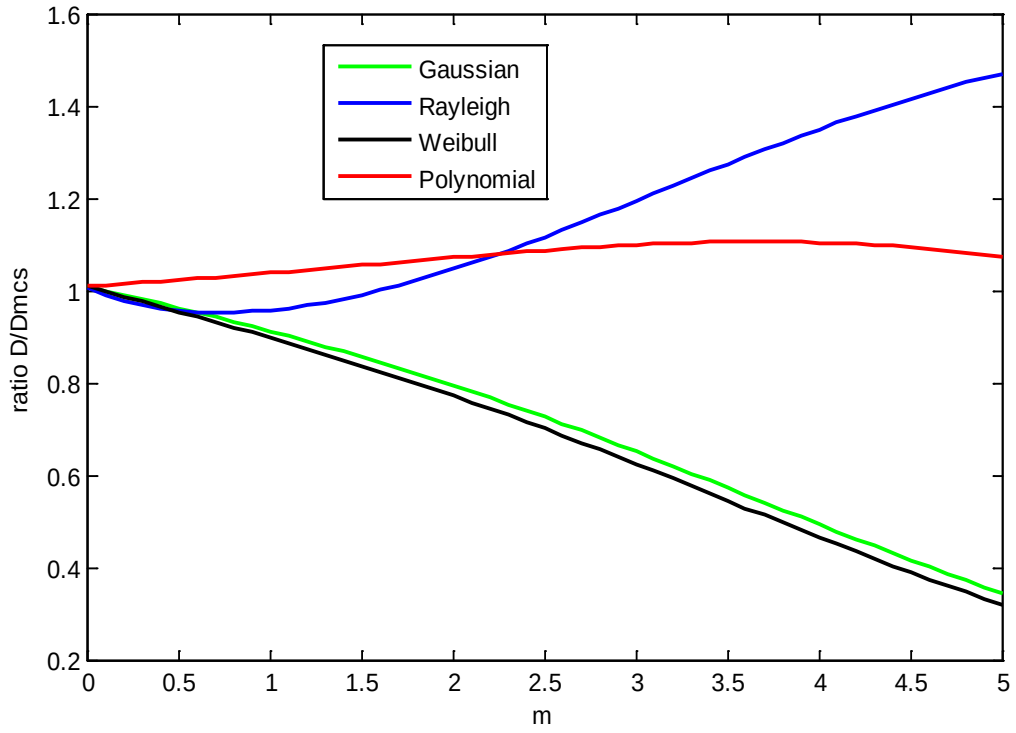

Fig 6 - 9 Comparison of D/Dmcs in each method

6.1.4 Conclusion

In conclusion, this example presents stochastic simulation by Monte Carlo Method in deterministic finite element model of wing structure. During this process, the parameters corresponding with geometry property and outside pressures are defined as input variables, while the maximum stress in the wing structure is searched in every certain sampling loop and transferred out as output variables. Three classical probability density functions, Gaussian, Rayleigh, and Weibull distribution are proposed and used to express the probability distribution of maximum stress in the wing structure. Polynomial expression method as a different method is suggested and provides satisfied results in fatigue analysis. Therefore, when deal with the huge amount of database of stochastic simulation, the regression method applied to obtain the appropriate polynomial expression is advantageous, it is more stable and approached to the precise results.

6.2 Airfoil shape optimization by heurist algorithms in surrogated model

6.2 .1 Airfoil CFD model

An airfoil is a streamlined shape that is capable of generating significantly more lift than drag. The shape of the airfoil can be chosen in the famous NACA 4 digits library. A numbering system is used to define NACA 4 digits wing sections. The first digit indicates the maximum value of the mean-line ordinate in percent of the chord[1]. The second integer indicated the distance from the leading edge to the location of the maximum camber in tens of the chord. The last two integers indicate the section thickness in percent of the chord. In addition, Four-digit series airfoils by default have maximum thickness at 30% of the chord (0.3 chords) from the leading edge. This information provides reasonable limits for variables in geometry in the process of optimization.

The formula for the shape of a NACA 00xx foil, with "xx" being replaced by the percentage of thickness to chord, is:

$$y_t = tc\left[a_1\sqrt{\frac{x}{c}} + a_2\left(\frac{x}{c}\right) + a_3\left(\frac{x}{c}\right)^2 + a_4\left(\frac{x}{c}\right)^3 + a_5\left(\frac{x}{c}\right)^4\right] \tag{6 - 8}$$

Where *c* is the chord length, *x* is the position along the chord from 0 to *c*, *y* is the half thickness at a given value of *x* (centerline to surface), and *t* is the maximum thickness as a fraction of the chord (so 100 *t* gives the last two digits in the NACA 4-digit denomination), $a_i\ (\mathrm{i} = 1, 2, \cdots, 5)$ are the constants,

The simplest asymmetric foils are the NACA 4 digit series foils, which use the same formula as that used to generate the 00xx symmetric foils, but with the line of mean camber bent. The formula used to calculate the mean camber line is:

$$y_c = \begin{cases} \frac{mx}{p^2}(2p - \frac{x}{c}), (0 \le x \le pc) \\ m\frac{c-x}{(1-p)^2}\left[1 + \frac{x}{c} - 2p\right], (pc \le x \le c) \end{cases} \tag{6 - 9}$$

Where *m* is the maximum camber (100 *m* is the first of the four digits), *p* is the location of maximum camber (10 *p* is the second digit).

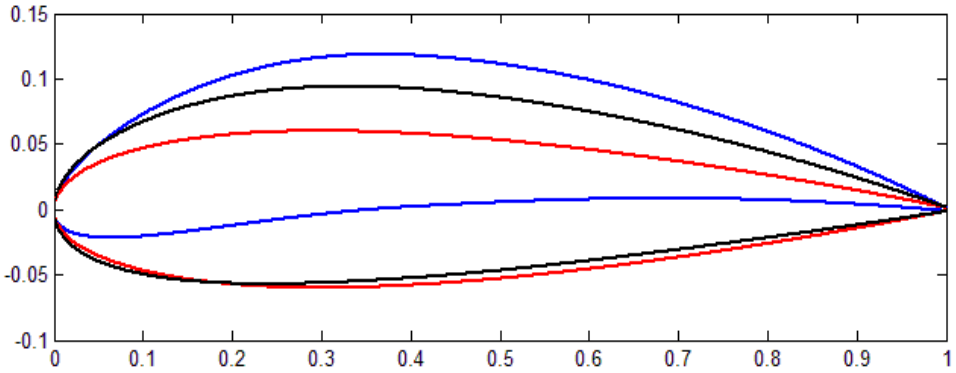

Fig 6 - 10 Examples of airfoil geometry model

The strength of CFD is its ability to inexpensively produce numerical simulations leading to understanding necessary of design. In the fluid element library of ANSYS FLOTRAN, Fluid 141 was chosen as the type of fluid finite element. Table 6.3 demonstrates the details of fluid property and flow environment. The results of certain nodes around airfoil in CFD calculation are captured and summarized as in Fig 6-10, Fig 6-11, Fig 6-12, namely the contour plot of nodal pressure result, total stagnation pressure and fluid velocity of nodal solution, respectively.

Table 6 - 3 Fluid property and flow environment

Table 1 Fluid property and flow environment	
Attack angle	3
Velocity	200 m/s
Temperature	230 K
Pressure	25000 Pa
Density	Air
Viscosity	0
Fluid element type	2D FLOTRAN 141

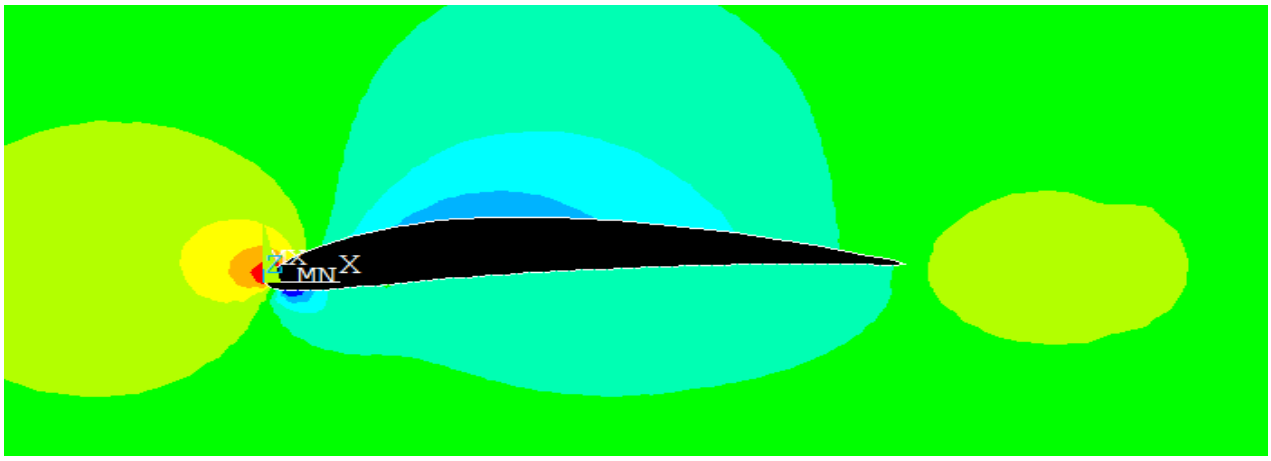

Fig 6 - 11 Nodal pressure result

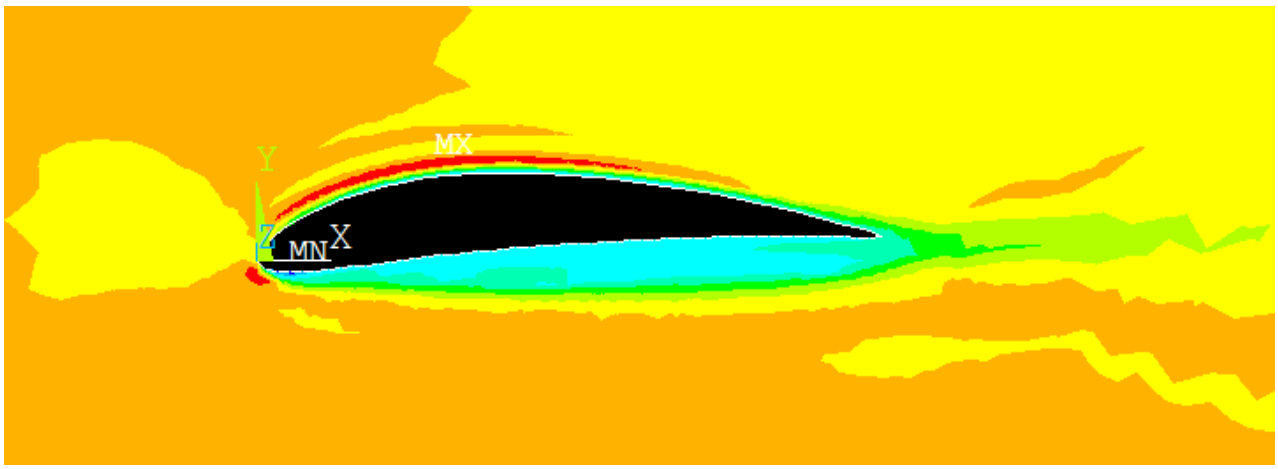

Fig 6 - 12 Total stagnation pressure

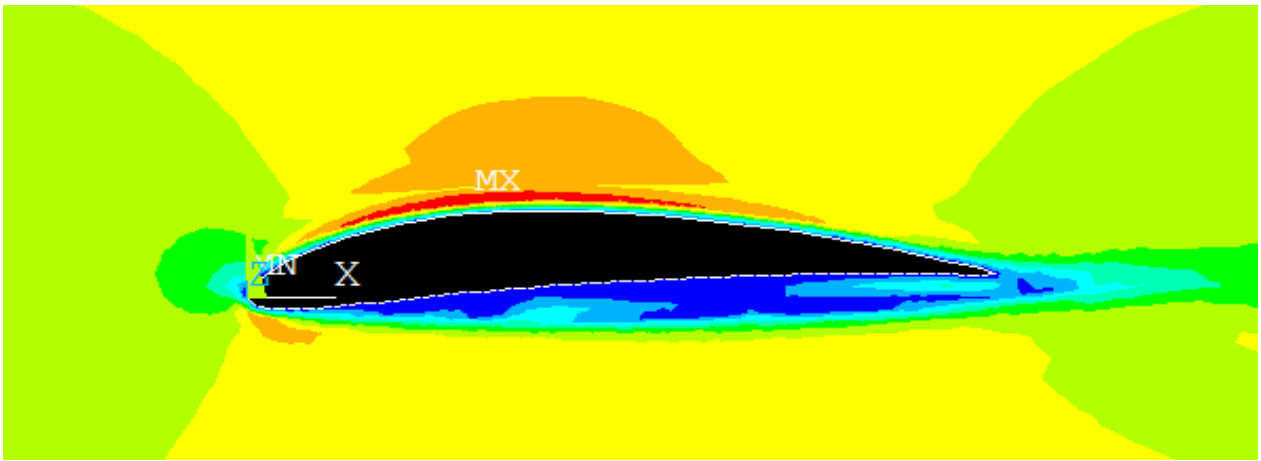

Fig 6 - 13 Fluid velocity of nodal solution

6.2.2 Surrogate model

Monte Carlo simulation (MCS) methods (sampling-based methods) perform repeated sampling and simulation. It is useful if one is trying to get a model to imitate a random

sampling from a population or for doing statistical experiments. It provides the most effective approach to the propagation and analysis of uncertainty for various combinations of the following reasons [101].

Firstly, a sampling based approach provides a full coverage of the range of each uncertain variable in a complicated system. Secondly, modification of the model is not required, and direct estimates of distribution functions are provided. In addition, in the process of sampling, a variety of sensitivity analysis procedures are available. Last but not the least, analysis procedures can be developed and allow the propagation of results through systems of linked models[102].

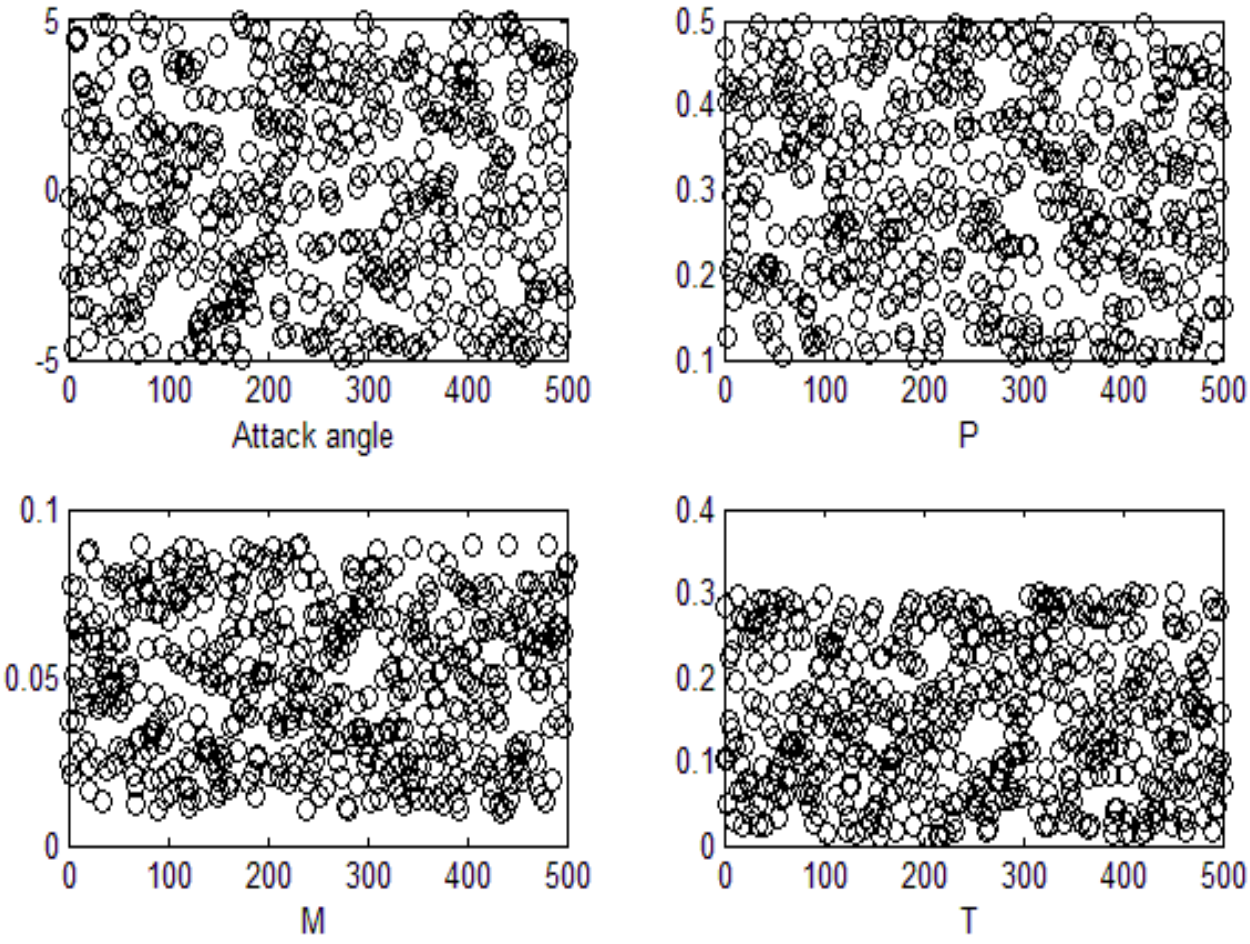

Fig 6 - 14 Samples of input variables

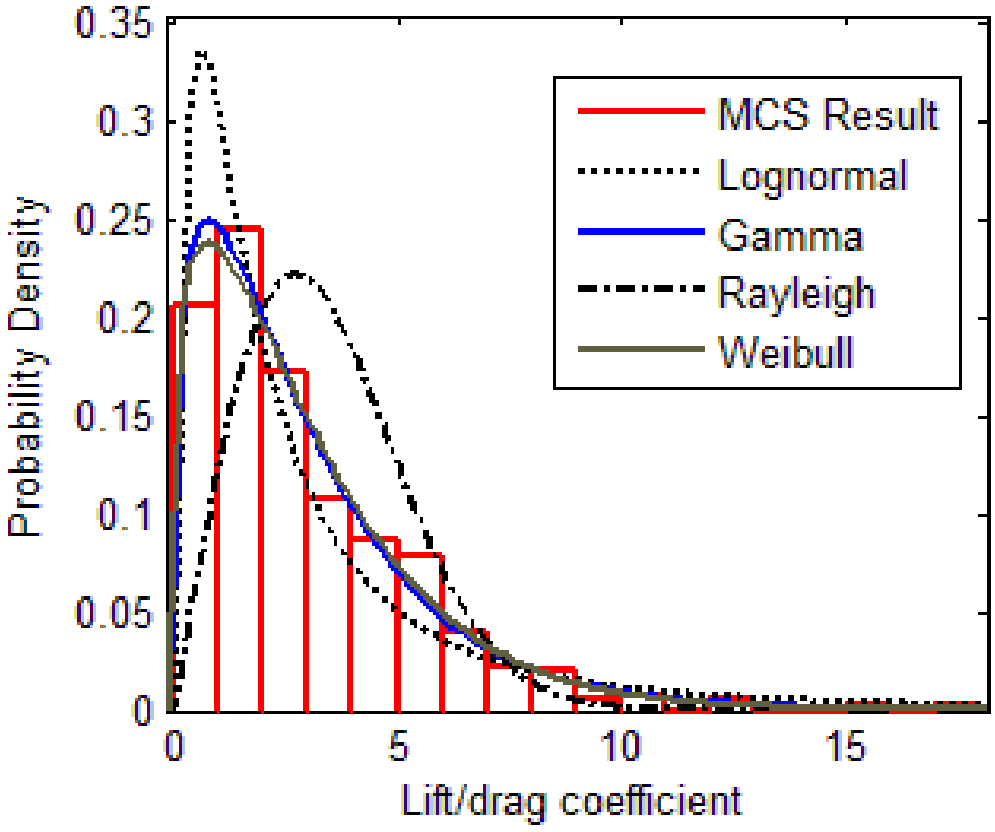

Fig 6 - 15 Probability density results of Lift/drag coefficient

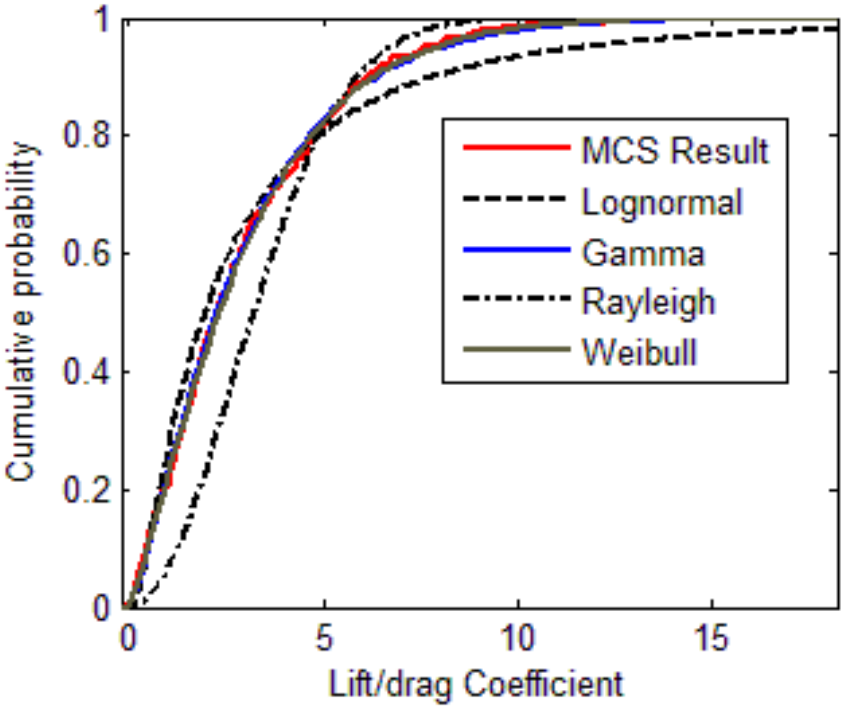

Fig 6 - 16 Cumulative probability of Lift/drag coefficient

As presented in Fig 6-13 attack angle, velocity and also parameters corresponding with geometry property of airfoil (m, p, t) were set as input variables in certain ranges as uniform probability distribution in Monte Carlo Simulation. In the other hand, the output parameter was Lift/drag coefficient calculated by performing CFD. The results showed in Fig 6-14 and Fig 6-15 respectively, as probability density and cumulative probability.

A surrogate model can be thought of as a regression to a set of data, where the data is a set of input-output pairing obtained by evaluating a black-box model of the complex system. Here, the black-box model is the system of performing MCS repeatedly in CFD. To conclude or capture the useful information from this black-box, surrogate model is considered.

A global surrogate model is a function that approximates the system across the design space. Kriging interpolators fit a spatial correlation function to a data set consisting of input-output pairs obtained by evaluating the underlying function[103].

$$G(x) = F(\beta : x) + z(x) \tag{6 - 10}$$

$$F(\beta : x) = \beta_0 + \sum_{i=1}^{n} \beta_i x_i \tag{6 - 11}$$

$$F(\beta : x) = \beta_0 + \sum_{i=1}^{n} \beta_i x_i + \sum_{i=1}^{n} \sum_{j=1}^{n} \beta_{ij} x_i x_j \tag{6 - 12}$$

Where $F(\beta : x)$ is a deterministic component defined by a regression model that gives an approximation to $G(x)$ in mean value and $z(x)$ is a stationary Gaussian process with zero mean and covariance ,

$$Cov[z(x), z(x')] = \sigma^2 R(\theta : x, x') \tag{6 - 13}$$

That interpolates the errors between the regression model predictions $F(\beta : x)$ and the true limit state function values $G(x)$ at the m realizations of the vector of basic random variables x, with σ^2 the constant process variance and R is a prescribed correlation function.

Several correlation functions are available, such as the exponential, linear and Gaussian correlation functions, the most widely used correlation function for structural reliability problems is the anisotropic Gaussian correlation function[104]

$$R(\theta : x, x') = \prod_{i=1}^{n} \exp(-\theta_i d_i^2) \qquad (6 - 14)$$

With $d_i = x_i - x_i'$ the distance between the evaluation point x and the reference point x' in the ith direction of the basic random variables space and $\theta = [\theta_1, \ldots, \theta_n]^T$ a vector of parameters that define the inverse of the correlation length in each direction.

A kriging interpolation model is completely defined by a vector of regression coefficients β , a vector of correlation parameter θ and the variance σ^2 of the stationary Gaussian process[. These parameters are estimated by fitting the Kriging model to a sample of support points.

Where F is the regression matrix and y is the vector of true limit state function values. A 0-order polynomial or first- and second –order polynomials are adopted as regression models $F(\beta : x)$. The matrix R defines the correlation between each pair of support points according to the prescribed correlation function.

A vector with the correlations between the prediction point and the m realizations $x^{(k)}$ $(k = 1, \ldots, m)$ of the vector of basic random variables used in the Kriging model fitting corresponds to the expected or mean value of the Kriging model prediction, an estimate for the variance or uncertainty associated with the model predictions can be given by:

$$\sigma_G^2 = \sigma^2 \left[1 + u(x)^T (F^T R^{-1} F)^{-1} u(x) - r(x)^T R^{-1} r(x) \right] \qquad (6 - 15)$$

$$u(x) = F^T R^{-1} r(x) - f(x) \qquad (6 - 16)$$

Kriging model is used to construct the approximations of the analysis code and describe the functional relationship between design variables and corresponding response. Reliable information form the sufficient number of MCS in CFD was

captured and concluded in the above mentioned Kriging model, zero order, first order and second order respectively.

Fig 6-16 compared the results of predictors of Kriging models (zero order, first order and second order) with the result of MCS, it proves that Kriging models have good property as fitting the result of MCS. The difference between the results and that of MCS is not evident and negligible. The accuracy of Kriging model is satisfied as a surrogate model. In the same time, Kriging model itself has stability of accuracy, the results of zero order, first order and second order are all closed to each other and approximated to the result of MCS. It also proves that the representation of stationary Gaussian process in Kriging model plays a very important role.

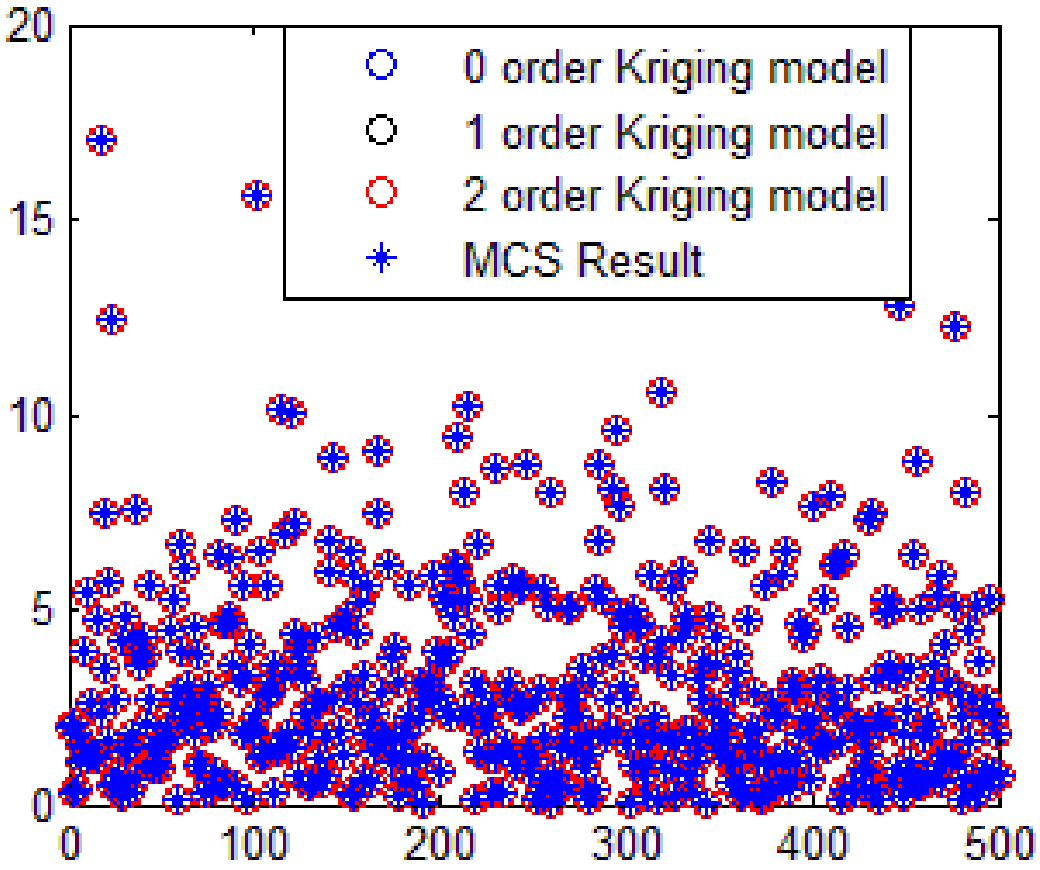

Fig 6 - 17 Results of Kriging models

Kriging model approximately describes the relationship between input variables and output parameters (Lift/drag coefficient). To compare the property of Kriging models which have different orders, the probability distributions of input variables (attack

angle, velocity and also parameters corresponding with airfoil geometry property) were changed in a reasonable range. The results predicted by Kriging models with different orders were presented in Fig 6-17, and Fig 6-18. Fig 6-17 presents that the variance of results predicted by zero order Kriging model is smaller than first order and second order Kriging models. Fig 6-18 also provides that the range of result of second order is wider that the else.

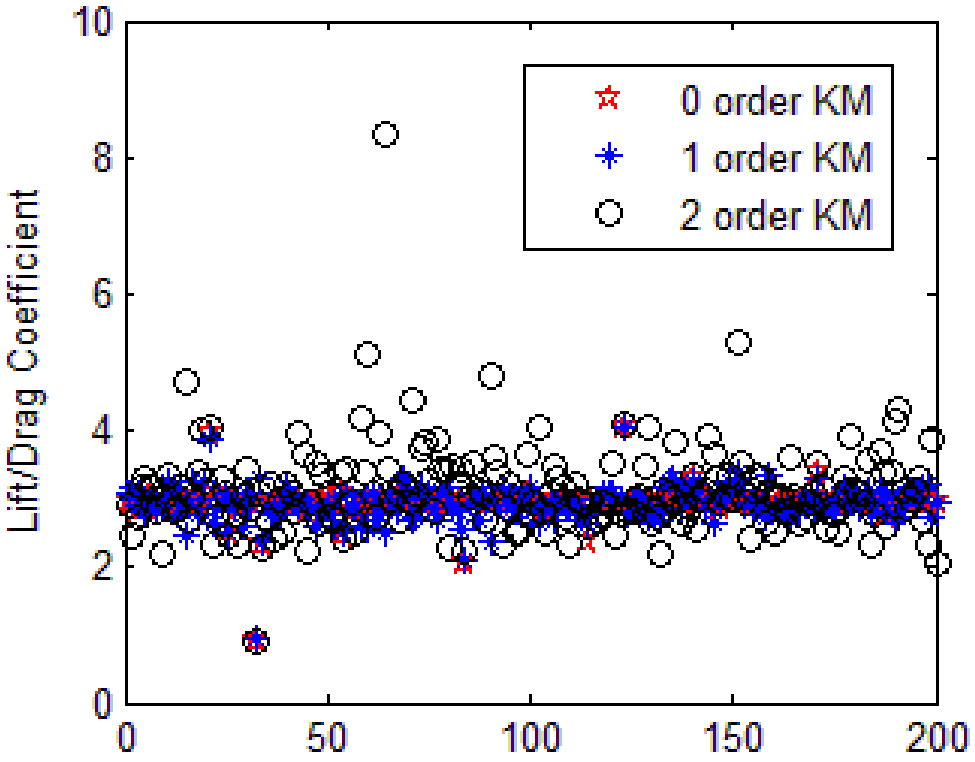

Fig 6 - 18 Results of Kriging models

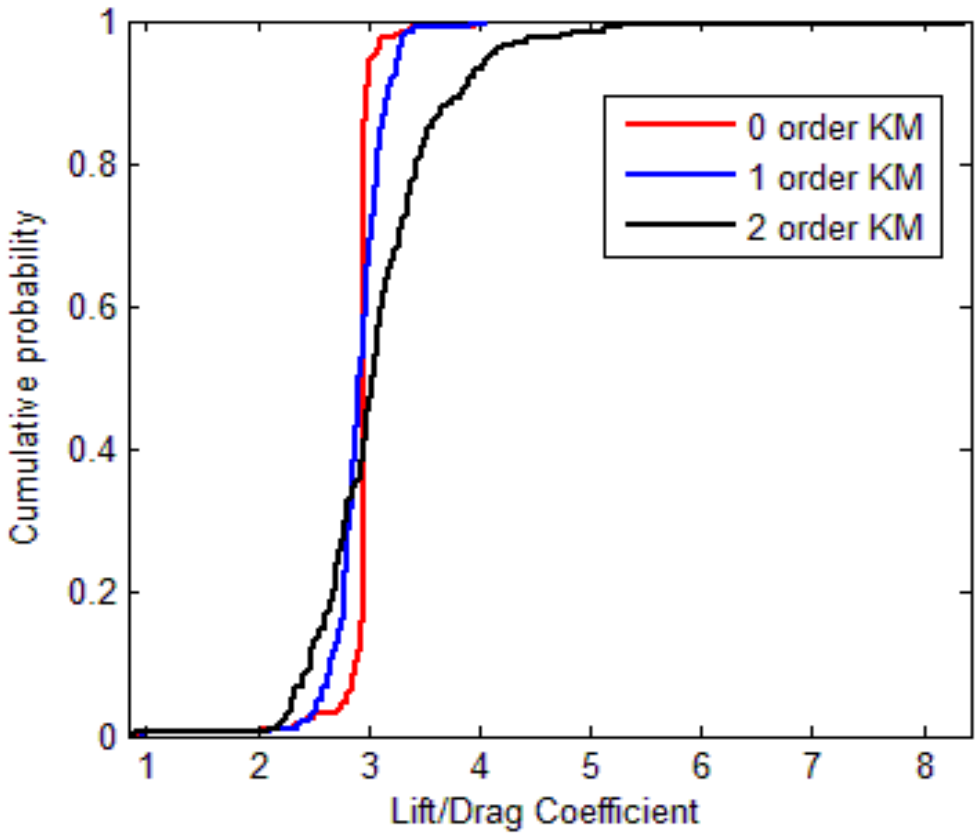

Fig 6 - 19 Results of cumulative probability in Kriging models

6.2.3 Optimization

Traditional methods confront the challenges from unacceptable time-complexity or natural drawbacks of premature convergence because of finding the nearest local optima of low quality. Simulated Annealing (SA) is a local search-based heuristic that makes us capable of escaping from being trapped into a local optimum[105]. It occasionally accepts solutions that are worse than the current. The probability of such acceptance is decreasing with time. SA has been applied successfully to a wide variety of highly complicated combinatorial optimization problems as well as various real-world problems[106].

Genetic Algorithm is a heuristic search technique and belongs to a class of the evolutionary computing. It draws inspiration from the principles and mechanisms of natural selection[107]. GA evolves a population of potential solutions via fitness-biased selection and breeding through genetic operators. Conventionally, selection of parents takes place at every generation and offspring are reproduced through

genetic operators like crossover and mutation. The process reiterates until some termination conditions are met[108]. Except SA and GA, there are other methods, such as Neural Networks (NN) and Support Vector Machines (SVM).

Simulated annealing algorithm and genetic algorithm are typical examples of heuristic algorithm. The concept of SA is originated from the "annealing" process in the metallurgical industry[109]. GA is inspired by the principles of natural evolution to perform search and optimization[110]. The optimization procedures of SA and GA search for a near global minimum mimicking.

In GA, every individual or chromosome is encoded into a structure that represents its properties. The set of individuals form the population. During each generation, the chromosomes are evaluated using some measures of fitness. A new generation is formed according to the fitness values of chromosomes by genetic operators (crossover operator, mutation operator and reproduction operator)[111]. Then the new generation is evaluated and this process is repeated until a stopping criterion is met.

GA is a class of adaptive stochastic optimization algorithms[112]. The processes of evolution and natural selection are computed on the population of candidate solution. Fitness basically represents the strength of the individual and it plays a vital role in the selection process. Evolution occurs with the formation of the new generation of the individuals with the mating process. Mutation as the small random change is also mimicked in the algorithm, it widens the search space[113].

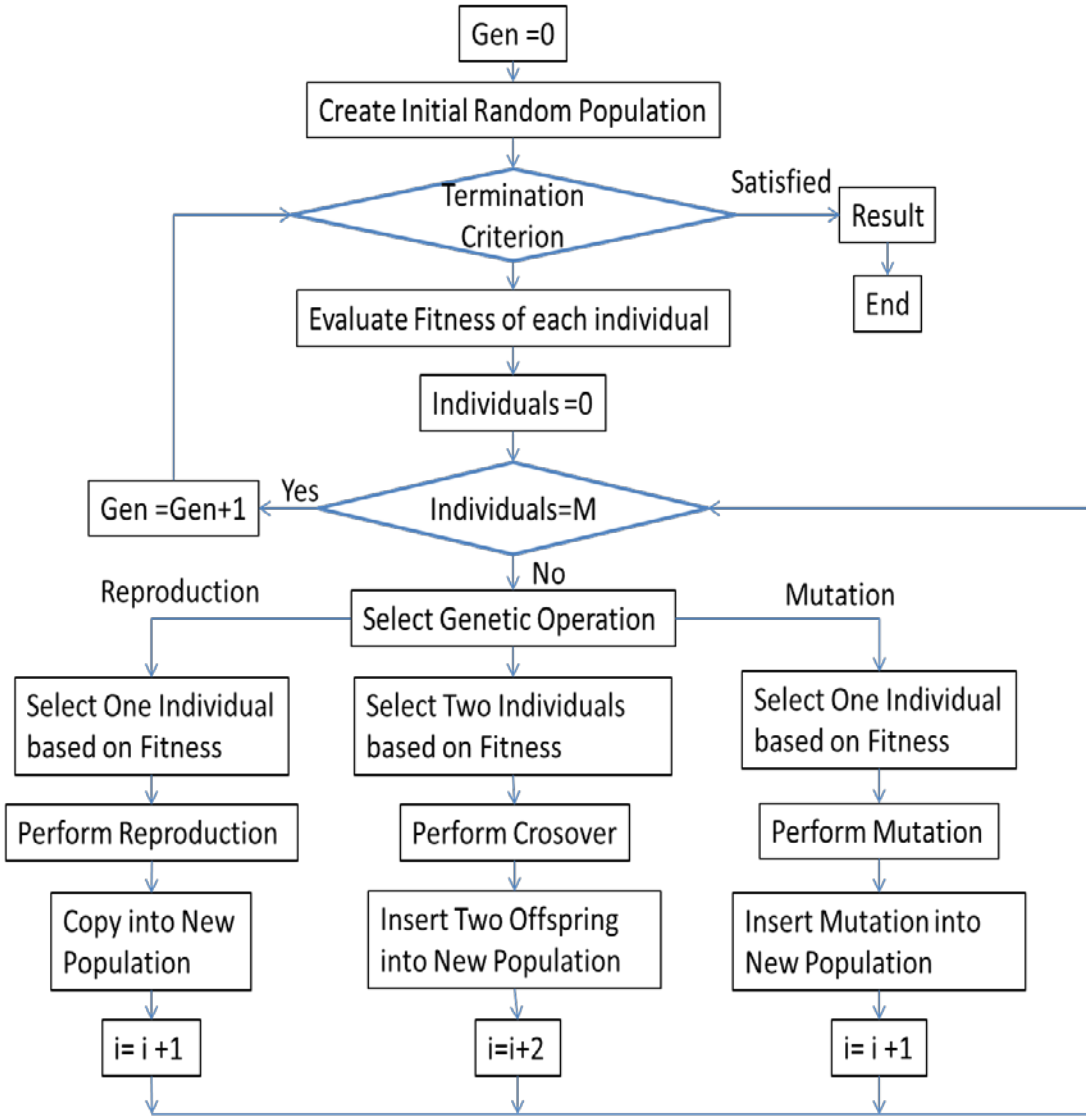

Fig 6 - 20 Flowchart of Genetic algorithm programming

SA starts from a random initial solution. A new solution is taken from the predefined neighbor-hood of the current solution[114]. The objective function value of this new solution is then compared with that of the current best solution in order to determine if an improvement has been achieved. In SA, the basic idea is not to restrict the search to those solutions that decrease the objective function value, but also allow moves that increase the objective function value[115]. This mechanism may avoid the procedure being trapped prematurely in a local minimum.

In SA, the basic idea is not to restrict the search to those solutions that decrease the objective function value, but also allow moves that increase the objective function value [116]. This mechanism may avoid the procedure being trapped prematurely in a local minimum.

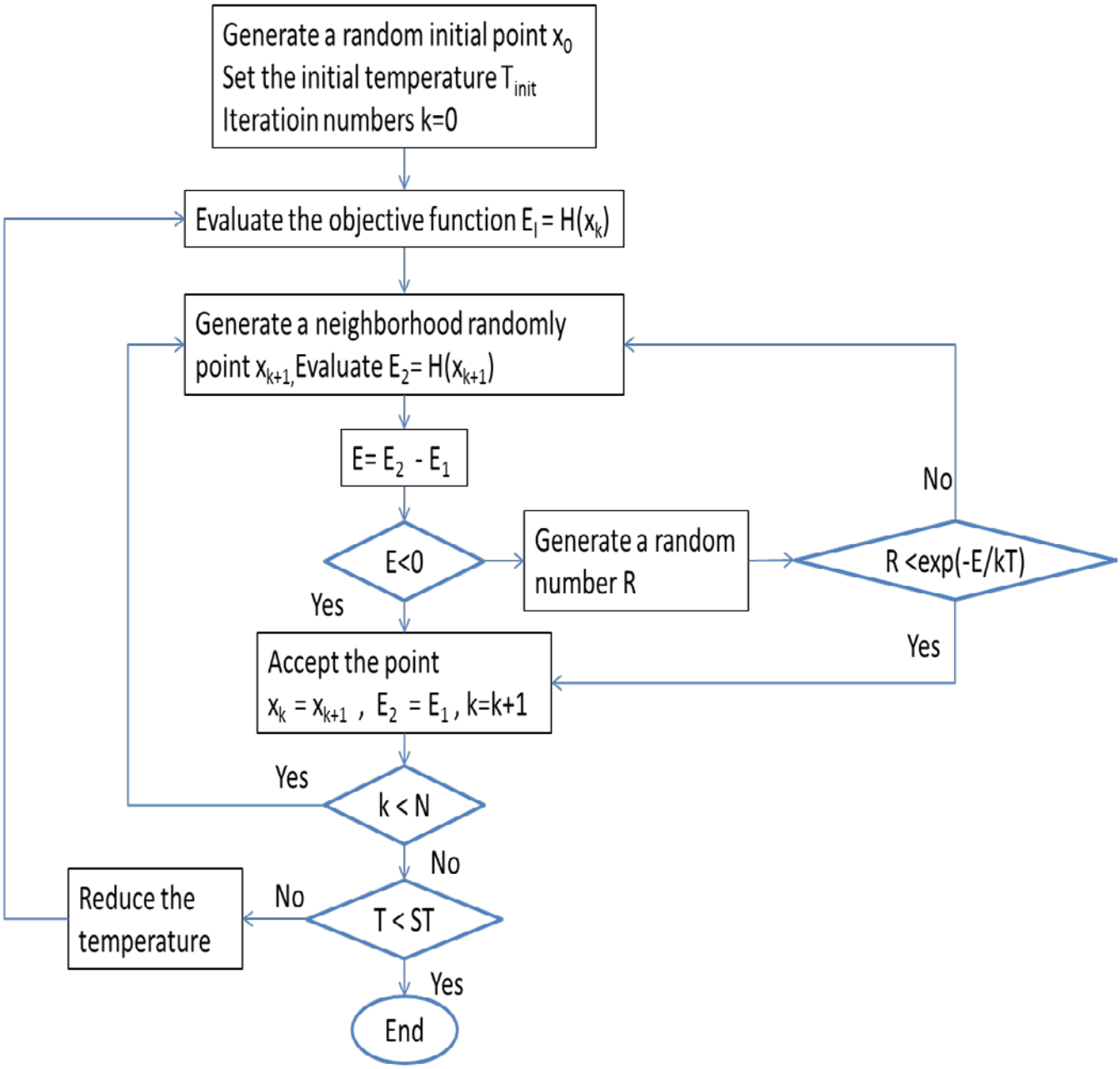

Fig 6 - 21 Flowchart of Annealing simulated algorithm programming

Based on the advantages of Kriging model, in the process of optimization, it is not necessary to perform CFD, while Kriging model can provide reliable results of Lift/drag coefficient of other parameters were settled down. Here we have attempt of airfoil shape optimization by GA and SA.

In our model, the velocity and attack angle were fixed as specific value (v=250 m/s, att=3), the searching methods of optimization were GA and SA, the variables in the

process optimization are parameters corresponding with airfoil geometry property (p, m, t), the objective of the optimization is to find the maximum Lift/drag coefficient. The formation of airfoil shape optimization in a traditional way can be written as

$$\text{Maximum } C = C(\mathrm{p}, \mathrm{m}, \mathrm{t}, \mathrm{v}, \mathrm{att}) \tag{6 - 17}$$

$$\text{Subject to } \begin{aligned} & V_{i,\min} \le V_i \le V_{i,\max}, \ i = 1, 2, 3; \\ & V_1 = p, V_2 = m, V_3 = t \\ & v = v_s, att = att_s \end{aligned} \tag{6 - 18}$$

Table 6 - 4 Results of SA and GA

	P	M	T	C	TIME (s)
SA (0)	0.1629	0.0704	0.0915	8.47	514.55
SA (1)	0.1612	0.0703	0.0909	8.48	610.48
SA (2)	0.1631	0.0704	0.0914	8.50	604.78
GA (0)	0.1632	0.0704	0.0915	8.47	299.50
GA (1)	0.1628	0.0704	0.0913	8.50	338.24
GA (2)	0.1627	0.0704	0.0913	8.50	315.86
CFD	0.16	0.07	0.09	8.43	6.7

Kriging models (zero order, first order, and second order) were applied in the airfoil shape optimization by heuristic algorithms (GA and SA). The results of optimization were listed in Table 6.4. Firstly, the results of GA and SA in Kriging models were extremely close. In the last range of the table, CFD were performed in ANSYS FLOTRAN by setting the parameters according to the result of optimization, it proves the sufficient accuracy of Kriging models. To offer more information for aerodynamic mechanism analysis, Fig 6-21, Fig 6-22, Fig 6-23 were the contour plot of CFD results.

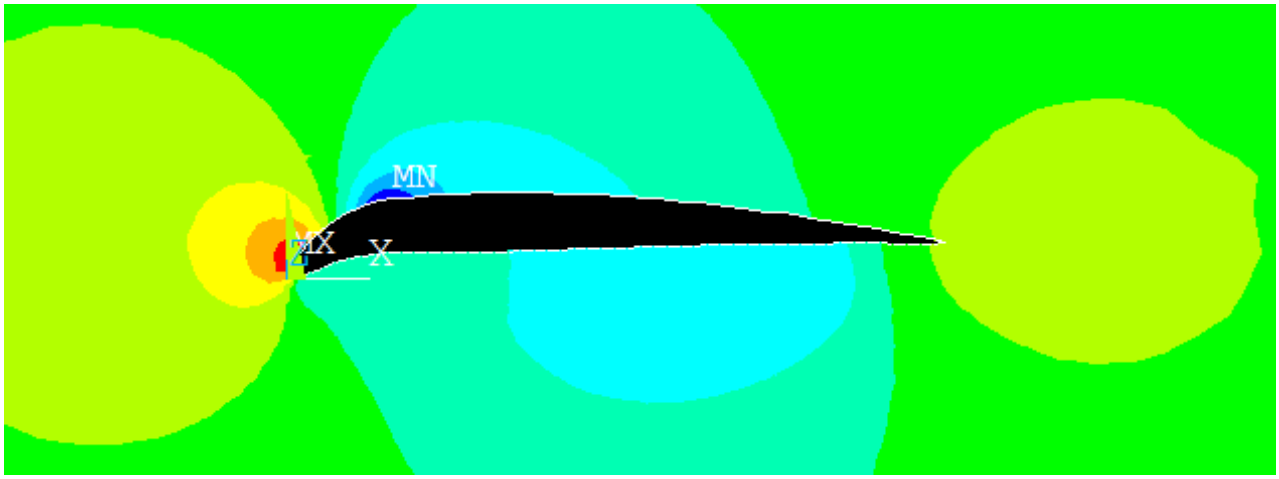

Fig 6 - 22 Nodal pressure result of optimized airfoil

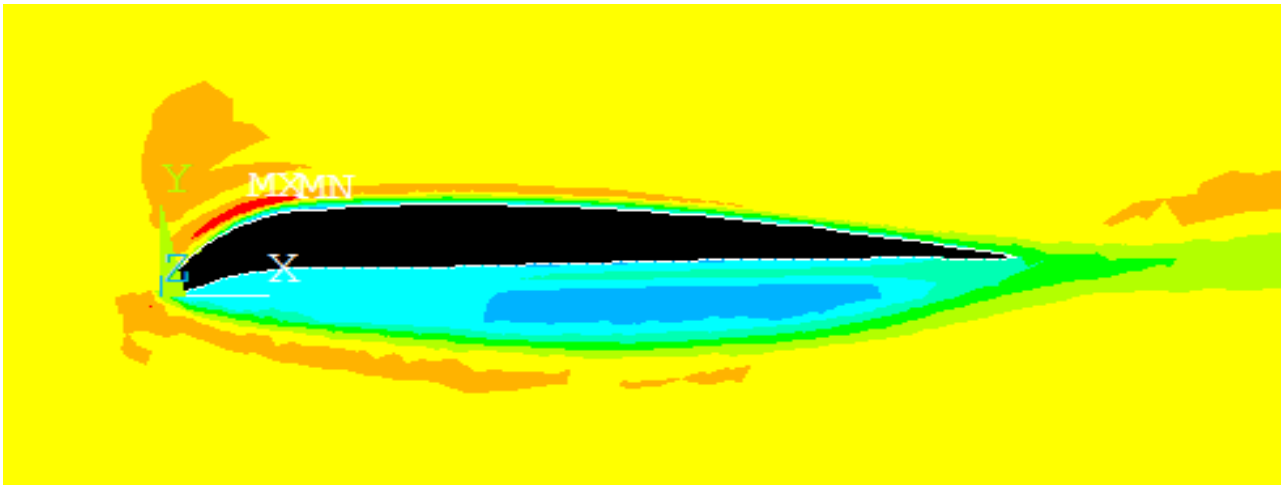

Fig 6 - 23 Total stagnation pressure of optimized airfoil

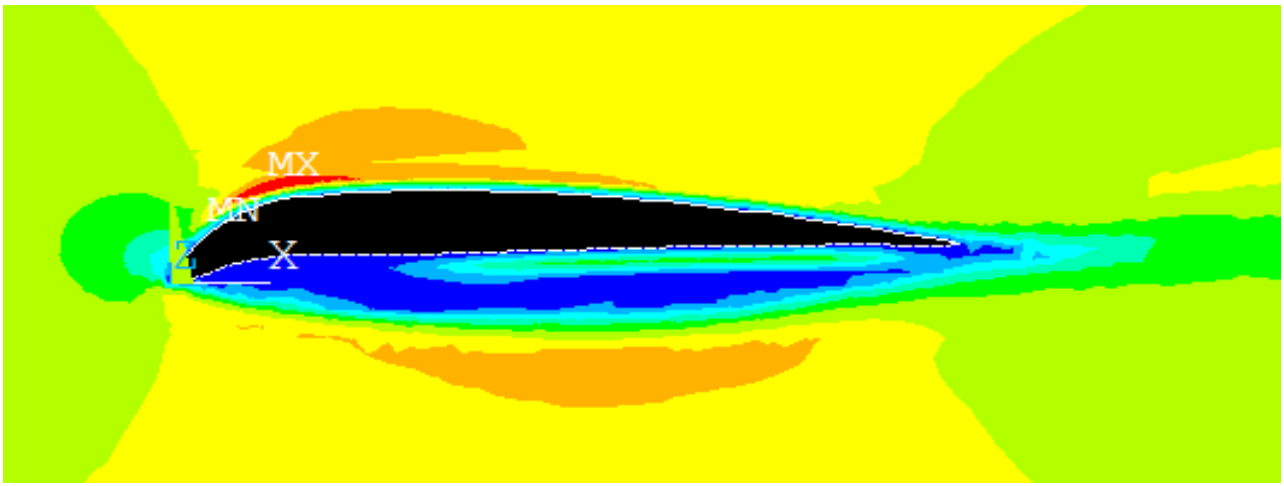

Fig 6 - 24 Fluid velocity of nodal solutionof optimized airfoil

On the other hand, we can find from Table 6.4 that for the computational expense, GA is more competitive than SA, it spent less time than SA, approximately half time

of the cost of SA. As optimization algorithm, GA is more economic than SA in this model. In addition, the results of GA were more convergent than SA in different Kriging models. It means that SA is more sensitive to the change of order of Kriging model. However, in the whole scope, the results of GA and SA were close as mentioned in the above.

6.2.4 Conclusion

A constructive method for airfoil shape optimization was proposed by creating surrogate model. Attempts of heuristic algorithms in optimization process were made in genetic algorithm and simulated annealing algorithm.

We find Kriging interpolation model has the interpolation capability for the huge amount database like the sample space of Monte Carlo. At the same time, it also has a high level of accuracy. Application of Kriging model can provide local uncertainty measures for the model predictions. Kriging model with different orders will cause difference of variance in prediction as discussed.

Heuristic algorithms were chosen for airfoil shape optimization to avoid the premature convergence in the process optimization. Simulated annealing and genetic algorithm work very well in Kriging model because of the advantages of random process in the program. As the different algorithm for airfoil shape optimization, genetic algorithm is more economic in computational expense than simulated annealing.

Chapter 7 Conclusion

Aircrafts have complicated operation environment and sophisticated mechanical structure itself. The traditional analysis of deterministic Finite Element Model ignores the fluctuation of parameters as uncertain variables in the real operation environment. Uncertainty is an inevitable issue in the process of manufacture, infrastructure, and engineering design. Quantifying and propagating the uncertainty in the simulation or design process as a key component of risk analysis, robustness evaluation or reliability based optimization attracts attention of researchers and designer. In this dissertation, Monte Carlo methods are chosen as an effective method to propogate uncertaintis in the system of structure, as discussed in Chapter 3. It is a non-intrusive, sampling based numerical method, but often requires a large ensemble of sampling points to provide a reliable and stable estimate of uncertainty. This makes MCS computationally expensive. However, Latin hypercube sampling is an appropriated sampling strategy can sharply reduce the number of sampling points while reach a certain level of accuracy.

Reliability based optimization struggles to seek for the best compromise between cost and safety while considering system uncertainties by incorporating reliability measures within the optimization. Despite the advantages of reliability based optimization, its application to practical engineering problem is still quite challenging. We propose an effective method to decouple the loops of reliability assessment analysis and optimization by creating surrogate models. Latin Hypercube sampling approach is performed in finite element model to obtain a reliable and believable database for surrogate models. In order to prevent the premature convergence in the process optimization, attempts in heuristic algorithms for optimization were made. Surrogate models are helpful in the reliability analysis of complex and realistic structural systems. The first proposals apply first- and second- order polynomial regression models as surrogates for the true limit state function, as applied in the example of cumulative damage analysis of wing structure by stochastic simulation in Chapter 6. In the other side, Kriging interpolation models for structural reliability problems hold several competitive features. It does not only have the interpolation capability, but also take the

flexibility to approximate arbitrary functions with a high level of accuracy, and it also explores the capability of providing a local uncertainty measure for the model predictions. Kriging model was applied in Chapter 4 for reliability analysis, Chapter 5 for reliability based optimization and also Chapter 6 for airfoil shaper optimization.

For optimization, traditional methods confront the challenges from unacceptable time-complexity or natural drawbacks of premature convergence because of finding the nearest local optima of low quality. The algorithm of Simulated Annealing (SA) is local search-based heuristic that makes us capable of escaping from being trapped into a local optimum. Genetic Algorithm (GA) draws inspiration from the principles and mechanisms of natural selection, it belongs to a class of the evolutionary computing. SA and GA were applied in the examples of Chapter 5 for reliability based optimization in surrogate model and in Chapter 6 for airfoil shape optimization.

Chapter 8 Résumé de la thèse en français

8.1 Motivation et objectif

Dans le domaine de la conception aérodynamique et de la fabrication des avions, les chercheurs ont fait beaucoup d'effort pour améliorer les performances des ailes en utilisant des techniques d'optimisation. Le développement de la mécanique des fluides numérique a permis de réduire les dépenses en soufflerie tout en fournissant des résultats convaincants pour simuler des situations compliquées des aéronefs. Dans cette thèse, il a été choisi une partie spécifique et importante de l'avion, à savoir, la structure de l'aile.

L'optimisation basée sur la fiabilité est une méthode très appropriées pour les structures sous incertitudes. Il s'agit d'obtenir le meilleur compromis entre le coût et la sécurité tout en tenant compte des incertitudes du système en intégrant des mesures de fiabilité au sein de l'optimisation. Malgré les avantages de l'optimisation de la fiabilité, son application à un problème d'ingénierie pratique est encore assez difficile.

Dans notre travail, l'analyse de l'incertitude dans la simulation numérique est introduite et exprimée par la théorie des probabilités. La simulation de Monte Carlo constitue une méthode efficace pour propager les incertitudes dans le modèle d'éléments finis de la structure, cette approche est ici appliquée pour simuler les situations compliquées qui peuvent se produire. Pour améliorer l'efficacité de la simulation Monte Carlo dans le processus d'échantillonnage, la méthode de l'Hypercube Latin est effectuée [89]. Cependant, l'énorme base de données de l'échantillonnage rend difficile le fait de fournir une évaluation explicite de la fiabilité. L'utilisation du polynôme de chaos est présentée et discutée. Le modèle de Kriging comme un modèle de substitution joue également un rôle important dans l'analyse de la fiabilité.

Les méthodes traditionnelles d'optimisation ont des inconvénients à cause du temps de calcul trop long, ou le fait d'être parasitées par un minimum local causant une convergence prématurée. Le recuit simulé est une méthode heuristique basée sur une recherche locale, les Algorithmes Génétiques puisent leur inspiration dans les principes

et les mécanismes de la sélection naturelle, qui nous rendent capables d'échapper aux pièges des optimums locaux. Dans l'optimisation de la conception de base de la fiabilité, ces deux méthodes ont été mise en place comme procédure d'optimisation. La boucle de l'analyse de fiabilité est testée sur le modèle de substitution.

8.2 Organisation du mémoire

Dans le chapitre 2, les méthodes d'analyse de l'incertitude sont présentées. Tout d'abord, la classification de l'incertitude et les sources d'incertitude dans la simulation de conception sont discutées. Ensuite, nous avons démontré la représentation de l'incertitude et de la modélisation comme l'a conclu dans les littératures. Après cela, la validation du modèle et l'analyse de sensibilité sont également pris en considération. Dans la dernière partie de ce chapitre, les méthodes de propagation de l'incertitude sont montrées et discutées.

Le chapitre 3 commence avec l'introduction de la formulation mathématique de Monte Carlo intégration. Ensuite, nous présentons des méthodes avancées de Monte Carlo, ainsi que l'importance de l'échantillonnage et l'échantillonnage Hypercube Latin. Ensuite, des méthodes de quadratures d'interpolation aléatoires, les méthodes de Monte Carlo pour les équations linéaires itératives et les chaînes de Markov et méthodes de Monte Carlo pour problème de valeurs propres sont également montrées dans ce chapitre. Enfin, nous avons un exemple numérique de la méthode d'échantillonnage qui souligne son intérêt. La simulation de Monte Carlo dans le modèle d'éléments finis de la structure de l'aile est effectué dans le chapitre 3.

Dans le chapitre 4, l'expansion stochastique pour l'analyse de probabilité est discutée. La théorie fondamentale de l'expansion du polynôme de chaos est présentée dans la première partie de ce chapitre. Ensuite, les polynômes d'Hermite et les séries de Gram - Charlier sont exprimés. Puis l'approche Karhunen - Loeve est une méthode très utile dans la simulation, et est également présentée. Dans ce chapitre, nous expliquons aussi la méthode spectrale stochastique des éléments finis, rôle de la transformation de Karhunen - Loeve et le rôle polynôme de chaos dans le cadre des méthodes spectrales des éléments finis stochastiques sont démontrées. Basé sur ces théories, nous avons aussi des exemples d'expansion stochastique pour l'analyse de probabilité.

Le chapitre 5 présente l'optimisation de la conception basée sur la fiabilité. Dans un premier temps, des remarques générales de RBDO [63] est illustré. Ensuite, la première commande et deuxième méthode de fiabilité sont expliquées. Ensuite, nous démontrons formulation mathématique de RBDO. Optimisation de la conception robuste est également sont introduit dans ce chapitre. Dans la dernière partie, des exemples de simulation numérique sont présentés.

Dans le chapitre 6, deux exemples Complet sont présentées. Le premier exemple est cumulatif de l'analyse des dommages de la structure de l'aile par une simulation stochastique.
Le deuxième exemple est l'optimisation de forme aérodynamique par des algorithmes heuristiques. Pour créer un modèle de substitution appropriée, la simulation de Monte Carlo a été effectuée en répétant calcul dynamique des fluides numérique, une information fiable et a été capturé et a conclu que interpolateurs Kriging. Afin d'éviter la convergence prématurée dans le processus d'optimisation, les tentatives dans algorithmes heuristiques d'optimisation ont été faites. Les résultats de l'algorithme génétique et algorithme de recuit simulé ont été testés en CFD pour confirmer la fiabilité de la méthode proposée dans le présent document.

Le chapitre 7 présente un résumé de cette thèse, les conclusions concernant les résultats.

8.2.1 Chapitre 2: Analyse de l'incertitude

Les incertitudes comprennent les erreurs de prédiction induites par hypothèse du modèle de conception et de simplification; l'incertitude de la performance découlant des propriétés des matériaux, et la tolérance de de la fabrication; et l'incertitude des conditions de charge appliquées sur la structure pendant le fonctionnement. Ces incertitudes peuvent entraîner des performances du système pour changer ou fluctuent, ou même de contribuer à la déviation grave et entraîner des défauts de fonction et la mission défaillance imprévue ou même sans précédent.

L'analyse d'incertitude est le prémisse de l'optimisation de la conception basée sur l'incertitude. Il comprend l'adoption de la taxonomie appropriée pour déterminer de

façon exhaustive et classer les sources d'incertitude; utilisant des outils mathématiques appropriés pour représenter et modéliser ces incertitudes; et l'application de l'analyse de sensibilité se rapproche pour filtrer les incertitudes avec des effets mineurs sur la conception de manière à simplifier les problèmes.

8.2.2 Chapitre 3: simulation de Monte Carlo

Echantillonnage d'importance

$$\mu = \int f(x)\pi(x)dx \tag{8- 1}$$

$f(x)$ est une fonction mesurable et $\pi(x)$ est une fonction de densité de probabilité.

La fonction de distribution d'importance $\mathrm{g}(x)$ est utilisé pour appliquer un changement de mesure

$$\mu = \int \frac{\pi(x)}{\mathrm{g}(x)} f(x)\,\mathrm{g}(x)dx \tag{8- 2}$$

$$\omega(\mathrm{X}_i) = \frac{\pi(\mathrm{X}_i)}{\mathrm{g}(\mathrm{X}_i)}, i = 1, \ldots, n \tag{8- 3}$$

$$\hat{\mu}_n^{IS} = \frac{1}{n}\sum_{i=1}^{n} \omega(\mathrm{X}_i) f(\mathrm{X}_i) \tag{8- 4}$$

Nous avons un exemple de répartition $\mathrm{T}(\nu, \theta, \sigma^2)$ avec la densité

$$\pi(x) = \frac{\Gamma((\nu+1)/2)}{\sigma\sqrt{\nu\pi}\,\Gamma(\nu/2)}\left(1 + \frac{(x-\theta)^2}{\nu\sigma^2}\right)^{-(\nu+1)/2} \mathrm{I}_R(x) \qquad (\theta = 0, \sigma = 1, \nu = 12) \tag{8- 5}$$

Les quantités d'intérêt sont (8- 6)

$$\begin{cases} f_1(x) = \left(\dfrac{\sin(x)}{x}\right)^5 \mathrm{I}(x)_{(2.1,+\infty)} \\ f_2(x) = \sqrt{\left|\dfrac{x}{1-x}\right|} \\ f_3(x) = \dfrac{x^5}{1+(x-3)^2}\mathrm{I}(x)_{[0,+\infty)} \end{cases}$$

T 8 - 1 Coût en temps de différent PDF par la méthode d'échantillonnage de importance

	f1	f2	f3
Student -T	7.634	7.628	7.600
Normal	5.974	5.956	5.940
Cauchy	3.807	3.563	3.923
Exact	1.768	1.172	1.719

T 8 - 2 Résultats de différent PDF par la méthode d'échantillonnage importance

	f1	f2	f3
Student -T	7.705e-5	1.157	4.523
Normal	7.444e-5	1.167	4.659
Cauchy	7.984e-5	1.165	4.514
Exact	7.749e-5	1.164	4.708

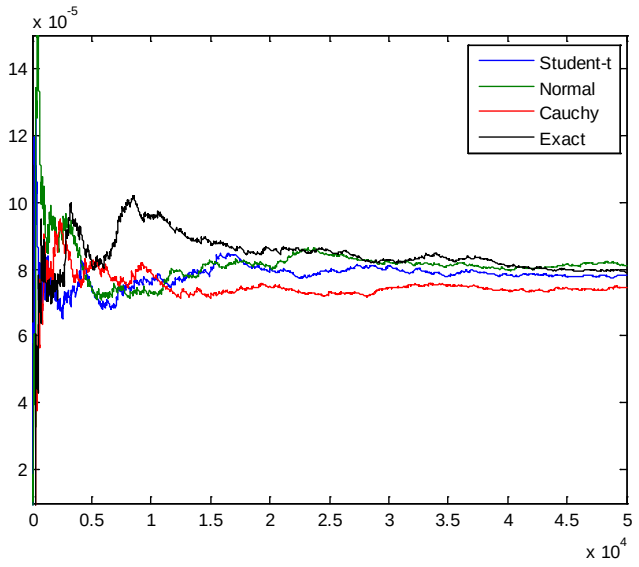

F 8 - 1 L'historique de la convergence de différentes PDF en fonction f1

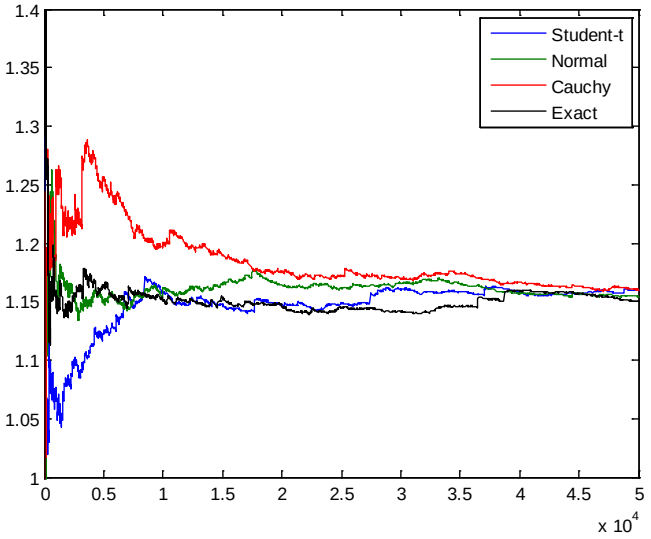

F 8 - 2 L'historique de la convergence de différentes PDF en fonction f2

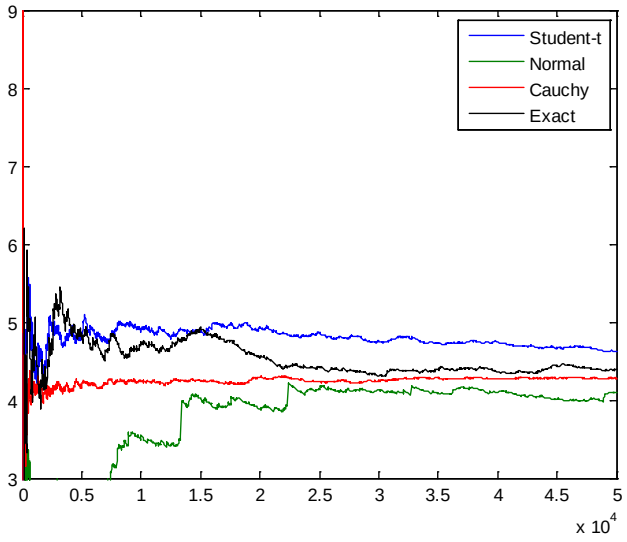

F 8 - 3 L'historique de la convergence de différentes PDF en fonction f3

‘Echantillonnage latin d’hypercube’ dans le modèle éléments finis de la structure

Modèle d'éléments finis de la structure de l'aile est construite par **ANSYS** ‘Paramètre Design Language’. Les paramètres du modèle déterministe d'origine correspondent aux propriétés géométriques et les propriétés des matériaux.

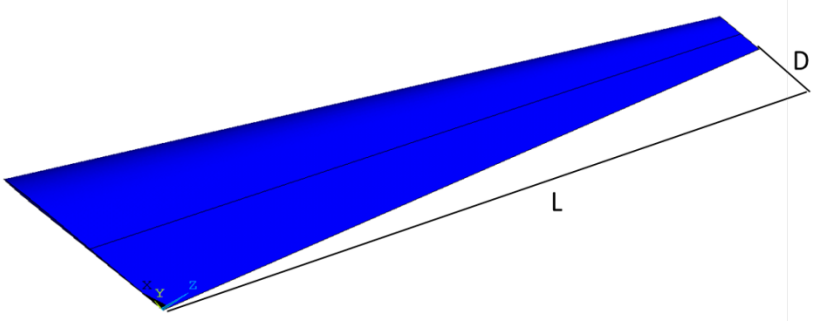

F 8 - 4 Modèle éléments finis de la structure de l'aile

Chaque fréquence propres, la structure d'aile a une déformation et le contour de la contrainte de Von-Mises.

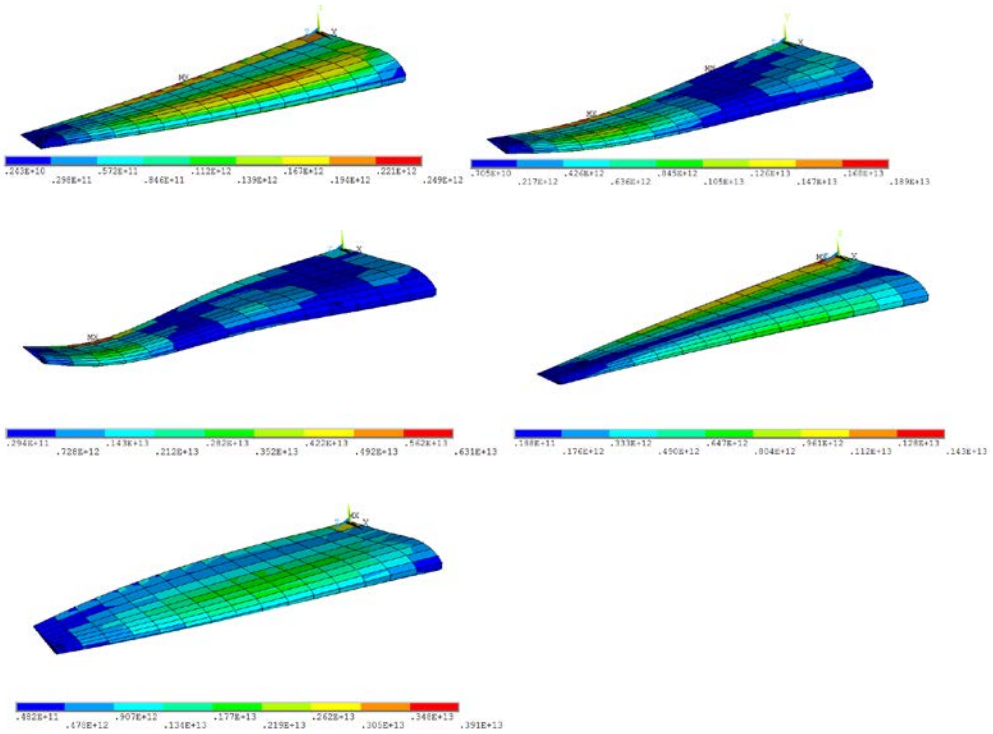

F 8 - 5 Photos du Contour des contraintes de Von-Mises en cinq fréquences propres

F 8 - 6 fournit les registres de fréquences propres dans le processus de simulation stochastique. Les probabilités cumulées de cinq fréquences propres de la structure de l'aile sont présentés dans F 8 - 7.

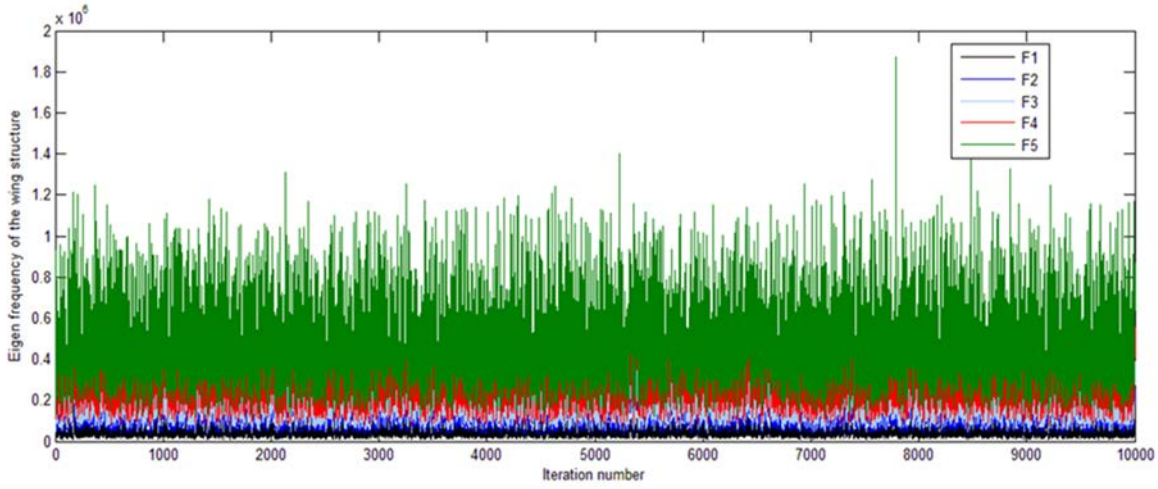

F 8 - 6 Fréquences propres dans le processus de l'échantillonnage Hypercube Latin

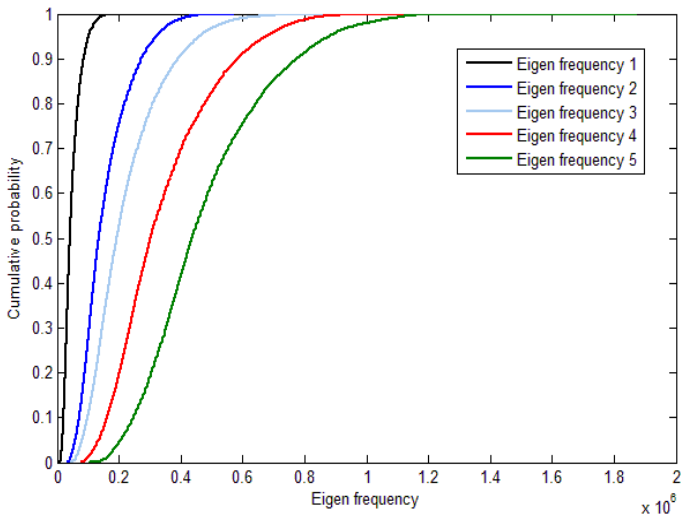

F 8 - 7 La probabilité cumulative de cinq fréquences propres dans MCS

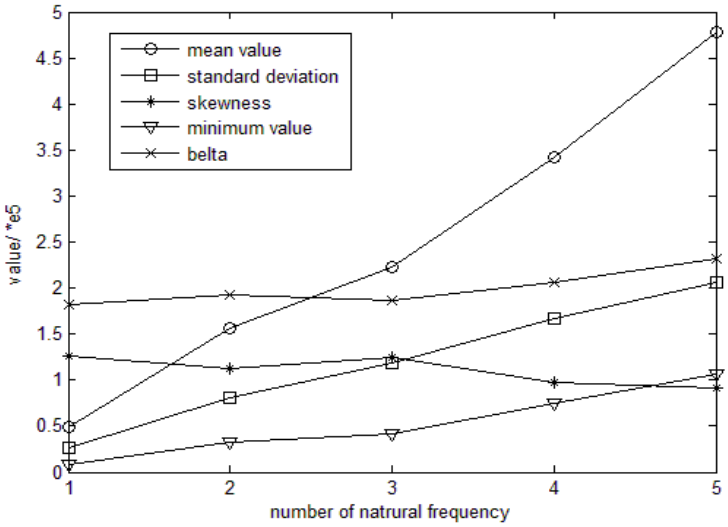

F 8 - 8 Statistique de la simulation stochastique

L'évaluation de la simulation stochastique dans la méthode d'échantillonnage latin d'hypercube est présentée dans le tableau. La valeur moyenne, écart-type, assymétrie, et aussi le minimum et le maximum sont donnés ainsi que la statistique dans la méthode d'échantillonnage.

T 8 - 3 Résultats de la méthode d'échantillonnage Hypercube Latin

	F1	F2	F3	F4	F5
Mean value /*e5 Hz	0.48595	1.5632	2.2246	3.4208	4.7813
Standard deviation /*e5 Hz	0.26679	0.81028	1.1919	1.6633	2.0616
Skewness /*e5 Hz	1.2572	1.1292	1.2509	0.96708	0.91258
Minimum /*e5 Hz	0.08809	0.32320	0.41714	0.74041	1.0691
Maximum /*e5 Hz	1.9210	5.7092	9.4982	11.670	18.737
Belta	1.8215	1.9292	1.8664	2.0566	2.3192

8.2.3 Chapitre 4: Expansion stochastique pour l'analyse de probabilité

Polynôme orthogonal

Dans le cas monodimensionnel, on peut élargir la réponse aléatoire u à l'aide de polynômes orthogonaux ξ, qui a une distribution de probabilité connue, avec comme unité normale $N[0,1]$. Si est une fonction d'une variable aléatoire x à distribution normale, qui a la moyenne μ_x et la variance connue σ_x^2, est une variable normalisée ξ:

$$\xi = \frac{x - \mu_x}{\sigma_x} \tag{8- 7}$$

En général, les polynômes d'Hermite à une dimension sont définis par

$$\Psi_n(\xi) = (-1)^n \frac{\varphi^n(\xi)}{\varphi(\xi)} \tag{8- 8}$$

$\varphi^n(\xi)$ est n^{th} dérivée de la fonction de densité normale, $\varphi(\xi) = 1/\sqrt{2\pi} e^{-\xi^2/2}$.

$$\{\Psi_i\} = \{1,\ \xi,\ \xi^2 - 1,\ \xi^3 - 3\xi,\ \xi^4 - 6\xi^2 + 3,\ \xi^5 - 10\xi^3 + 15\xi,\ \cdots\} \tag{8- 9}$$

Ainsi, 2-D PCE est

$$u(\theta) = b_0 + b_1\xi_1(\theta) + b_2\xi_2(\theta) + b_3(\xi_1^2(\theta) - 1) + b_4\xi_1(\theta)\xi_2(\theta) + b_5(\xi_2^2(\theta) - 1) \quad (8\text{- }10)$$

Supposons les quatre premiers moments d'une variable aléatoire x, sont donnés par, $m_x^1 = 2$, $m_x^2 = 3.2$, $m_x^3 = 7.5$, $m_x^4 = 45$. Estimer les coefficients b_i de z en utilisant le critère des moindres carrés donne:

$$\text{Minimiser} \quad \sum_{j=1}^{4} f_j^2(b_i) \quad (\mathrm{i} = 1, 2, 3) \quad (8\text{- }11)$$

$$f_1(b_i) = m_z^1 - m_x^1 = 0$$

$$f_2(b_i) = m_z^2(b_i) - m_x^2$$

$$f_3(b_i) = m_z^3(b_i) - m_x^3$$

$$f_4(b_i) = m_z^4(b_i) - m_x^4$$

Ensuite, nous pouvons effectuer l'optimisation afin d'avoir une solution de coefficients et en s'assurant de minimiser $\sum_{j=1}^{4} f_j^2(b_i)$,

$$E\left[\xi^k\right] = 0 \quad \forall k \ \ odd$$

$$m_z = b_0$$

$$m_z^2 = E\left[(\mathrm{z} - \mathrm{b}_0)^2\right] = b_1^2 + 2b_2^2 + 6b_3^2$$

$$m_z^3 = E\left[(\mathrm{z} - \mathrm{b}_0)^3\right] = 6b_1^2b_2 + 8b_2^3 + 36b_1b_2b_3 + 108b_2b_3^2$$

$$m_z^4 = E\left[(\mathrm{z} - \mathrm{b}_0)^4\right] = 3b_1^4 + 60b_2^4 + 3384b_3^4 + 24b_1^3b_3 + 60b_1^2b_2^2 + 252b_1^2b_3^2 + 576b_1b_2^2b_3 + 1296b_1b_3^3 + 2232b_2^2b_3^2$$

$$E\left[\xi^0\right] = 1,\ E\left[\xi^2\right] = 1,\ E\left[\xi^4\right] = 3,\ E\left[\xi^6\right] = 15 \ldots$$

$$b_0 = 2,\ b_1 = -1.545,\ b_2 = 0.628,\ b_3 = 0.141$$

$$x \approx z(\xi) = 2 - 1.545\xi + 0.628(\xi^2 - 1) + 0.141(\xi^3 - 3\xi)$$

$$m^1 = 2.0049,\ m^2 = 3.2364,\ m^3 = 7.0124,\ m^4 = 43.2743$$

Gram-Charlier série

Spécifiez les sept premiers coefficients de la série de Gram-Charlier

$$b_0 = \int_{-\infty}^{+\infty} f(x)dx, \tag{8- 12}$$

$$b_1 = -\int_{-\infty}^{+\infty} f(x)xdx, \tag{8- 13}$$

$$b_2 = \frac{1}{2}\int_{-\infty}^{+\infty} f(x)(x^2-1)dx, \tag{8- 14}$$

$$b_3 = -\frac{1}{6}\int_{-\infty}^{+\infty} f(x)(x^3-3x)dx, \tag{8- 15}$$

$$b_4 = \frac{1}{24}\int_{-\infty}^{+\infty} f(x)(x^4-6x^2+3)dx, \tag{8- 16}$$

$$b_5 = -\frac{1}{120}\int_{-\infty}^{+\infty} f(x)(x^5-10x^3+15x)dx, \tag{8- 17}$$

$$b_6 = \frac{1}{720}\int_{-\infty}^{+\infty} f(x)(x^6-15x^4+45x^2-15)dx, \tag{8- 18}$$

n^{th} moment central :

$$m_x^n = E\left[(\mathrm{X}-\mu_x)^n\right] = \int_{-\infty}^{+\infty}(X-\mu_x)^n f_X(x)dx \tag{8- 19}$$

$\mu_x = m^1 = 0$

$b_0 = 1$, $b_1 = 0$, $b_2 = \frac{1}{2}(m^2-1)$, $\mathrm{b}_3 = -\frac{1}{6}(m^3-3m^1)$

$\mathrm{b}_4 = \frac{1}{24}(m^4-6m^2+3)$, $b_5 = -\frac{1}{120}(m^5-10m^3+15m^1)$, $b_6 = \frac{1}{720}(m^6-15m^4+45m^2-15)$

Les coefficients de la série de Gram-Charlier peuvent être exprimées par des polynômes de Hermite en termes de moments centraux.

Supposons une matrice de covariance cible est donnée par

$$[C]=\begin{bmatrix} 1 & 0.63 & 0.75 & 0.92 \\ 0.63 & 1 & 0.96 & 0.84 \\ 0.75 & 0.96 & 1 & 0.72 \\ 0.92 & 0.84 & 0.72 & 1 \end{bmatrix}$$

Générer les variables aléatoires corrélées (distribution normale), et calculer la matrice de covariance $\left[\tilde{C}\right]$ donne :

$$P=\begin{bmatrix} 0.4320 & -0.4475 & 0.6166 & 0.4827 \\ 0.5744 & 0.3822 & -0.5195 & 0.5040 \\ -0.4851 & -0.5522 & -0.4547 & 0.5030 \\ -0.4981 & 0.5905 & 0.3784 & 0.5099 \end{bmatrix}$$

$$\Lambda=\begin{bmatrix} -0.0653 & 0 & 0 & 0 \\ 0 & 0.1733 & 0 & 0 \\ 0 & 0 & 0.4807 & 0 \\ 0 & 0 & 0 & 3.4114 \end{bmatrix}$$

$$[A]=[P][\Lambda]^{1/2}=\begin{bmatrix} 0 & -0.1863 & 0.4275 & 0.8915 \\ 0 & 0.1591 & -0.3602 & 0.9309 \\ 0 & -0.2299 & -0.3152 & 0.9291 \\ 0 & 0.2458 & 0.2623 & 0.9418 \end{bmatrix}$$

$$\left[\tilde{C}_{500}\right]=\begin{bmatrix} 1.1109 & 0.7590 & 0.8411 & 0.9690 \\ 0.7590 & 1.0681 & 0.9923 & 0.8565 \\ 0.8411 & 0.9923 & 1.1375 & 0.8227 \\ 0.9690 & 0.8565 & 0.8227 & 1.0850 \end{bmatrix}$$

Modèle de substitution pour l'analyse de la fiabilité

L'équation de la matrice résultante est de la forme

$$\{\Delta R\}=[S]\{\Delta P\} \qquad (8\text{- }20)$$

Lorsque les éléments $\{\Delta P\}$ sont les ajustements inconnus pour concevoir des variables qui sont nécessaires pour les changements $\{\Delta R\}$ entre le vecteur de réponse de référence et les réponses du système réels. La matrice de sensibilité $[S]$ contient les gradients de réponses par rapport à concevoir des variables:

$$[S] = S_{ij} = \frac{\partial R_i}{\partial P_j} \tag{8- 21}$$

T 8 - 4 Résultats de l'analyse de sensibilité pour les variables

	S	D	L	E	P	R
F1	-0.268	-0.103	-0.777	0.513	0.032	0.001
F2	0.013	-0.104	-0.806	0.542	0.028	0.005
F3	-0.260	-0.144	-0.764	0.528	0.026	0.002
F4	0.114	-0.089	-0.783	0.565	0.009	0.005
F5	-0.204	-0.050	-0.688	0.641	-0.053	0.001

Par conséquent, S, D, L, E sont choisis comme paramètres les plus sensibles aux fréquences naturelles.

F 8 – 9 et la F 8 - 10 sont les résultats de la régression différente dans le modèle Kriging en ajustant 1000 et 2000 des groupes de résultats de la méthode d'échantillonnage Hypercube Latin.

La discussion de la convergence pour le modèle de Kriging (régression de deuxième ordre) en ajustant montant différent de groupes d'échantillonnage est conclu dans la F 8 - 11.

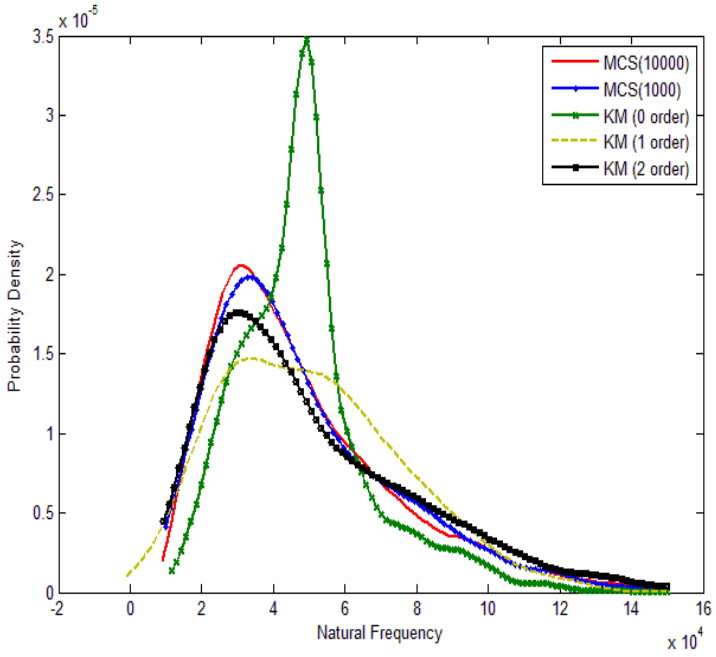

F 8 - 9 Résultat raccord pour modèle de Kriging 1000 points

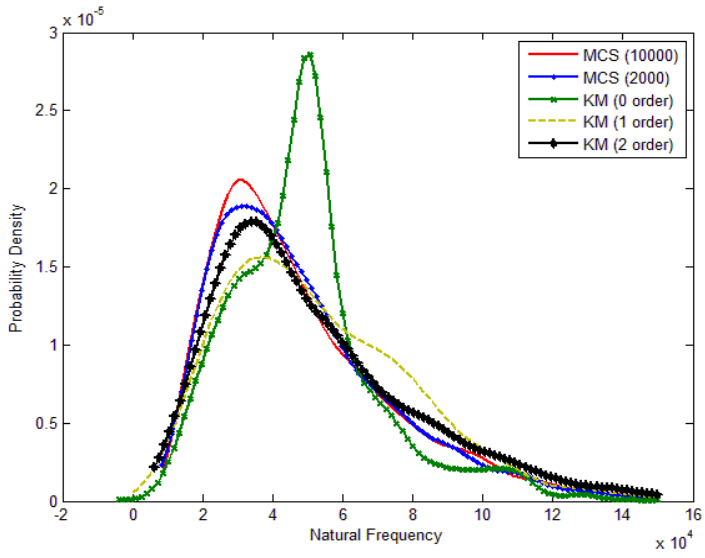

F 8 - 10 Résultat raccord pour modèle de Kriging 2000 points

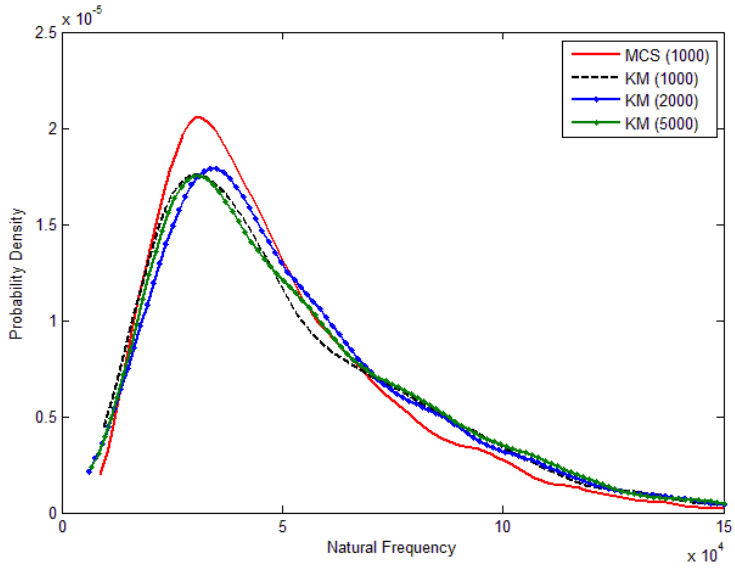

F 8 - 11 Résultats de Deuxième order de modèle Kriging

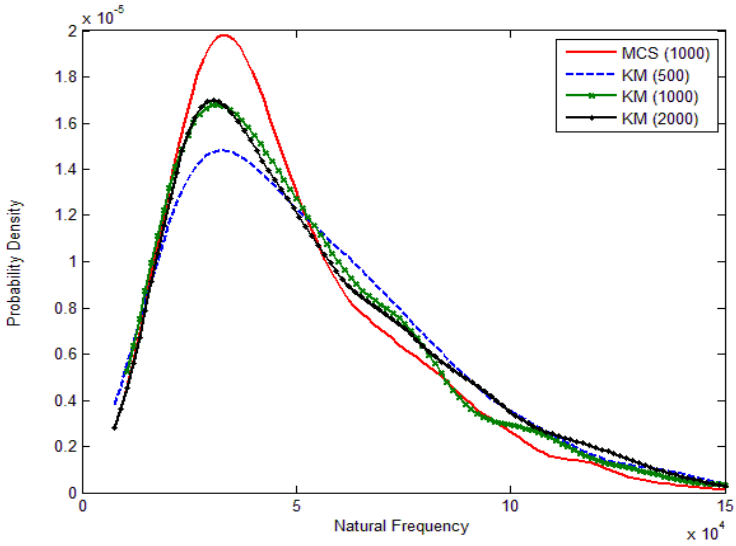

F 8 - 12 Stabilité des résultats dans le modèle Kriging

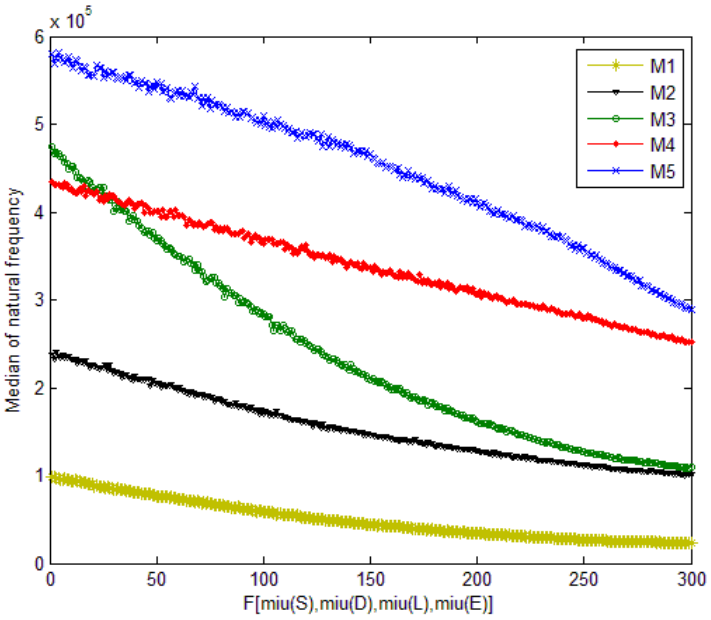

F 8 - 13 Résultats de valeur médiane de la fréquence propre

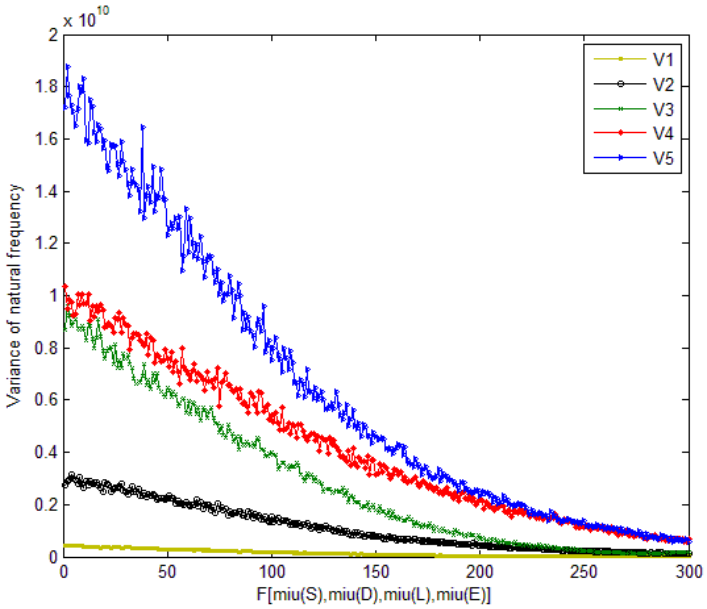

F 8 - 14 Résultats de la variance de la fréquence propre

F 8 – 13 et F 8 – 14 sont les résultats de valeur médiane et la variance de la fréquence propre de la structure de l'aile, respectivement. F 8 - 15 fournit des informations importantes que la différence de valeur médiane entre deux voisins première fréquence

propre. F 8 - 15 présente les résultats de Belta de la fréquence propre de la structure de l'aile.

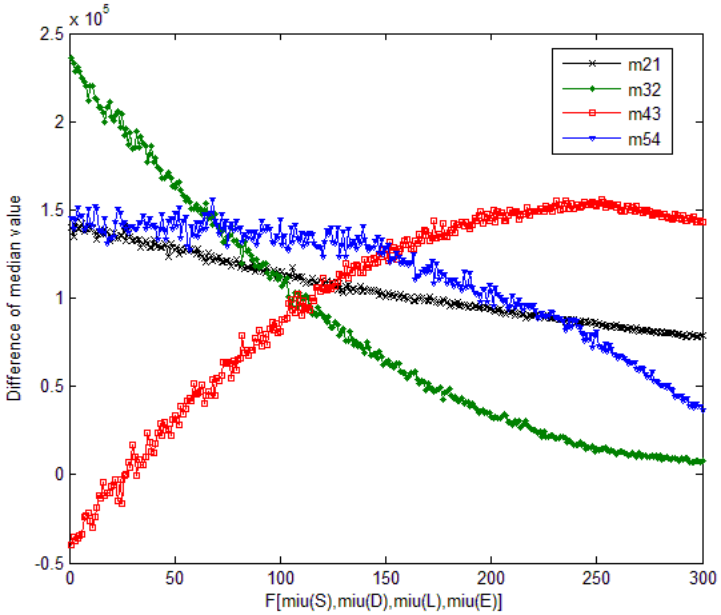

F 8 - 16 Différence de valeur médiane entre deux voisins fréquences propres

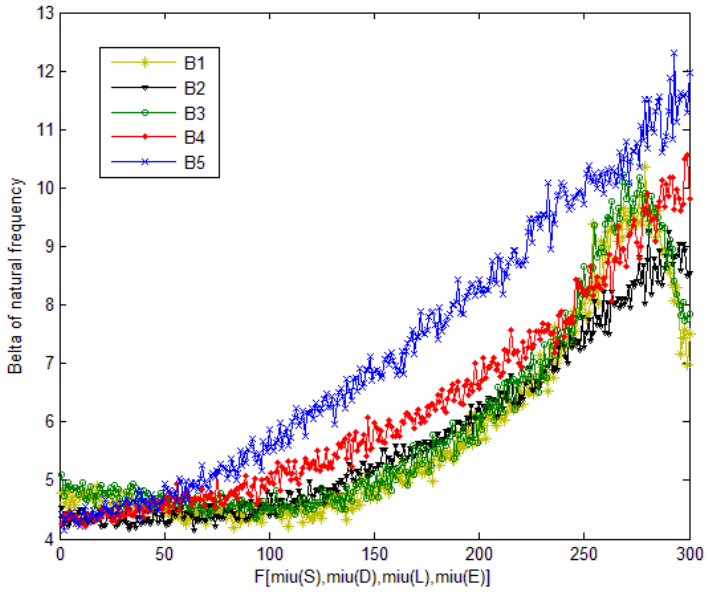

F 8 - 17 Résultats de belta de la fréquence propre de la structure de l'aile

8.2.4 Chapitre 5: Fiabilité et optimisation

Les procédures qui traitent de l'optimisation des incertitudes comprennent les points suivants:

1. Application des techniques d'optimisation efficaces qui nécessitent moins d'appels de fonction. Ces techniques peuvent profiter des caractéristiques spéciales du problème en introduisant des approximations successives pour les représentations de la fonction objectif et les contraintes par variable réciproque et / ou hybride.

2. Introduction des concepts de rapprochement à différents niveaux du processus d'optimisation.

3. Effectuer une simulation permettant de simuler des modèles d'incertitudes réalistes, impliquant paramètres incertains d'une manière efficace.

4. Une mise en œuvre appropriée de calcul, les aspects informatiques jouent un rôle clé, d'autant plus que les systèmes et les structures sont grands et nécessitent une modélisation détaillée. À cet égard, le calcul parallèle est devenu un outil qui prend de plus en plus l'intérêt des chercheurs et des ingénieurs.

Optimisation basée sur la fiabilité de modèle de substitution

Pour propager l'incertitude dans les paramètres du modèle élément fini (FEM), nous créons d'abord un FEM déterministe dans le logiciel ANSYS mécanique professionnelle via le langage de conception de paramètre. Paramètres correspondants ont été présentées dans le Tableau.

T 8 - 5 Paramètres de matériels et géométriques propriétés

Material and geometrical properties		
Certain parameters		
L	Length of the structure	10 m
E	Young's Module	2*10^5 MPa
P	Physical density	7000 kg/m^3
V	Poission ratio	0.3
Variables in Latin Hypercube sampling methods		

R1	Radius in the bottom	0.1 ~3 m
R2	Radius in the top	0.1~3 m
T1	Ratio of ring thickness	0.01~0.99
PP1	Pressure in the half surface	0~240
PP2	Force in the top	0~10^5 N

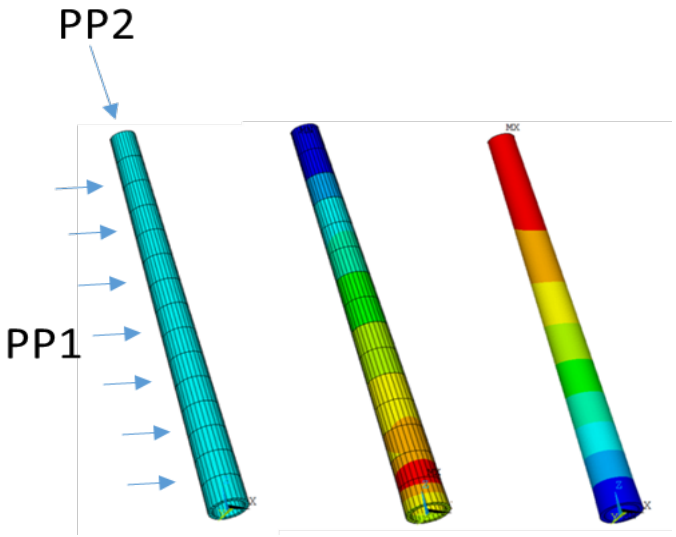

F 8 - 18 Résultats de l'analyse mécanique par éléments finis

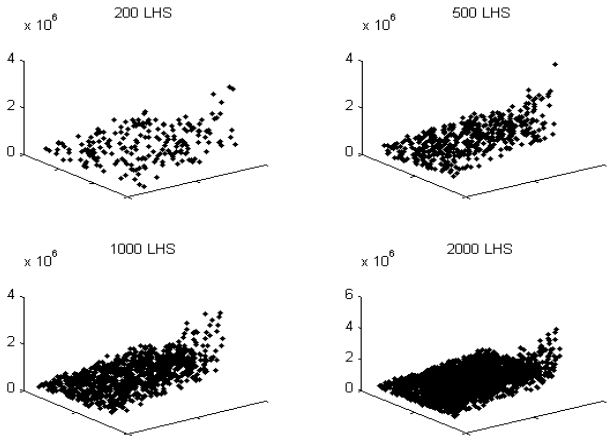

F 8 - 19 Résultats de la dispersion de la méthode d'échantillonnage Hypercube Latin

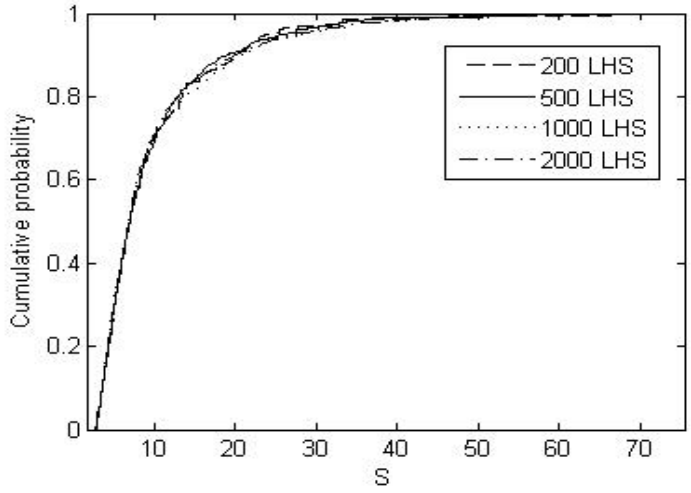

F 8 - 20 Probabilité cumulative de contrainte maximale

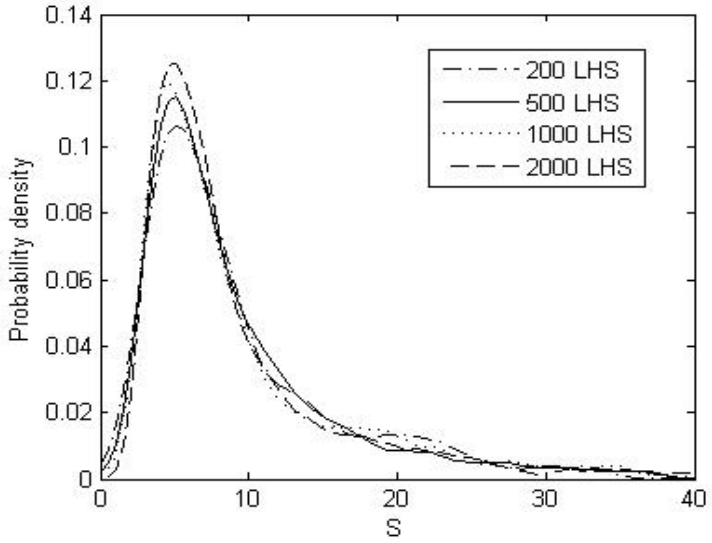

F 8 - 21 Densité de probabilité de contrainte maximale

T 8 - 6 Comparaison des résultats du modèle de substitution

	Correlation coefficient	D
Non-linear fitting	0.9933	1.0585
1-order regression	0.8002	23.7895
2-order regression	0.9471	6.8092

KM(0-order)	1	5.9341e-17
KM(1-order)	1	1.6060e-19
KM(2-order)	1	3.5514e-21

Pour être plus clair, les prédictions des modèles de substitution de la densité de probabilité et la probabilité cumulée ont été présentés dans la F 8 - 21 et la F 8 - 22, respectivement.

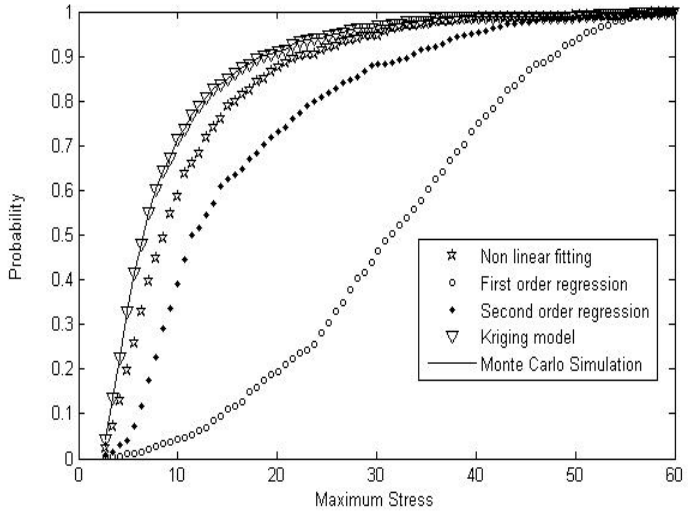

F 8 - 22 Prévision de la probabilité cumulative pour modèles de substitution

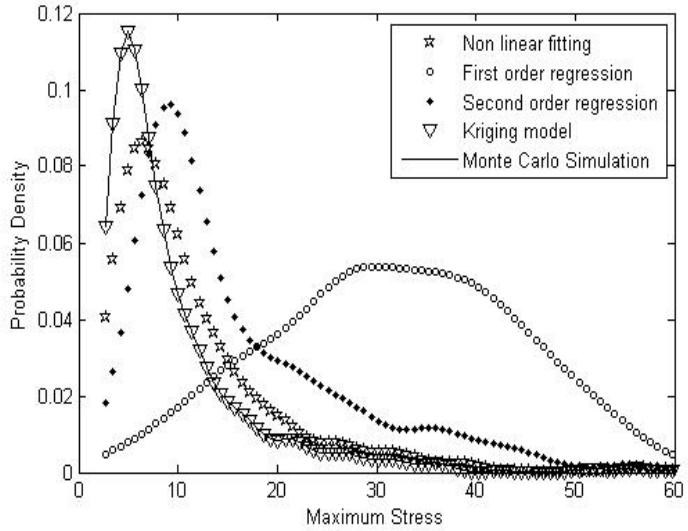

F 8 - 23 Prévision de densité de probabilité pour modèles de substitution

Les modèles de substitution décrits est représentés dans la F 8 - 23.

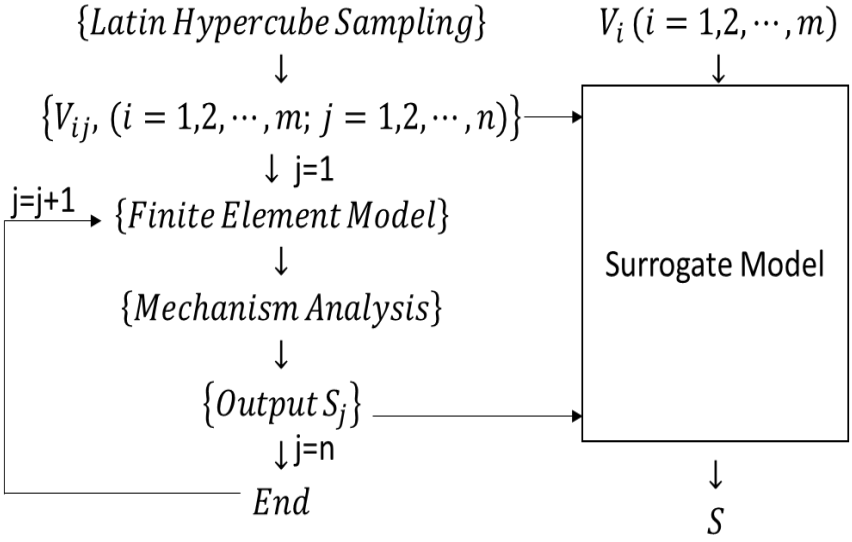

F 8 - 24 Organigramme du modèle de substitution

La formulation d'optimisation est exprimé sous la forme

$$V = V(\mathrm{R}1, \mathrm{R}2, T)$$
$$\mathrm{P} = P\left(F_M > F_s\right)$$

Le minimum (8- 22)

Sujet à

$$V_{i,\min} \le V_i \le V_{i,\max},\ i = 1,2,3; \quad (8\text{- }23)$$
$$V_1 = R1, V_2 = R2, V_3 = T$$

V est le volume de la structure, il est corrélé linéairement avec le poids et le coût de la structure, nous faisons comme l'un des objectifs et à trouver de petits valeur pour elle. P est égal à $P\left(F_M > F_s\right)$, elle est la probabilité de la situation lorsque la contrainte maximale dans toute la structure est plus grande que la limite d'élasticité du matériau dans la structure.

T 8 - 7 Résultats de l'optimisation de la fiabilité

	GA(KM)	GA(NF)	SA(KM)	SA(NF)
R1	1.1879	0.3532	1.1063	0.3399
R2	0.1092	0.1175	0.1022	0.1001

T	0.9887	0.9896	0.9872	0.9900
P	0.0100	0	0.0320	0
V	0.0349	0.0037	0.0342	0.0032
Time	2619	1.104	2244	4.436

T 8-7 présente les résultats de la fiabilité de l'algorithme d'optimisation génétique et recuit simulé sur la base de deux modèles de substitution, à savoir le modèle de Kriging et le modèle de non linéaire.

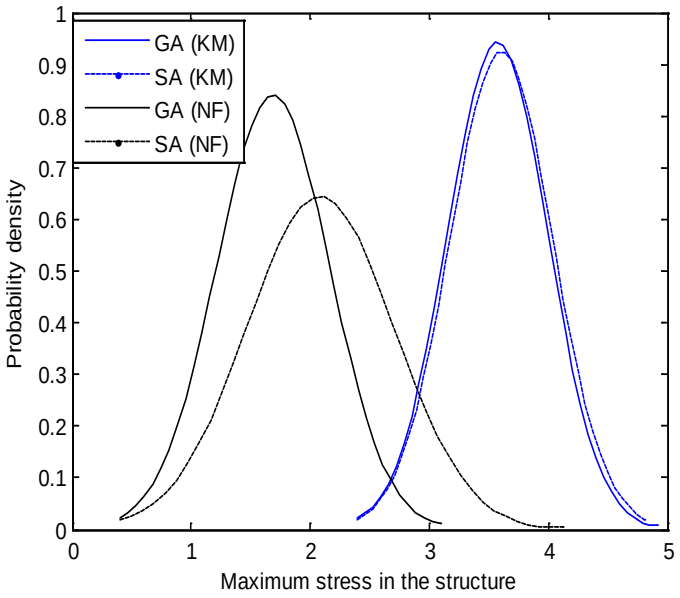

F 8 - 25 Probabilité densité d'échantillonnage Hypercube Latin

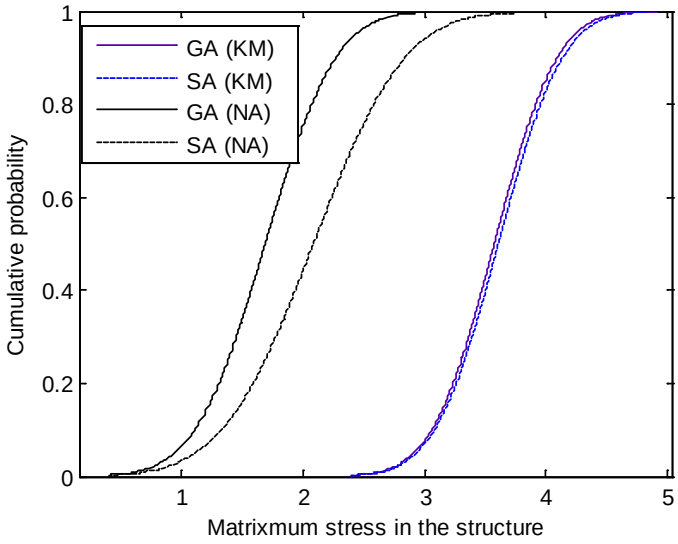

F 8 - 26 probabilité cumulative d'échantillonnage Hypercube Latin

F 8 - 24 et la F 8 - 25 sont les résultats de l'échantillonnage Hypercube Latin de la probabilité densité et de la probabilité cumulative respectivement.

8.2.5 Chapitre 6: Exemples

Analyse de dommages cumulatifs de la structure par simulation stochastique

Comme présente dans l'organigramme, les paramètres correspondant à la description du modèle de la géométrie et le chargement aléatoire sont définies comme des variables aléatoires d'entrée.

.

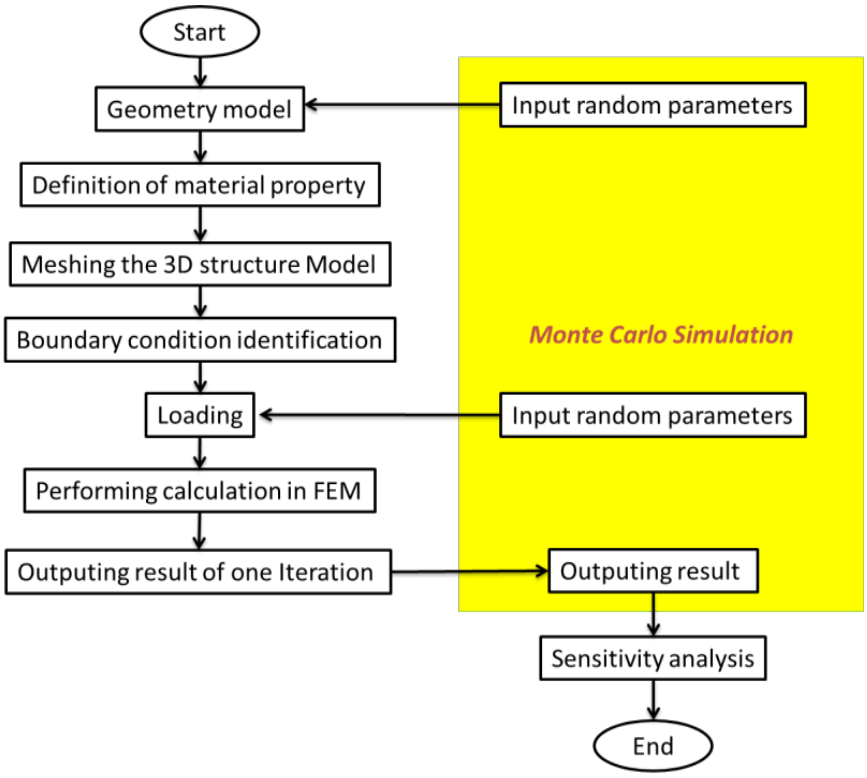

F 8 - 27 Organigramme de la simulation stochastique en Modèle éléments finis

Le déterministe FEM de la structure de l'aile a été créé par ANSYS paramétrique langage comme dans la F 8 – 27.

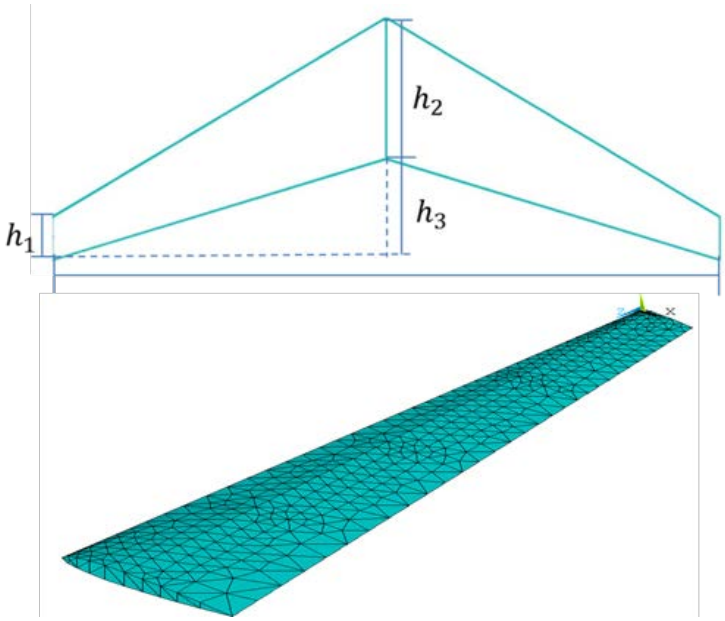

F 8 - 28 FEM de la structure de l'aile dans ANSYS

T 8 - 8 Les paramètres du FEM

Length	h_1 = 3.2 m h_2 = 10.5 m h_3 = 7.5 m l = 80 m
Airfoil	I_k $(k = 1, 2, \ldots, 8)$
Loading	P_j $(j = 1, 2, \ldots, 24)$
Material property	Physical density = 2800kg/m3 Young's module = 7e^10 Pa Poisson's ratio = 0.33

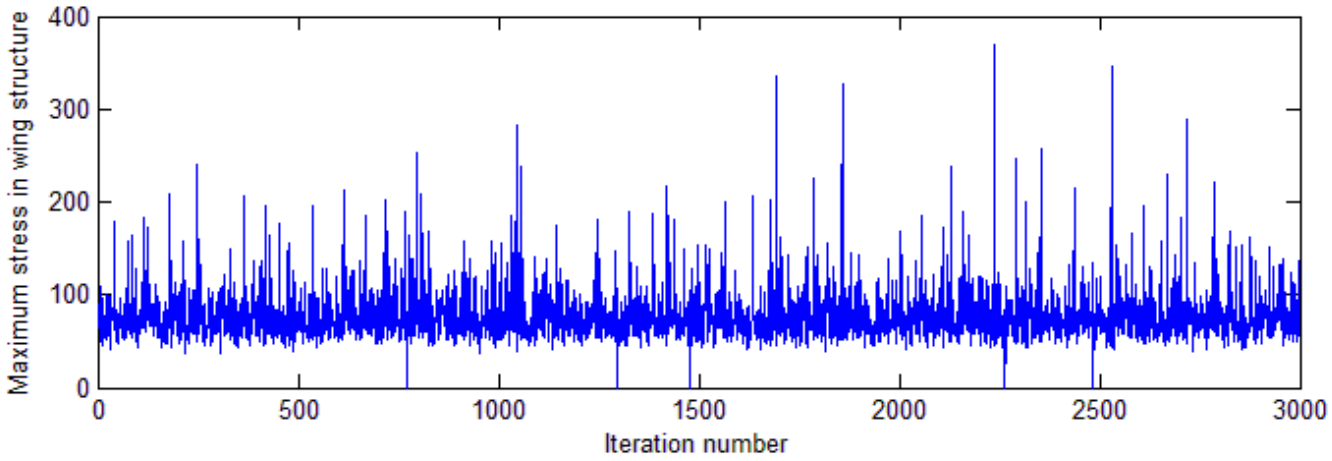

F 8 - 29 Contrainte maximale dans la structure de l'aile par LHS

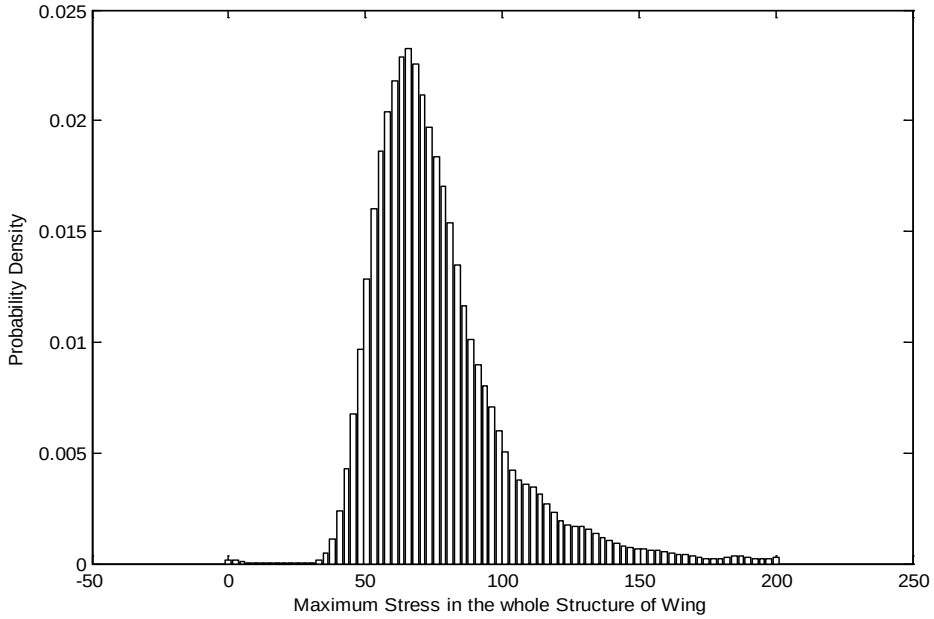

F 8 - 30 Histogramme de contrainte maximale par LHS

Analyse de la fatigue

Une loi linéaire d'accumulation des dommages à un point de la structure soumise à amplitude variable fonction du temps de stress est défini comme dans la formule

$$D = \sum_{i}^{m} \frac{n_i}{N_i} \tag{8- 24}$$

Si nous connaissons la fonction de densité de probabilité de la gamme de stress, l'équation est exprimée

$$D = \int_0^{\infty} \frac{n_T f(\Delta\sigma)}{N(\Delta\sigma)} d\Delta\sigma \tag{8- 25}$$

n_T est le nombre total de la gamme de stress $\Delta\sigma$, $f(\Delta\sigma)$ est le stress sonné PDF. La valeur de n_T peut être calculée à partir de la vie de la conception multiplié par $E[\Delta\sigma]$, taux attendu de la gamme de stress occurrence, et $N(\Delta\sigma)$ est le nombre de cycles à $\Delta\sigma$ donnée dans courbe SN:

$$N(\Delta\sigma)^m = C \tag{8- 26}$$

m et C sont des constantes des matériaux.

F 8 – 30 présente les résultats d'une analyse de sensibilité pour les variables d'entrée aléatoires dans ANSYS Design System probabiliste. Il est raisonnable de choisir les variables aléatoires d'entrée les plus importantes et de trouver la relation entre l'entrée des variables aléatoires et la variable de sortie (contrainte maximale dans la structure de l'aile).

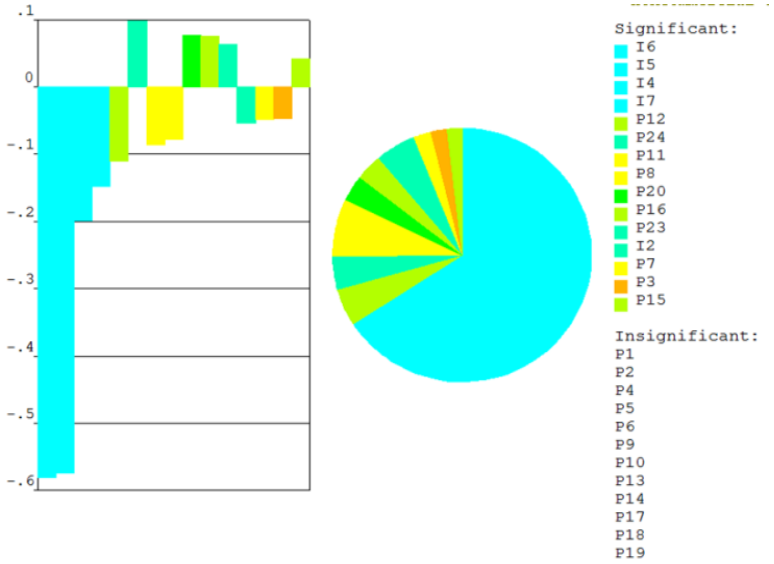

F 8 - 31 Résultat de l'analyse de sensibilité des variables d'entrée aléatoires

T 8-9 présente les résultats de coefficients dans l'équation polynomiale par la méthode de régression.

T 8 - 9 Résultats de coefficient dans l'expression polynomiale

	1	2	3	4	5	6	Average
C0	2.4184	2.3443	2.2619	2.5146	2.4276	2.8556	2.4704
C1	-1.5756	-0.8042	-0.2494	-1.6337	-0.5776	-1.9854	-1.1376
C2	-4.1768	-4.0053	-3.9237	-4.753	-4.2908	-6.0758	-4.5376
C3	-4.374	-4.9596	-4.7479	-5.0046	-5.5037	-4.8319	-4.9036
C4	-0.28	-0.3157	-0.6375	0.0775	-0.1375	-0.8884	-0.3600
C5	1.2423	0.7418	1.0502	2.1566	0.438	1.21	1.13982
C6	-0.5483	-1.1544	-2.2422	-0.3489	-1.933	0.9374	-0.8816
C7	0.6886	1.0282	-0.6858	0.2574	0.3405	0.7263	0.39253
C8	1.7323	0.5758	0.8964	0.8691	1.9482	1.8868	1.3181
C9	3.246	3.3491	3.1617	4.1428	3.8912	5.3302	3.8535
C10	5.7342	6.7796	6.3527	6.8503	7.0194	6.6274	6.5606
C11	-0.3678	-1.5251	-0.1858	-1.7806	-1.6474	-0.0055	-0.9187
C12	3.1091	3.53	3.8684	3.9861	4.5659	3.1202	3.69662
C13	-0.6524	-0.762	0.3015	-1.0879	-0.7102	0.0215	-0.4816
C14	-0.1657	1.1731	0.3854	0.5887	0.2194	0.3075	0.41807

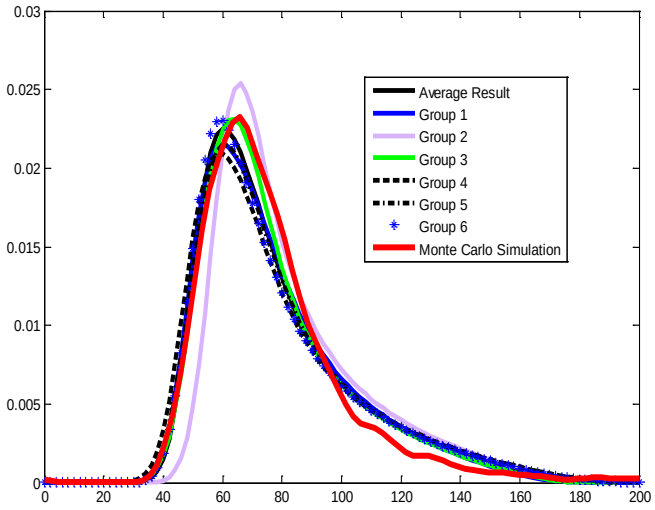

F 8 - 32 Probabilité densité d'équation polynomiale

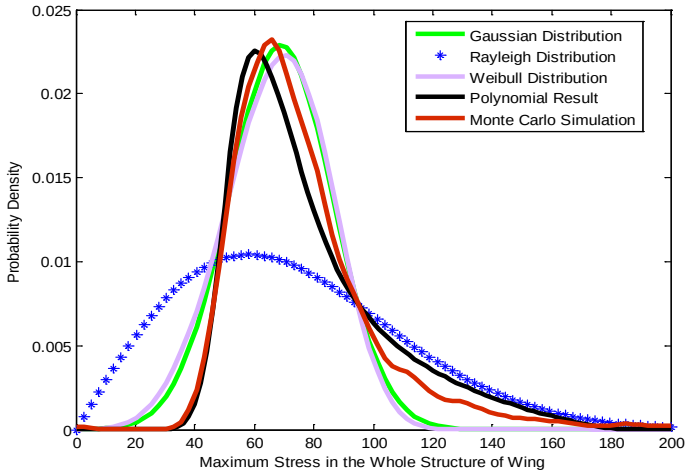

F 8 - 33 Probabilité densité par méthodes différentes

F 8 – 32 compare les résultats de la fonction classique de probabilité densité (gaussienne, Weibull et la distribution de Rayleigh), équation polynomiale (par la méthode de la delta de Dirac) et simulation de Monte Carlo. Les résultats sont obtenus statistiques de dommages cumulatifs, comme démontré dans F 8 – 33 et F 8 – 34.

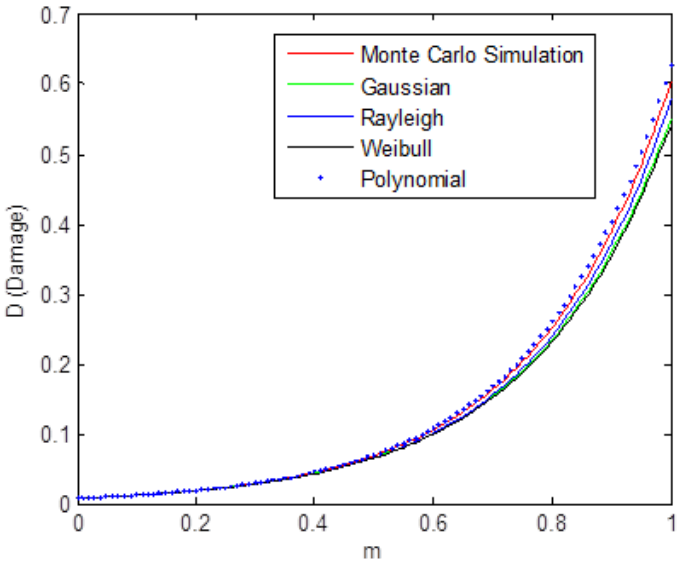

F 8 - 34 Résultats de dommages cumulatifs par méthodes différentes

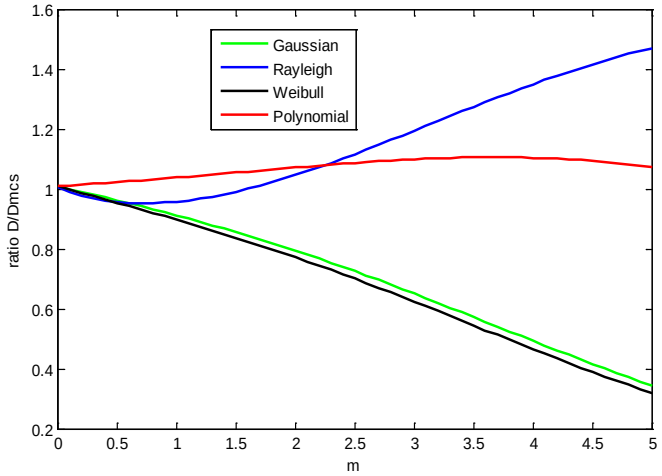

F 8 - 35 Comparaison des D/Dmcs par chaque méthode

L'optimisation de la forme aérodynamique par des algorithmes heuristiques en modèle de substitution

La formule pour la forme d'une feuille de 00xx NACA, «xx» étant remplacé par le pourcentage d'épaisseur accords, est:

$$y_t = tc\left[a_1\sqrt{\frac{x}{c}} + a_2\left(\frac{x}{c}\right) + a_3\left(\frac{x}{c}\right)^2 + a_4\left(\frac{x}{c}\right)^3 + a_5\left(\frac{x}{c}\right)^4\right] \qquad (8\text{- }27)$$

C est la longueur de la corde, x est la position le long de la corde de 0 à c, y est égal à la moitié de l'épaisseur à une valeur donnée de x (axe à la surface), et t est l'épaisseur maximale en une fraction de la corde (si 100 t donne les deux derniers chiffres de la NACA 4 chiffres dénomination), sont les constantes,
Les plus simples feuilles assymétriques sont les feuilles de la série NACA 4 chiffres, la formule utilisée pour calculer la ligne moyenne de carrossage est:

$$y_c = \begin{cases} \frac{mx}{p^2}(2p - \frac{x}{c}), (0 \le x \le pc) \\ m\frac{c-x}{(1-p)^2}\left[1 + \frac{x}{c} - 2p\right], (pc \le x \le c) \end{cases} \qquad (8\text{- }28)$$

m est la cambrure maximale (100 m est le premier des quatre chiffres), p est la position de la cambrure maximale (10p est le deuxième digit).

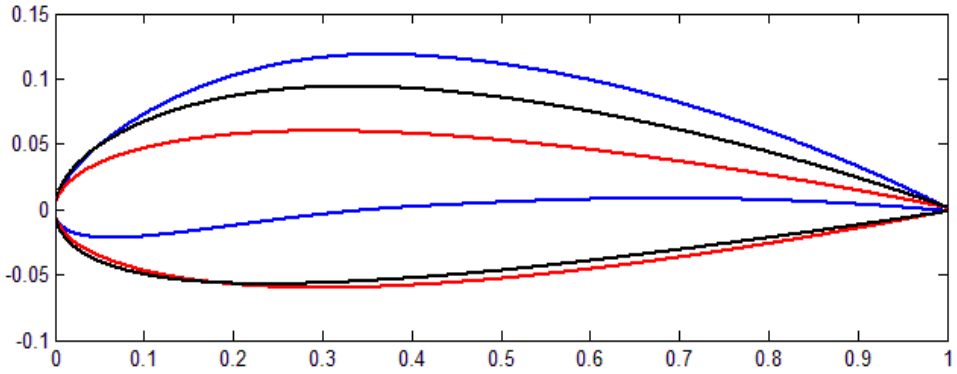

F 8 - 36 Exemples de modèle de la géométrie forme

Dans l'élément de fluide FLOTRAN ANSYS, Fluid 141 a été choisi comme type d'élément fini de fluide. Le tableau T 8 - 10 montre les détails de la propriété et de l'environnement fluide d'écoulement. Les résultats de certains nœuds autour de voilure dans le calcul CFD sont données et résumées comme dans F 8 – 36, F 8 – 37 et F 8 – 38, à savoir le tracé de contour du résultat de la pression nodale, pression de stagnation totale et la vitesse du fluide de la solution nodale, respectivement.

T 8 - 10 Propriété du fluide et de l'environnement de flux

Attack angle	3
Velocity	200 m/s
Temperature	230 K
Pressure	25000 Pa
Density	Air
Viscosity	0
Fluid element type	2D FLOTRAN 141

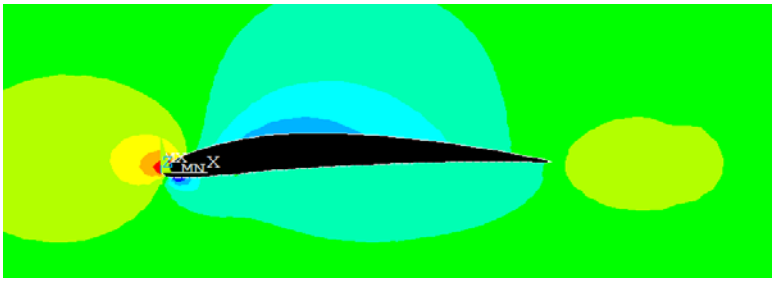

F 8 - 37 Résultat de la pression Nodal

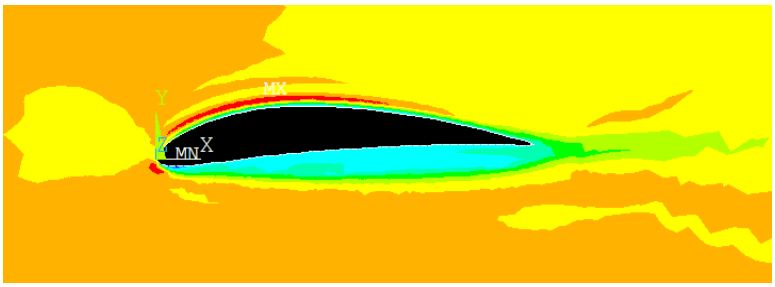

F 8 - 38 Pression totale de stagnation

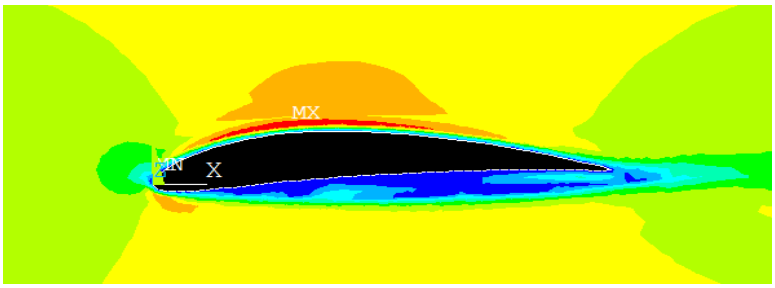

F 8 - 39 Vitesse du fluide de la solution nodale

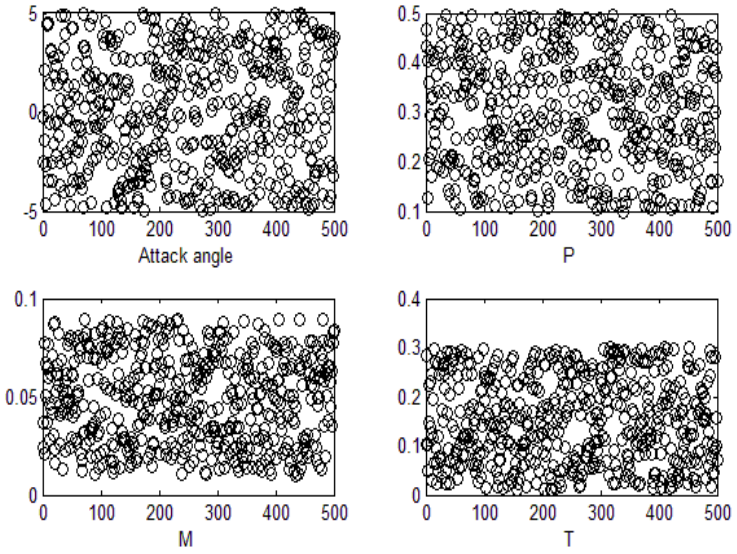

F 8 - 40 Echantillons de variables d'entrée

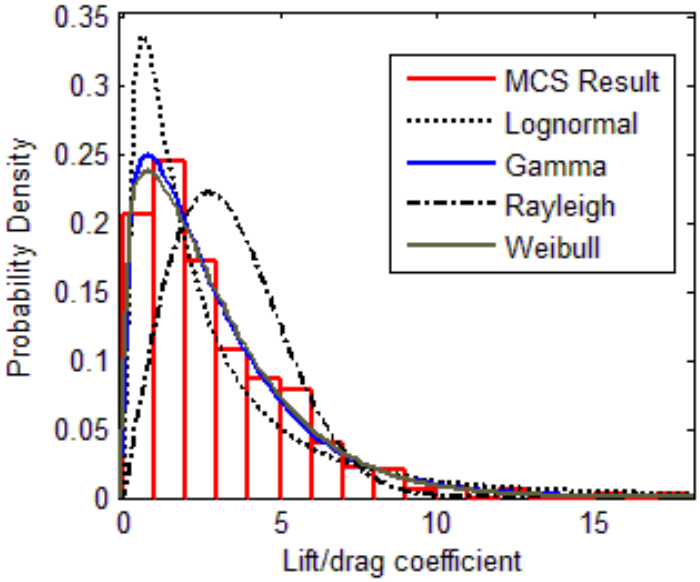

F 8 - 41 Résultats de la probabilité densité de Lift/drag coefficient

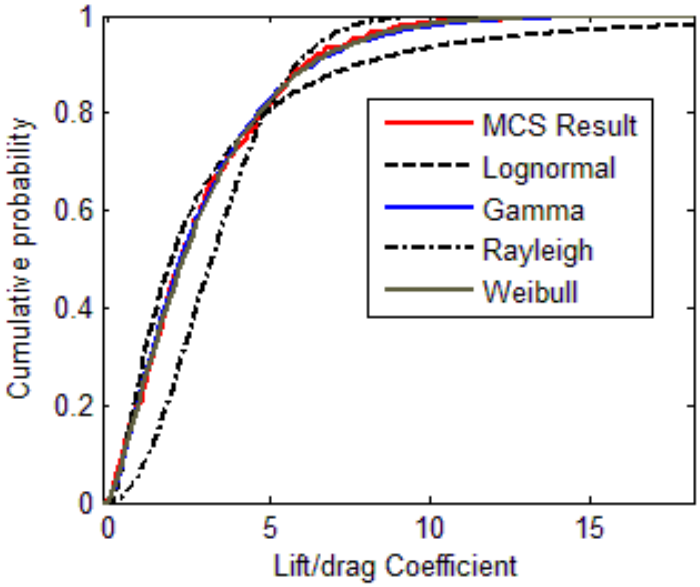

F 8 - 42 La probabilité cumulative de Lift/drag coefficient

F 8 – 42 a comparé les résultats des prédicteurs de modèles Kriging (d'ordre zéro, de premier ordre et de second ordre) avec le résultat de MCS, cela prouve que les modèles de Kriging ont une bonne propriété comme le montage du résultat de MCS.

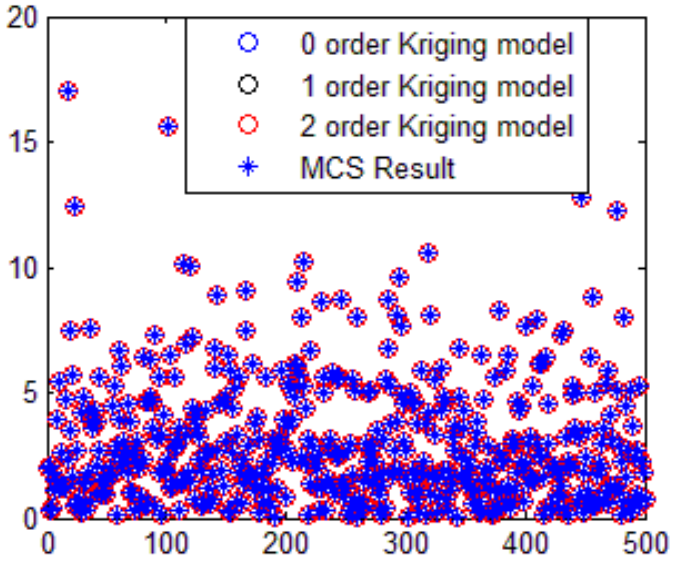

F 8 - 43 Résultats prédits par les modèles Kriging

Les résultats prédits par les modèles Kriging avec différents ordres ont été présentés dans la F 8 – 43 et la F 8 – 44.

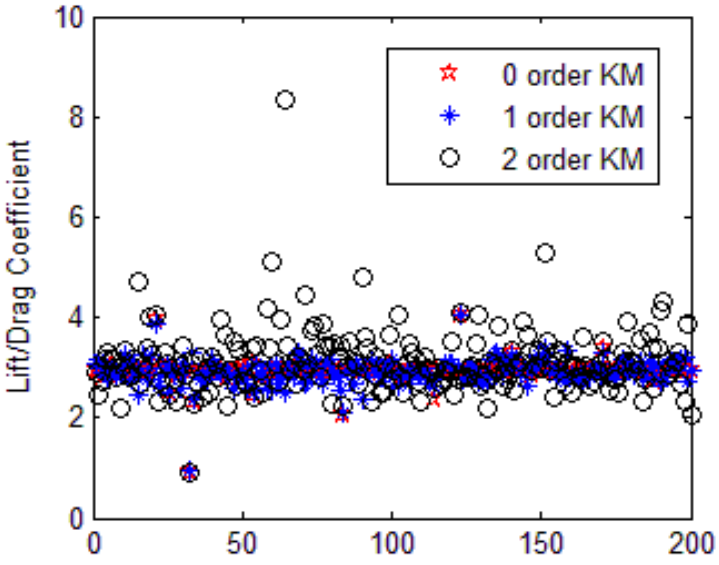

F 8 - 44 Résultats prédits par les modèles Kriging

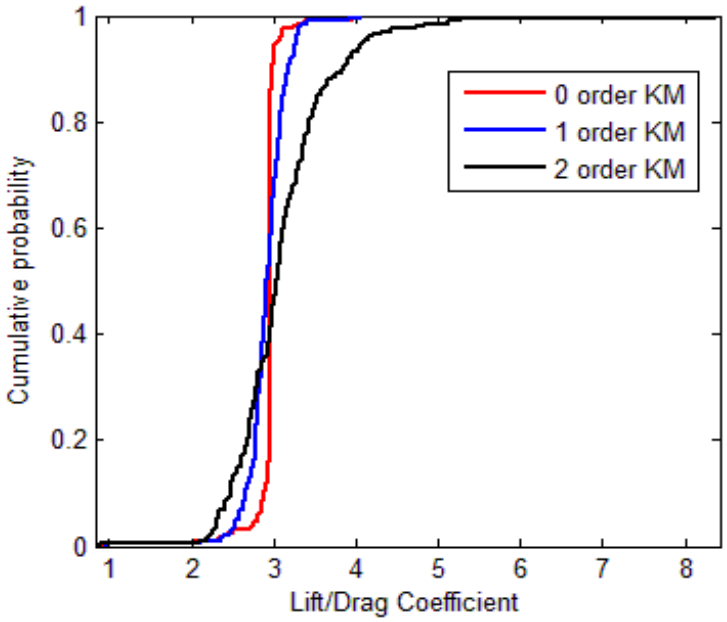

F 8 - 45 Résultats de probabilité cumulative dans les modèles Kiging

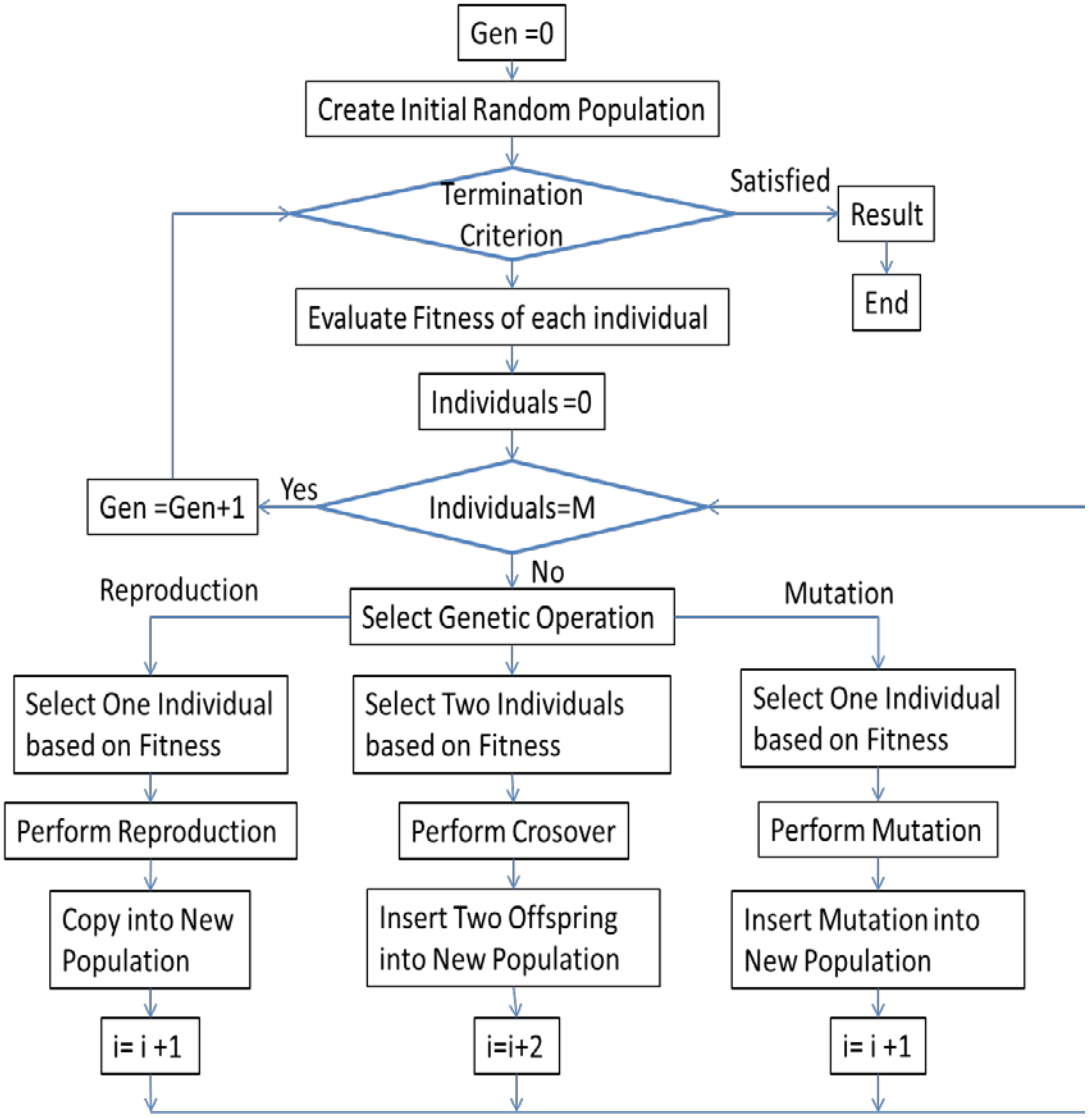

F 8 - 46 Organigramme de la programmation de l'algorithme génétique

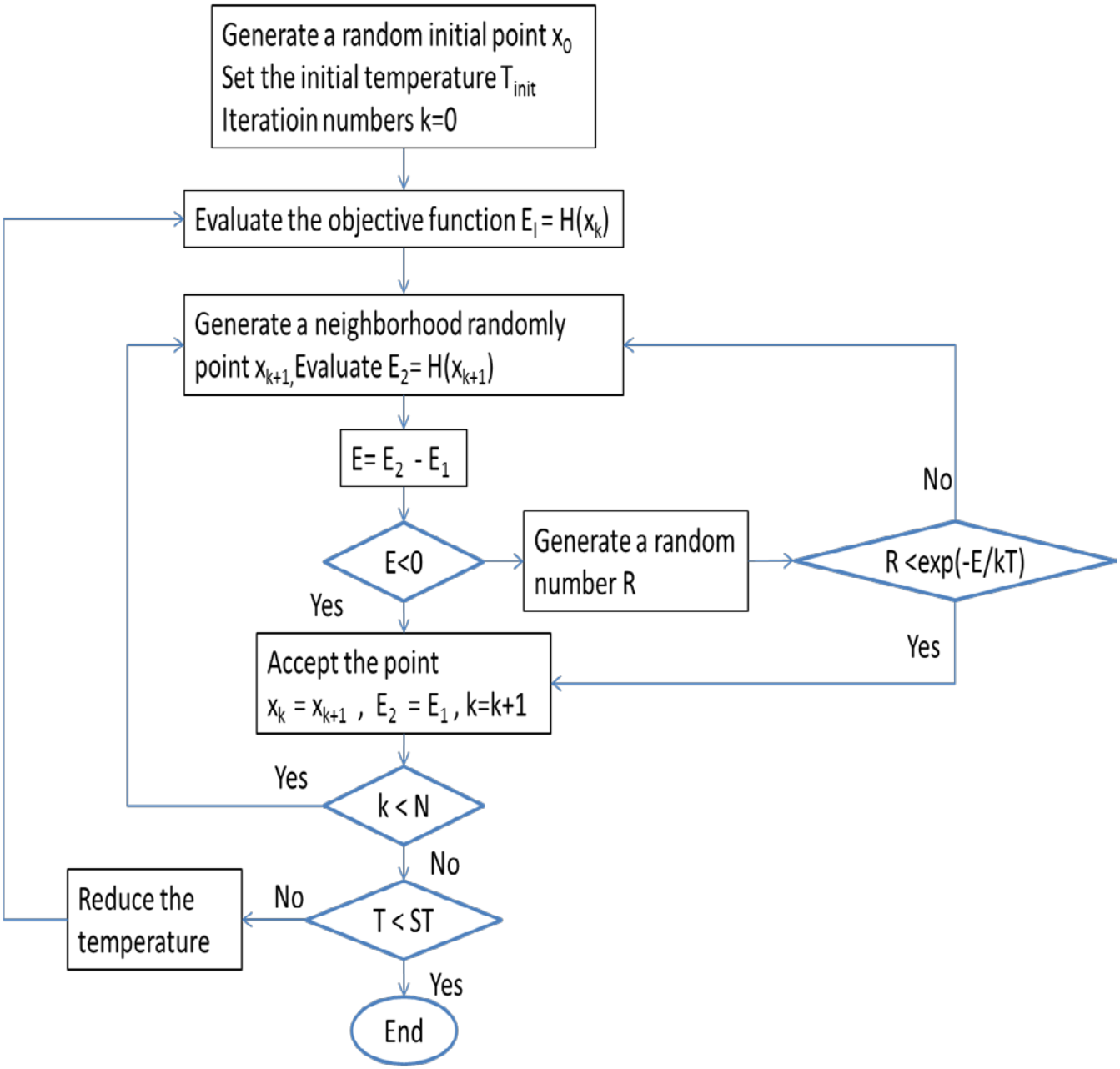

F 8 - 47 Organigramme du la programmation de l'algorithme recuit simulé

La formation de l'optimisation de forme aérodynamique de façon traditionnelle peut être écrite comme

$$\text{Maximum} \quad C = C(\mathrm{p}, \mathrm{m}, \mathrm{t}, \mathrm{v}, \mathrm{att}) \tag{8- 29}$$

$$V_{i,\min} \le V_i \le V_{i,\max},\ i = 1,2,3;$$
$$V_1 = p, V_2 = m, V_3 = t$$
Sujet à $$v = v_s,\ att = att_s \qquad (8\text{- }30)$$

T 8 - 11 Résultats de la SA et GA

	P	M	T	C	TIME (s)
SA (0)	0.1629	0.0704	0.0915	8.47	514.55
SA (1)	0.1612	0.0703	0.0909	8.48	610.48
SA (2)	0.1631	0.0704	0.0914	8.50	604.78
GA (0)	0.1632	0.0704	0.0915	8.47	299.50
GA (1)	0.1628	0.0704	0.0913	8.50	338.24
GA (2)	0.1627	0.0704	0.0913	8.50	315.86
CFD	0.16	0.07	0.09	8.43	6.7

Pour offrir plus d'informations pour l'analyse de mécanisme aérodynamique, F 8 – 47, F 8 – 48 et F 8 – 49 était le tracé de contour des résultats CFD.

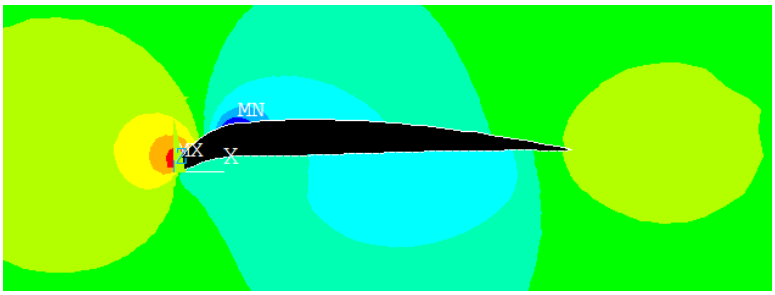

F 8 - 48 Résultat de la pression nodale du profil aérodynamique optimisée

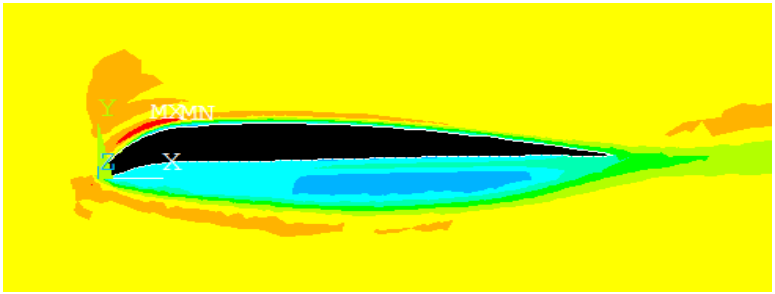

F 8 - 49 Pression de stagnation totale du profil aérodynamique optimisée

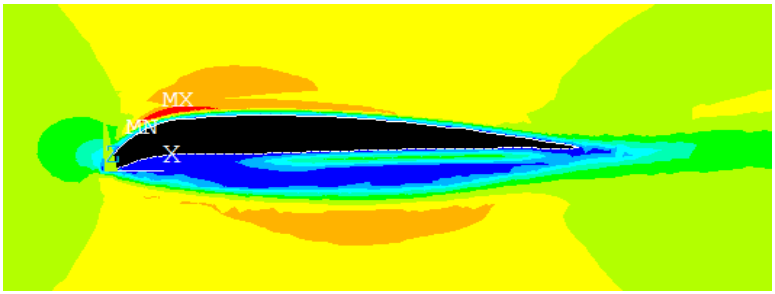

F 8 - 50 Vitesse de fluide de solution nodal de profil aérodynamique optimisée

8.3 Conclusion

Aéronefs est un problème compliqué car l'environnement de fonctionnement et la structure mécanique sont sophistiqués. L'analyse traditionnelle des modèles éléments finis déterministe ignore la fluctuation des paramètres comme variables incertaines dans l'environnement de fonctionnement réel. L'incertitude est un problème inévitable dans le processus de fabrication, les infrastructures et l'ingénierie de conception. La quantification et la propagation de l'incertitude dans le processus de simulation ou comme un élément clé de l'analyse des risques, l'optimisation de l'évaluation robustesse ou la fiabilité basée attire l'attention des chercheurs et des ingénieurs. Dans cette thèse, les méthodes de Monte Carlo sont choisies comme une méthode efficace pour propager des incertitudes dans le système de la structure, comme nous l'avons vu dans le chapitre 3. Il d'agit d'une méthode non-intrusive, l'échantillonnage basé méthode, mais nécessite souvent un grand ensemble de points d'échantillonnage pour fournir une estimation fiable et stable de l'incertitude. Cela rend l'approche MCS coûteuse en calcul. Cependant, l'échantillonnage latin hypercube est une stratégie d'échantillonnage appropriée pouvant réduire le nombre de points d'échantillonnage tout en atteignant un certain niveau de précision.

L'optimisation basée sur la fiabilité à trouver le meilleur compromis entre le coût et la sécurité tout en tenant compte des incertitudes du système en intégrant des mesures de fiabilité au sein de l'optimisation. Malgré les avantages de l'optimisation de la fiabilité, son application à problème d'ingénierie pratique est encore assez difficile. Nous proposons une méthode efficace pour découpler les boucles de l'analyse de l'évaluation

de la fiabilité et l'optimisation en créant des modèles de substitution. L'échantillonnage latin hypercube est utilisé dans le modèle des éléments finis pour obtenir une base de données fiable et crédible pour les modèles de substitution. Afin d'éviter la convergence prématurée dans le processus d'optimisation, des ajustements dans les algorithmes heuristiques d'optimisation ont été faits. Les modèles de substitution sont utiles dans l'analyse de la fiabilité des systèmes structuraux complexes. Les premières propositions appliquent des modèles de régression première et de deuxième ordre polynôme comme substituts pour la véritable fonction d'état limite, telle qu'elle est appliquée dans l'exemple de l'analyse cumulative du dommage de la structure de l'aile par simulation stochastique au chapitre 6. Par ailleurs, les modèles de Kriging d'interpolation pour des problèmes structurels de fiabilité détiennent plusieurs caractéristiques compétitives. Il n'a pas seulement la capacité d'interpolation à souligner, mais aussi le fait de prendre la flexibilité pour se rapprocher des fonctions arbitraires avec un haut niveau de précision, et il explore également la capacité de fournir une mesure de l'incertitude locale pour les prédictions du modèle. Le modèle de Kriging a été appliqué dans le chapitre 4 pour l'analyse de la fiabilité, dans le chapitre 5 pour l'optimisation de la fiabilité et sur la base également et dans le chapitre 6 pour l'optimisation de forme aérodynamique.

Pour l'optimisation, les méthodes traditionnelles engendrent un coût important en temps ou des inconvénients naturels de convergence prématurée parce que de trouver l'optimum local le plus proche de faible qualité. L'algorithme du recuit simulé (SA) est une heuristique basée sur la recherche locale qui nous rend capables d'échapper à être pris au piège par un optimum local. Algorithme génétique (GA) puise son inspiration dans les principes et les mécanismes de la sélection naturelle, il appartient à une classe de l'informatique évolutive. SA et GA ont été appliquées dans les exemples du chapitre 5 pour l'optimisation en fonction de la fiabilité de modèle de substitution et dans le chapitre 6 pour l'optimisation de forme aérodynamique.

List of figures

Fig 2 - 1 Comparaison between aleatory uncertainty and epistemic uncertainty..... 7
Fig 2 - 2 Uncertainty sources in the simulation-based design..... 9
Fig 2 - 3 Examples of probability density function.....10
Fig 3 - 1 Convergence history of different PDF in function f1.....48
Fig 3 - 2 Convergence history of different PDF in function f2.....48
Fig 3 - 3 Convergence history of different PDF in function f3.....49
Fig 3 - 4 Finite element model of wing structure.....51
Fig 3 - 5 Contour picture of Von-Mises stress in five natural frequencies 52
Fig 3 - 6 Records of natural frequencies in the process of Latin Hypercube sampling.....54
Fig 3 - 7 Cumulative probability of five natural frequencies in MCS.....54
Fig 3 - 8 Numerical statistic in the stochastic simulation.....55
Fig 4 - 1 Hermite polynomials.....62
Fig 4 - 2 5000 Gaussian sampling points are generated in the Monte Carlo simulation.....73
Fig 4 - 3 Kriging model 1000 points fitting result.....82
Fig 4 - 4 Kriging model 2000 points fitting results.....82
Fig 4 - 5 Second order Kriging model fitting results.....83
Fig 4 - 6 Stability of results in Kriging model.....83
Fig 4 - 7 Results of median value of natural frequency.....84
Fig 4 - 8 Results of variance of natural frequency 85
Fig 4 - 9 Difference of median value between two neighbour natural frequencies 86
Fig 4 - 10 Results of belta of natural frequency in wing structure 87
Fig 5 - 1 Finite element model and results of mechanical analysis 118
Fig 5 - 2 Scatter results of Latin Hypercube sampling method.....119
Fig 5 - 3 Cumulative probability of maximum stress 119
Fig 5 - 4 Probability density of maximum stress 120
Fig 5 - 5 Prediction of surrogate models in cumulative probability 123
Fig 5 - 6 Prediction of surrogate models in probability density.....123
Fig 5 - 7 Flowchart of surrogate model.....124
Fig 5 - 8 Probability density of Latin Hypercube sampling 127
Fig 5 - 9 Cumulative probability of Latin Hypercube sampling 128

Fig 6 - 1 Flowchart of Stochastic simulation in Finite Element Model 131
Fig 6 - 2 Finite Element Model of wing structure in ANSYS 132
Fig 6 - 3 Record of maximum stress in the whole structure of the wing in LHS.....133
Fig 6 - 4 Histogram of maximum stress in LHS 133
Fig 6 - 5 Result of sensitivity analysis of random input variables 135
Fig 6 - 6 Probability density of polynomial equation.....137
Fig 6 - 7 Probability density of different method.....138
Fig 6 - 8 Results of accumulative damage in different method 139
Fig 6 - 9 Comparison of D/Dmcs in each method 140
Fig 6 - 10 Examples of airfoil geometry model.....142
Fig 6 - 11 Nodal pressure result 143
Fig 6 - 12 Total stagnation pressure.....143
Fig 6 - 13 Fluid velocity of nodal solution.....143
Fig 6 - 14 Samples of input variables 144
Fig 6 - 15 Probability density results of Lift/drag coefficient 145
Fig 6 - 16 Cumulative probability of Lift/drag coefficient 145
Fig 6 - 17 Results of Kriging models.....148
Fig 6 - 18 Results of Kriging models.....149
Fig 6 - 19 Results of cumulative probability in Kriging models 150
Fig 6 - 20 Flowchart of Genetic algorithm programming 152
Fig 6 - 21 Flowchart of Annealing simulated algorithm programming 153
Fig 6 - 22 Nodal pressure result of optimized airfoil.....155
Fig 6 - 23 Total stagnation pressure of optimized airfoil 155
Fig 6 - 24 Fluid velocity of nodal solutionof optimized airfoil 155

List of tables

Table 3 - 1 Time cost of different PDF by importance sampling method.....47
Table 3 - 2 Results of different PDF by importance sampling method 47
Table 3 - 3 Results of deterministic finite element model.....52
Table 3 - 4 Results of Latin Hypercube Sampling method.....55
Table 4 - 1 Representation of various distributions as functionals of normal random variables .60
Table 4 - 2 Results of sensitivity anlysis for input variables 77
Table 5 - 1 Parameters of material and geometrical properties 118
Table 5 - 2 Comparison of results of surrogate model.....121
Table 5 - 3 Results of reliability based optimization.....126
Table 6 - 1 Parameters in Finite Element Model.....132
Table 6 - 2 Results of coefficient in the polynomial expression.....136
Table 6 - 3 Fluid property and flow environment.....142
Table 6 - 4 Results of SA and GA 154

Reference

[1] J.B. Ingram-Cotton, M.J. Hecht, Reliability program requirements for space systems, Aerospace Report NO, TOR-2007(8583)-6889, US, Aerospace Corporation, 2007.

[2] W. Yao, X.Q. Chen, Review of uncertainty-based multidisciplinary design optimization methods for aerospace vehicles, Progress in Aerospace Science 47(2011)450-479.

[3] L. Bermúdez, A. Velázquez, A. Matesanz, Viscous– inviscid method for the simulation of turbulent unsteady wind turbine airfoil flow, Journal of Wind Engineering and Industrial Aerodynamics, 2002.

[4] A. Haldar, S. Mahadevan, Probability, reliability, and statistical methods in engineering design, John Wiley & Sons Inc. 2000.

[5] Rubinstein, R. Y, Kroese, D. P. (2007), Simulation and the Monte Carlo Method (2nd ed.), New York: John Wiley & Sons, ISBN 978-0-470-17793-8.

[6] P. Doubilet, C.B. Begg, M.C. Weinstein, Probabilistic sensitivity analysis using Monte Carlo simulation, A practical approach, Journal of the Society for Medical Decision Making [1985, 5(2):157-177].

[7] J.C. Helton, F.J. Davis, Latin hypercube sampling and the propagation of uncer-tainty in analyses of complex systems, Reliability Engineering & System Safety, 2003.

[8] D.A. DeLaurentis, D.N. Mavris, Uncertainty modeling and management in multidisciplinary analysis and synthesis, In: 38th aerospace sciences meeting and exhibit, Reno, NV, AIAA-2000-0422, 200.

[9] A.K. Noor, Non-deterministic approaches and their potential for future aerospace system, NASA/CP-2001-211050, Langley Research Center 2011.

[10] J.B. Ingram-Cotton, M.J. Hecht, Reliability program requirements for space systems, Aerospace Report NO.TOR-2007(8583)-6889, US Aerospace Corporation, 2007.

[11] Helton J.C, Burmaster D.E, Treatment of aleatory and epistemic uncertainty in performance assessments for complex systems, Reliability Engineering and System Safety 1996; 54(2-3):91-4.

[12] W.L. Oberkampf, S.M. Deland, B.M. Rutherford, Estimation for total uncertainty in modeling and simulation, SAND2000-0824, Sandia National Laboratories 2000.

[13] Haldar A, Mahadevan S, Probability, reliability, and statistical methods in engineering design, John Wiley & Sons Inc. 2000.

[14] Pawitan Y, In all likelihood: statistical modeling and inference using likelihood, USA: Oxford University Press, 2001.

[15] Youn BD, Kloess A, Bayesian reliability analysis with evolving, insufficient, and subjective data sets, Journal of Mechanical Design 2009; 131(11):111008.

[16] Yager R, Kacprzy KJ, Fedrizzi M, Advances in the Dempster-Shafer theory of evidence, New York: John Wiley AND Sons. 1994.

[17] Sentz K, Ferson S, Combination of evidence in Dempster-Shafer theory, SAND 2002-0835, Sandia National Laboratories; 2002.

[18] P. Soundappan, R. Grandhi, R. Canfield, Comparison of evidence theory and Bayesian theory for uncertainty modeling, Reliab.Eng.Syst.Saf. 85(2004)295-311.

[19] E.Alyanak, R.Grandhi, H.R.Bae, Gradient projection for reliability-based design optimization using evidence theory, Eng. Optim40 (10)(2008)923-935.

[20] Y.C. Bai, C. Jiang, Evidence-theory-based structural static and dynamic response analysis under epistemic uncertainties, Finite Elements in Analysis and Design 68(2013)52-62.

[21] H. Agarwal, J.E. Renaud, E.L. Preston, Uncertainty quantification using evidence theory in multidisciplinary design optimization, Reliability Engineering & System Safety 85(2004)281-294.

[22] Z.P. Mourelatos, J.Zhou, A design optimization method using evidence theory, J.Mech.Des. 128(2006)270-279.

[23] H.A. Jensen, Structural optimal design of systems with possibility theory, Advances in Engineering Software 32(2001)937-948.

[24] I. Lopez, N. Sarigul-Klijn, A review of uncertainty in flight vehicle structural damage monitoring, diagnosis and control: Challenges and opportunities, Progress in Aerospace Sciences, 46(2010) 247-273.

[25] M. Inuiguchi, H. Ichihashi, Modality constrained programming problems: A unified approach to fuzzy mathematical programming problems in the setting of possibility theory, Information Sciences, 67(1993), 93-126.

[26] G. Mauris, Possibility distributions: A unified representation of usual direct-probability-based parameter estimation methods, International Journal of Approximate Reasoning, 52(2011) 1232-1242.

[27] Ü.S. Sakallı, Ö.F. Baykoç, Can the uncertainty in brass casting blending problem be managed A probability/possibility transformation approach, Computers & Industrial Engineering, 61 (2011), 729-738.

[28] E. Miranda, S. Destercke, On the connection between probability boxes and possibility measures, Information Sciences, Volume 224, (2013) 88-108.

[29] D. Dubois, H. Prade, Bayesian conditioning in possibility theory, Fuzzy Sets and Systems, 92(1997) 223-240.

[30] C. Baudrit, I. Couso, D. Dubois, Joint propagation of probability and possibility in risk analysis: Towards a formal framework, International Journal of Approximate Reasoning, 45(2007) 82-105.

[31] N. Impollonia, G. Muscolino, Interval analysis of structures with uncertain-but-bounded axial stiffness, Computer Methods in Applied Mechanics and Engineering, 200(2011) 1945-1962.

[32] C. Jiang, X. Han, F.J. Guan, An uncertain structural optimization method based on nonlinear interval number programming and interval analysis method, Engineering Structures, 29(2007) 3168-3177.

[33] L. Majumder, S.S. Rao, Interval-based optimization of aircraft wings under landing loads, Computers & Structures, 87(2009)225-235.

[34] W. Verhaeghe, W. Desmet, D. Vandepitte, D. Moens, Interval fields to represent uncertainty on the output side of a static FE analysis, Computer Methods in Applied Mechanics and Engineering, 260 (2013) 50-62.

[35] Y. Ben-Haim, I. Elishakoff. Convex models of uncertainty in applied mechanics, Elsevier,1990 - Psychology - 221 pages.

[36] Y. Ben-Haim, Convex Models of Uncertainty: Applications and Implications, Erkenntnis: An International Journal of Analytic Philosophy, 1994, 41: 139-156.

[37] M. Fuchs, A.Neumaier, Uncertainty modeling with clouds in autonomous robust design optimization, REC 2008, USA.

[38] M. Troffaes, G. Walter, D. Kelly, A robust Bayesian approach to modeling epistemic uncertainty in common-cause failure models, Reliability Engineering & System Safety, Volume 125, May 2014, Pages 13-21

[39] J.C. Heltona, J.D. Johnsonb, Quantification of margins and uncertainties: Alternative representations of epistemic uncertainty, Reliability Engineering & System Safety. Volume 96, Issue 9, September 2011, Pages 1034–1052.

[40] J.C. Heltona, J.D. Johnsonb, W.L. Oberkampfc, An exploration of alternative approaches to the representation of uncertainty in model predictions, Reliability Engineering & System Safety. Volume 85, Issues 1–3, July–September 2004, Pages 39–71.

[41] S.John, The Relationship between the Coefficient of Correlation and the Angle Included between Regression Lines, Journal of Educational Research 41 (4).

[42] K. Pearson (1895), Notes on regression and inheritance in the case of two parents, Proceedings of the Royal Society of London, 58 : 240–242
.
[43] G.R. Shorack, J.A. Wellner, Empirical Processes With Applications to Statistics, Philadelphie, Society for Industrial & Applied Mathematics, 4 septembre 2009, 998 p. (ISBN 978-0-89871-684-9, LCCN 2009025143).

[44] Stephens. M.A (1974), EDF Statistics for Goodness of Fit and Some Comparisons, Journal of the American Statistical Association 69: 730–737.

[45] F. Galton, Regression towards mediocrity in hereditary stature, Journal of the Anthropological Institute of Great Britain and Ireland, 15 : 246–263.

[46] Lehman, Ann (2005), Basic Univariate And Multivariate Statistics: A Step-by-step Guide. Cary, NC: SAS Pres, p.123, ISBN 1-59047-576-3.

[47] W.H. Kruskal, Ordinal Measures of Association , Journal of the American Statistical Association, vol. 53, no 284, 1958, p. 814–861.

[48] A. Saltelli, T.H. Andres, T. Homma, Sensitivity analysis of model output: An investigation of new techniques, Computational Statistics & Data Analysis, Volume 15, Issue 2, February 1993, Pages 211-238.

[49] J.C. Helton, J.E. Bean, B.M. Butcher, J.W. Garner, J.D. Schreiber, P.N. Swift, P. Vaughn, Uncertainty and sensitivity analysis for gas and brine migration at the Waste Isolation Pilot Plant: Permeable shaft with panel seals, Journal of Hazardous Materials, Volume 45, Issues 2–3, February 1996, Pages 107-139.

[50] S. Acharjee, N. Zabaras, A non-intrusive stochastic Galerkin approach for modeling uncertainty propagation in deformation processe, Computers & Structures, Volume 85, Issues 5–6, March 2007, Pages 244-254.

[51] H.M. Panayirci, M.F. Pellissetti, Efficient component-wise and solver-based intrusive SFEM analysis of complex structures, Finite Elements in Analysis and Design, Volume 46, Issue 5, May 2010, Pages 449-459.

[52] R.H. Lopez, A non-intrusive methodology for the representation of crack growth stochastic processes, Mechanics Research Communications, Volume 64, March 2015, Pages 23-28.

[53] L. Goel, R. Billinton, Monte Carlo simulation applied to distribution feeder reliability evaluation, Electric Power Systems Research, Volume 29, Issue 3, May 1994, Pages 193-202.

[54] S. Balopoulou, M. Grigoriu, Sensitivity of seismic response to uncertainties in restoring force model: a Monte Carlo simulation case study, Engineering Structures, Volume 16, Issue 7, 1994, Pages 518-533.

[55] Q. Long, M. Scavino, R.Tempone, S.J. Wang, Fast estimation of expected information gains for Bayesian experimental designs based on Laplace approximations, Computer Methods in Applied Mechanics and Engineering, Volume 259, 1 June 2013, Pages 24-39.

[56] K. Durga Rao, V. Gopika, V.V.S. Sanyasi Rao, H.S. Kushwaha, A.K. Verma, A. Srividya, Dynamic fault tree analysis using Monte Carlo simulation in probabilistic safety assessment, Reliability Engineering & System Safety, Volume 94, Issue 4, April 2009, Pages 872-883.

[57] S. Engelund, R. Rackwitz, A benchmark study on importance sampling techniques in structural reliability, Structural Safety, Volume 12, Issue 4, November 1993, Pages 255-276.

[58] J. Roshanian, M. Ebrahimi, Latin hypercube sampling applied to reliability-based multidisciplinary design optimization of a launch vehicle, Aerospace Science and Technology, Volume 28, Issue 1, July 2013, Pages 297-304.

[59] I. Dimov, R. Georgieva, T. Ostromsky, Monte Carlo sensitivity analysis of an Eulerian large-scale air pollution model, Reliability Engineering & System Safety, Volume 107, November 2012, Pages 23-28.

[60] S. Franceschini, C. Tsai, M. Marani, Point estimate methods based on Taylor Series Expansion – The perturbance moments method – A more coherent derivation of the second order statistical moment, Applied Mathematical Modelling, Volume 36, Issue 11, November 2012, Pages 5445-5454.

[61] U. Kirsch, Approximate structural reanalysis based on series expansion, Computer Methods in Applied Mechanics and Engineering, Volume 26, Issue 2, May 1981, Pages 205-223.

[62] Z.K. Nagy, R.D. Braatz, Distributional uncertainty analysis using power series and polynomial chaos expansions, Journal of Process Control, Volume 17, Issue 3, March 2007, Pages 229-240.

[63] Y.J. Lee, J.H. Song, Finite-element-based system reliability analysis of fatigue-induced sequential failures, Reliability Engineering & System Safety, Volume 108, December 2012, Pages 131-141.

[64] F. Biondini, F. Bontempi, P.G. Malerba, Fuzzy reliability analysis of concrete structures, Computers & Structures, Volume 82, Issues 13–14, May 2004, Pages 1033-1052.

[65] V.J Romero, L.P Swiler, A.A Giunta, Construction of response surfaces based on progressive-lattice-sampling experimental designs with application to uncertainty propagation, Structural Safety, Volume 26, Issue 2, April 2004, Pages 201-219.

[66] H. Agarwal, J.E. Renaud, E.L. Preston, D. Padmanabhan, Uncertainty quantification using evidence theory in multidisciplinary design optimization, Reliability Engineering & System Safety, Volume 85, Issues 1–3, July–September 2004, Pages 281-294.

[67] R.H. LopezI, A.T. BeckII, Reliability-based design optimization strategies based on FORM: a review, J. Braz. Soc. Mech. Sci. & Eng. vol.34 no.4 Rio de Janeiro Oct./Dec, 2012.

[68] D. Geman (1984), Stochastic Relaxation, Gibbs Distributions, and the Bayesian Restoration of Images, IEEE Transactions on Pattern Analysis and Machine Intelligence 6 (6): 721–741.

[69] A.L. Herbert (1986), Metropolis, Monte Carlo and the MANIAC, Los Alamos Science 14: 96–108.

[70] R. W.Bailey (1994), Polar Generation of Random Variates with the t-Distribution, Mathematics of Computation 62 (206): 779–781.

[71] S.K. Choi, R. Grandhi, R.A. Canfield, Reliability-based Structural Design - 2006 - Technology & Engineering, P.60.

[72] R. Grimmett, D.R. Stirzaker (1992), Probability and Random Processes, 2nd Edition, Clarendon Press, Oxford, ISBN 0-19-853665-8.

[73] J. Roshanian, M. Ebrahimi, Latin hypercube sampling applied to reliability-based multidisciplinary design optimization of a launch vehicle, Aerospace Science and Technology, Volume 28, Issue 1, July 2013, Pages 297-304.

[74] S. Eugene, O. Donnell (1997), Incidence algebras, Pure and Applied Mathematics 206, Marcel Dekker, ISBN 0-8247-0036-8.

[75] T. Crestauxa, O. Maitreb, J.M. Martinezc, Polynomial chaos expansion for sensitivity analysis, Reliability Engineering & System Safety, Volume 94, Issue 7, July 2009, Pages 1161–1172.

[76] R. Lia, R. Ghanem, Adaptive polynomial chaos expansions applied to statistics of extremes in nonlinear random vibration, Probabilistic Engineering Mechanics, Volume 13, Issue 2, April 1998, Pages 125–136.

[77] X.L. Wan, G.E. Karniadakis, Multi-element generalized polynomial chaos for arbitrary probability measures, Journal of Scientific Computing, 28 (3) 2006, pp 901 - 928.

[78] M. Shinozuka, G. Deodatis, Simulation of stochastic processes by spectral representation, ASME, Applied Mechanics Review, 44 (4) (1991), pp. 191–204.

[79] S. Dham, R. Ghanem, Finite element analysis of multiphase flow in porous media with the polynomial chaos expansion, Second International Conference on Computational Stochastic Mechanics, Athens, Greece (June, 1994).

[80] G.P. Howell, Truncated Taylor series solutions to a generalized Burgers' equation, Journal of Sound and Vibration, Volume 108, Issue 1, 8 July 1986, Pages 133-14.

[81] D. Wallach, D. Makowski, J.W. Jones, F. Brun, Parameter Estimation with Bayesian Methods, Working with Dynamic Crop Models (Second Edition), 2014, Pages 277-309.

[82] J. Berger, 1985, Statistical Decision Theory and Bayesian Analysis, Springer-Verlag, New York.

[83] J.M. Bernardo (1992), On the development of the reference prior method, Bayesian Statistics 4, Oxford University Press, Oxford, pp. 35-60.

[84] Kenney, J. F. Keeping, E. S. (1962) Linear Regression and Correlation, Ch. 15 Mathematics of Statistics, Pt. 1, 3rd ed. Princeton, NJ: Van Nostrand, pp. 252-285.

[85] M. Georges (1969). Part 1 of Cahiers du Centre de morphologie mathématique de Fontainebleau, Le krigeage universel, École nationale supérieure des mines de Paris.

[86] R.E. Melchers, Importance sampling in structural systems, Structural Safety, Volume 6, Issue 1, July 1989, Pages 3-10.

[87] M.Z. Miguel, G. Josselin, R. Emmanuel, An original sensitivity statistic within a new adaptive accelerated Monte-Carlo method, Procedia - Social and Behavioral Sciences, Volume 2, Issue 6, 2010, Pages 7712-7713.

[88] Y.N. Liu, M.Y. Hussaini, G. Ökten, Optimization of a Monte Carlo variance reduction method based on sensitivity derivatives, Applied Numerical Mathematics, Volume 72, October 2013, Pages 160-171.

[89] Aleš Florian, An efficient sampling scheme: Updated Latin Hypercube Sampling, Probabilistic Engineering Mechanics, Volume 7, Issue 2, 1992, Pages 123-130.

[90] B. Gaspar, A.P. Teixeira, C.G. Soares, Assessment of the efficiency of Kriging surrogate models for structural reliability analysis, Probabilistic Engineering Mechanics, Volume 37, July 2014, Pages 24-34.

[91] M. Miki, Y.Murotsu, T.Tanaka, S.W. Shao, Reliability-based optimization of fibrous laminated composites, Reliability Engineering & System Safety, Volume 56, Issue 3, June 1997, Pages 285-290.

[92] A.D. Kiureghian, T. Dakessian, Multiple design points in first and second-order reliability, Structural Safety, Volume 20, Issue 1, 1998, Pages 37-49.

[93] S.Q. Shan, G. Wang, Reliable design space and complete single-loop reliability-based design optimization, Reliability Engineering & System Safety, Volume 93, Issue 8, August 2008, Pages 1218-1230.

[94] G.I. Schuëller, H.A. Jensen, Computational methods in optimization considering uncertainties – An overview, Computer Methods in Applied Mechanics and Engineering, Volume 198, Issue 1, 15 November 2008, Pages 2-13.

[95] K.Y. Tam, Genetic algorithms, function optimization, and facility layout design, European Journal of Operational Research, Volume 63, Issue 2, 10 December 1992, Pages 322-346.

[96] P.S. Laursen, Simulated annealing for the QAP — Optimal trade-off between simulation time and solution quality, European Journal of Operational Research, Volume 69, Issue 2, 10 September 1993, Pages 238-243.

[97] W.L. Goffe, G.D. Ferrier, John Rogers. Global optimization of statistical functions with simulated annealing, Journal of Econometrics, Volume 60, Issues 1–2, January–February 1994, Pages 65-99.

[98] C.Bathias, There is no infinite fatigue life in metallic materials, Fatigue & Fracture of Engineering Materials & Structures 22 (7): 559–565. doi:10.1046/j.1460-2695.1999.00183.x.

[99] P. Doubilet, C.B. Begg, M.C. Weinstein, Probabilistic sensitivity analysis using Monte Carlo simulation, A practical approach, Journal of the Society for Medical Decision Making [1985, 5(2):157-177].

[100] D.H. Ted, T. Kendall (2000), Linear algebra and linear operators in engineering with applications in Mathematics, Academic Press, ISBN 0-12-206349-X.

[101] P. Doubilet, C.B. Begg, M. C. Weinstein, Probabilistic sensitivity analysis using Monte Carlo simulation, A practical approach.Journal of the Society for Medical Decision Making [1985, 5(2):157-177].

[102] E. Cherchi, C.A. Guevara, A Monte Carlo experiment to analyze the curse of dimensionality in estimating random coefficients models with a full variance–covariance matrix Transportation Research Part B: Methodological, 2012.

[103] J.P.C. Kleijnen. Kriging metamodeling in simulation: A review, European Journal of Operational Research, Volume 192, Issue 3, 1 February 2009, Pages 707-716.

[104] J. Mira, Prediction of deterministic functions: an application of a Gaussian kriging model to a time series outlier problem, Computational Statistics & Data Analysis, Volume 44, Issue 3, 1 January 2004, Pages 477-491.

[105] W.L. Goffe, G.D. Ferrier, J. Rogers, Global optimization of statistical functions with simulated annealing, Journal of Econometrics, Volume 60, Issues 1–2, January–February 1994, Pages 65-99.

[106] P.S. Laursen, Simulated annealing for the QAP — Optimal trade-off between simulation time and solution quality, European Journal of Operational Research, Volume 69, Issue 2, 10 September 1993, Pages 238-243.

[107] K.Y. Tam, Genetic algorithms, function optimization, and facility layout design, European Journal of Operational Research, Volume 63, Issue 2, 10 December 1992, Pages 322-346.

[108] D. Simon, R. Rarick, M. Ergezer, D. Du, Analytical and numerical comparisons of biogeography-based optimization and genetic algorithms, Information Sciences, Volume 181, Issue 7, 1 April 2011, Pages 1224-1248.

[109] J.R. Harland, P. Salamon, Simulated annealing: A review of the thermodynamic approach, Nuclear Physics B - Proceedings Supplements, Volume 5, Issue 1, September 1988, Pages 109-115.

[110] A. Georgieva, I. Jordanov. Global optimization based on novel heuristics, low-discrepancy sequences and genetic algorithms, European Journal of Operational Research, Volume 196, Issue 2, 16 July 2009, Pages 413-422.

[111] N.F. Wang, X.M. Zhang, Y.W. Yang, A hybrid genetic algorithm for constrained multi-objective optimization under uncertainty and target matching problems, Applied Soft Computing, Volume 13, Issue 8, August 2013, Pages 3636-3645.

[112] G. Whittaker, R. Färe, A hybrid genetic algorithm for multiobjective problems with activity analysis-based local search, European Journal of Operational Research, Volume 193, Issue 1, 16 February 2009, Pages 195-203.

[113] A.F. Shahraki, R. Noorossana, Reliability-based robust design optimization: A general methodology using genetic algorithm, Computers & Industrial Engineering, Volume 74, August 2014, Pages 199-207.

[114] T.L. Friesz, G. Anandalingam, N. J. Mehta, K. Nam, The multiobjective equilibrium network design problem revisited: A simulated annealing approach, European Journal of Operational Research, Volume 65, Issue 1, 19 February 1993, Pages 44-57.

[115] R.W. Eglese, Simulated annealing: A tool for operational research, European Journal of Operational Research, Volume 46, Issue 3, 15 June 1990, Pages 271-281.